Ph.D. thesis

Instituto Universitario de Investigación
de Ingeniería de Aragón
Universidad Zaragoza

Characterization, detection and quantification of acute myocardial ischemia from depolarization ECG-derived indices

Daniel Romero Pérez

Directors:
Esther Pueyo Paules
Pablo Laguna Lasaosa

Aragón Institute for Engineering Research (I3A)
University of Zaragoza

June 2013

Characterization, detection and quantification of acute myocardial ischemia from depolarization ECG-derived indices

Thesis submitted for the Ph.D. degree in Biomedical Engineering

Daniel Romero Pérez

Supervised by

Esther Pueyo Paules
Pablo Laguna Lasaosa

Aragón Institute for Engineering Research (I3A)
University of Zaragoza

June 2013

"Para Aragón, en España,
Tengo yo en mi corazón
Un lugar todo Aragón,
Franco, fiero, fiel, sin saña."

"Estimo a quien de un revés
Echa por tierra a un tirano:
Lo estimo, si es un cubano;
Lo estimo, si aragonés."

José Martí
Fragmentos de la Poesía VII
de los Versos Sencillos.

Abstract

Diagnosis and risk stratification of patients with acute coronary syndromes has been shown to be improved by adding information from the depolarization phase (QRS complex) to the conventionally used ST-T segment of the electrocardiogram (ECG). In this thesis robust and reliable methods for characterizing ventricular depolarization from the ECG in the setting of acute myocardial ischemia have been implemented and evaluated. Two different ischemic models have been used for this purpose. The first one is a short-term ischemic model of approximately 5-min balloon occlusion in patients undergoing percutaneous coronary intervention (PCI) in one of the major coronary arteries. The second one is an experimental model of myocardial infarction in pigs, consisting in 40-min balloon occlusion in the mid-left anterior descending artery.

In chapters 2 and 3 the three main slopes within the QRS complex, the upward and downward slopes of the R wave as well as the upward slope of the terminal S wave, were evaluated in the first ischemic model. In ECG recordings at baseline (control recordings) and during PCI-induced ischemia (occlusion recordings), the QRS slopes were quantified using a developed methodology that incorporates dynamic ECG normalization to improve the sensitivity in the detection of ischemia-induced changes. The method was applied in standard leads as well as in leads obtained by projection of spatial QRS loops, where slope changes in response to the induced-ischemia were seen to be emphasized. Analyses in the temporal and spatial domains were performed based on the quantified absolute (during PCI) and relative (with respect to baseline) changes in the QRS slopes. Additionally, other ECG indices, like the ST level deviation, the R and S wave amplitudes and the QRS complex duration, were measured and compared with the QRS slopes. Changes in all those indices were characterized and correlated with the extent and severity of the induced ischemia, quantified by myocardial perfusion imaging (MPS). Correlation analyses were carried out independently for each index and also by combining indices from the depolarization and repolarization phases. Results showed that the QRS slopes correlated

well with ischemia characteristics and could be used as adjunct tools to ST-T analysis for risk stratification in acute ischemia.

In chapter 4 ischemia was assessed by evaluation of three angles within the QRS complex: the R wave angle, the up-stroke angle and the down-stroke angle. Changes in the R wave angle, seen as a surrogate of QRS duration, were suggested to be used for predicting the extent and severity of ischemia. Changes in the up-stroke and down-stroke angles in response to the induced ischemia were more abrupt than those in the R wave angle and were suggested to be used in the development of an ischemia detector. The detector was implemented by modeling ischemia-induced changes as step-like changes with a linearly gradual transition plus additive Laplacian noise.

Finally, in chapter 5 the QRS methods developed in the thesis, as well as other vectorcardiogram-derived indices related to both the depolarization and repolarization phases, were extrapolated to the experimental model of myocardial ischemia and infarction in pigs. Changes in the analyzed indices, quantified at positions of noticeable peaks and valleys observed during occlusion, were correlated with the myocardium at risk and the infarct size, quantified by MPS at the end of the experiment. Indices associated with the latter part of the depolarization correlated better with the ischemia characteristics than indices associated with the earlier part of the depolarization or the ST segment. Additionally, correlation values were computed all along the occlusion to estimate the time intervals where the quantified ECG changes were more strongly related to the ischemic region and the region with the irreversible damage. Depolarization indices and ST segment deviation were used as predictor variables in a multiple linear regression analysis. Results corroborated the importance of using indices corresponding to different phases of the ECG to better describe the myocardium at risk and the infarct size.

Resumen y Conclusiones

Diversos estudios han demostrado que el diagnóstico y la estratificación del riesgo en pacientes con síndromes coronarios agudos pueden mejorarse sensiblemente mediante la adición de información relativa a la fase de despolarización (complejo QRS), a la que se utiliza convencionalmente relativa al segmento ST-T, ambas obtenidas del electrocardiograma (ECG). En esta tesis se han implementado y evaluado métodos robustos y fiables para la caracterización de la despolarización ventricular en el ECG, en el contexto de la isquemia aguda de miocardio. Para este propósito se han utilizado dos modelos de isquemia distintos. El primero es un modelo isquémico de corta duración, obtenido en pacientes sometidos a una intervención coronaria percutánea (ICP), en la cual se ocluye de forma total una de las principales arterias coronarias por medio de un balón durante aproximadamente 5 min. El segundo es un modelo experimental de infarto de miocardio obtenido en cerdos, que consistió en la oclusión de la arteria coronaria descendente anterior izquierda durante 40 min usando un procedimiento similar.

En los capítulos 2 y 3 de la tesis se evaluaron las tres principales pendientes dentro del complejo QRS, la pendiente de subida y de bajada de la onda R, así como la pendiente de subida de la onda terminal S en el primer modelo de isquemia. Dichas pendientes se cuantificaron en registros ECG adquiridos en situación de reposo (registros de control) y durante la isquemia inducida a través de la ICP (registros de oclusión), mediante una metodología desarrollada que incorpora una normalización dinámica del ECG, con vistas a mejorar la sensibilidad en la detección de los cambios inducidos por la isquemia. El método fue aplicado en las derivaciones estándares, así como en derivaciones obtenidas a partir de la proyección del loop espacial del complejo QRS, donde los cambios de las pendientes en respuesta a la isquemia inducida fueron más destacados. Además, se realizaron análisis en los dominios temporal y espacial basados en los cambios absolutos (durante la ICP) y relativos (con respecto a los valores en control), cuantificados a partir de los valores de las pendientes evaluadas. Otros índices derivados del ECG como la desviación del segmento ST, la amplitud de las ondas R y S, y la duración

del complejo QRS fueron además evaluados y comparados con las pendientes del QRS. Los cambios ocurridos en todos los índices fueron caracterizados y correlacionados con la extensión y la severidad de la isquemia inducida, características que fueron cuantificadas a partir de imágenes de perfusión miocárdica (MPS). Los análisis de correlación se realizaron de forma independiente para cada índice, y también mediante la combinación de índices asociados con las fases de despolarización y repolarización ventricular. Los resultados mostraron que las pendientes del QRS correlacionan bien con las características de la isquemia, y que éstas podrían ser utilizadas como herramienta adjunta al análisis del segmento ST-T en la estratificación del riesgo en la fase aguda de la isquemia.

En el capítulo 4 se estudiaron los cambios inducidos por la isquemia mediante la evaluación de tres ángulos obtenidos dentro complejo QRS: el ángulo de la onda R, el ángulo de subida y el ángulo de bajada. Los cambios en el ángulo de la onda R, vistos como un potencial sustituto de la duración del complejo QRS, se utilizaron para predecir la extensión y la severidad de la isquemia. Los cambios ocurridos en los ángulos de subida y de bajada en respuesta a la isquemia inducida, resultaron ser más abruptos que los observados en el ángulo de la onda R, y se utilizaron en el desarrollo de un detector de isquemia. El detector se desarrolló modelando los cambios observados como cambios de tipo escalón con una transición linealmente gradual, más ruido aditivo con distribución Laplaciana.

Por último, en el capítulo 5 se extrapolaron al modelo experimental de isquemia e infarto de miocardio obtenido en cerdos, los métodos derivados del QRS desarrollados en esta tesis, así como otros índices derivados del vectorcardiograma, relacionados tanto con la fase de despolarización como con la repolarización. Los cambios en los índices analizados se cuantificaron en aquellas posiciones correspondientes a los picos y valles más notables observados durante la oclusión coronaria, y se correlacionaron con el miocardio en riesgo y el tamaño final del infarto, ambos cuantificados por medio de MPS tomadas al final del experimento. Los índices relacionados con la última parte de la despolarización correlacionaron mejor con las características de la isquemia que los índices asociados a la primera parte de la despolarización, o al segmento ST. Los valores de correlación también fueron calculados a lo largo de la oclusión para estimar los intervalos de tiempo en los que, los cambios cuantificados en el ECG, estuvieron más fuertemente relacionados con la zona isquémica y con la zona donde el daño fue irreversible. Tanto los índices derivados de la despolarización como la desviación del segmento ST se utilizaron en un análisis de regresión lineal múltiple como variables predictivas de las características de la isquemia. Los resultados corroboraron la importancia de utilizar índices asociados a las diferentes fases del ECG para describir en mejor medida tanto el miocardio en riesgo como el tamaño final del infarto.

Contents

List of Figures

List of Tables

Chapter 1
Introduction

1.1 Cardiovascular diseases

Cardiovascular disease (CVD), according to the definition of the American Heart Association, includes coronary artery disease (atherosclerosis), cerebrovascular disease (stroke), high blood pressure (hypertension) or rheumatic heart disease (damage of myocardium and heart valves) [1]. Coronary artery disease (CAD) and cerebral artery disease are major causes of death in industrialized countries, representing one third of global mortality. CVD mainly affects people over 60 years old who live in developed countries. In the United States, CVD is the leading cause of death and disability, especially among Hispanics [2]. Over 600 000 people die each year from this cause, which means 26% of all deaths that occur in the country. In Spain, CVD accounts for 33% of the total number of deaths, as reported by the National Institute of Statistics (INE: www.ine.es). Important modulators of CVD are so called "modifiable risk factors", such as unhealthy diet, lack of exercise, consumption of snuff and alcohol, and stress. "Non-modifiable risk factors" include age and heredity. Improvement of CVD management is a primary task that requires advances in its diagnosis, treatment and prevention.

1.1.1 Coronary artery disease

CAD is the most common type of heart disease. CAD occurs when the arteries that supply blood to the heart muscle become hardened and narrowed. This is due to accumulation of cholesterol and other materials, called plaque, on the inner wall of the artery. This buildup is called "atherosclerosis" (see Fig. 1.1). As it progresses, less blood flows through the arteries. As a result, the heart muscle cannot receive blood and oxygen, which can lead to chest pain (angina) or myocardial infarction (MI). Most infarctions occur when a blood clot suddenly interrupts the blood supply to the heart, causing permanent heart damage.

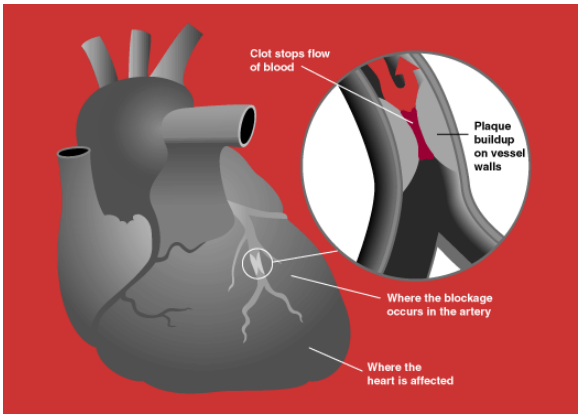

Figure 1.1: Plaque buildup inside a coronary artery and its consequences. Figure based on the image en.wikimedia.org/... diagram.png.

Over time, CAD can also weaken the heart muscle and contribute to the presence of heart failure [3,4] and arrhythmias [5–7] . Heart failure occurs when the heart is no able to effectively pump blood to the body, whereas arrhythmias are changes in the normal rhythm of the heart.

1.1.2 Cardiac arrhythmogenesis and sudden cardiac death

Arrhytmias: An arrhythmia is a disorder of the regular rhythm of the heartbeat, in which the heart beats either too fast (tachycardia), too slow (bradycardia) or irregularly. Each heart beat begins with an electrical discharge originated in a special area (natural pacemaker), which then follows a given path within the heart. The electrical discharge acts as a trigger for mechanical contraction. If a malfunction occurs in the generation or propagation of the electrical impulse, and thus contraction is disturbed, the state is set for arrhythmia development [8].

Arrhythmias can be divided into two different categories: ventricular and supraventricular. Ventricular arrhythmias occur in the two lower chambers of the heart, called ventricles. Supraventricular arrhythmias occur in the structures above the ventricles, mainly the atria (the two upper chambers of the heart).

Ventricular arrhythmias include: Ventricular tachycardia (VT), ventricular fibrillation (VF) and premature ventricular contractions (PVCs).

Supra-ventricular arrhythmias include: supraventricular tachycardia (SVT) or paroxysmal supraventricular tachycardia (PSVT), atrial fibrillation (AF), Wolff-Parkinson-White syndrome (WPW), atrial flutter (AFL) and supraventricular premature contractions (SPCs).

There are several factors that cause irregularities of the heartbeat. In some people, arrhythmias are a congenital defect. Some diseases, including

certain types of heart disease, high blood pressure and hemochromatosis (iron accumulation in the body), can also contribute to the generation of arrhythmias. In addition, stress, caffeine, snuff, alcohol and some medical prescriptions for cough and catarrh can affect the natural rhythm of the heartbeat.

The presence or absence of symptoms and specific types of symptoms depend on the state of the heart and the type of arrhythmia. Symptoms also depend on the severity, frequency and duration of the arrhythmia. Some arrhythmias do not cause warning symptoms. Symptoms may be very mild when present, or may be serious and even life-threatening.

Diagnosis and treatment of arrhythmias: Arrhythmias can be diagnosed using various techniques. The most commonly used test to diagnose an arrhythmia is the standard electrocardiogram (ECG or EKG) which allows to assess the electrical currents produced by the heart and determine the type of arrhythmia[9,10]. Other techniques: the Holter monitoring, providing a continuous readout of the frequency and heart rate during a period of 24 hours (or more); electrophysiology study (EPS), which is usually performed in a cardiac catheterization laboratory and records the electrical pathways of the heart; and the tilt test, as a way to evaluate the heart rate in cases of fainting associated with, among others, the presence of arrhythmias.

Often, the first step to treat the arrhythmia is the administration of antiarrhythmic drugs such as digitalis, beta blockers and calcium channel blockers. Other treatments include transcatheter interventions, implantable devices and surgery (in extreme cases).

Sudden cardiac death (SCD): SCD is the abrupt loss of heart function, leading in most cases to patient's death. It is mainly triggered by arrhythmias, including bradycardia, ventricular tachycardia and, more often, ventricular fibrillation. It is estimated that 12.5% of deaths that occur naturally are sudden deaths and of these, 88% are of cardiac origin.

Of all cases of sudden cardiac death, 80% occur in patients with ischemic heart disease and among them, CAD and peripheral artery desease[11]. Both artery occlusion and reperfusion can cause arrhythmias, such as ventricular fibrillation, leading to sudden death. These cases usually occur in elderly people exposed to cardiovascular risk factors like those mentioned in section 1.1.

1.2 The surface electrocardiogram (ECG)

The ECG measures the variations in the electrical activity of the heart (myocardial fibers) along time. These variations are normally captured with electrodes located at the skin surface and represent the result of the depolarization (activation) and repolarization (relaxation) of the cardiac muscle, which produce electrical changes that reach the body surface.

The ECG recording provides a wealth of information about the heart function, allowing to diagnose a great variety of cardiac alterations [9]. Some of the problems that can be detected through the ECG are: arrhythmias, MI, angina pectoris and changes in the size of the heart. The ECG also helps to support the diagnosis of other diseases such as changes in the potassium and calcium ions in the body and certain lung and thyroid problems.

1.2.1 The electrical activity of the heart

The heart is divided into four chambers, the two higher or atria and the two lower or ventricles. The ventricles are bigger than the atria and present a thicker wall because their pumping action is also higher. The wall of the left ventricle is thicker than the right one, as it pumps blood to the whole body whereas the right ventricle sends blood just to the pulmonary circuit.

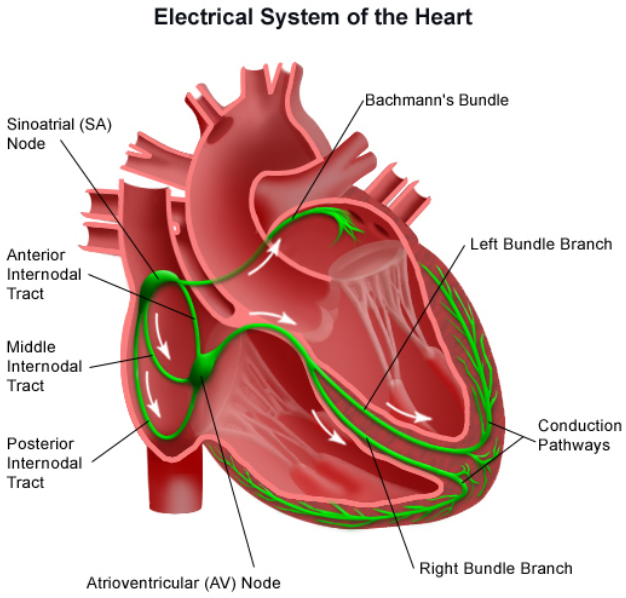

Figure 1.2: Electrical conduction system of the heart. Figure based on the image http://mdmedicine ... system.jpg.

To make the cyclic contraction of the heart synchronous and ordered, there is an electrical conduction system consisting of specialized cardiac muscle fibers that allows the transmission of the electrical impulses and the stimulation of the atria and ventricular myocardium. Although the heart is innervated by the sympathetic nervous system, it beats even without this stimulus, as the conduction system is autoexcitable.

The conduction system consists of the following elements: the sinoatrial (SA) node, the atrioventricular (AV) node, the bundle of Hiss with its right

and left branches and the Purkinje fibers (see Fig. 1.2). The SA node acts as the natural pacemaker of the heart, having the property of automaticity, that is, it spontaneously generates electrical impulse that then spread to excite other cells of the myocardium.

The electrical stimulus passes to the atria coming from the SA node, activating the right atrium and then the left one. Once the impulse reaches the AV node, it is delayed to give time to the blood to pass from the atria to the ventricles before the valves that separate them get closed [12]. Subsequently, the AV node transmits the electrical stimulus across the right and left branches of the bundle of His until the stimulus reaches the ventricles and causes their contraction. In order to achieve a coordinated contraction of the ventricles, the electrical impulse must be transmitted quickly, which occurs through a number of conductive branches ending in the Purkinje network (see Figure 1.2).

Action potential at cellular level

For the development of a contractile response of the cardiac cells, an electrical response in the cell membrane needs to be first generated. This electrical response is called the cardiac action potential (AP).

The morphology of the AP varies from one cell to another depending on their location. A general characteristic of the AP in the cardiac cells is its long duration, ranging between 150 and 300 ms, in contrast with the skeletal muscle and neurons, that present a duration of 1-5 ms. This long duration has important functional consequences, as it allows the overlapping in time of the action potential (electrical phenomenon) with the contraction of the fiber (mechanical phenomenon). As a consequence of this lengthened time, the refractory periods will also be lengthened, ensuring that the muscle can not be re-excited at any time, except at the very end of the contraction.

The two most differentiated APs in the heart are the AP of cells with slow response and the AP of the fibers or cells with fast response. In the SA node and AV node cells, the resting membrane potential is not maintained in a stable level, but presents a series of rhythmic fluctuations that result in the automatic generation of action potentials. In all other cardiac fibers (atrial and ventricular) the AP presents the following phases, which are shown in Fig. 1.3:

- Phase 0: Fast depolarization with an initial fast upstroke due to the opening of the inward fast Na^+ channels that allows a rapid inflow of Na^+ ions into the cell.
- Phase 1: Brief repolarization occurring simultaneously with the inactivation of the fast Na^+ channels.
- Phase 2: This phase is called the “plateau” phase, in which the AP

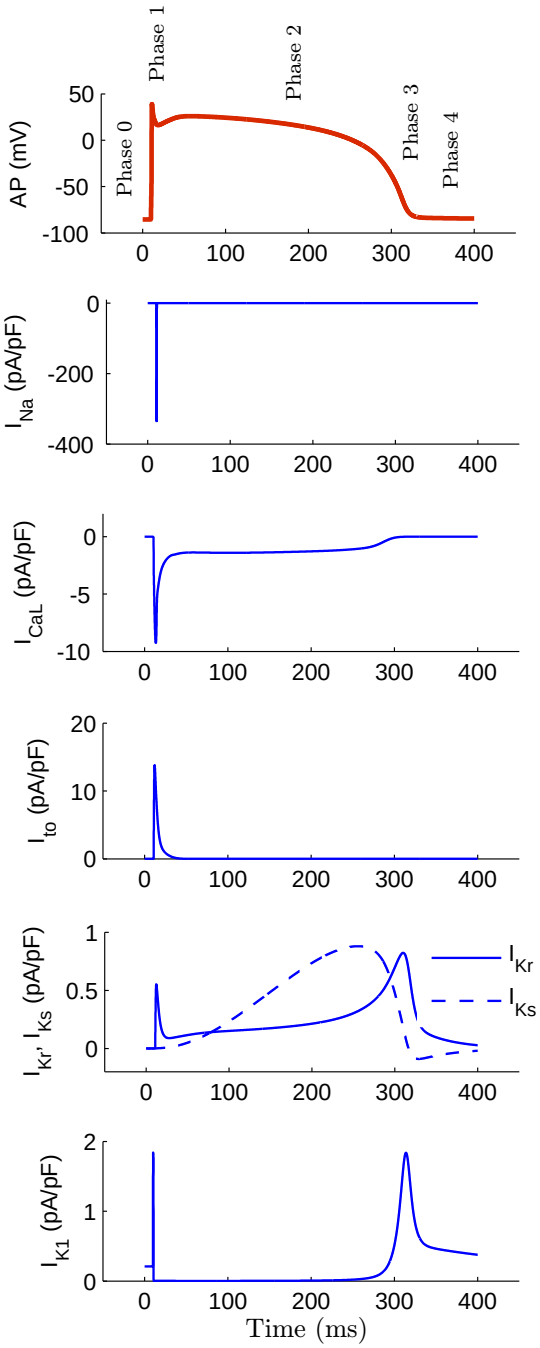

Figure 1.3: Action potential of the ventricular cells of the heart and the most important ionic currents involved in the different phases (phases are marked by numbers at the top graph) generated using a model by Ten Tusscher and Panfilov[13] from the Cellular Open Resource (COR) software.

duration (APD) of the cardiac cells is prolonged. The main event here is the entry of the slow currents of Ca^{2+} ions. This event triggers the release of calcium from the sarcoplasmic reticulum, an essential event for electromechanical coupling.

- Phase 3: Fast repolarization mainly due to the massive outflow of K^{+} ions outside the cell and the marked decrease in the inflow of Ca^{2+} ions, thereby returning the cell to its resting state.

- Phase 4: Resting membrane potential. In basal conditions these fibers exhibit a high permeability to potassium, which makes its resting value close to its equilibrium point ($-90\ mV$). The cell remains in this state until activated by an electrical stimulus, which typically comes from an adjacent cell.

Propagation of the action potentials in tissue and ECG generation

The propagation of the electrical stimulus trough the myocardium results in the generation of APs at different intervals in time and space, which originate a variable electrical field on the body surface. The sum of those AP gradients along the entire cardiac cycle measured on the body surface is is reflected in the ECG.

Figure 1.4 shows the shape of different APs corresponding to different types of cardiac cells. Likewise, the final ECG signal obtained by the sum of all these APs at a particular placement of the body is shown.

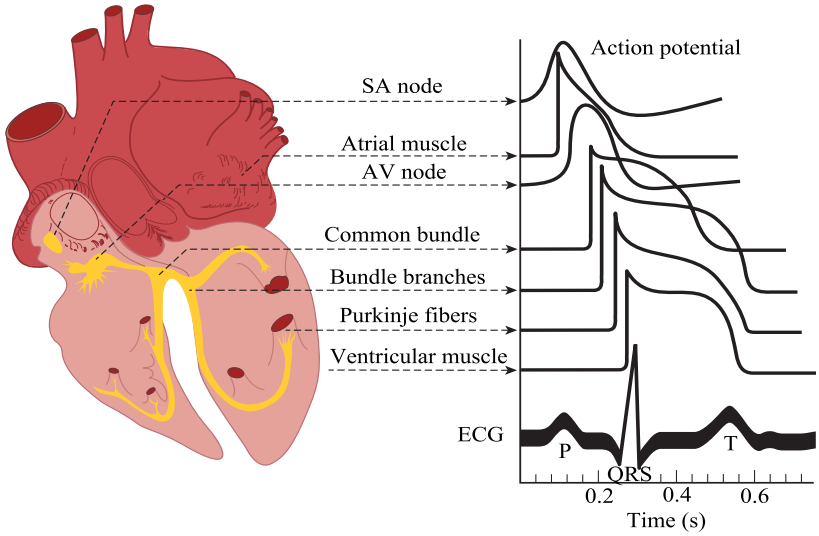

Figure 1.4: Shape of different APs corresponding to different cells found in the heart. Modified and reproduced from Ganong et al. [14]

1.2.2 Lead systems and ECG acquisition

The first electrocardiograph was developed by Willem Einthoven in 1903. Einthoven used a galvanometer to record the first ECG leads (I, II and III) known as standard or Einthoven leads. These three leads are peripheral and measure the potential difference between electrodes located in the members as described below:

- Lead **I**: potential difference between the electrode of the right arm (RA, -) and the left arm (LA, +).
- Lead **II**: potential difference between the right arm (RA,-) and the left leg (LL,+).
- Lead **III**: potential difference between the left arm (LA,-) and the left leg (LL,+).

Peripheral electrodes form the angles of what is known as Einthoven's triangle, which is shown in Fig. 1.5. From the three points of the Einthoven´s triangle, an imaginary point V_{WCT} (the centroid of the triangle, called the Wilson's central terminal, or WCT), located in the center of the chest and above the heart is defined. These three peripheral leads are bipolar, i.e. they have a positive and a negative pole.

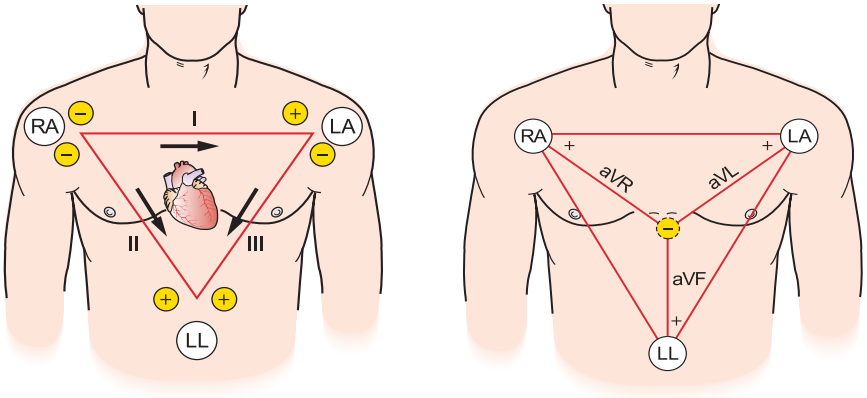

Figure 1.5: Einthoven's triangle and representation of: (left) the limb leads, (right) the augmented limb leads. Reproduced from Jones[15].

At present, twelve leads are commonly used to record an ECG for clinical diagnosis: limb leads, augmented limb leads and chest leads. The limb leads are the ones previously described, whereas the augmented limb leads and the chest leads are defined as follows:

1. Augmented limb leads

- Lead **aVL**= $-\mathbf{I} - \frac{\mathbf{II}}{\mathbf{2}}$
- Lead **aVR**= $\frac{\mathbf{-I+II}}{\mathbf{2}}$
- Lead **aVF**= $-\mathbf{II} - \frac{\mathbf{I}}{\mathbf{2}}$

2. Chest limb leads or precordial leads: They consist of six unipolar leads called V1-V6 whose electrodes are placed directly on the chest as shown in Fig. 1.6. Specific electrode placements are summarized in table 1.1. Due to their close proximity to the heart, these leads do not require any augmentation when acquired. These unipolar leads measure voltage variations of electrodes **V1-V6** with respect to the WCT reference, V_{WCT}, which is represented as $\mathbf{V}_{WCT} = \frac{1}{3}(\text{ RA} + \text{LA} + \text{LL})$.

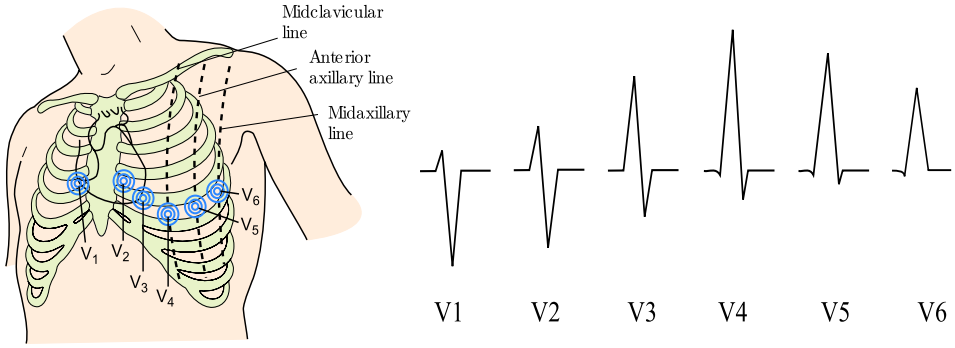

Figure 1.6: Position of the electrodes used to record the precordial leads V1-V6. Representative waveforms of the QRS complex in each precordial lead V1-V6 are also shown (bottom). Reproduced and modified from Jones[15].

Table 1.1: Standard chest leads electrode placements.

Lead	amp; **Positive electrode placement**	amp; **View of heart**
V1	amp; 4-*th* Intercostal space to right of sternum	amp; Septum
V2	amp; 4-*th* Intercostal space to left of sternum	amp; Septum
V3	amp; Directly between **V2** and **V4**	amp; Anterior
V4	amp; 5-*th* Intercostal space at left midclavicular line	amp; Anterior
V5	amp; Level with **V4** at left anterior axillary line	amp; Lateral
V6	amp; Level with **V5** at left midaxillary line	amp; Lateral

Another lead system commonly used in the clinical setting is the vectorcardiographic (VCG) lead system, composed of orthogonal leads. In particular, the Frank's lead configuration is the most popular[16]. The placements of the electrodes is defined by the points A, E, I, and M, which correspond to the left, front, right, and back, respectively. The point C, close to the heart,

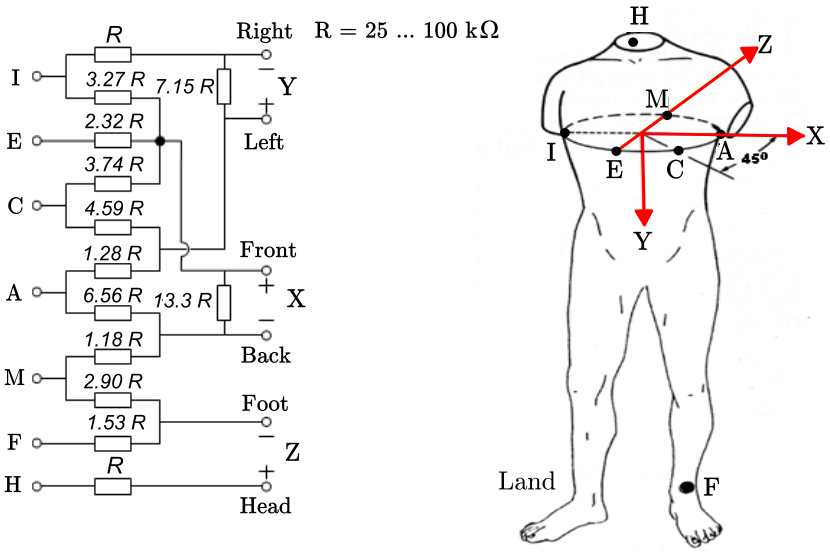

Figure 1.7: Frank's lead system configuration.

is defined located between points A and E. In addition, a point on the neck (H) and one on the left foot (F) are included. The resistor matrix employed by Frank in order to establish a normalized three-lead vector, with the leads denoted by X(back-to-front component), Y (right-to-left component) and Z (foot-to-head component) is illustrated in Fig. 1.7.

A way widely used in the literature to reproduce the orthogonal Frank´s lead system, is the one in which a transformation matrix is used to synthesize the Frank's leads from the standard 12-lead ECG and viceversa. Among the most commonly used transformation matrices are highlight the Dower inverse matrix[17] and the Kors matrix[18].

1.2.3 ECG waveforms

1.2.3.1 Features in the temporal domain

A normal cardiac cycle is reflected in the ECG signal as illustrated in Fig. 1.8. Different positive and negative deflections can be observed due to the atrial and ventricular activity. Such deflections are named by the consecutive letters P, Q, R, S and T, which are repeated in every cardiac cycle. The meaning of each of those characteristic ECG waves are described in the following:

P wave: It reflects the depolarization of the atria. This wave usually presents a positive polarity with amplitude lower than the rest of

waves. If this wave is absent, it may indicate, for example, the existence of a ventricular ectopic focus prevailing over the SA node that makes the depolarization of the atria coincide with the depolarization of the ventricles.

Q, R and S waves: These three waves together form the "QRS complex". The QRS complex represents the depolarization of the ventricles, forming a peaked waveform in the ECG. The complex appears after the P wave and, considering that the ventricles have much more mass than the atria, the QRS complex is larger than the P wave. A normal QRS complex has a duration between $60 - 100$ ms and a voltage no greater than 3.5 mV. Not all QRS complexes contain the three waves, Q, R and S. Convention dictates that any combination of these waves can be referred to as a QRS complex. Some authors use lowercase letters to designate a small wave and capital letters for larger waves. For example, a complex Rs would be predominantly positive (the R wave being much higher than the S wave), while a rS complex would be predominantly negative. In Fig. 1.9 different morphologies of the QRS complex and their corresponding nomenclature are shown.

T wave: It reflects the repolarization of the ventricles. In most of the leads, the T wave is usually positive with a duration of around $150 - 350$ ms. Negative T waves may be a symptom of disease, although an inverted T wave is normal in lead aVR and sometimes in lead V1. The T wave amplitude is quite variable from one lead to another, but should never exceed 0.6 mV. Symmetrical inversion of the T wave, especially in left precordial leads, is usually characteristic of myocardial ischemia and mechanical overload of the ventricles.

From all the above characteristic ECG waves observed in each cardiac cycle, some important time segments and intervals are defined. The segments are normally isolelectrical and the intervals combined waves and segments. The most important segments and intervals used in the development of this thesis are:

PQ interval: At the end of the P wave there is an electrically silent period due to the delay suffered by the physiological stimuli in the AV node, whose duration varies between 120-220 ms. Lengthening of this segment indicates AV conduction disturbances (AV block) while shortening below 120 ms is typical by a syndrome of accelerated AV conduction (Wolff-Parkinson-White and Lown-Ganong-Levine).

QRS duration: It is a measurement of the duration of the QRS complex that indicates the total time required for ventricular depolarization.

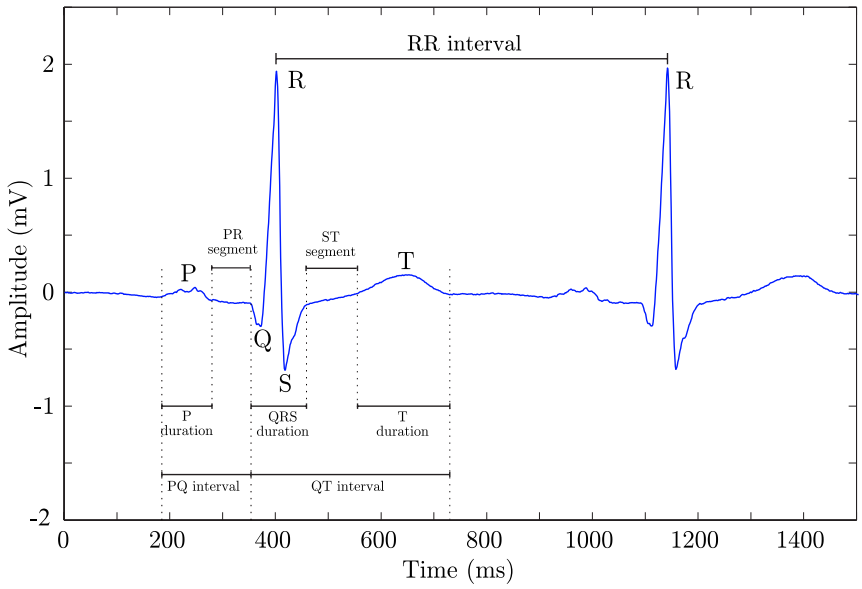

Figure 1.8: Characteristic ECG waves and commonly measured segments and intervals. Reproduced from Sörnmo and Laguna[9].

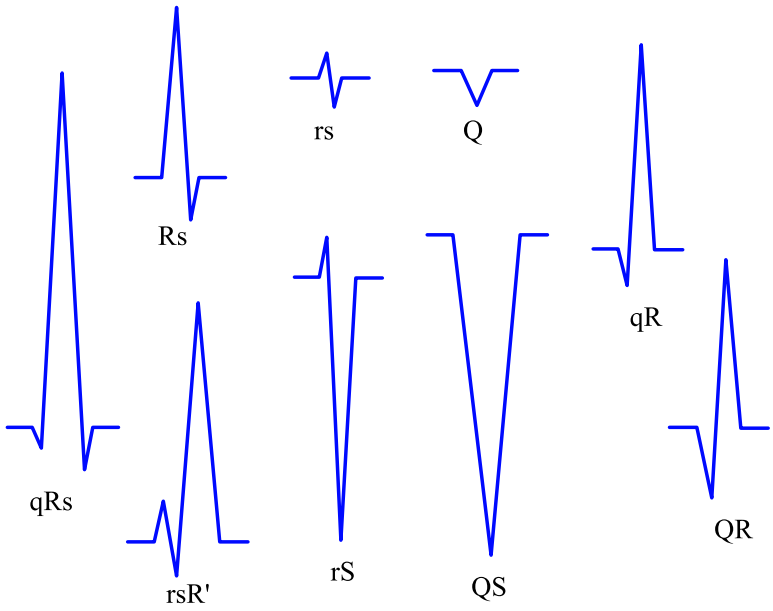

Figure 1.9: Different morphologies of the QRS complex and their associated nomenclature. Figure based on the image https://commons.wikimedia ... QRS_nomenclature.svg.

ST segment: The ST segment connects the QRS complex and the T wave. It covers from the end of the QRS complex (J point) to the start of the T wave. The ST amplitude is measured as the displacement of the ECG signal at (or the J point plus a set period of time) the J point with respect to the isoelectric line. From a clinical point of view, positive or negative deviations of the ST segment larger than 1-2 mm, measured at 60-80 ms after the J point, can be in most cases clear indicators of myocardial ischemic disorders.

Other typical intervals of the ECG are:

RR interval: It measures the distance between the peaks of two consecutive R waves. This interval is used to evaluate the heart rate (HR: defined as 1/RR) variability (HRV) by the analysis of the RR series. The heart rate is normally between 60-100 beats/min. A reduction in the HRV may be a predictor of mortality after MI.

QT interval: It is a measure of the time interval between the beginning of the Q wave and the end of the T wave. The QT interval is dependent on heart rate (higher HR corresponds to smaller QT interval) and must be tailored to HR for its interpretation. The standard correction uses the Bazett's formula[19], in which the corrected QT interval, QTc, is calculated as:

$$QTc = \frac{QT}{\sqrt{RR}} \tag{1.1}$$

This equation is not normally very accurate, because of the overestimation and underestimation of the relationship between the QT and RR intervals at high and low frequencies, respectively, so that alternative equations are frequently used, including the Friderica formula[20] and the Framingham method[21]. Those methods are expressed in equations 1.2 - 1.3 described below:

$$QTc = \frac{QT}{RR^{1/3}}. \tag{1.2}$$

$$QTc = QT + 0.154 \cdot (1 - RR). \tag{1.3}$$

STT interval: This interval comprises the ST segment and the T wave.

1.2.3.2 Features in the frequency domain

The ECG frequency components are approximately between 0.05 and 70 Hz. The frequency components corresponding to the P and T waves achieve up

to 15 Hz, while in the case of the QRS complex they reach up to 40 Hz. In Fig. 1.10 these different frequency components are represented. Nevertheless, other higher frequency components have also been associated with the different ECG waves. For example, in the case of the P wave, such frequency components can be useful to predict certain types of atrial arrhythmias. Likewise, high frequency components present in the latter part of the QRS complex have been used to investigate late potentials [22]. In addition, frequency components in the band 150-250 Hz of the QRS complex have been widely used as a marker for detecting acute myocardial ischemia [23–26].

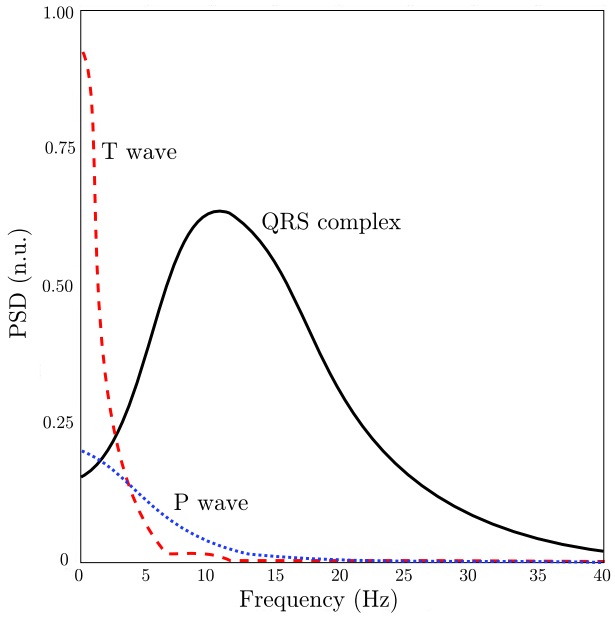

Figure 1.10: Frequency components of the different characteristic ECG waves. Reproduced from Sörnmo and Laguna [9].

1.2.3.3 Interferences and noise in the ECG signal

The noise can be classified depending on whether it is deterministic or random, or according to their origin, external or internal to the measurement system. The term "noise" is normally used when its source is internal to the measuring system and its nature is random. In contrast, the term "interference" applies to the case of signals external to the measuring system, whose time evolution tends to follow a pre-established law that can be known in advance, although its value at any given time may come characterized by a random variable. For example, interferences may come from the power line, or produced by electrical or electronic equipments close to the measurement system.

Sources of noise and interferences that are commonly found in the ECG are described below.

- **Noise sources:**

Electromyographic (EMG) noise: The EMG is the main source of noise in the ECG recording. Its origin can be found in the action potentials associated with the muscle activity of the skeletal muscles. Noise reduction is difficult in this case and requires the cooperation of the patient or subject in which is being measured. Various techniques for EMG noise reduction have been described in the literature[27].

Baseline wander: The baseline wander consists of a low frequency signal superimposed on the ECG, making the isoelectric line not to be well defined. This variation may be due to respiration, body movements or bad contact between the electrodes and the skin. Its frequency content usually remains below 1 Hz. There are different signal processing techniques for baseline wander removal.

Electrode-patient interface: The electrodes are the major element in the measurement chain. Therefore, the noise generated by the electrodes is especially important. The electrodes acts as a transducer. They must convert the ionic currents that are the driving mechanism of the bioelectric signals in the tissues into electrical currents. This transduction should not disturb the signal to be measured. The most important parameters are, therefore, the impedance and the noise. The impedance should be as low as possible to minimize the loading effect of the post-amplification phase of the acquisition equipment and the effect of common mode interference appearing at the input.

Measuring system: The amplification and recording of biopotentials are often accompanied by problems caused by the power line network. The presence of the power line network leads to the development of electric and magnetic fields that interact with the measuring system and the patient. As these are low frequency fields they will always be in near-field.

- **Interference sources:**

The interferences of internal origin come from the measurement equipment itself and the underlying causes are varied. The most common cause is the power supply when the equipment is connected to power line network. A distinction can be made: interferences caused by the electric field, capacitive coupling, and interferences caused by the magnetic field.

Interferences produced by the electric field include:

- Capacitive coupling to the measurement leads
- Capacitive coupling to the electrodes
- Coupling on the patient

Interferences caused by the magnetic field include:

- Interferences caused by the differential mode voltage across the thorax by the currents induced within the patient by an external magnetic field.

- Interferences induced in the loop measured by an the presence of a magnetic field.

Another effect that occurs with relative frequency in ECG signal is the superposition of an interference signal from the power line network (50-60 Hz). To reduce the effect of that interference there are a number of techniques[9] based primarily on the design of various types of filters (e.g. a band removal filter centered at the frequency of the interference network and with a bandwidth sufficiently narrow as to not impair the remaining signal components).

1.3 ECG manifestations of myocardial ischemia and infarction

Ischemic heart disease is the most common form of heart disease and, with few exceptions, is secondary to coronary atherosclerosis. In this disease, the development of blockages at the level of the coronary arteries result in a limitation on the blood flow to the myocardium. When this flow is not sufficient to satisfy myocardial oxygen demand, tissue ischemia occurs. Ischemia produces a series of alterations in myocardial tissue that are responsible for notable clinical and electrocardiographic features. Ischemic changes are initially reversible, but when ischemia becomes acute and sustained, those changes can be irreversible and result in death or necrosis of the myocardial tissue.

In patients with coronary atherosclerosis, MI can be present on a chronic basis, in the event that the coronary flow is insufficient even under basal conditions, or episodically, when the coronary flow is sufficient in resting conditions, but not in circumstances that increase oxygen demand (physical exercise, infections, etc.) or that cause a decrease in oxygen supply (hypoxia, anemia, etc.). In the case of acute coronary syndromes, there is a sharp decrease in coronary perfusion as a result of the rupture of an atherosclerotic plaque and thrombus formation. In these cases, acute ischemia occurs, which may or may not cause necrosis depending on the severity and duration of the blockage in the affected vessel.

From the electrocardiographic point of view, typical changes can be observed, which vary according to the severity of the ischemia and the presence or absence of necrosis. Such alterations are called picture of ischemia, injury and necrosis, which correspond to successively higher degrees of ischemia. There is not an exact correspondence between the electrocardiographic picture of ischemia, injury or necrosis and clinical ischemia. The latter can be present without apparent changes in the ECG, and on the other hand, an

ECG may show changes not necessarily due to ischemia (false positives).

Additionally, the electrocardiographic changes may be displayed transiently or permanently, which corresponds to the nature of episodic or chronic myocardial ischemia. Those changes occur characteristically in electrocardiographic leads facing the area suffering from myocardial ischemia, which, in turn, depend on the obstructed coronary vessels.

1.3.1 Picture of ischemia

The electrocardiographic picture of ischemia is characterized by the presence of T wave abnormalities. Those alterations are the result of a late repolarization in the ischemic zone and vary depending on whether the area affected by the ischemia is mainly subendocardial or subepicardial. When the ischemia is transmural, the subepicardial area prevails.

Subendocardial ischemia: In this case, repolarization of the subendocardial area is delayed and creates a vector that is directed from the subendocardium to subepicardium, resulting in the development of a positive T wave in the leads facing the ischemic zone. That T wave is usually peaked and higher than normal in amplitude, and tends to be symmetrical (Fig. 1.11 a).

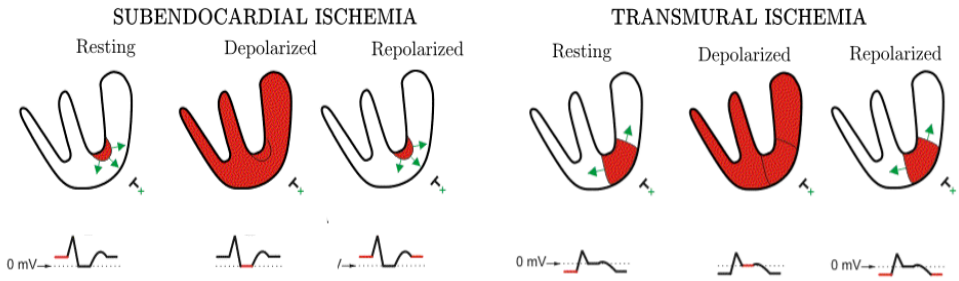

Figure 1.11: ECG alterations according to the ischemic zone in the myocardium. Reproduced and modified from www.cvphysiology ... changes.gif.

Usually this picture is detected in a transient and fleeting way, in connection with acute ischemic processes. Outside this context, the differential diagnosis is very difficult with similar morphologies found in other circumstances, including normal variants, pericarditis, hyperkalemia, and others.

Subepicardial ischemia: Subepicardial or transmural ischemia causes a flattened or negative T wave, wide base and usually symmetrical, an expression of a repolarization vector directed from the subepicardium to the subendocardium as a result of the delayed repolarization in the subepicardial area (Fig. 1.11 b).

This picture may occur in cases of acute or chronic ischemia, being often persistent, and it is commonly accompanied by the appearance of a mirror picture (symmetric positive T) in the frontal plane, in those leads opposite to the ischemic zone. Similar manifestations arise in various other situations: normal variant (hyperventilating, adolescents, mostly women), pericarditis in chronic phase, pulmonary embolism, myocarditis, stroke, alcoholism, left ventricular hypertrophy, etc.

1.3.2 The injury current

Ischemia has a complex time dependent effect on the electrical properties of the myocardial cells. Acute and severe ischemia reduces the resting potential of the cell membrane and shortens the action potential duration (see Fig. 1.12). Those changes determine a voltage gradient between the normal and ischemic areas. Consequently, current flows appear between those regions. Such current flows are called injury currents and are represented in the surface ECG as a ST-segment deviation.

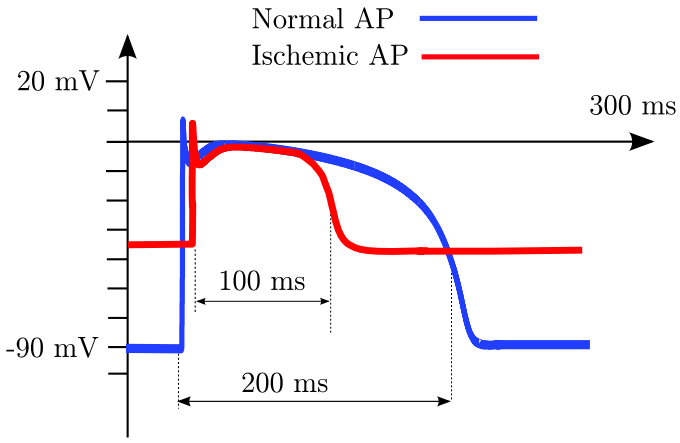

Figure 1.12: Representation of normal and ischemic APs.

ST segment elevation is usually a sign of severe subepicardial injury with frequent involvement of transmural myocardium and subsequent development of necrosis except in the case of vasospastic angina (see Fig. 1.13 b). ST segment elevation in two or more contiguous leads during the acute phase of MI represents the main finding to indicate the need for an early reperfusion (fibrinolysis / primary transluminal coronary angioplasty (PTCA)).

On the other hand, ST segment depression is usually a sign of lower subendocardial injury (Fig. 1.13 a). The subendocardial myocardium is particulary susceptible to ischemia. An established significant criterion for diagnose subendocardial ischemia is a ST segment depression of at least 1 mm below the isoelectric line and 80 *ms* after *J* point.

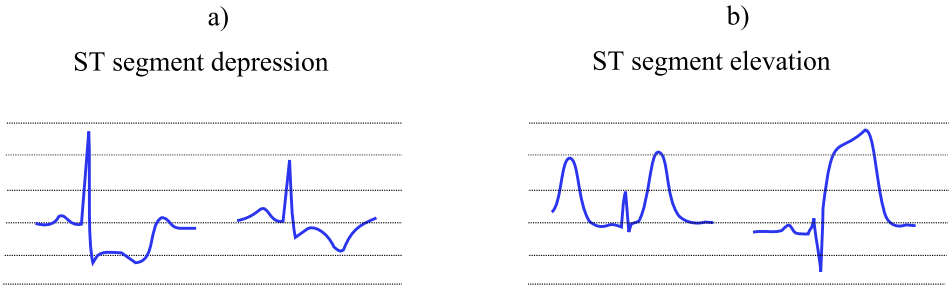

Figure 1.13: ST-segment deviation caused by severe subendocardial (ST depression) and subepicardial (ST elevation) ischemic injuries.

There are multiple factors that modify the amplitude of acute ischemic ST segment deviations. Deep ST elevation or ST depression in various leads usually indicates very severe ischemia. From a clinical perspective, the division of acute myocardial infarction in two types (presence of ST segment elevation and no segment elevation) is useful, since treatment based on acute reperfusion is only effective in the first case.

1.3.3 Necrosis

The necrotic area is electrically silent, i.e. it is typically not depolarized. Necrosis is commonly and is represented by pathological Q waves. To differentiate Q waves with pathological significance from those without different criteria are established including:

- Duration (width) of the Q waves gt; 0.04 sec.nbsp;
- Greater amplitude of Q wave with respect to the R wave:
  $\geqq$ 25% of R wave amplitude in leads II, III and aVF.
  $\geqq$ 15% of R wave amplitude in leads V4-V6.
  $\geqq$ 50% of R wave amplitude in lead aVL.
- Q wave only present in lead V1 or III has not significance, unless it is accompanied by other signs in close leads.
- Q waves with ST-T alterations are more significant than without them.

1.3.4 Localization of the ischemic zone

Changes in ECG leads are useful to locate ischemic regions (see different ischemic regions in Fig. 1.14). For instance, acute transmural ischemia of the anterior wall is reflected in ST segment elevation or in an increase in T wave positivity in one or several precordial leads (V1-V6) and in leads I and

aVL. Ischemia of the inferior wall induces changes in leads II, III and aVF, whereas ischemia in the posterior wall is recognized indirectly by reciprocal ST segment depression in leads V1 to V3. Prominent and reciprocal ST segment depression in these leads is also recorded in some infarcts of the inferior wall, especially in those with extension to the posterior and lateral wall.

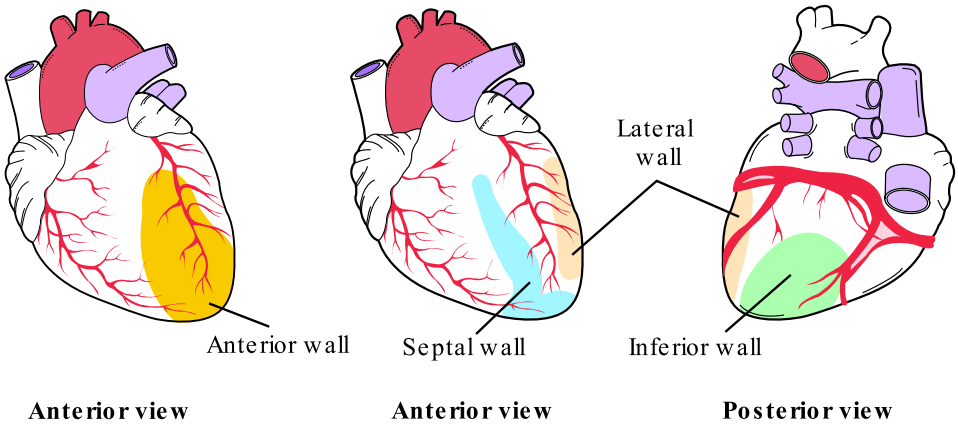

Figure 1.14: Different localizations of MI based on the ischemic zone and viewed from both the anterior and posterior walls. Reproduced from Jones[15].

Right ventricular ischemia usually produces ST segment elevation in the right precordial leads. When the first sign of acute infarction is ischemic ST-segment elevation, within a few hours or days, this anomaly is accompanied by T wave inversion and often of Q waves in the same leads. Reversible transmural ischemia due, for example, to coronary vasospasm (Prinzmetal's variant angina) may cause a transient elevation of the ST segment without the development of Q waves. ST segment elevation may disappear completely in a few minutes or be followed by T-wave inversion persisting for hours or even days, depending on the severity and duration of the ischemia. Patients with ischemic chest pain showing a deep inversion of the T wave in variousnbsp; precordial leadsnbsp; (eg., V1 to V4), with or without elevated cardiac enzymes, usually have an obstruction of the coronary arteries of the anterior descending branch. In contrast, those with a basal anomalous inversion of the T wave sometimes exhibit a normalization (pseudonormalization) of the T wave during episodes of acute transmural ischemia.

Severe ischemia of the anterior wall (with or without infarction) can cause a significant inversion of the T wave in the precordial leads. This pattern is sometimes associated with severe stenosis of the anterior descending branch of the left coronary artery.

Changes in the depolarization phase (QRS complex) that occur in myocardial infarction often accompany repolarization (ST-T) abnormalities.

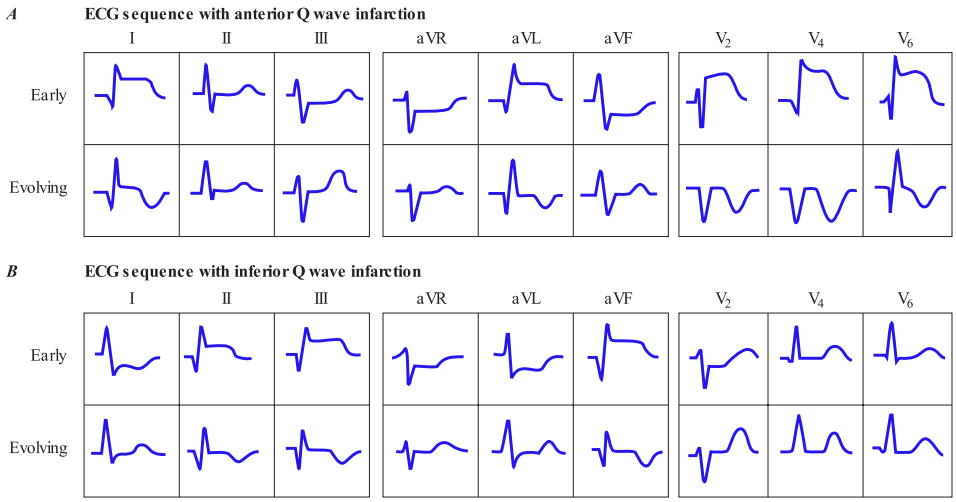

Figure 1.15: Sequence of depolarization and repolarization changes corresponding to (A) infarction of the anterior wall with Q-wave and (B) of the inferior wall with Q-wave. In the anterior wall infarction, ST segment elevation in leads I and aVL as well as in precordial leads is accompanied by a reciprocal depression in leads II, III and aVF. By contrast, patients with acute infarction of the inferior wall (or later) is associated with reciprocal ST depression in leads V1 to V3. Reproduced from Fauci et al.[28].

Sufficient necrosis of myocardial tissue determines a reduction in R-wave amplitude or quite abnormal Q waves in the anterior and inferior leads (see Fig. 1.15). Abnormal Q waves were formally considered as a marker of transmural infarction. Subsequent studies have proved that transmural infarcts may develop without Q-wave and that subendocardial infarcts sometimes are accompanied by Q waves. Therefore, it has been suggested to classify the infarct as “with Q-wave” or “without Q-wave”.

The loss of depolarization strength due to either a posterior or lateral infarct determines a reciprocal increase in the R wave amplitude in leads V1 and V2, without diagnostic Q waves in any of the conventional leads. Atrial infarction is associated with PR segment deviations (produced by a current of injury), changes in the morphology of the P wave or atrial arrhythmias. During the weeks or months following the attack, these ECG changes persist or begin to resolve. The complete normalization of the ECG after infarction with Q wave is uncommon but can occur, especially with smaller infarcts. In contrast, ST segment elevations that persist for several weeks or months after infarction with Q wave usually correspond to a serious deterioration of wall motion (akinetic or dyskinetic area), but are not always a manifestation of ventricular aneurysm.

1.4 Imaging techniques to quantify myocardial ischemia and infarction

Knowledge of the myocardial area at risk, size of myocardial infarction, and myocardial salvage is fundamental to understand the pathophysiology of ischemia-reperfusion injury, as well as to assess the efficacy of treatments aimed at improving myocardial salvage. Figure 1.16 illustrates how the area at risk, the infarct size and the myocardial salvaged can be determined with imaging techniques. Today, the most relevant and widely used techniques for cardiovascular imaging are single-photon emission computed tomography (SPECT) and cardiac magnetic resonance imaging (MRI) as reviewed recently by Florian et al.[29], Arai[30] and Ishida et al.[31].

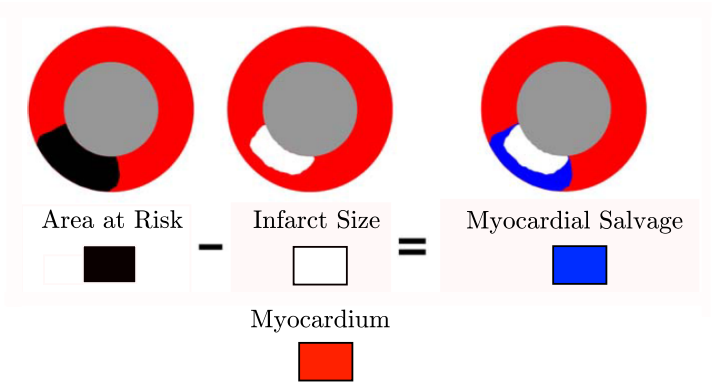

Figure 1.16: Diagram basis on how is evaluated the area at risk, infarct size, and myocardial salvage by MPI. Based on image of the Fig. 1 in Arai[30].

1.4.1 Magnetic resonance imaging (MRI)

MRI characterizes tissues based on specific nuclear magnetic properties such as T1 and T2. In brief, T1 relaxation time (spin-lattice relaxation time) is the rate constant describing how quickly protons realign with the main magnetic field. T1- weighted images can differentiate tissues showing differences in intrinsic or pathological T1. T1-weighted images are commonly used to image the tissue distribution of "gadolinium Gd" contrast. Currently, in the routine clinical setting MI imaging after Gd administration is done by an inversion-recovery T1-weighted sequence, which achieves an increased contrast between normal and pathological tissue (dark vs. bright). Using this technique, infarcted myocardial tissue weighting as low as 1 gram can be visualized (vs. 10 grams with SPECT). On the other side, T2 relaxation time (spin-spin relaxation time) is the rate constant describing how long protons remain synchronous or in-phase after being tipped perpendicular to

the main magnetic field (i.e., in the transverse plane). T2-weighted images generally show fluids as having high or bright signal intensity, while solid tissue, like the myocardium, has intermediate signal intensity (see Fig 1.17). An increase in free water content of tissue increases the signal intensity on T2-weighted images[32]. Thus, in the case of myocardial edema associated with acute MI, the area at risk appears slightly brighter than remote myocardium when imaged with T2-weighted methods. While this summary cannot cover the subtleties of MRI, it provides hints of why some tissues or part of them may be bright or dark depending on the intrinsic characteristics, pathologic changes in tissue magnetic properties, or differential accumulation of gadolinium contrast.

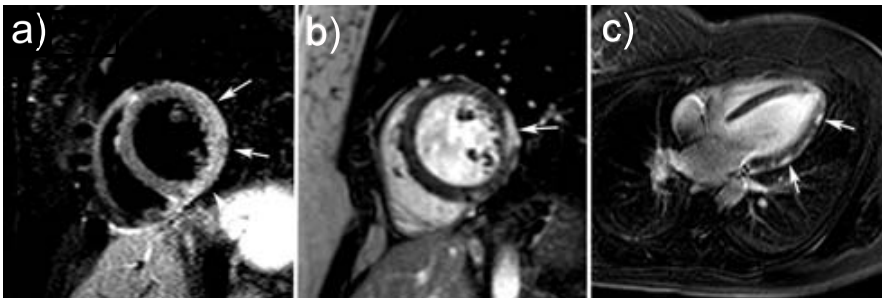

Figure 1.17: Reproduced from Florian et al.[29]: MRI study in an 18 year old male with acute chest pain in which acute myocarditis was diagnosed. Mid ventricular short axis T2-weighted short-inversion-time inversion-recovery (T2w-STIR) image shows edema (increased signal intensities) in the lateral wall (arrows, a) and short and vertical long-axis ce-MRI show typical subepicardial enhancement in the lateral wall (arrows, b, c).

Clinically available Gd contrast agents are injected into the intravascular space and rapidly distribute into the extracellular space. Due to the size and charge, these contrast agents are excluded from the intracellular space. Acute MI is enhanced because cell rupture allows Gd into a higher fraction of the tissue than in viable myocardium. Chronic infarcts are enhanced because the collagenous scar that forms is relatively acellular and thus has a high-effective extracellular space. Myocardial contrast wash-in and washout are dynamic processes, so one of the most important factors in imaging post contrast administration is timing. The optimal time window for infarct imaging is between 10-25 minutes post contrast administration, which is referred to as late contrast enhancement ce-MRI (or late Gd enhancement, LGE images), opposed to early ce-MRI (or early Gd enhancement EGE images).

Regarding infarct size, late ce-MRI is a well-validated, accurate and reproducible tool for sizing acute, healing and healed infarcts[33,34]. Due to its high spatial resolution, enabling depiction of small MIs, late ce-MRI is con-

sidered the reference imaging modality for infarct sizing and is increasingly being used to determine the relationship between infarct size, ventricular remodeling and patient outcome[33,35–37].

1.4.2 Single photon emission computed tomography (SPECT)

SPECT is a nuclear medicine technique that uses radiopharmaceutical substances or radiotracers, a rotating camera (single or multiple-head) and a computer to produce three-dimensional (3D) images representing slices through the body in different planes[38]. SPECT images are functional in nature rather than being purely anatomical such as ultrasound, computed tomography (CT) and MRI.

Single-photon emission computed tomography has been applied to the heart for myocardial perfusion imaging (MPS) (see Fig. 1.18). It is an effective non-invasive diagnostic technology when evaluating patients for clinically significant coronary artery disease (CAD) in the following circumstances: diagnosing CAD in patients with an abnormal resting ECG and restricted exercise tolerance; or assessing myocardial viability before referral for myocardial re-vascularization. Thus, when SPECT is performed to look for damaged heart muscle following a heart attack, injury or infection, it is called *myocardial viability testing*. When SPECT is performed to assess how the heart pumps blood out to the rest of the body, it is called *ventricular function scanning*.

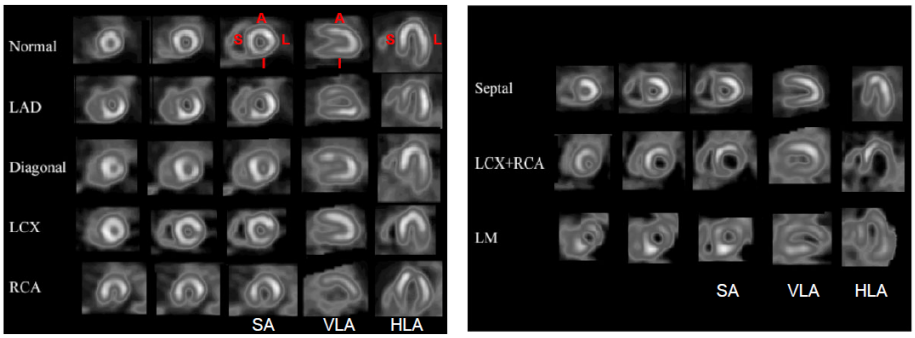

Figure 1.18: Pattern of ischemia in various coronary artery territories in SPECT images. Reproduced from Fuster et al.[39]

The U.S. Food and Drug Administration (FDA) has approved several radiotracers that are used for SPECT cardiac imaging, including:

- Thallous chloride - Thallium-201

- Technetium Tc-99m sestamibi (also known as methoxyisobutylisonitrile) - Cardiolite®

- Technetium Tc-99m tetrofosmin - Myoview ™

Also the FDA has approved pharmaceutical agents that are used to stress the heart during testing, including the following:

- Adenosine
- Dipyridamole
- Dobutamine

Once a cardiac specific radiopharmaceutical is administered, the heart rate is raised to induce myocardial stress, either by exercise or pharmacologically (adenosine, dobutamine, or dipyridamole). SPECT imaging performed after stress reveals the distribution of the radiopharmaceutical, and therefore the relative blood flow to the different regions of the myocardium. Diagnosis is made by comparing stress images to a further set of images obtained at rest. MPS has been demonstrated to have an overall accuracy of about 83% (sensitivity: 85%; specificity: 72%) [40] and is comparable with (or better than) other non-invasive tests for ischemic heart disease.

1.4.3 Comparison between SPECT and MRI

Despite the fact that there are other accepted alternative imaging modalities for differentiating and sizing the jeopardized and the infarcted myocardium in patients with suspected/stable CAD, SPECT and MRI are the ones mostly used in clinical trials and animal experiments, and hence, in the studies described in this thesis.

Myocardial perfusion has been evaluated by SPECT, but patients are exposed to radiation and the diagnostic accuracy is sometimes limited by relatively low spatial resolution and artifacts from photon scatter and tissue attenuation. In the case of MRI, the spatial resolution is substantially higher than that of SPECT, allowing visualization of subendocardial ischemia.

Over the past 5 years, a large number of articles have documented that MRI can non invasively determine the area at risk, infarct size, and myocardial salvage. While T2-weighted imaging has been the method most commonly used, precontrast T1-weighted images and EGE images can also determine the size of the area at risk. All three of these MRI methods detect the area at risk based on myocardial edema resulting from ischemia. LGE images provide a well-accepted reference for infarct size quantification.

1.5 Objectives and outline of the thesis

Analysis of the standard 12-lead ECG is a valuable tool in the clinical evaluation of suspect acute MI, in both pre-hospital and hospital settings. In addition to ischemia detection, the ECG recorded in the acute phase of myocardial infarction (both “snapshot” ECG and ECG retrieved from a monitoring system) can also add further information about prognosis and risk stratification to improve early triage and tailoring of the acute treatment

for better outcome. To achieve that, other information within the ECG signal than the conventional ST-T analysis needs to be evaluated. Myocardial ischemia in more severe stages also affects the depolarization phase. Some of the depolarization changes are considered to represent already necrotic areas (Q waves), but other, potentially reversible changes in the QRS complex also appear, although they are less well understood and are usually not considered for clinical decision making. These changes have been reported to be stronger predictors of clinical outcome than ST measures alone. To facilitate clinical implementation, more robust and clinically feasible methods of QRS complex analysis are needed, as well as better understanding of the pathophysiological bases of the depolarization changes.

In the present thesis a number of ECG signal processing methods are developed to investigate ventricular depolarization in ECG recordings acquired during PCI-induced ischemia. The **main objective of the thesis** is the characterization, detection and quantification of the ischemia-induced alterations in the QRS complex. Two different ischemic models, describing a short-term model of myocardial ischemia in humans and a long-term model of myocardial infarction in animals, respectively, have been studied using the proposed methods.

The thesis is organized as follows:

In **Chapter 2**, the three main slopes within the QRS complex, the upward ($\mathcal{I}_{\text{US}}$) and downward ($\mathcal{I}_{\text{DS}}$) slopes of the R wave as well as the upward ($\mathcal{I}_{\text{TS}}$) slope of the terminal S wave, were evaluated as to represent a robust measure of pathological changes within the depolarization phase. The full methodology for quantification of $\mathcal{I}_{\text{US}}$, $\mathcal{I}_{\text{DS}}$ and $\mathcal{I}_{\text{DS}}$, which incorporates a dynamic ECG normalization so as to improve the sensitivity in the detection of ischemia-induced changes, is presented. Furthermore, the method is also applied on leads obtained by projection of QRS loops (obtained either from the VCG or from orthogonal leads derived from the PCA technique) onto their dominant directions. ECG recordings both in a resting state and during elective PCI-induced transmural ischemia are analyzed using these methods for their characterization in the temporal domain.

- D. Romero, M. Ringborn, P. Laguna, O. Palhm, E. Pueyo. Depolarization changes during acute myocardial ischemia by evaluation of QRS slopes. Standard lead and vectorial approach. *IEEE Transactions on Biomedical Engineering*, 2011, 58(1), 110-120.

- D. Romero, E. Pueyo, M. Ringborn, P. Laguna. QRS slopes for ischemia monitoring in PCI recording. In *World Congress on Medical Physics and Biomedical Engineering, September 7-12, 2009, Munich, Germany* (pp. 1695-1698). Springer Berlin Heidelberg.

- D. Romero, M. Ringborn, P. Laguna, O. Pahlm, E. Pueyo. Análisis Espacial en la Evaluación de Cambios de la Despolarización Cardíaca durante Isquemia Aguda de Miocardio. *In V Congreso Latinoamericano de Ingeniería Biomédica*, CLAIB2011, pp:1-4

Chapter 3 comprises the spatial characterization of the changes in the proposed QRS slopes indice during ischemia with the objective of assessing whether the slope changes hold spatial information regarding coronary occlusion site. Since the amount of myocardial ischemia induced by elective PCI is available (as quantified by MPS), the QRS slope changes are correlated to the extent and severity of ischemia and compared to other conventional depolarization indices (R-wave amplitude and QRS duration). The complementariness of QRS slopes with respect to conventional ST-deviation regarding the explanation of the amount of ischemia is investigated by multiple linear regression (MLR) analysis.

- M. Ringborn, D. Romero, E. Pueyo, O. Pahlm, G.S. Wagner, P. Laguna and P.G. Platonov. Evaluation of depolarization changes during acute myocardial ischemia by analysis of QRS slopes. *Journal of Electrocardiology,* 2011, 44(4), 416-424.

- D. Romero, E. Pueyo, M. Ringborn, P. Laguna. Spatial characterization of ischemia in 12-lead ECG recordings during PCI using both depolarization and repolarization indices. *In Computers in Cardiology, 2009.* IEEE, 2009. p. 113-116.

- D. Romero, M. Ringborn, E. Pueyo, O. Palhm, G.S. Wagner, P. Laguna, P. Platanov. Análisis de la despolarización en isquemia de miocardio mediante la evaluación de las pendientes del QRS. *Proceedings XXIX Congreso Anual de la Sociedad Española de Ingeniería Biomédica.* pp. 41-44.

- M. Ringborn, D. Romero, O. Pahlm, G. Wagner, P. Laguna, E. Pueyo, P. Platonov. Analysis of QRS slopes as a measure of depolaritazion change during acute myocardial ischemia. *37th International Congress on Electrocardiology*, 2010. Lund, Sweden.

A new angle-based methodology applied to the QRS complex is proposed in **Chapter 4**. Those QRS angles, denoted by ϕ_{R} (R-wave angle), ϕ_{U} (upstroke angle) and ϕ_{R} (down-stroke angle), are evaluated in the same study population analyzed in chapters 2 and 3, as another way to quantify morphologic changes within the QRS complex due to ischemia. Under the hypothesis that the R-wave angle ϕ_{R} can be a robust surrogate of QRS width, it was involved in a correlation analysis with the ischemia markers as quantified by MPS. The other two remaining angles are used as a trigger of acute

ischemia in a designed ischemia detector, which is based on a laplacian noise model considering the shape of acute ischemia changes as a step-like change with a gradual transition.

- D. Romero, M. Ringborn, P. Laguna and E. Pueyo. Detection and quantification of acute myocardial ischemia by morphologic evaluation of QRS changes by an angle-based method. *Journal of Electrocardiology* 2013, 46(3), 204-214.
- D. Romero, P. Laguna, E. Pueyo. "Detecting acute myocardial ischemia by evaluation of QRS angles". *International Journal of Bioelectromagnetism*, 2013, 15(1), 77-82.

Chapter 5 extrapolates the QRS-based analysis performed in chapters 2 and 3 to an experimental model of myocardial infarction in pigs. This model consists of a long PCI–induced ischemia produced by 40-min coronary balloon inflation inside the left anterior descending (LAD) artery. Characterization of the dynamics of the depolarization indices during balloon-induced ischemia is carried out in the precordial ECG leads (V1-V6), normalized leads and QRS loop-derived leads. SPECT and MRI images acquired at the end of the experiment allow quantification of myocardium at risk (MaR) and the final infarct size (IS), respectively, and these two markers of ischemic damage are correlated with changes in the ECG-derived indices.

- D. Romero, M. Ringborn, M. Demidova, S. Koul, P. Laguna, P. Platonov, E. Pueyo. Characterization of ventricular depolarization and repolarization changes in a porcine model of myocardial infarction. *Physiological Measurement*, 2012, 33(12), 1975.

Chapter 6 summarizes the conclusions of the thesis and describe future lines of research to expand the work of this thesis.

Chapter 2

Depolarization ECG markers for quantifying acute MI

2.1 Introduction

Changes in the repolarization phase of the ECG (ST-T complex) are most widely used for detection and localization of acute myocardial ischemia. Several prior studies have additionally reported changes in the depolarization phase both in humans and animals when suffering ischemia. These include changes in QRS amplitudes [41–43], QRS duration [44], Karhunen-Loève transform derived indices [45], intra-QRS potentials [22] and "distortion of the terminal part of the QRS complex" [46] in the standard ECG. The latter, in addition to relating to more severe ischemia, also correlates to worse clinical outcome in a large cohort. Changes in high-frequency QRS components (in the frequency band 150-250 Hz) of the high-resolution signal-averaged ECG have been reported as well [23,47,48]. These methods have, however, not been implemented clinically. Among various limitations, one is the difficulty of correctly delineating the end of the QRS complex when there is pronounced ST elevation. In recent studies more reliable methods for characterizing changes in the QRS complex due to both amplitude and duration changes have been proposed [24,49]. In [24], Pueyo *et al.* quantified changes in the QRS complex during myocardial ischemia induced by elective PCI by measuring the up-slope and down-slope of the R wave. In that study, the variability of the QRS slopes in the control recording was used as a reference for quantification of the ischemia-induced changes. However, the stability of this reference was not further explored by means of the normal or intra-individual variation within or between different recordings, nor was an analysis performed to properly characterize factors that affect the measurement of the QRS slopes by modulation of the QRS amplitude. Another way to evaluate depolarization changes during ischemia is by analyzing different shape features derived from the electrical heart vector loop obtained from

the orthogonal ECG leads as in [50] and [51]. Prolonged PCI provides an excellent human model to investigate the electrophysiological changes during the initial minutes of transmural ischemia [45], [47]. During this procedure, a balloon is inserted and inflated inside a coronary artery to induce controlled ischemia due to the balloon occlusion. After deflation the blood flow is immediately restored. During the PCI the occlusion site is perfectly defined in space and time and therefore allows to study the ischemia-induced changes in both domains.

The specific aims of this chapter were to:

- Evaluate the normal variation of the QRS slopes in the 12 standard leads at resting state (control recordings) in a large population, with the purpose of determining reliable limits of significant QRS slope changes due to an ischemic pathophysiological process.
- Apply a normalization procedure to both control and PCI recordings to attenuate low-frequency variation in the slopes and stabilize the slope reference for better quantification of pathophysiologically significant changes.
- Test the performance of this improved method in monitoring QRS slope changes along the dynamic ECG recordings during PCI-induced ischemia on the standard 12-lead ECG and leads derived from the spatial QRS loop.
- Determine the timing of significant changes during PCI.

2.2 Materials and Methods

2.2.1 Databases

The total study population analyzed in this chapter comprised 152 patients, 73 of whom were referred to the Department of Clinical Physiology at Lund University Hospital, Sweden for exercise testing (STRESS dataset). The other 79 patients were taken from the STAFF III dataset, with patients admitted to the Charleston Area Medical Center in West Virginia, USA, for prolonged, elective PCI due to stable angina pectoris [41], [45]. Further details of both datasets are described in the following section.

ECG acquisition: All ECGs were recorded using the same equipment provided by Siemens-Elema AB, Solna, Sweden. Nine standard leads (V1-V6, I, II and III) were recorded and digitized at a sampling rate of 1 kHz with an amplitude resolution of 0.6 μV. The precordial leads V1 to V6 were obtained using the standard electrode placements. For the limb leads, the Mason-Likar electrode configuration was used to minimize the noise level [52].

The three augmented leads aVL, -aVR and aVF were then generated from the limb leads to yield the complete standard 12-lead ECG.

Inclusion criteria: The following inclusion criteria had to be met for both subpopulations: no clinical or ECG evidence of an acute or recent myocardial infarction, no intraventricular conduction delay with QRS duration equal to or more than 120 ms (including left bundle branch block (LBBB) and right bundle branch block (RBBB)), no pacemaker rhythm, low voltage, atrial fibrillation/flutter or any ventricular rhythm at inclusion (or during the PCI for that subpopulation). Patients were also excluded if either they underwent an emergency procedure, or presented signal loss during acquisition.

2.2.1.1 STRESS dataset

The STRESS dataset comprises a total of 73 patients who were admited for a stress testing using an ergonomic bike for the test (see Fig. 2.2). Five ECG recordings (a-e) of 5-min duration were acquired during the entire protocol. The first three recordings (a-c)are control recordings acquired at different times prior to the stress test. The fourth (d) recording was acquired during the recovery of patient starting just after the end of the stress test. The fifth (e) recording was an additional control recording acquired after the recovery phase. No ECG recording was taken during the stress testing because of the persistent electromyographic noise caused by the movement of the patients while pedaling. For this particular dataset, the first two control recordings acquired before the stress test (b and c) were used for the analysis that will be described later.

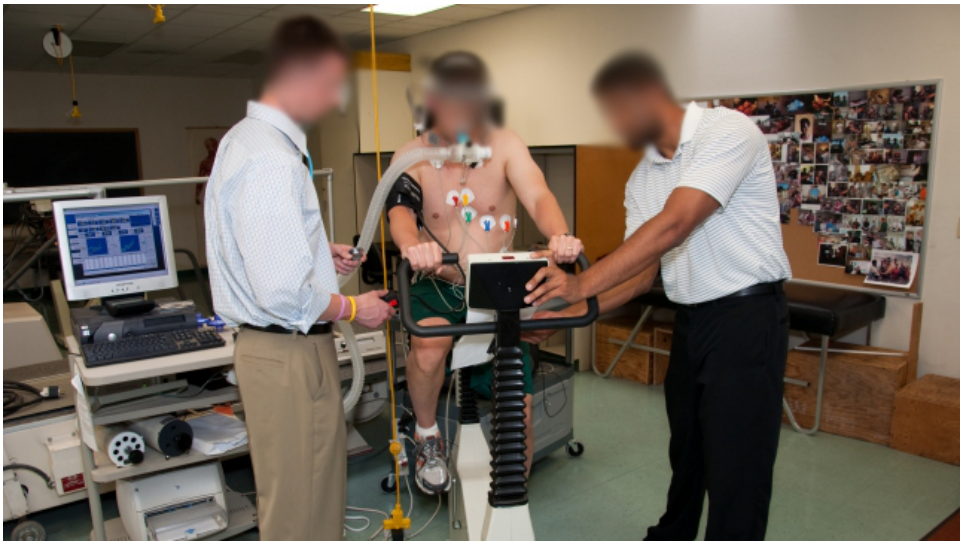

Figure 2.1: Typical ergonomic bicycle used for exercise stress testing.

2.2.1.2 STAFF III dataset

The original population of this dataset comprises 102 patients undergoing prolonged PCI (> 100 sec) in one of the major coronary arteries. This occlusion period was considered to be larger than usual PCI procedures because the protocol included a unique prolonged occlusion instead of a series of short occlusions. The study was approved by the local investigational review board, and informed consent was obtained from each patient before enrolment. Balloon inflation was maintained for 5 minutes or more whenever clinically feasible.

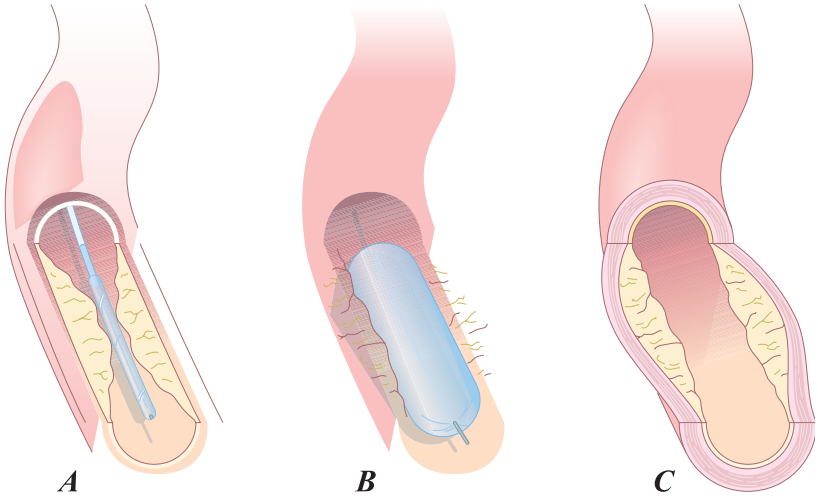

Figure 2.2: Representation of an angioplasty (or PCI) procedure. A) Plaque formation inside the coronary artery; B) Balloon inflation and C) Blood flow restitution. Reproduced from Fauci et al. [28].

Control recordings: For each patient two or more control recordings were acquired continuously for 5 min, at rest in supine position prior to the PCI procedure, during clinical stable situations, with a time interval of maximum one hour. At least another additional control recording in the same conditions was also acquired after the PCI procedure. The two control recordings acquired just before the PCI procedure are those used for analysis.

PCI recordings: In the subset of 79 analyzed patients, a continuous ECG was acquired during the PCI, starting before and ending after balloon inflation and deflation, respectively, for the analysis of QRS slopes during ischemia. The duration of the occlusions ranged from 1 min 30 s to 7 min 17 s (mean: 4 min 26 s). If more than 1 balloon inflation was performed during the procedure, only the first one was considered, to avoid possible bias due to either ischemia-induced collateral recruitment and preconditioning within the area of a previous inflation or persistent ischemia in the myocardium. The occlusion sites of the PCI procedures were: left anterior descending

(LAD) coronary artery in 25 patients (mean occlusion duration: 3 min 54 s), right coronary artery (RCA) in 38 patients (mean occlusion duration: 4 min 37 s), and left circumflex artery (LCX) in 16 patients (mean occlusion duration: 4 min 51 s). In Figure 2.3 are represented the number of patients who remain under occlusion, determined every 30 seconds, for the whole population (n=79) as well as for the different occluded artery subgroups.

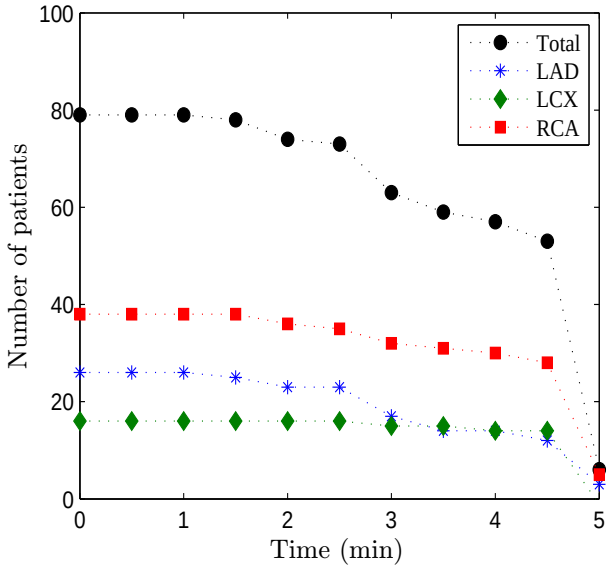

Figure 2.3: Number of analyzed patients of the STAFF III dataset who remain under occlusion at specific time instants.

For each patient of the two datasets, two control recordings were acquired continuously for 5 min, at rest in supine position prior to the stress test or the PCI procedure, respectively, during clinical stable situations, with a time interval of maximum one hour. The electrodes were either retained on the patient between the recordings, or removed and their positions marked, to enable accurate comparisons of the ECG variables.

These control recordings from all 152 subjects were later used for determining the intra- and inter-individual variation of the QRS slopes.

2.2.2 Preprocessing

All ECG signals involved in the analysis were preprocessed before evaluating the investigated indices as follows: (1) QRS complex detection, (2) selection of normal beats according to[53], (3) baseline drift attenuation via cubic spline interpolation and (4) wave delineation using a wavelet-based technique[54].

2.2.3 QRS slopes in single ECG leads

To quantify ischemic QRS changes the following indices were evaluated for each beat and lead:

- $\mathcal{I}_{\mathrm{US}}$: the upward slope of the R wave.
- $\mathcal{I}_{\mathrm{DS}}$: the downward slope of the R wave.
- $\mathcal{I}_{\mathrm{TS}}$: the upward slope of the S wave (in leads V1-V3).

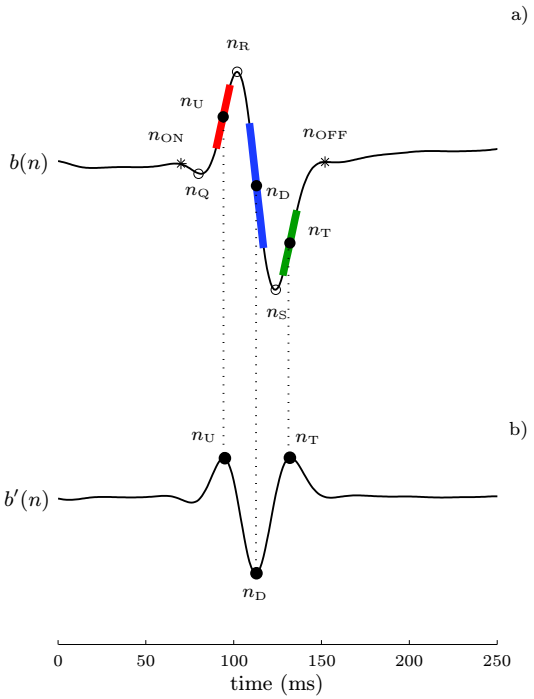

Figure 2.4: a) Example of an ECG beat with the delineation marks used to evaluate the QRS slopes; b) ECG beat derivative with the marks of relative maximum and minimum values within the QRS complex.

A three-step procedure was applied to compute the above indices. First, the time locations of the Q, R and S wave peaks were determined, denoted by n_{Q}, n_{R} and n_{S}, respectively. Beats for which n_{R} could not be successfully determined were rejected from further analysis. Beats for which the delineator determined a valid n_{R}, but was unable to determine n_{Q} or n_{S} due to the absence of the Q or the S waves, a second search was performed to delimit the reference points used in the QRS slopes calculation. For the Q wave, the interval ranging from 2 ms after QRS onset, n_{ON}, to 2 ms prior

to n_{R} was examined and the time instant associated with the lowest signal amplitude was identified as n_{Q}. Analogously, n_{S} was determined considering the interval from 2 ms after n_{R} to 2 ms prior to QRS offset, n_{OFF}. It should be noted that the determination of n_{Q}, n_{R} and n_{S} is not critical since they just delimit the interval over which the maximum and minimum slopes are reached for[24]. Importantly, $\mathcal{I}_{\mathrm{TS}}$, corresponding to the upslope of the S wave, was only computed for leads V1-V3, where the S wave is usually more pronounced. In addition, during more pronounced ischemia, the final part of the QRS complex might get highly distorted, thus making it difficult to delineate the S wave, or it might disappear. In those cases, the $\mathcal{I}_{\mathrm{TS}}$ measure was discarded.

The second step consisted of determining the time instant: n_{U}, associated with the maximum slope of the ECG signal between n_{Q} and n_{R} (global maximum of the ECG signal derivative between n_{Q} and n_{R}); n_{D}, associated with the minimum slope between n_{R} and n_{S} (global minimum of the ECG signal derivative between n_{R} and n_{S}); and finally n_{T}, corresponding to the maximum slope between n_{S} and the QRS complex offset n_{OFF} (see Fig. 2.4).

Finally, three lines were fitted in the least squares sense to the ECG signal in 8-ms windows centered around n_{U}, n_{D}, and n_{T}, respectively; the resulting slopes of those three lines were denoted by $\mathcal{I}_{\mathrm{US}}$, $\mathcal{I}_{\mathrm{DS}}$ and $\mathcal{I}_{\mathrm{TS}}$ (see thick red, blue and green lines in Fig. 2.4-a).

2.2.4 QRS slopes from spatial QRS loops

2.2.4.1 QRS loop from the vectorcardiogram (VCG)

From the standard 12-lead ECG, $l_1(n), \ldots, l_{12}(n)$, it is possible to generate the three orthogonal leads $x(n)$, $y(n)$, and $z(n)$ by applying the Dower Inverse Matrix (D^{-1}) over leads V1-V6, I and II[17], contained in the vector $\mathbf{l}(n) = [l_1(n), l_2(n), \ldots, l_8(n)]^T$. These three orthogonal leads can be represented in a 3D space so that one can observe the variations of the electrical heart vectorcardiogram (VCG), given by $\mathbf{v}_{\mathrm{VCG}}(n) = [x(n), y(n), z(n)]^T$ which is computed as:

$$\mathbf{v}_{\mathrm{VCG}}(n) = D^{-1} \cdot \mathbf{l}(n) \tag{2.1}$$

where the D^{-1} matrix is:

$$D^{-1} = \begin{bmatrix} -0.172 & -0.074 & 0.122 & 0.231 & 0.239 & 0.194 & 0.156 & -0.010 \\ 0.057 & -0.019 & -0.106 & -0.022 & 0.041 & 0.048 & -0.227 & 0.887 \\ -0.229 & -0.310 & -0.246 & -0.063 & 0.055 & 0.108 & 0.022 & 0.102 \end{bmatrix}$$

In order to enhance the sensitivity of the QRS slopes for detecting ischemic-induced changes, a new lead obtained from spatial QRS loop is proposed here as an alternative to the standard single leads. During depolarization, the dominant direction $\mathbf{u}$ (see Fig. 2.5) of the QRS loop ($\mathrm{QRS}_{\mathrm{VCG}}$)

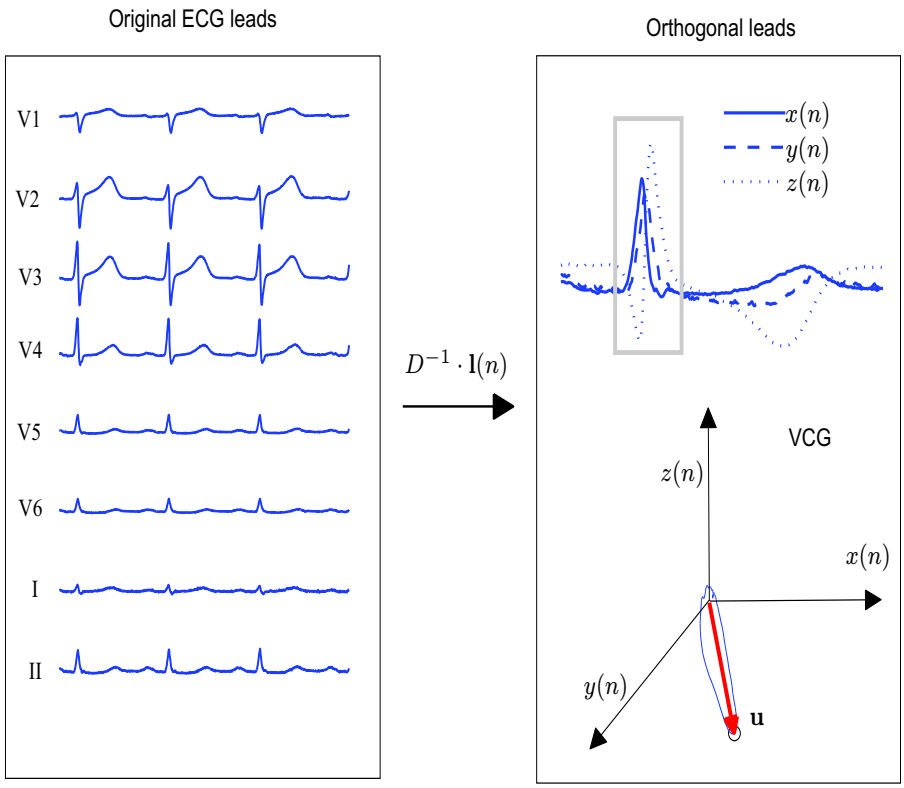

Figure 2.5: Representative diagram of the transformation used to obtain the VCG from the standard 12-lead ECG signal as well as an illustration of the main direction within the QRS loop determined to generate $g(n)$.

points to the QRS loop tip, called the *mean electrical axis*. Thus, determining the main direction of the $\mathrm{QRS_{VCG}}$ loop, the new lead can be obtained by projecting the loop onto that vector. For this analysis we first searched for the main direction $\mathbf{u}$ by maximizing the following equation:

$$\mathbf{u} = [u_x, u_y, u_z]^T = [x(n_0), y(n_0), z(n_0)]^T,$$

with

$$n_0 = \arg\max_n [x^2(n) + y^2(n) + z^2(n)] \tag{2.2}$$

where n spans over the samples of the running beat from 10 ms before n_{ON} to 130 ms after n_{ON}. Then the new projected lead $g(n)$ was calculated by projecting the points of the $\mathrm{QRS_{VCG}}$ loop onto the $\mathbf{u}$ axis :

$$g(n) = \frac{\mathbf{v}_{\mathrm{VCG}}^T(n)\ \mathbf{u}}{\|\mathbf{u}\|}. \tag{2.3}$$

The indices described in the previous section were then evaluated on this new lead.

2.2.4.2 QRS loop using PCA

Principal component analysis (PCA) is a technique commonly employed in signal processing. One way to implement PCA is by applying singular value decomposition (SVD) on the standard 12-lead ECG to generate a new lead system that concentrates the most energy of the signal in a small set of leads[55]. Specifically, the SVD was applied over leads V1-V6, I and II to obtain 8 transformed leads $\mathrm{w}_k(n)$, $k = 1, 2, \ldots, 8$, by using the following transformation:

$$\mathbf{w}(n) = \mathbf{U}^T\ \mathbf{l}(n) \tag{2.4}$$

where $\mathbf{U}$ is the matrix containing the right singular vectors (or the principal components) obtained from matrix $\mathbf{L}$ decomposition according to:

$$\mathbf{L} = \mathbf{V}\mathbf{\Sigma}\mathbf{U}^T \tag{2.5}$$

being $\mathbf{L}$= $[\mathbf{l}_1, \ldots, \mathbf{l}_8]$, with $\mathbf{l}_k = [l_k(1), l_k(2), \ldots, l_k(N)]^T$ and N the number of samples in the recording, $\mathbf{V}$ represents the matrix containing the left singular vectors and $\mathbf{\Sigma}$ a nonnegative diagonal matrix containing the singular values. The columns of the matrix $\mathbf{U}$ represent the principal components (orthogonal components), ordered by importance according to the variance of the data in the new orthogonal system, whereas each element of the column vectors represent the contribution of each lead.

Figure 2.6 shows this lead-reducing transformation. It is evident that the energy of the original leads is mostly concentrated in the first 3 of the 8

transformed leads $w_k(n)$. The new lead system given by the first three orthogonal transformed leads $w_1(n)$, $w_2(n)$ and $w_3(n)$ was subsequently used to represent the QRS loop in a different way, called the QRS_{PCA} loop. Anal-

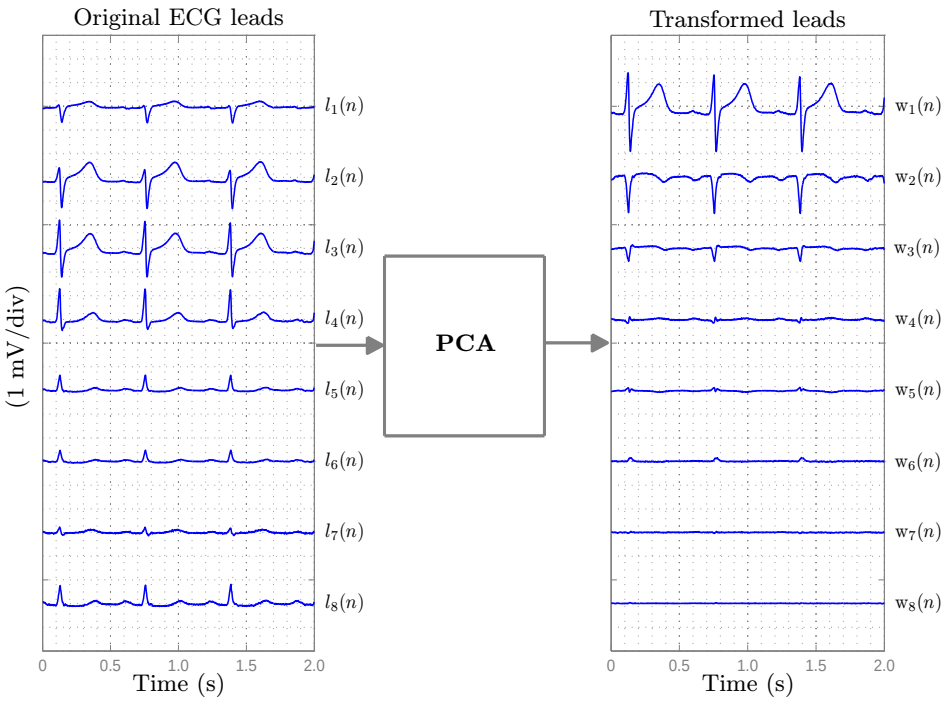

Figure 2.6: Left side: Standard 12-lead ECG signal (only $l_1(n), ..., l_8(n)$ are displayed); Right side: Transformed orthogonal ECG leads obtained from the PCA technique.

ogously to the process described in section 2.2.4.1, the same methodology was applied here to compute a new lead by projecting the QRS_{PCA} loop onto its dominant direction using equations (2.2) and (2.3). The only difference with respect to 2.2.4.1 is that $\mathbf{v}_{VCG}(n)$ was replaced with $\mathbf{v}_{PCA}(n)$, defined as:

$$\mathbf{v}_{PCA}(n) = [w_1(n), w_2(n), w_3(n)]^T . \tag{2.6}$$

Examples of the two approaches described above are presented in Fig. 2.7, where three consecutive beats in three orthogonal leads are shown, corresponding to each of the two vectorial techniques (VCG or PCA) used in this study. Corresponding QRS loops are shown as well. The QRS slopes were evaluated in the new leads obtained by projection of QRS loops in order to compare these results with those obtained from individual leads of the standard 12-lead ECG system.

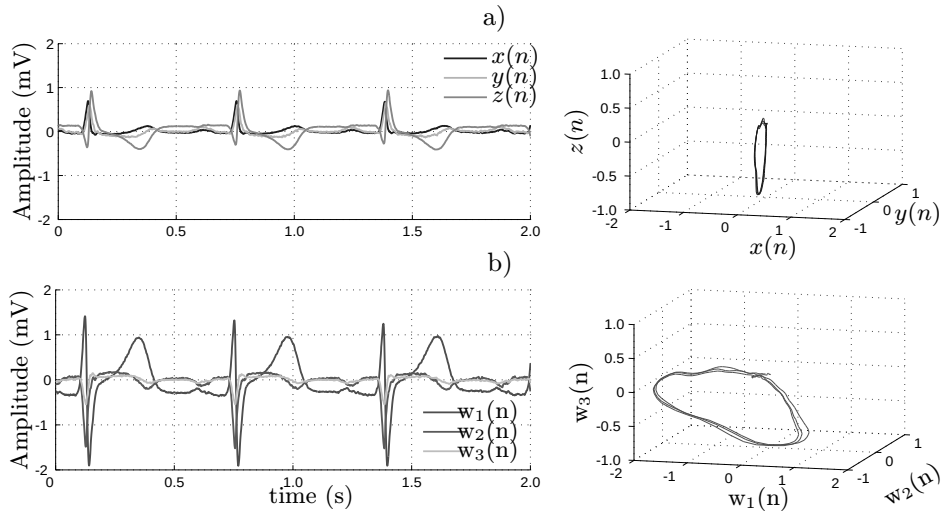

Figure 2.7: a) Orthogonal X, Y and Z leads derived from Dower Inverse Matrix in a time segment, and their corresponding loops; b) Transformed orthogonal ECG leads obtained from the PCA technique, and their corresponding loops.

2.2.5 Quantification of ischemic changes

The ability of a certain index $\mathcal{I}$ to track PCI-induced ischemic changes in relative terms with respect to the normal variation measured at resting state was characterized by the parameter $\mathcal{R}_{\mathcal{I}}$[45]. This parameter, evaluated at time instant t_ϕ taken in increments of 10 s from $t = 0$ (occlusion start) until the end of the occlusion, was defined as the ratio between the change observed during PCI up to time t_ϕ, denoted by $\Delta_{\mathcal{I}}(t_\phi)$, and the normal fluctuations observed during the control recording immediately prior to the PCI, as defined by the standard deviation (SD) of $\mathcal{I}$ in this control recording denoted by $\sigma^{\mathcal{I}}$:

$$\mathcal{R}_{\mathcal{I}}(t_\phi) = \frac{\Delta_{\mathcal{I}}(t_\phi)}{\sigma^{\mathcal{I}}}. \tag{2.7}$$

2.2.6 ECG normalization

When large physiological variations occur in the ECG signal at resting state, the potential value of $\mathcal{R}_{\mathcal{I}}$ as a marker of ischemia is highly reduced because of the increase in $\sigma^{\mathcal{I}}$ in the denominator of $\mathcal{R}_{\mathcal{I}}$ (2.7). This occurs when respiration or other low-frequency modulations of the ECG affect the

QRS complex amplitude and the slope estimates. To compensate for this, an ECG signal normalization procedure was employed[56]. In brief, the normalization uses a running window of 15-s duration centered around the R

wave of each processed beat $b_i(n)$, with i denoting beat index. The median of the R wave amplitudes corresponding to the M (or $M+1$) beats within the 15-s window was computed: $R_{m_i} = \text{median}\{R_{[i-M/2]}, ..., R_{[i+M/2]}\}$, and the normalized beat $\hat{b}_i(n)$ was defined as:

$$\hat{b}_i(n) = \frac{R_{m_i}}{R_i} b_i(n). \tag{2.8}$$

Figure 2.8 shows this ECG normalization procedure. This procedure was applied to both the control and PCI recordings in all the processed leads, either standard ones or derived from the QRS_{VCG} and QRS_{PCA} loops.

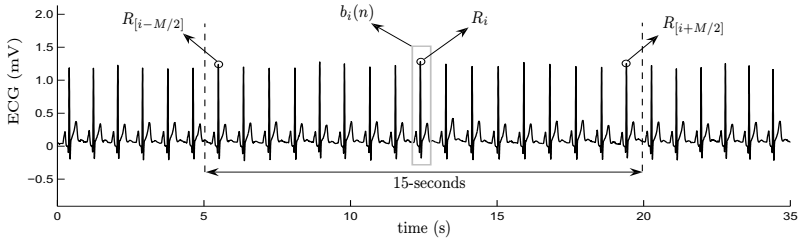

Figure 2.8: ECG normalization used to compensate for low-frequency oscillations. The gray rectangle represents the analyzed beat and the dashed lines the boundaries of the 15-s window.

2.2.7 Normal variations of the QRS slopes

Intra-individual variability analysis: To assess the intra-individual variability of QRS slope variations, $\mathcal{I}_{\text{US}}$ and $\mathcal{I}_{\text{DS}}$ were measured on the normalized beats of each of the two control recordings analyzed per patient. The SD of $\mathcal{I}$ ($\mathcal{I}_{\text{US}}$ or $\mathcal{I}_{\text{DS}}$), denoted by $\sigma^{\mathcal{I}}_{k,c}(j)$, was computed for each patient $j = 1, ..., J$, and lead $k = 1, ..., 12$, in each of the two control recordings ($c = 1, 2$). The difference between the SDs of the two control recordings was quantified:

$$d^{\mathcal{I}}_k(j) = \sigma^{\mathcal{I}}_{k,1}(j) - \sigma^{\mathcal{I}}_{k,2}(j) \tag{2.9}$$

A statistical test (1-sample t-test) was applied to the difference $d^{\mathcal{I}}_k(j)$ evaluated for the whole set of patients, and each lead k and index $\mathcal{I}$, with the purpose of contrasting the following hypothesis:

- $\mathcal{H}_0$: the intra-individual change ($\bar{d}^{\mathcal{I}}_k$) is $= 0$.
- $\mathcal{H}_1$: the intra-individual change ($\bar{d}^{\mathcal{I}}_k$) is $\neq 0$.

where

$$\bar{d}^{\mathcal{I}}_k = \frac{1}{J} \sum_{j=1}^{J} d^{\mathcal{I}}_k(j). \tag{2.10}$$

Inter-individual variability analysis: To assess the inter-individual variability of QRS-slope variations, the mean of the two SDs $\sigma^{\mathcal{I}}_{k,c}(j)$, $c = 1, 2$, was computed for each patient j, lead k, and index $\mathcal{I}$:

$$\sigma^{\mathcal{I}}_{k}(j) = \frac{1}{2}\{\sigma^{\mathcal{I}}_{k,1}(j) + \sigma^{\mathcal{I}}_{k,2}(j)\}. \tag{2.11}$$

Then the SD of $\sigma^{\mathcal{I}}_{k}(j)$ over patients was quantified, and denoted by $s^{\mathcal{I},\updownarrow}_{k}$. Additionally, the SD of the $\sigma^{\mathcal{I}}_{k,c}(j)$, $c = 1, 2$, for each patient j was also computed and denoted by $s^{\mathcal{I},\leftrightarrow}_{k}(j)$

$$s^{\mathcal{I},\leftrightarrow}_{k}(j) = \frac{1}{\sqrt{2}}|\sigma^{\mathcal{I}}_{k,1}(j) - \sigma^{\mathcal{I}}_{k,2}(j)| = \frac{1}{\sqrt{2}}\left|d^{\mathcal{I}}_{k}(j)\right|. \tag{2.12}$$

A statistical test (1-sample t-test) was applied to compare the intra-individual variability, $s^{\mathcal{I},\leftrightarrow}_{k}(j)$, $j = 1, ..., J$, with the inter-individual variability of the whole population, $s^{\mathcal{I},\updownarrow}_{k}$.

2.2.8 Time course of QRS slope changes during ischemia

Absolute $\Delta_{\mathcal{I}}(t)$ and relative $\mathcal{R}_{\mathcal{I}}(t)$ ischemia-induced changes during occlusion were computed for each patient j and lead k. These values were averaged over the whole population as well as over each of the three groups defined according to the occlusion site. In addition, determination of significant changes in the QRS slopes due to the induced ischemia during PCI, and their timing, was performed by applying a statistical test of the type described in section 2.2.7. In this case, differences were computed between the mean, $\mathcal{I}_{\text{REF}}$, of the analyzed index $\mathcal{I}$ ($\mathcal{I}_{\text{US}}$ or $\mathcal{I}_{\text{DS}}$) during the first five seconds of the PCI recording (taken as a reference) and the current values of $\mathcal{I}$ in the PCI recording, $\mathcal{I}(t)$, evaluated at time instants t taken in increments of 3 s from the onset of occlusion ($t = 0$), in each lead k.

2.2.9 Calculation of ST-segment change

The ST level measured at J point, $\mathcal{I}_{\text{ST}}$, was also quantified in all of the analyzed recordings. Subsequently, the corresponding absolute $\Delta_{\mathcal{I}_{\text{ST}}}$ and relative $\mathcal{R}_{\mathcal{I}_{\text{ST}}}$ changes during PCI were calculated, and compared with those corresponding to QRS slope indices.

2.3 Results

2.3.1 Methodological analysis

An example of the effect of the normalization technique described in section 2.2.6 is presented in Fig. 2.9, which shows sequences of $\mathcal{I}_{\text{DS}}$ values

measured before and after application of the ECG normalization. It is clear from the figure that normalization attenuates the low-frequency oscillations,

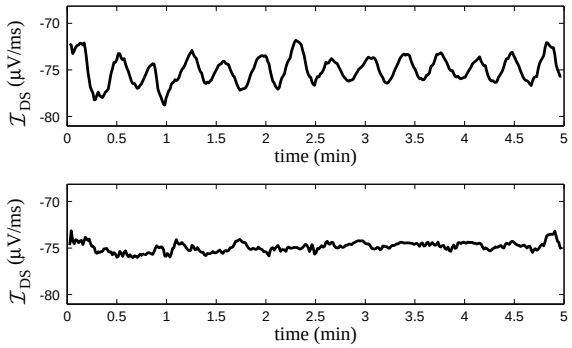

Figure 2.9: $\mathcal{I}_{DS}$ values measured in lead II in a control recording of a patient from the STAFF III dataset before (top) and after (bottom) applying ECG normalization.

most likely generated by respiration or other very low-frequency components of uncertain origin, which affect the slope measurements through modulation of the QRS amplitude. In those patients presenting this low-frequency oscillatory behavior (31 out of a total of 152) the mean of the oscillation frequency was 0.04 ± 0.01 Hz. As a consequence, the variability observed in $\mathcal{I}_{US}$, $\mathcal{I}_{DS}$ and $\mathcal{I}_{TS}$ in any recording at rest becomes substantially lower after applying the normalization procedure (e.g. for $\mathcal{I}_{DS}$ a reduction of 20.3% was observed among the 12 leads in the STAFF III dataset, with maximum of 33.4% in lead II), thus making those measurements in normalized ECG suitable for assessing ischemia-induced changes through evaluation of the relative ratio $\mathcal{R}_{\mathcal{I}}$.

Figure 2.10 shows the QRS slope series evaluated in two control recordings and the PCI recording for a particular patient in lead V2 (LAD occlusion). It can be observed from the first two columns (control recordings) that the three QRS slopes show high stability. More importantly, their degree of variation in the two control recordings is very similar between them. During PCI, the amount of change in $\mathcal{I}_{US}$ was much lower than in $\mathcal{I}_{DS}$ or $\mathcal{I}_{TS}$.

2.3.2 Intra-individual variability of the QRS-slope variations

The low intra-individual variability of the QRS-slope variations is confirmed by the results of the statistical test described in section 2.2.7. In all the leads, except for V3, I, -aVR and II, the p-value is < 0.05 and the hypothesis $\mathcal{H}_0$ of the intra-individual variability of QRS-slope variations being negligible is accepted. In leads V3, I, -aVR and II, despite the p-value being > 0.05,

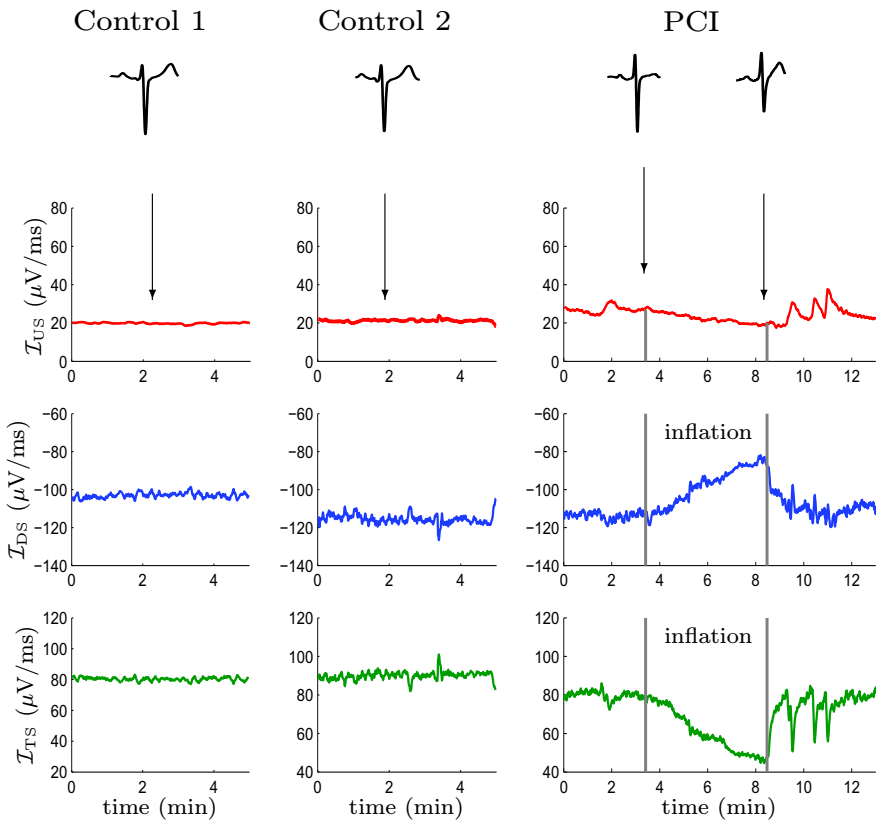

Figure 2.10: QRS slopes in normalized ECGs of a patient in lead V2. On top, representative beats during control and PCI (LAD occlusion) are shown. Each row corresponds to an evaluated index ($\mathcal{I}_{\mathrm{US}}$, $\mathcal{I}_{\mathrm{DS}}$, and $\mathcal{I}_{\mathrm{TS}}$), whereas each column represents a different recording. Gray vertical lines in the right column mark the beginning and end of the occlusion.

the differences between the two control recordings were very close to 0. To illustrate that, Fig. 2.11 presents averaged results and dispersion of $d_k^{\mathcal{I}}(j)$.

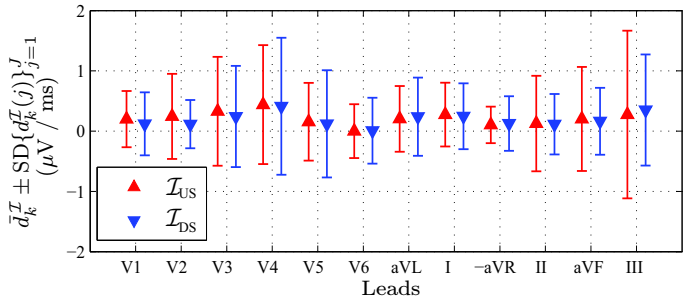

Figure 2.11: Mean ± SD over patients of the intra-individual variations $d_k^{\mathcal{I}}(j)$ for $\mathcal{I}_{\mathrm{US}}$ and $\mathcal{I}_{\mathrm{DS}}$.

2.3.3 Inter-individual variability of QRS-slopes variations

The inter-individual variability of the QRS-slope variations as a representation of how the SDs of $\mathcal{I}_{\mathrm{US}}$ and $\mathcal{I}_{\mathrm{DS}}$ at resting state vary within the whole population is presented in Fig. 2.12.

The statistical test described in section 2.2.7 confirms that, in all leads, the differences between intra-individual variations $s_k^{\mathcal{I},\leftrightarrow}(j)$ and the SD $s_k^{\mathcal{I},\updownarrow}$ of the whole dataset are highly significant ($p < 0.05$), being $s_k^{\mathcal{I},\updownarrow} > \bar{s}_k^{\mathcal{I},\leftrightarrow}$ in all cases, with $\bar{s}_k^{\mathcal{I},\leftrightarrow} = \dfrac{1}{J}\displaystyle\sum_{j=1}^{J} s_k^{\mathcal{I},\leftrightarrow}(j)$.

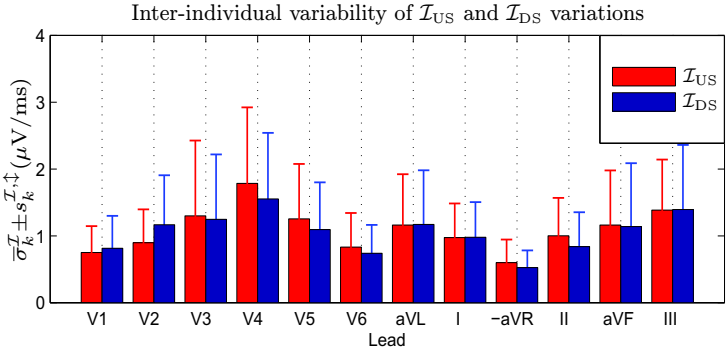

Figure 2.12: Mean ± SD over patients of the variations $\sigma_k^{\mathcal{I}}$ for $\mathcal{I}_{\mathrm{US}}$ and $\mathcal{I}_{\mathrm{DS}}$.

2.3.4 Dynamic changes of the QRS slopes during ischemia in standard leads

2.3.4.1 Global analysis

Relative changes of the QRS slopes measured during PCI, and averaged over patients, were computed for the standard 12-lead ECG. First, the performances of the three QRS slopes ($\mathcal{I}_{\text{US}}$, $\mathcal{I}_{\text{DS}}$ and $\mathcal{I}_{\text{TS}}$) were analyzed for the precordial leads V1-V3. In these leads, we found that the two last slopes within the QRS complex (i.e. $\mathcal{I}_{\text{DS}}$ and $\mathcal{I}_{\text{TS}}$) present a similar behavior along time, but not so for $\mathcal{I}_{\text{US}}$. Figure 2.13 shows the relative factor of change ($\mathcal{R}_{\mathcal{I}}$) for the three slopes during 5 min of coronary occlusion in leads V2 and V3. It is clear that there is a strong relationship between the slopes. In all the other leads, where the $\mathcal{I}_{\text{TS}}$ index was not evaluated, the $\mathcal{I}_{\text{DS}}$ slope presented higher sensitivity to the ischemia-induced changes, with maximum values reached in leads V3 and V5. In lead V3, the maximum averaged factors of change of $\mathcal{I}_{\text{DS}}$ and $\mathcal{I}_{\text{US}}$, quantified by the parameter $\mathcal{R}_{\mathcal{I}}$, were found to be 9.31 and 5.11, respectively. In lead V5, the maximum factors of change were 8.06 and 6.01.

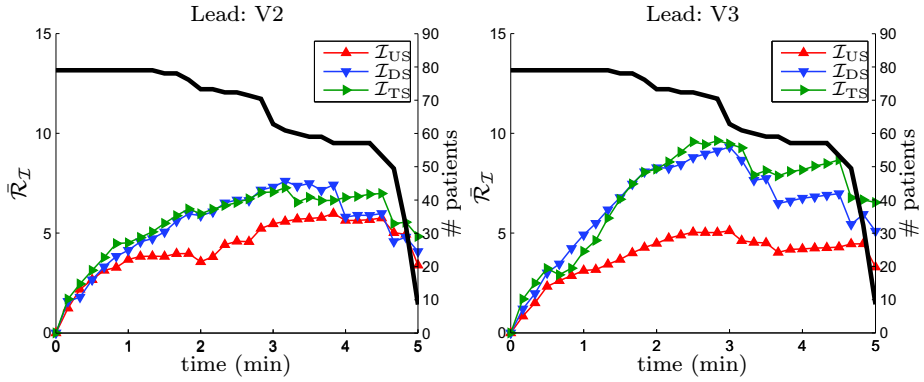

Figure 2.13: Relative changes $\mathcal{R}_{\mathcal{I}}$ of the three QRS slopes ($\mathcal{I}_{\text{US}}$, $\mathcal{I}_{\text{DS}}$ and $\mathcal{I}_{\text{TS}}$) in leads V2 and V3. The black lines represent the number of patients that remain under occlusion at each time instant.

This means that QRS slopes are very sensitive to the ischemia-induced changes, and their values during PCI change by at least a factor of 5 (in leads V3 and V5) with respect to their normal variations during control.

The amount of relative change, $\mathcal{R}_{\mathcal{I}}$, averaged for all patients and leads was found to increase by 27.3% when the ECG normalization described in section 2.2.6 was applied prior to measuring $\mathcal{I}_{\text{US}}$ and $\mathcal{I}_{\text{DS}}$.

2.3.4.2 Analysis restricted to the occlusion site

The results described in section 2.3.4.1 were obtained from the total population without separating into groups according to the occlusion site. In order to see whether changes in the slopes vary as a function of the occlusion site, the same analysis described in 2.3.4.1 was performed, but clustering patients in three different groups according to the occluded artery. Fig. 2.14 presents the three leads with the largest sensitivity to the ischemia-induced changes for each group, both in absolute and relative terms. For the LAD group the greatest changes were found in the anterior leads V2-V4, being V3 the most sensitive one with maximum values of $\bar{\Delta}_{\mathcal{I}_{\mathrm{DS}}} = 47.11$ μV/ms and $\bar{\mathcal{R}}_{\mathcal{I}_{\mathrm{DS}}} = 28.7$ times their normal variation in the control recordings. For the LCX group leads V4-V6 presented the largest changes, with $\bar{\Delta}_{\mathcal{I}_{\mathrm{DS}}} = 10.41$ μV/ms and $\bar{\mathcal{R}}_{\mathcal{I}_{\mathrm{DS}}} = 8.05$ in lead V5. Finally, in the RCA group the largest changes were found in leads II, aVF and III. Although lead III showed the largest absolute change, $\bar{\Delta}_{\mathcal{I}_{\mathrm{DS}}} = 7.02$ μV/ms, the greatest relative change, $\bar{\mathcal{R}}_{\mathcal{I}_{\mathrm{DS}}} = 8.61$, was seen in lead II.

2.3.5 Dynamic changes of QRS slopes during ischemia in loop-projected leads

2.3.5.1 Slopes evaluated from QRS loops

Figure 2.15 shows averaged QRS loops ($\mathrm{QRS}_{\mathrm{VCG}}$ and $\mathrm{QRS}_{\mathrm{PCA}}$) for the control recording of a particular patient as well as their evolution during PCI. For the control recording the loops corresponding to all beats contained within the last minute of the recording were averaged and shown in the left panel of top and middle rows (Fig. 2.15 (a) for $\mathrm{QRS}_{\mathrm{VCG}}$, and (b) for $\mathrm{QRS}_{\mathrm{PCA}}$). The evolution of the loops along the occlusion time using both approaches is presented in the remaining panels of Fig. 2.15 (a)-(b). Fig. 2.15 (c) shows the beats obtained by projecting $\mathrm{QRS}_{\mathrm{VCG}}$ and $\mathrm{QRS}_{\mathrm{PCA}}$ onto their dominant directions. It can be observed how the magnitude of the loop varies while increasing the degree of ischemia, and how it looks very similar to the control loop in the first 30 seconds of the PCI process.

In the same way that the shape of the loop varies, so does its dominant direction and, consequently, the morphology, duration and amplitude of the projected beats. In Fig. 2.15 (c) a reduction in the QRS amplitude and a prolongation of the QRS duration can be observed at the different stages of the PCI as compared to the control.

Sequences of the slope values ($\mathcal{I}_{\mathrm{US}}$ and $\mathcal{I}_{\mathrm{DS}}$) evaluated on the projected leads during PCI are shown in Fig. 2.16 for a representative patient of the STAFF III dataset. As can be observed, the magnitudes of the slope changes measured in leads projected from $\mathrm{QRS}_{\mathrm{PCA}}$ are greater in absolute values than those obtained from $\mathrm{QRS}_{\mathrm{VCG}}$, which can be confirmed by looking

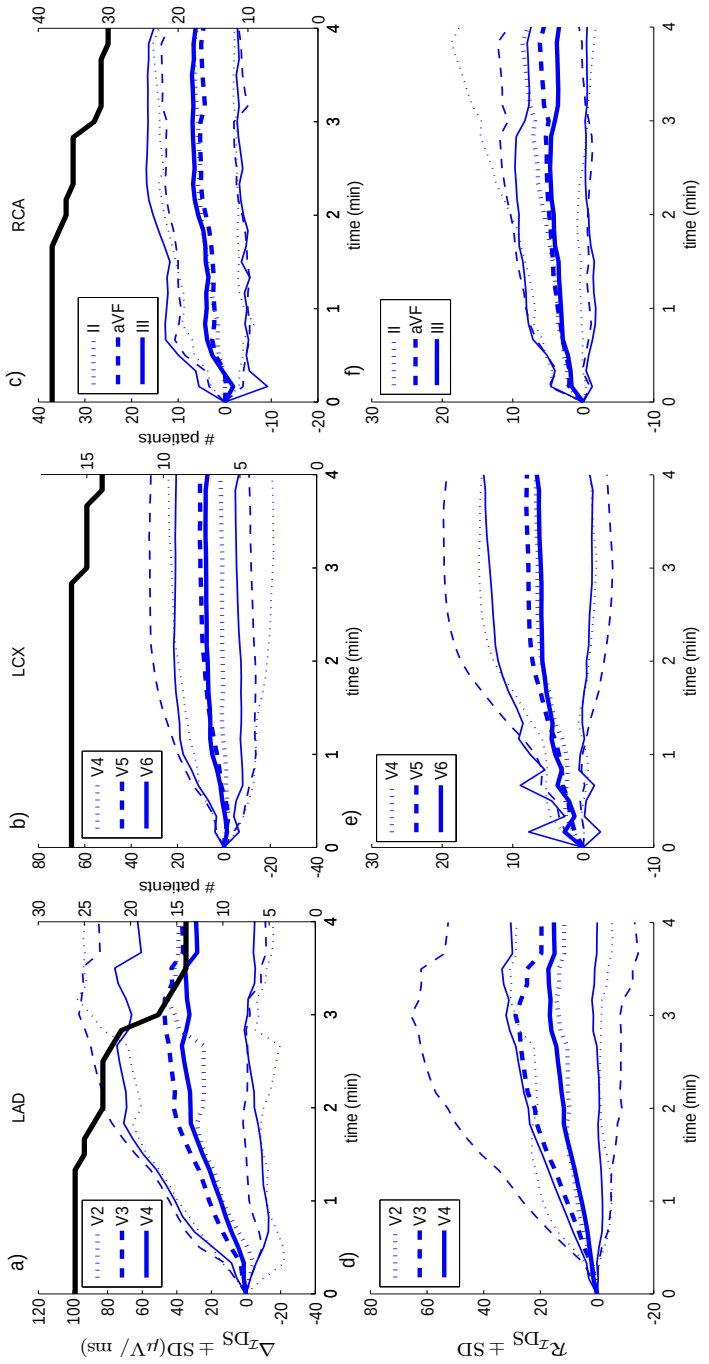

Figure 2.14: Leads with the highest ischemia-induced changes according to the occluded artery. (a), (b) and (c): Mean (thick lines) ± SD (thin lines) over patients of $\Delta_{\mathcal{I}_{DS}}$ in groups LAD, LCX and RCA, respectively; d), e) and f): Mean ± SD of $\mathcal{R}_{\mathcal{I}_{DS}}$ for the same leads and groups showed in (a), (b) and (c), respectively. Black lines represent the number of patients under occlusion.

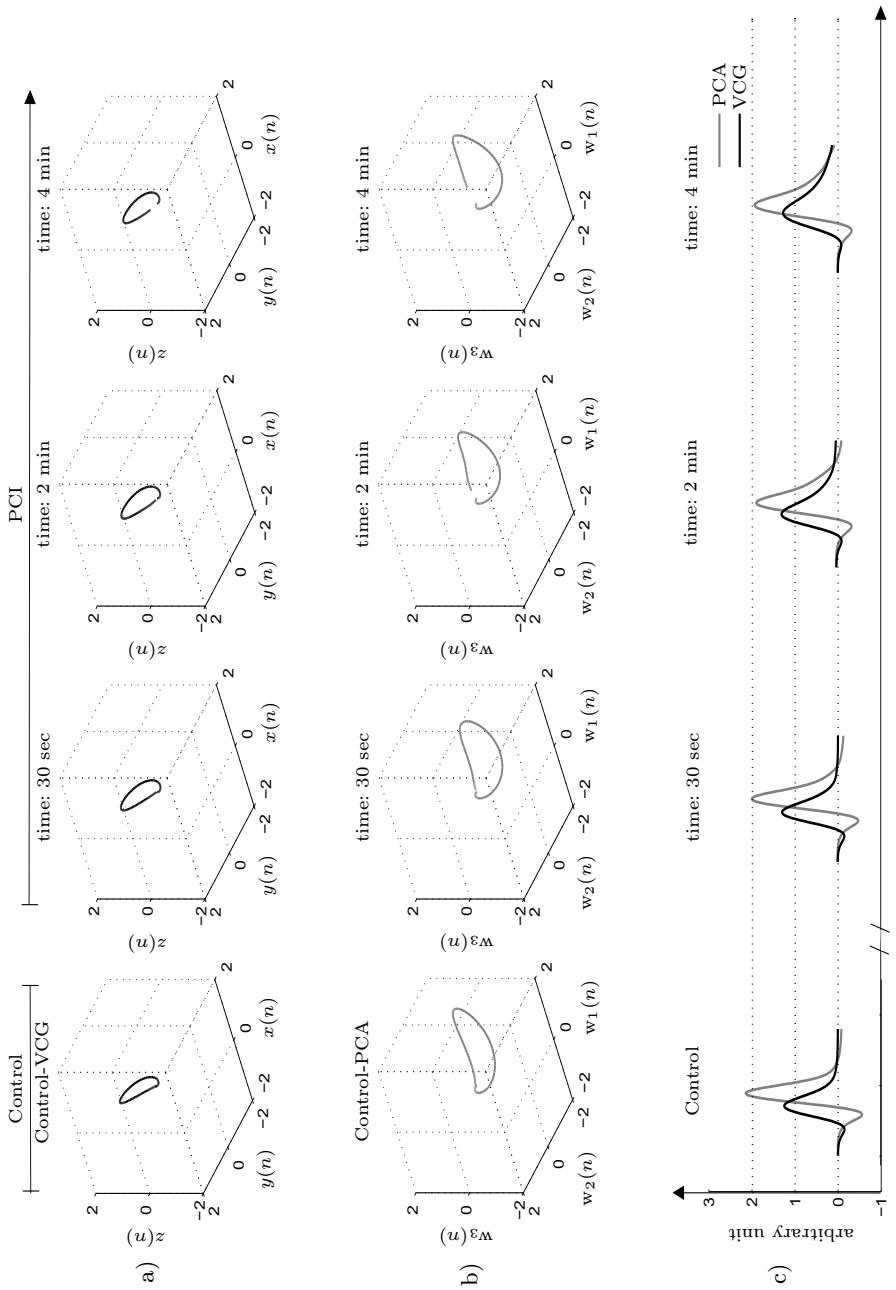

Figure 2.15: Averaged loops in control (average over the last minute) and at different times during the PCI procedure (in each case the average corresponds to the previous 30 seconds) using: a) the VCG technique, and b) the PCA technique; c) beats obtained by projection onto the dominant direction of each loop.

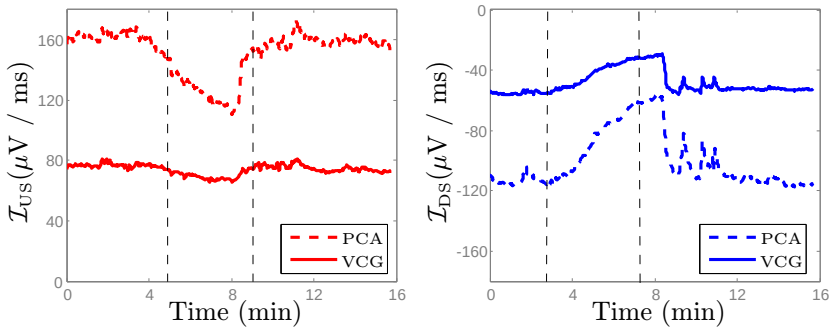

Figure 2.16: Sequences of $\mathcal{I}_{US}$ and $\mathcal{I}_{DS}$ during the PCI recording of a representative patient evaluated on the new leads obtained by projecting QRS loops (PCA and VCG). Dash lines mark the beginning and end of occlusion.

at the heartbeats shown in Fig. 2.15 (c). However, the variability ($\sigma^{\mathcal{I}}$) of the slopes during the control recording is smaller for VCG projected leads than for PCA ones (see numbers at the top of Fig. 2.16), thus compensating somehow the quantification of the relative change ($\mathcal{R}_{\mathcal{I}}$) during PCI.

2.3.5.2 Standard 12-lead ECG vs QRS loop methods

In order to corroborate whether the new approaches based on the QRS loop provide QRS slope measurements that perform better than those directly measured on the standard 12-lead ECG system, we compared the relative slope changes averaged over the whole population in lead V3 and the two leads obtained by projection of the QRS loops (QRS_{VCG} and QRS_{PCA}). As can be observed in Fig. 2.17 (a), the methods based on the QRS loop seem superior.

Regarding $\mathcal{I}_{US}$, the PCA-derived lead was more sensitive to the ischemia-induced relative changes ($\mathcal{R}_{\mathcal{I}}$) than the VCG-derived lead, with their maximum values being 10.5 (103% higher than in V3) and 7.87 (54% higher than in V3), respectively. In the case of $\mathcal{I}_{DS}$ the two loop methods showed very similar behavior, with maximum relative factors of 12.4 and 13.7 for PCA- and VCG-derived leads, which were 36% and 47% higher, respectively, compared to lead V3. Despite the fact that the maximum absolute change for $\mathcal{I}_{DS}$ in the VCG-derived lead was slightly inferior to that of the PCA-derived lead, its variation in the control was substantially smaller, thus explaining the slightly superior relative factor of change found for $\mathcal{I}_{DS}$ in the VCG-derived lead.

2.3.6 Comparison with ST level

Relative changes of the ST level ($\mathcal{R}_{\mathcal{I}_{ST}}$) were superior to those of the QRS slopes in most of the standard leads, even when the comparison was per-

formed for the different subgroups, where in lead V3 for LAD subgroup and lead II for the RCA one, the relative change of $\mathcal{I}_{ST}$ were around three times greater with respect to the $\mathcal{I}_{DS}$ change. Correlation between $\mathcal{I}_{ST}$ and $\mathcal{I}_{DS}$ changes in leads V3 and II were, 0.36 and 0.38, respectively, corroborating that both measures represent different underling physiological phenomena. However, in those leads with lower projection of the ST-T complex, like V6, I and -aVR, a clear superiority of $\mathcal{I}_{DS}$ with respect to the ST level was observed , which was accentuated for $\mathcal{I}_{DS}$ measured in loop-derived leads (see Fig. 2.17 (a)-(b)).

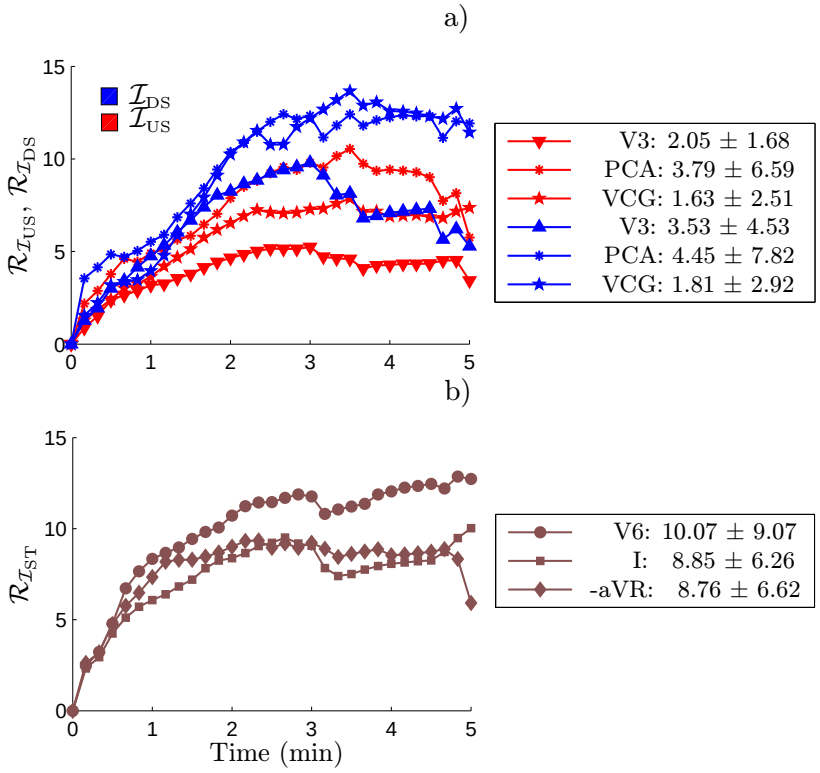

Figure 2.17: Evolution of the relative factor of change $\mathcal{R}_{\mathcal{I}}$ during PCI for: a) $\mathcal{I}_{US}$ and $\mathcal{I}_{DS}$; b) $\mathcal{I}_{ST}$. Mean ± SD of $\sigma^{\mathcal{I}}$ over patients in the control recordings are displayed on the right of each graph.

2.3.7 Timing of significant QRS slope change during PCI

Figure 2.18 shows examples of the time course during PCI of the p-values computed for the statistical test described in section 2.2.8. A p-value $<$ 0.05 implies that significant changes in the QRS slopes occur due to the induced ischemia. In leads V4 and V5 significant changes in $\mathcal{I}_{US}$ and $\mathcal{I}_{DS}$ were found to occur between 1 and 2 min after initiation of the coronary

occlusion. In lead V3 significant changes were already seen at around 30 sec. In leads V3 and V4 significant changes occurred in $\mathcal{I}_{\text{DS}}$ earlier than in $\mathcal{I}_{\text{US}}$. This performance was representative of most of the other leads. Notice that, as time progresses, there is a decline in the number of patients that remain under occlusion and, consequently, the p-values shown in Fig. 2.18 are computed for a different number of patients at each time instant.

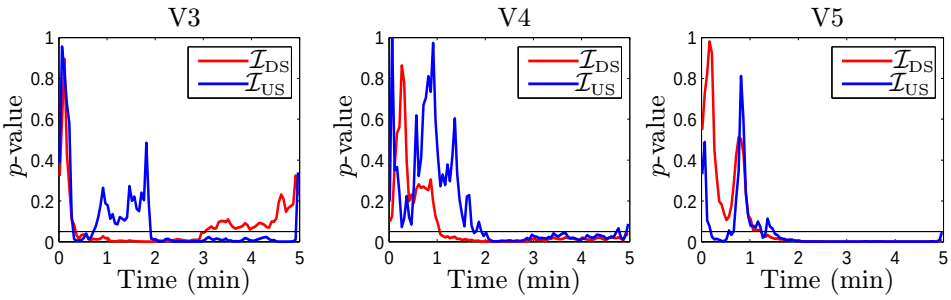

Figure 2.18: Significance of changes in $\mathcal{I}_{\text{US}}$ and $\mathcal{I}_{\text{DS}}$ along time during PCI as evaluated by the p-value of the statistical test described in section 2.2.8. The threshold for significance, $p = 0.05$, is shown in black solid line.

2.4 Discussion

In this study we measured the slopes of the QRS complex ($\mathcal{I}_{\text{US}}$, $\mathcal{I}_{\text{DS}}$ and $\mathcal{I}_{\text{TS}}$) and assessed their performances for evaluation of myocardial ischemia induced by coronary occlusion during prolonged PCI. QRS slopes were first introduced in [49] and [24] as a method for characterizing ECG alterations due to myocardial ischemia on the standard 12-lead ECG system. We propose an improvement for the quantification of QRS slope changes with the purpose of providing more sensitive and reliable estimates of the occurrence of significant changes in the depolarization phase during ischemia. Our proposal is to dynamically normalize the QRS signal amplitude so as to avoid low and very low-frequency oscillations that directly influence the variability of the estimated slopes. Results obtained after applying normalization provide measurements of relative QRS slope changes, $\mathcal{R}_{\mathcal{I}}$, during PCI that are 27.3% larger than those measured without normalization in the standard 12-lead ECG. The reason for that improvement is that the SD of the QRS slopes in normalized control recordings is substantially reduced, while absolute changes during PCI are of the same magnitude, thus leading to an increase in the relative ratio $\mathcal{R}_{\mathcal{I}}$ and, thus, in the sensitivity. In the present study the QRS slopes were also evaluated in leads derived from the QRS loops. The results obtained using the methods based on the QRS loop far exceeded those obtained in the standard 12-lead ECG system, reaching up to a 103% improvement for $\mathcal{I}_{\text{US}}$ and a 46% for $\mathcal{I}_{\text{DS}}$ measured in $\mathcal{R}_{\mathcal{I}}$ with respect

to lead V3. The superiority of the QRS slopes evaluation using loop-derived leads as compared to standard leads holds also true when the analysis is separately performed in each of the three patients subgroups. That superiority is justified by the fact that the slopes measured from the QRS loop show higher absolute values, since the loop-derived leads result from the projection onto a dominant vector with maximized amplitude, either generated from the VCG loop or the PCA loop. In addition, by definition of the loop-derived leads, the timing of the $\mathcal{I}_{\text{US}}$ and $\mathcal{I}_{\text{DS}}$ will always be in the first and the second half, respectively, of the QRS complex, so this potential drawback when dealing with single (and interchanged) leads will not appear when dealing with loop derived ones.

Regarding the dynamic analysis for the different groups according to the occluded artery, the LAD group showed the most pronounced changes, reaching a relative factor of change three times higher than that of the other two groups, particularly when analyzing lead V3 (see Fig. 2.14), a finding suggestive of a correlation to the amount of ischemia. In any case, the index $\mathcal{I}_{\text{DS}}$ proved to be the most sensitive of the slope indices, as evaluated either using absolute or relative change. It also presents the advantage of being possible to be evaluated for any possible QRS morphology regardless of the analyzed lead or occlusion site. Analysis of changes in the S wave slope $\mathcal{I}_{\text{TS}}$ for leads V1-V3 in LAD occlusions showed a similar pattern and amount of change compared to $\mathcal{I}_{\text{DS}}$.

Analysis of the intra-individual slope variability in different control recordings showed that the QRS slopes present high stability for each patient, thus providing a reliable reference for the evaluation of ischemia-induced changes in the QRS complex. On the other hand, the inter-individual variability was significantly larger, thereby supporting the proposal of having a patient dependent normalization of the $\mathcal{R}_{\mathcal{I}}$ index, $\mathcal{R}_{\mathcal{I}} = \Delta_{\mathcal{I}}/\sigma^{\mathcal{I}}$, provided that the reference $\sigma^{\mathcal{I}}$ used in the proposed method is taken from the same patient so as to be able to assess ischemia variations. The same observations were corroborated from the loop derived leads.

Significant changes in QRS slopes during PCI-induced ischemia were found to occur around 30 s after initiation of the artery occlusion in some of the analyzed leads and up to 2 min in other leads. The $\mathcal{I}_{\text{DS}}$ index showed earlier reaction than $\mathcal{I}_{\text{US}}$ to the induced changes in most leads. In both cases a kind of rebound or backwards behavior (see Fig. 2.18) was observed between 30 s and 2 min after the start of the occlusion that can be justified by a remarkable R wave amplitude increase during that period that compensates the QRS widening [57].

Analysis of the time evolution of $\mathcal{I}_{\text{DS}}$ showed an oscillatory behavior after balloon release (Fig. 2.16). This behavior was observed in several recordings resulting from oscillatory QRS amplitudes, which are very similar to those one reported for the ST-T segment where, in most cases, have been

associated with unfavorable outcome [58–60]. In Fig. 5 of the study by Laguna *et al.* [58] similar oscillations can be observed when analyzing the shape of ECG waveforms on the same database used in this study.

The applicability of the slope indices for ischemia detection is limited by the fact that the QRS slopes present high inter-individual variability, which implies the need of a reference baseline measurement to be used for computation of relative ischemia-induced slope changes. On the other hand, the fact that intra-individual variability of QRS slopes is minor suggests that the slope indices could potentially be used for monitoring ischemia over time in scenarios like chest pain units, intensive care units and as monitoring in a pre-hospital setting. This applicability, however, needs to be tested in future studies, since issues like the sensitivity of the slope indices to body postural changes deserve further analysis. The use of slope indices evaluated in leads derived from spatial QRS loops could not only lead to higher sensitivity to the ischemia-induced changes, as reported in this study, but also to a minor dependence on other factors such as body postural changes. Another limitation to this study is the fact that PCI-induced, short-time ischemia of 5 minutes might not produce severe enough ischemia to give rise to more pronounced changes of the QRS slopes. The clinical information within the QRS complex additive to that of the ST-T changes could be used for risk stratification of STEMI patients with more severe ischemia and also evolving infarction, which could guide treatment and give prognostic information. Future studies are planned to further evaluate this.

Chapter 3

Spatial analysis of depolarization ECG changes

3.1 Introduction

In addition to ischemia detection, localization of the ischemic area and estimation of its severity are clinically relevant and may provide very valuable information for risk stratifying patients and for tailoring their treatment. Beyond conventional ST-T analysis important ischemia-induced changes occur in both the depolarization and repolarization phase, which might add further information for risk stratification. Several studies in the literature have quantified ischemia induced changes in the ECG during PCI, and have investigated the relationship between those ECG changes and the occlusion site. In García et al.[61], global ECG indices derived from the Karhunen-Lòeve transform were compared with local ECG indices, and combinations of both types of indices were used for identification of the occluded artery. In[54], analysis of T wave alternans (TWA) was used to provide spatial distributions of ischemia induced ECG changes as a function of the occlusion site.

Prolongation of the QRS complex has been described as a marker of more severe ischemia with slow conduction, both in animal studies and in humans during PCI and acute MI[44,62–64]. Also, in a large cohort of STEMI patients, Wong et al reported an independent, positive relationship between QRS duration on admission ECG and 30-day mortality for anterior infarct location[65,66]. Prolongation of QRS duration is, however, difficult to determine correctly, because ST elevation commonly obscures the delineation between the end of the depolarization and the beginning of the repolarization. In the Sclarovsky-Birnbaum ischemia grading system, distortion of the terminal part of the depolarization, in addition to pronounced ST elevation (grade 3 ischemia), has, in several studies, been found to be a sign of more severe myocardial ischemia and to predict larger infarct size, lesser

degree of ST segment resolution, impaired microvascular patency, and worse clinical outcome after revascularization by either thrombolysis or primary PCI[46,67–69]. Those changes have been reported to be stronger predictors of clinical outcome than ST measures alone. The ischemia grading system or any other method of assessing depolarization changes has not, however, been implemented in clinical practice. To facilitate clinical implementation, a more robust and clinically feasible method of QRS complex analysis is needed, as well as better understanding of the pathophysiological bases of the depolarization changes.

During coronary artery occlusion by PCI, the QRS slopes introduced in the previous chapter became considerably less steep than in the control situation, particularly the downward slope ($\mathcal{I}_{\mathrm{DS}}$) of the R wave, as a combined result of both changes in the QRS amplitude and duration. In this thesis, the method for computation of QRS slopes was developed further from its original definition,[24] making it more robust, as associated with very low intraindividual variation in a control situation. Additionally, calculation of the most terminal slope for leads with an S wave ($\mathcal{I}_{\mathrm{TS}}$). Changes in the QRS slopes were temporally characterized in the previous chapter, however, they were not spatially characterized in terms of the occlusion site, nor correlated to the actual amount of ischemia or compared with other conventional ECG indices of ischemia.

In the present chapter the same ECG recordings (a control recording just prior the PCI, and the PCI recording) from the STAFF III database were analyzed, with the purpose of assessing the lead-by-lead spatial profiles of the ischemic changes in the ECG, with emphasis on depolarization. The following ECG-derived indices were analyzed: ST elevation, QRS duration, R and S wave amplitude and QRS slopes, evaluated in groups of patients clustered according to the occluded artery (LAD, LCX and RCA).

In a small subset of patients of the total study population, MPS images were available[70,71], as a reliable method for detecting and quantifying myocardial ischemia induced by elective PCI. For this particular subset of recordings, the specific aims were to:

- Test if the amount of QRS slope changes correlates to the extent and severity of ischemia as determined by MPS and to compare the correlation to that of conventional depolarization parameters (R wave amplitude change and QRS prolongation).
- Evaluate the extent to which QRS slope changes add information to conventional ST elevation analysis in the correlation to the extent and severity of ischemia.
- Assess whether the slope changes hold spatial information regarding coronary occlusion site.

3.2 Materials and Methods

3.2.1 Study population

In addition to the 79 patients analyzed in the previous chapter, which were also involved in the study described in this chapter, the subset of 38 patients with available MPS data were considered to carry out further spatial analysis. The average age for this subset of patients was 63 ± 12 [range 33-80] years, from which 25 (66%) were men. The distribution and mean duration of coronary artery occlusion was as follows: LAD, 8 patients (mean occlusion duration: 4 min 45 sec); LCX, 9 patients (mean occlusion duration: 4 min 47 sec); and RCA, 21 patients (mean occlusion duration: 4 min 52 sec). For these 38 patients, MPS was performed during the PCI and the following day, as a control, to provide a means for quantifying the ischemia.

3.2.2 Radionuclide images

3.2.2.1 Acquisition

Approximately 30 mCi (1100 MBq) of sestamibi was injected intravenously in each patient after confirmation of total coronary artery occlusion by the balloon. The scintigraphic imaging carried out by a single-head rotating gamma camera (Elscint, Haifa, Israel) was obtained within 3 hours after completion of the PCI procedure. The acquisitions were made with a high-resolution collimator in a 64 × 64 matrix, 6.9-mm pixel size, using 30 projections (25 seconds/ projection) at 180° (from 45° right anterior oblique to 45° left posterior oblique). Using filtered back projection with a Butterworth filter, transverse sections were reconstructed, without attenuation correction. Short-axis sections were reconstructed for further analysis[72].

For the control study, another injection of approximately 30 mCi (1110 MBq) technetium-99m-sestamibi was administered, and imaging was performed 2 to 3 hours later with the same gamma camera and acquisition protocol as for the PCI study. All patients were clinically stable between the 2 examinations. Examples of this technique are shown in Fig. 3.1.

3.2.2.2 Images evaluation for ischemia quantification

The Cedars-Sinai and Emory quantitative analysis programs (CEqual; ADAC Laboratories, Milpitas, CA)[73,74] were used for making volume-weighted bull's eye plots from the short-axis slices. Any loss of perfusion during the PCI study compared with the control study was determined by an automatic procedure by comparing the bull's eye plots of the 2 studies for each patient[72] and was expressed as both "extent" and "severity" of the myocardial ischemia, as described earlier.[75] Reduction of perfusion by 25% or more was used as the threshold for indicating significantly hypoperfused

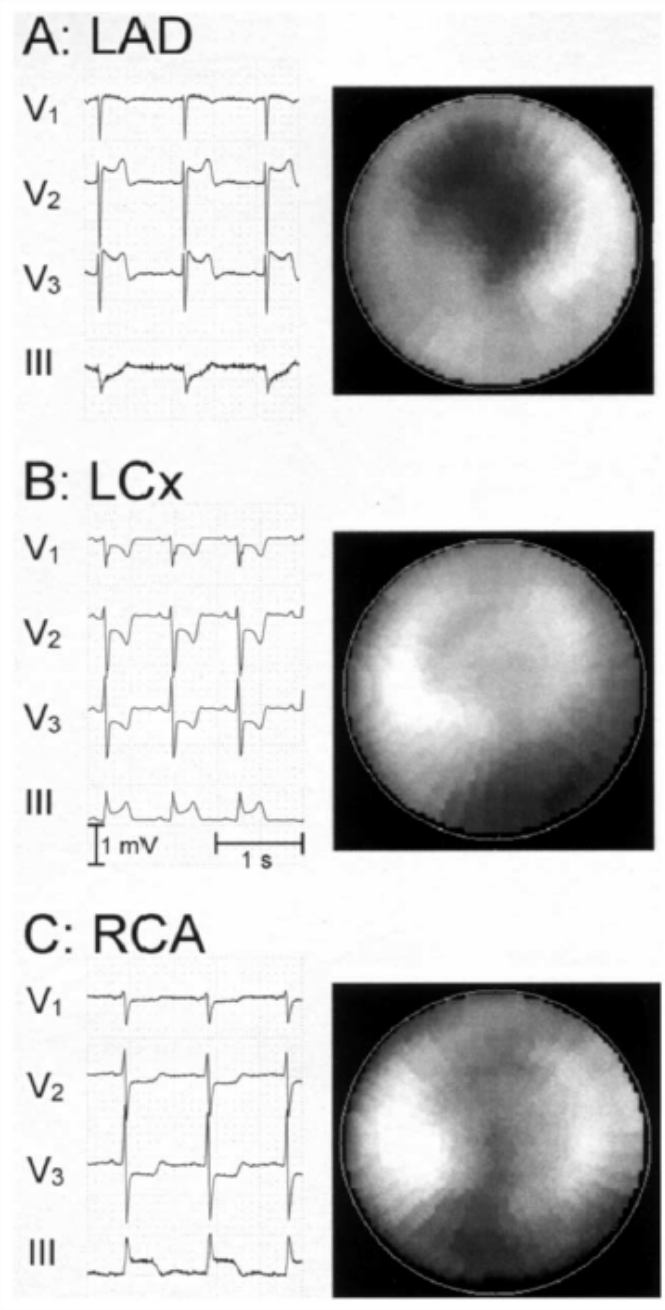

Figure 3.1: Examples of scintigraphic images taken for different patients of the STAFF III dataset, occluded at different vessels. Representative ECG patterns during occlusion are also shown (reproduced from Persson et al.[72])

myocardium[72]. This area in the bull's eye plot was delineated as an "extent map", representing all added slices (or volume) of the left ventricular myocardium, expressed as a percentage of the left ventricle and defining the extent of ischemia. The total pixel count difference (or local perfusion loss) between the control and occlusion study within this delineated hypoperfused area in the "extent map" was the severity, expressed as a percentage of the total pixel count in the control situation within the same area.[72] The extent and severity of the ischemia were calculated for each patient. All the scintigraphic data analyses were performed at the Department of Clinical Physiology, Lund University, Sweden, blinded to the ECG data.

3.2.3 Depolarization analysis

3.2.3.1 QRS slopes indices

Using the same methodology described in chapter 2, the two main slopes of the R wave of the QRS complex, $\mathcal{I}_{\mathrm{US}}$ and $\mathcal{I}_{\mathrm{DS}}$, and the upward slope of the S wave, $\mathcal{I}_{\mathrm{TS}}$, were evaluated here from the standard 12-lead ECG. The absolute delta change of QRS slopes at the end of the PCI was calculated ($\Delta\mathcal{I}_{\mathrm{US}}^{\mathrm{PCI}}$, $\Delta\mathcal{I}_{\mathrm{DS}}^{\mathrm{PCI}}$, $\Delta\mathcal{I}_{\mathrm{TS}}^{\mathrm{PCI}}$). In contrast to section 2.2.5, the delta values were just calculated at the end of the occlusion ($t = t_{\mathrm{PCI}}$) rather than during the entire PCI process, and it was denoted as:

$$\Delta\mathcal{Y}_{\mathrm{PCI}} = \ell \cdot t_{\mathrm{PCI}} \tag{3.1}$$

where ℓ is the slope obtained from fitting in a least square sense the values of index $\mathcal{Y}$ ($\mathcal{Y} = \mathcal{I}_{\mathrm{US}}$, $\mathcal{I}_{\mathrm{DS}}$, $\mathcal{I}_{\mathrm{TS}}$), from the beginning ($t$=0) to the end of the occlusion. A graphic representation of this strategy is shown in Fig. 3.2. Among the 12 standard leads, the maximal positive change ($\Delta\mathcal{Y}_{max}^{pos}$) of the $\mathcal{I}_{\mathrm{DS}}$ deflection (positive change: $\mathcal{I}_{\mathrm{DS}}$ slope getting less steep) and maximal negative change ($\Delta\mathcal{Y}_{max}^{neg}$) of the $\mathcal{I}_{\mathrm{US}}$ deflection (negative change: $\mathcal{I}_{\mathrm{US}}$ slope getting less steep) was determined for each patient. The sum of all positive delta changes of the $\mathcal{I}_{\mathrm{DS}}$ deflection ($\Delta\mathcal{Y}_{sum}^{pos}$) and negative changes of the $\mathcal{I}_{\mathrm{US}}$ deflection ($\Delta\mathcal{Y}_{sum}^{neg}$) were calculated as to quantify the changes.

3.2.3.2 R- and S-wave amplitude:

R- and S-wave amplitudes were automatically measured using the PR segment as the isoelectric level. Delta changes of the R- and S-wave amplitudes (ΔR_{PCI} and ΔS_{PCI}) were determined in the same way as that used for the QRS slopes (described in previous section) in each lead at the end of the PCI recording.

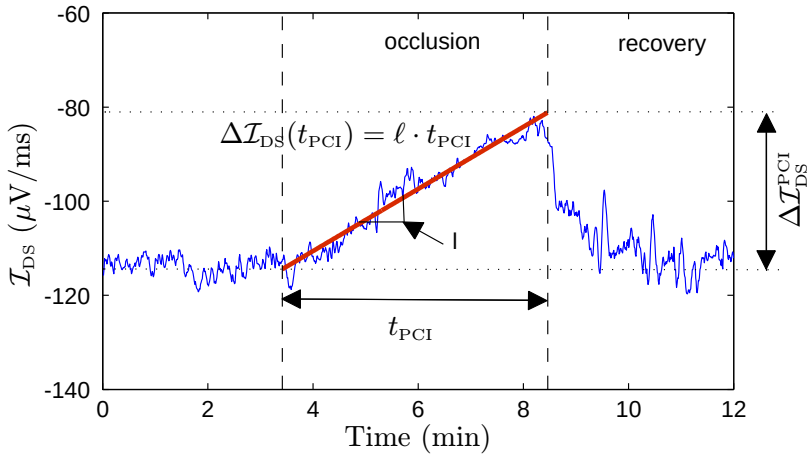

Figure 3.2: Representation of the strategy by which a line is fitted (red line) to the averaged $\mathcal{I}_{\rm DS}$ values during the PCI procedure in a least square sense to reduce the effect of possible outlier measurements on the $\mathcal{I}_{\rm DS}$ change computation.

3.2.3.3 QRS complex duration

The QRS duration was determined by taking a global measurement from the 12 standard leads. In each beat, the earliest QRS onset and the latest QRS offset among leads (see Fig. 3.3) were selected as the beginning and end, respectively, of the depolarization phase taken as the longest temporal projection for the electrical activity of the depolarization. In addition, a multilead detection rule was applied to reduce the risk of misestimation, for example, due to large simultaneous ST-segment deviation or noise [76]. In brief, with this multilead detection rule, the earliest mark of the QRS onset and the latest mark of the QRS offset, respectively, in any of the 12 leads were accepted only if they did not differ from the 3 closest corresponding marks in other leads by more than 6 and 10 milliseconds, respectively, for each beat. The automatically determined QRS onset and offset were also manually validated, with no disagreement about the delineations provided by the two methods. Finally, the absolute delta change of the QRS duration, $\Delta QRS_{\rm PCI}$, was determined using the same methodology applied for the above indices.

3.2.4 Repolarization analysis: ST-segment

ST-segment measurements were made automatically in each lead at the ST-J point, using the PR interval as the isoelectric level. Absolute ST-deviation $\Delta ST_{\rm PCI}$ at the end of the PCI recording relative to the ST level at rest was determined for each lead. In addition, the maximal ST elevation ΔST_{max}^{pos}

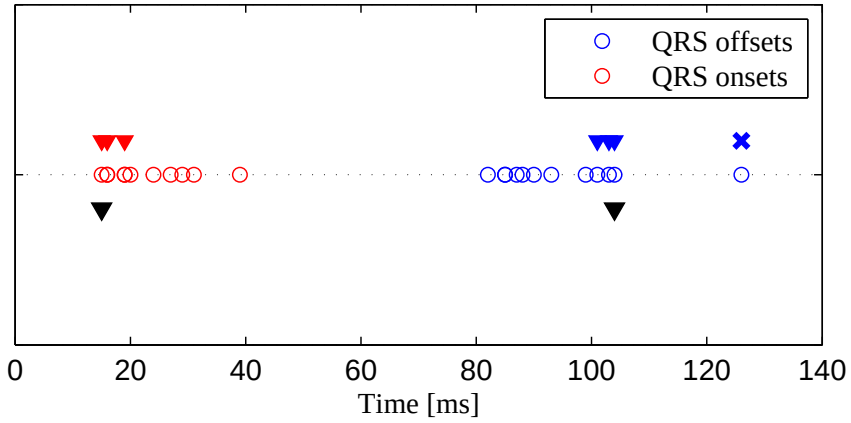

Figure 3.3: Example of the multilead detection rule used to determine the QRS duration. Empty circles represent the onset and offset marks for one arbitrary beat in the 12 standard leads. Red and blue solid triangles indicate the 3 closest marks determined under the rules and the x mark the rejected one. Black solid triangles represent the final marks accepted as onset and offset of the beat.

and the sum of ST elevation ΔST^{pos}_{sum} (positive values for ΔST_{PCI}) among all leads at the end of the PCI recording were determined for each patient.

3.2.5 Spatial analysis related to the occlusion site

All the indices described above were evaluated on the standard 12-lead ECG. However, to study the three-dimensional profile of the changes in the analyzed indices across different projections (sagittal, frontal and transverse), the inverse Dower matrix (see section 2.2.5) was applied in two different ways:

1. The inverse Dower matrix was applied to generate the three orthogonal leads X, Y and Z from the standard 12-lead ECG signals and the absolute ischemia-induced changes $\Delta\mathcal{Y}_{\text{PCI}}$ at the end of the occlusion were computed over those X, Y, and Z leads.

2. Ischemia-induced absolute changes $\Delta\mathcal{Y}_{\text{PCI}}$ were evaluated over each of the 12 standard leads ($l = 1, 2, ..., 12$), and the inverse Dower matrix was then applied on the resulting 12 delta values to generate three transformed orthogonal delta values $\Delta\tilde{\mathcal{Y}}_{\text{PCI}}$ representative of those changes.

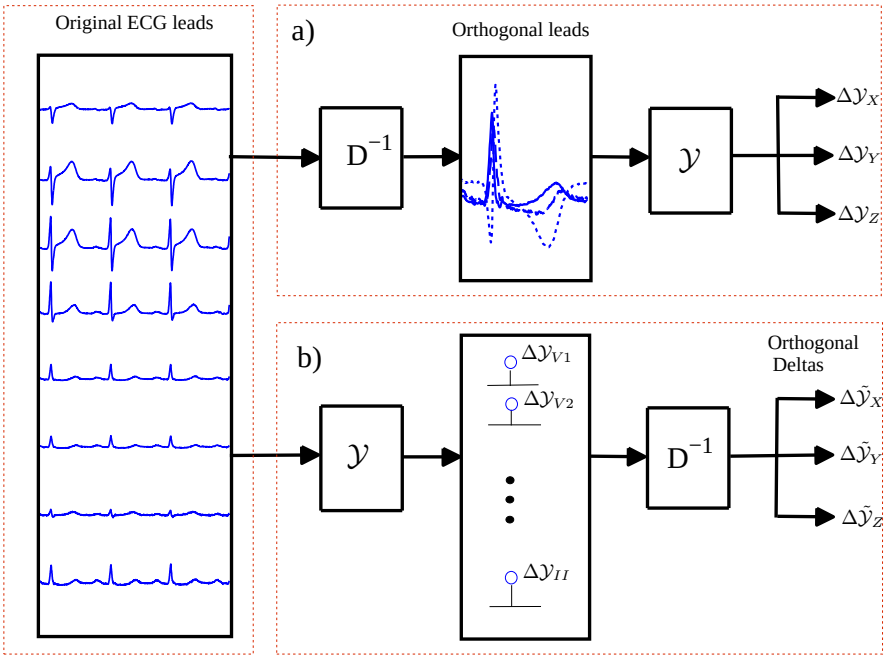

Figure 3.4: Diagram used for the two orthogonal transformations. a) Transformation where D^{-1} is applied over the original leads to generate the orthogonal leads X, Y and Z. b) Transformation where D^{-1} is applied after calculation of the absolute delta values.

Figure 3.4 illustrates the diagrams used for the two different 3D techniques previously defined.

In order to spatially characterize myocardial ischemia the mean $\Delta\overline{\mathcal{Y}}_{\mathrm{PCI}}(l)$ and the standard deviation $\sigma^{\Delta\mathcal{Y}}_{\mathrm{PCI}}(l)$ over patients of the absolute changes $\Delta\mathcal{Y}_{\mathrm{PCI}}$ ($\mathcal{Y} = \mathcal{I}_{\mathrm{US}}, \mathcal{I}_{\mathrm{DS}}, R, S, ST$) were computed. Computations were performed for the standard and orthogonal leads as well as for the transformed orthogonal deltas. For this analysis, patients of the whole study population were clustered into three groups according to the occluded artery (LAD, RCA and LCX).

3.2.6 Statistical methods and prediction of the amount of ischemia

Results obtained for the subset of 38 patients with available MPS data are also presented as mean ± SD, as made for the whole study population. Because of the small number of patients in this subset, nonparametric tests were used. Spearman rank correlation coefficient (r) was used for correlation

analysis with the extent and severity of the ischemia. Mann-Whitney U test was used for comparison between groups. Multiple linear regression analysis was also used to evaluate additional value of different QRS changes to ST changes in predicting the amount of ischemia. All these variables were considered continuous. All statistical tests were 2-sided, and significance was defined as $p < 0.05$. The statistical analysis was performed by SPSS, version 15.0, for Windows (SPSS, Chicago, IL).

3.3 Results

3.3.1 Spatial distribution of ischemic changes

3.3.1.1 Measurements in the whole study population

Spatial characterization of ischemia-induced changes across leads for the whole population (n=79) is presented in Figure 3.5. Each of the rows in that figure shows $\overline{\Delta\mathcal{Y}}_{\mathrm{PCI}}(l)\ \pm\sigma^{\Delta\mathcal{Y}}_{\mathrm{PCI}}(l)$ for each lead l, when computed for any of the indices ST, S and $\mathcal{I}_{\mathrm{DS}}$. Each of the columns corresponds to an occlusion group (LAD, LCX, and RCA). It can be observed that the three indices present similar spatial profiles and that those profiles are highly dependent on the occlusion site. In the LAD group the most prominent changes were seen in leads V2-V4. In the LCX and RCA groups the most pronounced changes were noticed in leads V4-V6 and II, aVF and III, respectively. If relative changes $\mathcal{R}_{\mathcal{Y}}$ are used for the spatial characterization, comparable lead-by-lead profiles are obtained. Table 3.1 shows averaged values of $\Delta\mathcal{Y}$ computed for each of the occlusion groups in those leads identified as most sensitive to ischemia-induced changes. The averaged relative changes over patients and leads were $\mathcal{R}_{ST} = 14.5$, $\mathcal{R}_{S} = 15.2$ and $\mathcal{R}_{\mathcal{I}_{\mathrm{DS}}} = 6.2$ times their normal variations in control. Two of the other analyzed indices, R and $\mathcal{I}_{\mathrm{US}}$, show similar profiles between them, but those are weakly distinctive in terms of the occlusion site.

Figure 3.6 shows the frontal, transverse, and sagittal projections of the 3D spatial $\mathcal{I}_{\mathrm{DS}}$ vector computed at the end of the occlusion for each artery group (LAD, RCA and LCX). In figure 3.6-(a), where the inverse Dower matrix is applied to the ECG signals, the RCA group shows smaller averaged vectors than those of the other groups, while the LAD group presents the largest averaged vectors. In Figure 3.6-(b), where the inverse Dower matrix is applied over the $\Delta\mathcal{I}_{\mathrm{DS}}$ values, the LCX and RCA groups are less overlapping than in Figure 3.6-(a) and the three occlusion groups can be separated in a better way.

3.3.1.2 Measurements in the subpopulation with MPS data

The extent and severity of the ischemia produced by PCI-induced coronary occlusion, as estimated by myocardial scintigraphy, are presented in Table

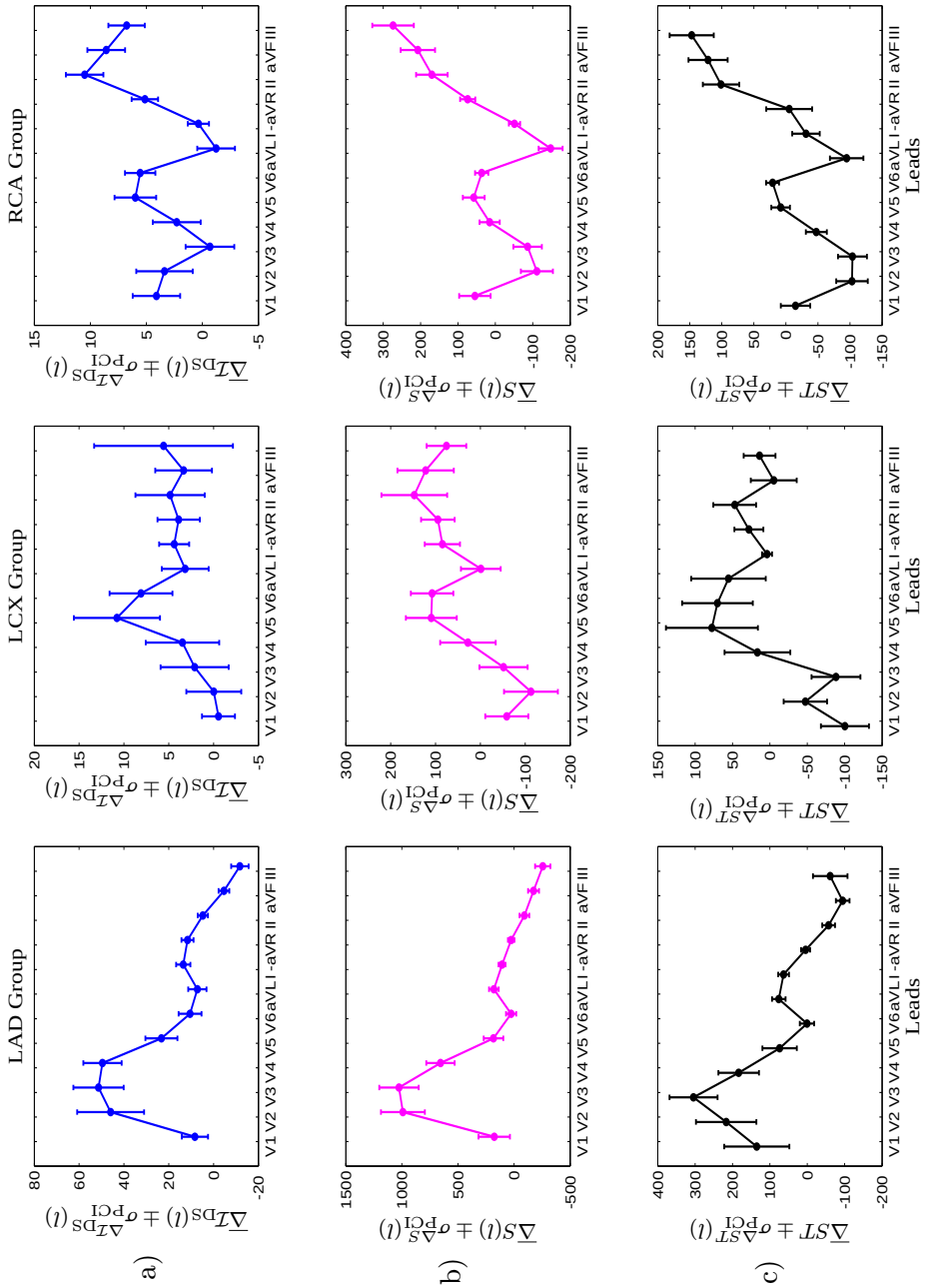

Figure 3.5: Spatial distribution (expressed as mean ± SD) across leads of (a) $\Delta\mathcal{I}_{\mathrm{DS}}$, (b) ΔS and ΔST in the LAD, LCX and RCA subgroups.

Table 3.1: Averaged $\Delta\mathcal{Y}$ and $\mathcal{R}_{\mathcal{Y}}$ values of ST, S, and $\mathcal{I}_{\text{DS}}$ in each of the occlusion groups and leads identified as most sensitive to ischemia-induced changes.

Changes	**LAD (V2-V4) mean ± SD**	**LCX(V4-V6) mean ± SD**	**RCA(II-aVF-III) mean ± SD**
$\Delta ST(\mu\text{V})$	234.8 ± 66.4	54.7 ± 50.9	123.2 ± 31.1
$\Delta S(\mu\text{V})$	890.8 ± 165.8	81.6 ± 55.3	216.9 ± 47.9
$\Delta\mathcal{I}_{\text{DS}}(\mu\text{V/ms})$	48.9 ± 11.5	7.5 ± 4.1	8.6 ± 1.7
$\mathcal{R}_{ST}$	29.8 ± 7.74	10.7 ± 4.55	24.4 ± 5.49
$\mathcal{R}_{S}$	39.2 ± 8.12	13.7 ± 4.05	21.4 ± 5.01
$\mathcal{R}_{\mathcal{I}_{\text{DS}}}$	16.1 ± 3.25	5.08 ± 1.28	6.13 ± 0.98

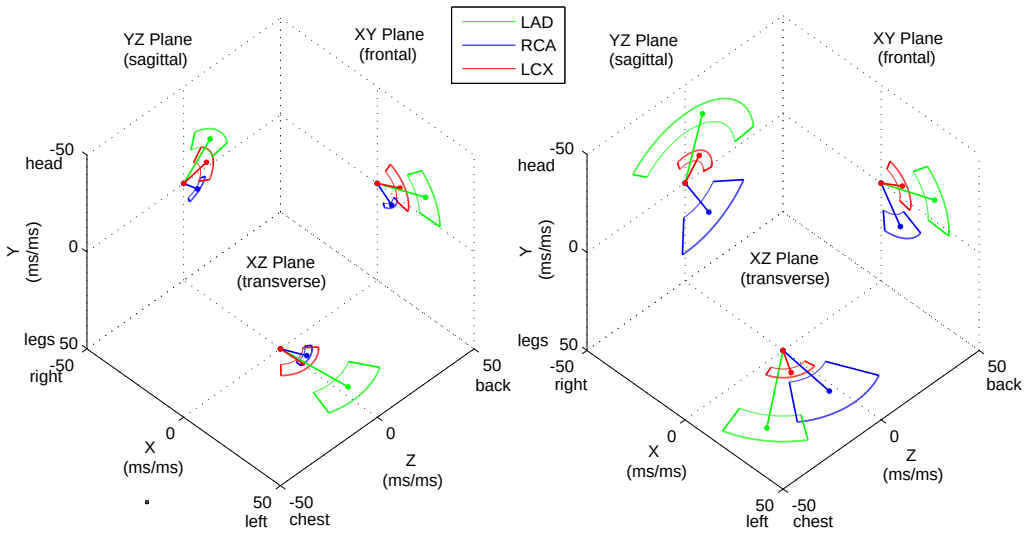

Figure 3.6: Averaged 3D vector $\Delta\mathcal{I}_{\text{DS}}$ for each of the three occlusion groups in the frontal, transverse, and sagittal projections: (a) D^{-1} applied over 12-lead ECG; (b) D^{-1} applied over delta values. The lines represent the group average vectors, with circular sectors covering once the standard deviation in magnitude and angle of the axis.

3.2, for the subset of patients with available MPS data (n=38) and subgroups of it according to the occluded artery. Among all patients, the extent varied between 0 and 65% of the left ventricle (mean ± SD, 20% ± 17%) and the severity between 26% and 63% (mean ± SD, 38% ± 8%).

Table 3.2: Myocardial ischemia during PCI expressed as extent and severity in the subset of patients with available MPS data and subgroups based on occluded coronary artery.

Coronary artery occluded	**Extent (% of LV) mean ± SD (range)**	**Severity(%) mean ± SD(range)**
Total (n = 38)	20 ± 17 (0-65)	38 ± 8 (26-63)
LAD (n = 8)	43 ± 15 (15-65)	47 ± 9 (33-63)
LCX (n = 9)	19 ± 14 (4-45)	35 ± 5 (29-43)
RCA (n = 21)	12 ± 10 (0.1-32)	35 ± 7 (26-51)

In Fig. 3.7, mean ± SD of QRS slope changes for LAD (anterior leads) and RCA occlusions (inferior leads) are shown, respectively. Changes in $\mathcal{I}_{\text{US}}$ and $\mathcal{I}_{\text{DS}}$ were statistically different in leads V2 to V4 and in II, aVF and III for the two ischemia locations, whereas differences between $\mathcal{I}_{\text{DS}}$ and $\mathcal{I}_{\text{TS}}$ changes in the LAD group were non significant (NS). The overall amount of slope change was greater in the LAD group than in the RCA group. In Fig. 3.8, changes in $\mathcal{I}_{\text{DS}}$ are shown for patients with LAD, LCX, and RCA occlusions, respectively. The spatial distribution of $\mathcal{I}_{\text{DS}}$ changes was most evident for anterior and inferior ischemia, with the most marked changes found in leads V2 to V5 and leads II, aVF, and III, respectively. In the LCX group, the most pronounced changes were noted in leads V5 and aVL. Because of the present finding of $\mathcal{I}_{\text{TS}}$ being less or equally affected by the ischemia as compared with $\mathcal{I}_{\text{DS}}$ (in line with the results shown in the previous chapter) and the variable presence of S waves in most leads except from V1 to V3, only $\mathcal{I}_{\text{US}}$ and $\mathcal{I}_{\text{DS}}$ were considered in the following correlation analysis.

3.3.2 Correlation between depolarization changes and ischemia

3.3.2.1 R-wave downslope ($\mathcal{I}_{\text{DS}}$) change

Changes in $\mathcal{I}_{\text{DS}}$ at the end of the PCI were found to be positive in 299 (66%) of the total analyzed leads by 14.8 ± 18.2 (0.1-124.9) μV/ms and negative in 157 (34%) leads by 8.6 ± 11.2 (0-58.8) μV/ms. The quantitative distribution among the patients of the maximum positive $\mathcal{I}_{\text{DS}}$ change in any lead, the sum of all positive $\mathcal{I}_{\text{DS}}$ change, and the sum of all $\mathcal{I}_{\text{DS}}$ change regardless of direction, respectively, are presented in Table 3.3-A. In addition, the correlation between the different quantifications of $\mathcal{I}_{\text{DS}}$ change and the extent and severity of ischemia is shown. For all $\mathcal{I}_{\text{DS}}$ measures, there were significant

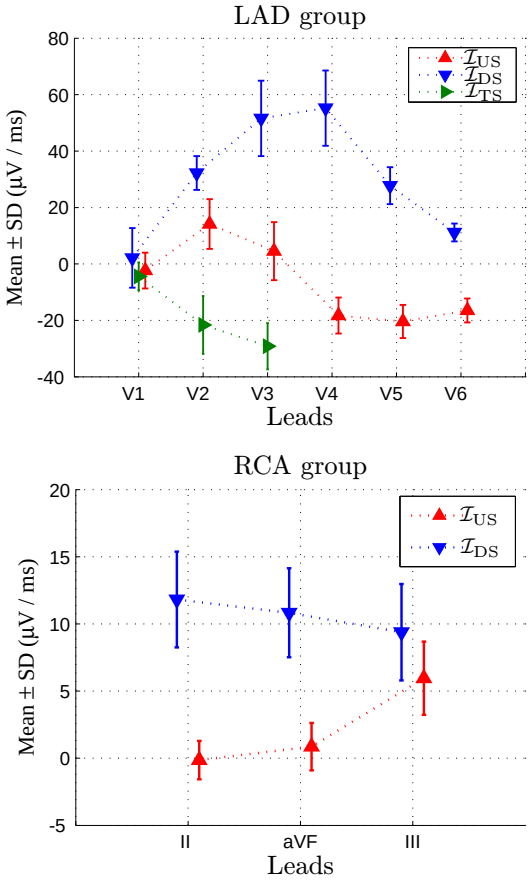

Figure 3.7: Mean ± SD of QRS slope changes for LAD (leads V1-V6) and RCA occlusions (leads II, aVF, and III). Changes in $\mathcal{I}_{TS}$ are shown only for leads V1 to V3 in the LAD group.

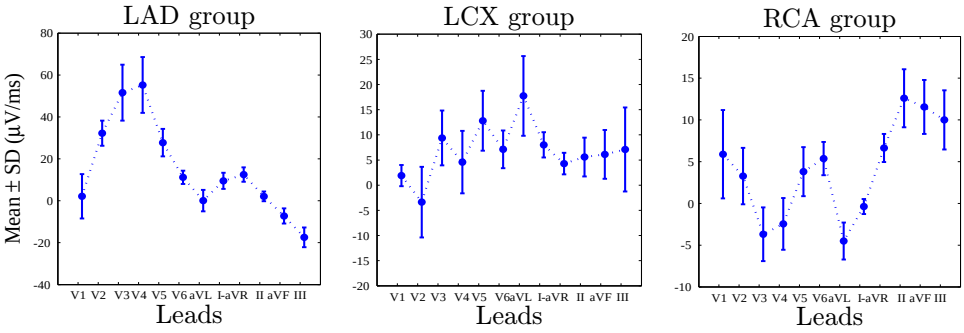

Figure 3.8: Spatial distribution of $\mathcal{I}_{DS}$ changes in the 12 standard leads for LAD, LCX and RCA subgroups, respectively.

correlations to the amount of ischemia, with the highest Spearman rank correlation coefficient found for the sum of positive $\mathcal{I}_{\mathrm{DS}}$ change among all 12 leads ($r = 0.71$, $p < 0.0001$ for extent, and $r = 0.73, p < 0.0001$ for severity).

3.3.2.2 R-wave upslope ($\mathcal{I}_{\mathrm{US}}$) change

At the end of the PCI, the $\mathcal{I}_{\mathrm{US}}$ showed a negative mean change by 7.6 $\pm$ 10.2 (0-94.2) μV/ms in 301 (66%) leads, whereas 155 (34%) leads presented a positive change by 7.8 $\pm$ 13.1 (0-94) μV/ms. In Table 3.3-B, the correlations between corresponding quantifications of $\mathcal{I}_{\mathrm{US}}$ change and amount of ischemia are presented, as well as the distribution of the different patient specific $\mathcal{I}_{\mathrm{US}}$ measures. A comparison between $\mathcal{I}_{\mathrm{US}}$ change and $\mathcal{I}_{\mathrm{DS}}$ change with respect to correlation to ischemia is presented in Fig. 3.9, where the $\mathcal{I}_{\mathrm{DS}}$ change shows the strongest correlation.

3.3.2.3 R-wave amplitude (R) change

The R-wave amplitude at the end of the PCI decreased in 284 (62%) leads by 115.3 $\pm$ 128.7 (0.7-851.9) μV and increased by 120.5 $\pm$ 158.8 (0.2-866.3) μV in 172 (38%) of the total analyzed leads. In Table 3.3-C, the Spearman rank correlation coefficients are presented regarding the correlation between R-wave amplitude changes (sum of all R-wave increase and decrease and sum of all R-wave changes among the leads, respectively) and the measures of ischemia. All correlations were significant, with the sum of total R-wave amplitude change among all leads showing the highest correlation coefficient ($r = 0.63$, $p < 0.0001$, and $r = 0.60$, $p < 0.0001$ for extent and severity, respectively). In the same panel, also the distribution of the R-wave measures among the subjects is displayed.

3.3.2.4 QRS duration (QRS) change

At the end of the PCI, 24 patients (63%) showed a prolongation of the QRS duration, whereas 14 patients (37%) showed a decrease as displayed in Table 3.3-D. For both subgroups, the correlation between $\Delta QRS_{\mathrm{PCI}}$ and the amount of ischemia was very weak and non significant.

3.3.2.5 ST-segment analysis

The maximal ST elevation in any lead, ΔST^{pos}_{max}, and the summed ST elevation among all 12 leads, ΔST^{pos}_{sum}, are presented in Table 3.4, with the largest changes in the LAD group followed by the LCX and RCA group, respectively. The correlation between maximal ST elevation, ΔST^{pos}_{max}, and extent and severity of ischemia was $r = 0.73$ ($p < 0.0001$) for both ischemia measures. The corresponding correlations for summed ST elevation were $r = 0.67$ ($p < 0.0001$) and $r = 0.73$ ($p < 0.0001$) for extent and severity, respectively.

Table 3.3: Quantitative distribution of depolarization changes

QRS index	**Mean ± SD** (range)	**Extent** (% of LV) r (p)	**Severity** (%) r (p)
(A)			
$\Delta\mathcal{I}_{\mathrm{DS}}$ (μV/ms)			
$\Delta\mathcal{I}_{\mathrm{DS}}{}^{pos}_{max}$	35 ± 28 (3-125)	0.60 (<.0001)	0.58 (<.0001)
$\Delta\mathcal{I}_{\mathrm{DS}}{}^{pos}_{sum}$	116 ± 97 (8-125)	0.71 (<.0001)	0.73 (<.0001)
$\Delta\mathcal{I}_{\mathrm{DS}}{}^{tot}_{sum}$	154 ± 114 (17-552)	0.62 (<.0001)	0.62 (<.0001)
(B)			
$\Delta\mathcal{I}_{\mathrm{US}}$ (μV/ms)			
$\Delta\mathcal{I}_{\mathrm{US}}{}^{neg}_{max}$	15 ± 13 (0.9-54)	0.50 (=.0015)	0.47 (=.0032)
$\Delta\mathcal{I}_{\mathrm{US}}{}^{neg}_{sum}$	60 ± 60 (1-295)	0.62 (<.0001)	0.55 (=.0004)
$\Delta\mathcal{I}_{\mathrm{US}}{}^{tot}_{sum}$	92 ± 74 (16-319)	0.39 (=.0155)	0.33 (=.0390)
(C)			
ΔR (μV)			
ΔR^{pos}_{sum}	701 ± 862 (39-3291)	0.41 (=.0110)	0.46 (=.0040)
ΔR^{neg}_{sum}	871 ± 811 (79-3668)	0.52 (=.0010)	0.45 (=.0040)
ΔR^{tot}_{sum}	1574 ± 1377 (190-6291)	0.63 (<.0001)	0.60 (<.0001)
(D)			
ΔQRS (ms)			
QRS widening (n=24)	8.4± 6.6 (0-23)	0.17 (NS)	0.30 (NS)
QRS narrowing (n=14)	4.0 ± 5.0 (0.3-17.1)	0.39 (NS)	0.28 (NS)

Table 3.4: Delta changes of ST expressed as maximum ST elevation in any of the 12 leads and sum of ST elevation among all leads (μV).

ECG index	**LAD** (μV)	**RCA** (μV)	**LAD** (μV)
ΔST^{pos}_{max}	567 ± 459 (25-1384)	150 ± 133 (0-486)	214 ± 239 (18-727)
ΔST^{pos}_{sum}	1622 ± 1514 (36-4858)	520 ± 561 (0-1979)	552 ± 540 (52-1557)

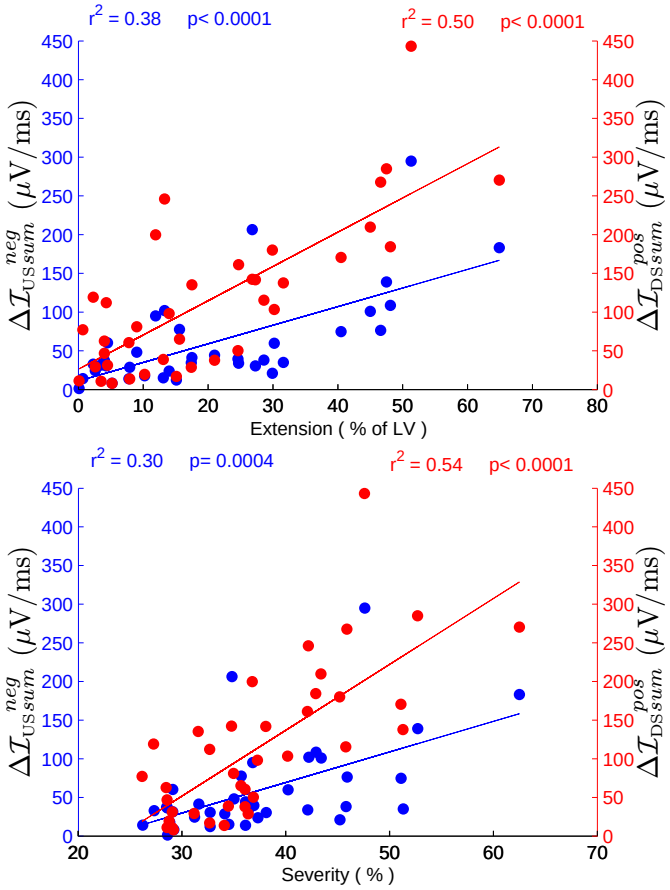

Figure 3.9: Correlation between QRS slope changes ($\Delta\mathcal{I}_{\mathrm{US}}{}^{neg}_{sum}$ and $\Delta\mathcal{I}_{\mathrm{DS}}{}^{pos}_{sum}$) and amount of ischemia (extent and severity). LV indicates left ventricle. Red color: $\mathcal{I}_{\mathrm{DS}}$ changes vs Extent/Severity; Blue color: $\mathcal{I}_{\mathrm{US}}$ changes vs Extent/Severity.

3.3.3 Association between QRS slope and ST segment changes

The correlation between QRS slope ($\mathcal{I}_{\text{US}}$ and $\mathcal{I}_{\text{DS}}$) changes and ST-segment changes considering both maximum ST elevation and sum of ST elevation is presented in Fig. 3.10. The correlation between $\mathcal{I}_{\text{DS}}$ changes and ΔST^{pos}_{sum} or ΔST^{pos}_{max} was stronger than that of $\mathcal{I}_{\text{US}}$ ($r = 0.75$ and $r = 0.69$, respectively, for $\mathcal{I}_{\text{DS}}$, compared with $r = 0.44$ and $r = 0.61$ for $\mathcal{I}_{\text{US}}$), all highly significant.

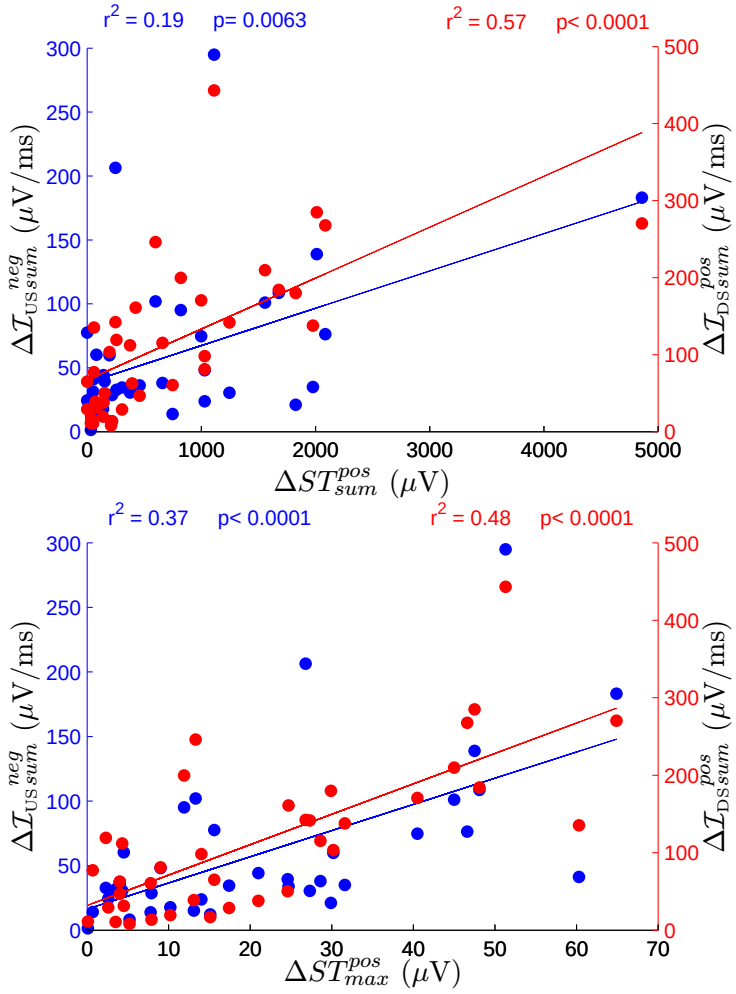

Figure 3.10: Correlation between QRS slope changes ($\Delta\mathcal{I}^{neg}_{\text{US}sum}$ and $\Delta\mathcal{I}^{pos}_{\text{DS}sum}$) and sum of ST elevation ΔST^{pos}_{sum} (top panel) and maximal ST elevation ΔST^{pos}_{max} (bottom panel). Red and blue colors indicate the scatter plots of $\mathcal{I}_{\text{DS}}$ vs ST changes and $\mathcal{I}_{\text{US}}$ vs ST changes, respectively.

To evaluate if depolarization changes provide information to predict the extent and severity of the ischemia in addition to the conventional ST eleva-

tion analysis, a MLR was performed. The results obtained for $\mathcal{I}_{\text{US}}$ and $\mathcal{I}_{\text{DS}}$ are displayed in Fig. 3.11, which provided the largest increase above and beyond that of the ST segment.

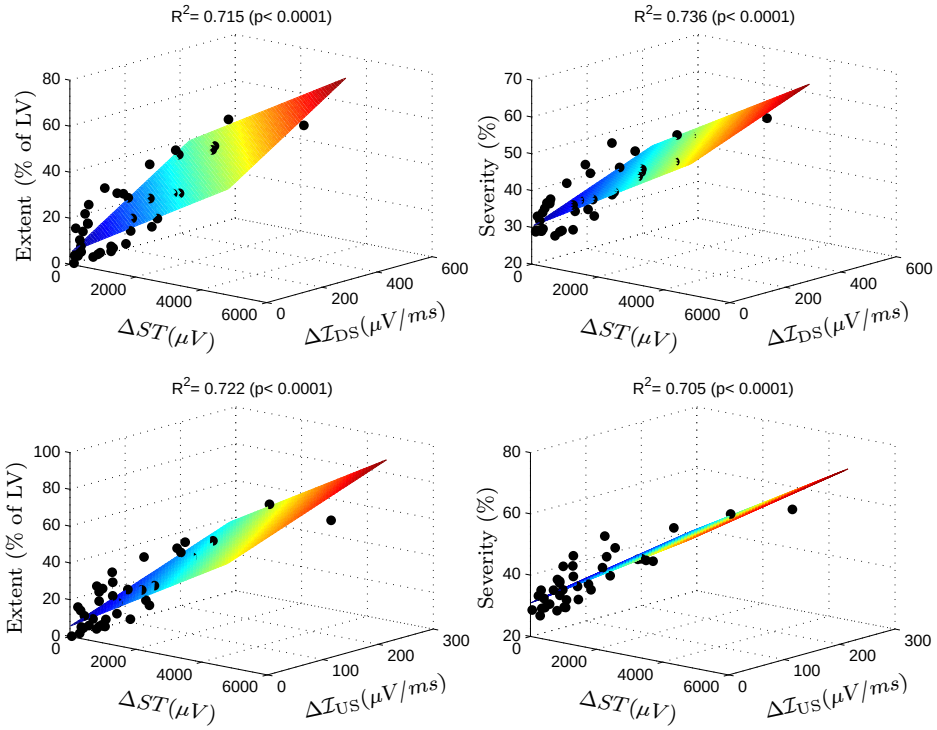

Figure 3.11: Regression analysis when adding QRS slopes changes to ST changes for explaining the extent and severity of the ischemia.

Regarding the extent of ischemia, the portion of the dependent variable explained by the independent variables, R^2, increased by 12.9% after adding $\mathcal{I}_{\text{US}}$ and by 12.2% after adding $\mathcal{I}_{\text{DS}}$ as illustrated in Table 3.5. A combination of the 2 increased the prediction of the extent by 14.5%. The corresponding values for the severity of ischemia were 4.0%, 7.1%, and 7.1%, respectively. The additive effect of the R-wave amplitude change was lower.

3.4 Discussion

In addition to conventional ST segment changes, ECG-derived indices from the final part of the QRS complex ($\mathcal{I}_{\text{DS}}$ and S) show high sensitivity for-characterization of PCI-induced ischemia. Spatial profiles of the ischemia-induced changes for the indices ST, S and $\mathcal{I}_{\text{DS}}$, either when computed using absolute values $\Delta_{\mathcal{Y}}$ or relative values $\mathcal{R}_{\mathcal{Y}}$, are clearly different for the three

Table 3.5: Results of the MLR. Prediction of extent and severity of ischemia by adding QRS slope ($\mathcal{I}_{\text{US}}$ and/or $\mathcal{I}_{\text{DS}}$ in μV/ms) changes or R-wave amplitude changes (R in μV) to sum of ST changes in leads with ST elevation (ST in mV). LV indicates left ventricle; arrow, increase of the explanation of the dependent variable by the added independent variable/s.

ECG indices	**Dependent variable** Extent(% of LV) $R^2(p)$	**Dependent variable** Severity(%) $R^2(p)$
ST	0.593 (<.0001)	0.665 (b.0001)
ST, $\mathcal{I}_{\text{US}}$	0.722 (<.0001), $\Uparrow$ 12.9%	0.705 (<.0001), $\Uparrow$ 4.0%
ST, $\mathcal{I}_{\text{DS}}$	0.715 (<.0001), $\Uparrow$ 12.2%	0.736 (<.0001), $\Uparrow$ 7.1%
ST, $\mathcal{I}_{\text{DS}}$, $\mathcal{I}_{\text{US}}$	0.738 (<.0001), $\Uparrow$ 14.5%	0.736 (<.0001), $\Uparrow$ 7.1%
ST, R sum neg	0.688 (<.0001), $\Uparrow$ 9.5%	0.693 (<.0001), $\Uparrow$ 2.8%
ST, R sum pos	0.593 (<.0001), $\Uparrow$ 0.0%	0.669 (<.0001), $\Uparrow$ 0.4%
ST, R sum tot	0.644 (<.0001), $\Uparrow$ 5.1%	0.673 (<.0001), $\Uparrow$ 0.8%

occlusion site groups. In each group, the spatial profiles show the largest changes in the leads closest to the ischemia region, in agreement with results reported by Martínez et al.[54] and García et al.[61] when investigating other indices in the same study population. The occlusion site clustering is more pronounced when indices are analyzed in a 3D space generated by Dower transformation of the 12-lead ischemia-induced changes rather than when the indices are computed on the X, Y, and Z leads and ischemia-induced changes are subsequently evaluated. The presented analysis of depolarization changes presented hence allows the spatial characterization of regional ischemia, where the marked and distinctive spatial profiles in both 3D and across standard 12- lead ECG system could be considered for occlusion site identification.

The other important finding in this chapter was that changes in the downward slope $\mathcal{I}_{\text{DS}}$ significantly correlate to both the extent and severity of ischemia. The correlation coefficient was higher than that between conventional QRS parameters and ischemia and similar to that of ST elevation. The sum of positive $\mathcal{I}_{\text{DS}}$ change among all leads showed higher correlation coefficients than other QRS slope quantifications. The change in $\mathcal{I}_{\text{DS}}$ correlated to simultaneous ST elevation but also gave separate, additive predictive information about the amount of ischemia beyond that provided by conventional ST-segment changes alone. The severity of ischemia and, hence, risk of fast development of irreversible myocardial necrosis due to a sudden, total coronary occlusion, depend on a number of local factors such as the presence of collaterals and ability of the myocardium to adapt to anaerobic metabolism (preconditioning). Fast development of new acute treatment regimens for STEMI (more aggressive antiplatelet therapy and

especially invasive strategies with primary PCI) have improved clinical outcome. It has, however, also resulted in a higher number of referrals to more remotely located PCI centers as well as early, often pre-hospital ECG-based triage. Using as much information as possible from the standard 12-lead ECG is essential for early ischemia detection, risk stratification based on ischemia severity assessment, and prediction of outcome. In addition to ST-T changes caused by the injury current, more severe ischemia affects the myocytes and conduction system, thus slowing down the conduction and affecting the depolarization phase of the ECG. Localized conduction delay may lead to the loss of cancellation effects from opposite electrical forces, changing the QRS-wave amplitudes and slightly increasing the QRS duration. Depolarization changes are more challenging than ST-T changes to measure and quantify. In the study of this chapter, we apply a new robust method to evaluate changes of the slopes in the QRS complex in a well-defined situation of ischemia due to coronary occlusion. We have shown in the previous chapter that the downward slope $\mathcal{I}_{\mathrm{DS}}$ is more sensitive to ischemia than the upward slope $\mathcal{I}_{\mathrm{US}}$ in a larger patient population using the same ischemia model. Although $\mathcal{I}_{\mathrm{DS}}$ in different leads represents different timing during the depolarization phase, we here show its dynamic change as a sum of all leads to correlate to the amount of ischemia and also display lead specific, spatial information with respect to coronary occlusion site. In the Sclarovsky-Birnbaum ischemia grading system, loss of anteroseptal S waves during anterior STEMI and changes in the R-wave amplitude/ST-J point ratio in inferior STEMI, respectively, indicate more severe ischemia, less salvage, worse microvascular flow, failure of ST-segment resolution, and worse prognosis.[67–69] In a canine model of ischemia, QRS prolongation was a sign of less myocardial protection and more severe ischemia.[63] The QRS slope changes and especially changes in the $\mathcal{I}_{\mathrm{DS}}$ evaluated in the present study represent variations in the R- and S-wave amplitudes, as well as changes in the total depolarization duration. The slope measurement is not affected by simultaneous ST elevation and J-point drift, making it stable to calculate. In this study, there was a correlation between the ST elevation and the sum of $\mathcal{I}_{\mathrm{DS}}$ change; however, it was not high enough, implying that changes are most due to exactly the same pathogenesis, but instead suggesting $\mathcal{I}_{\mathrm{DS}}$ to be influenced by reduced conduction due to the ischemia. By regression analysis, we also found the $\mathcal{I}_{\mathrm{DS}}$ change to add another 12% and 7%, respectively, for predicting the extent and severity of ischemia quantified by myocardial scintigraphy, although this is observed after just 5 minutes of ischemia. It could be hypothesized that longer ischemia duration would produce even more pronounced depolarization changes in addition to ST changes. Therefore, it is plausible to suggest that depolarization analysis presented by $\mathcal{I}_{\mathrm{DS}}$ change could add relevant information about the severity of ischemia in addition to the conventional ST-T analysis.

3.5 Limitations

The study population used in the correlation analyses is small, and therefore, the statistical finding must be interpreted with this in mind. This human model of about 5 minutes of controlled ischemia by PCI with myocardial scintigraphy as the criterion standard is unique. Nevertheless, it just represents the first few minutes of ischemia, and the method should also be applied to situations with longer periods of ischemia, where even more severe grades of ischemia could be expected, possibly affecting the QRS complex in a more extensive way. This method is applied on continuous ECG recordings with calculations of dynamic changes and it is suitable for sequential ECGs recorded in a monitoring situation rather than a snapshot ECG without known baseline values.

Chapter 4

A QRS angle-based method for detecting acute MI

4.1 Introduction

As pointed out previously, the ST deviation has been traditionally considered as the most sensitive marker to diagnose ischemia in clinical practice. Hence, most of the ischemia detectors are mainly based on ST segment-derived indices[77–80]. ST-based are developed should be able to distinguish between ischemic and non-ischemic episodes, however, nowadays this task is still a challenge because ST segment changes may also result from other causes such as changes in the heart electrical axis due to body position changes (BPC) and heart rate-related events, among others.

Ischemia detectors are commonly applied in long-duration ECG monitoring (using Holter monitors, typically 24 hours), which are used to evaluate patients with suspected or known CAD. Several techniques to detect myocardial ischemia in long-duration ECGs have been reported, being most of them based on the identification of ST segment deviations and changes in the T wave morphology. However, when ischemia becomes acute, ECG changes start to be reflected also in the QRS complex, and thus, those changes could be used to trigger an alert indicating the presence of a more severe ischemia.

In chapters 2 and 3, a reliable method for characterizing changes in the QRS complex due to both amplitude and duration changes was proposed by measuring the two main slopes of the QRS complex, i.e. the upward and downward slopes of the R wave[24]. The method was strengthened by incorporating a normalization process to attenuate the normal variations of the slopes at baseline, thereby increasing its sensitivity to ischemia-induced changes[81] and its correlation with ischemia characteristics.

As an evolution of that method, three QRS angles were evaluated in this chapter, which were obtained as the angles of the triangle formed by the lines of the QRS complex shown in Fig. 4.1 b). The main objectives of the

present chapter were to:

- Assess the dynamics of those indices during coronary occlusion.
- Characterize the spatial distribution of their changes in relation to the occlusion site and correlate such changes with the amount of ischemia.
- Test their performance for acute myocardial ischemia detection using a Laplacian noise model with gradual transitions.

4.2 Methods

4.2.1 ECG data

The study population analyzed in this chapter was the STAFF III dataset (n=79) already described in chapter 2. Most of the analyses were carried out in the total study population, while others focused on the subset including SPECT data (n= 38).

4.2.2 QRS angle-based indices

The QRS angles proposed in this chapter are illustrated in Fig. 4.1:

- the R wave angle ϕ_{R}: the angle opposite to the R line l_{R}.
- the up-stroke (U) angle ϕ_{U}: the angle opposite to the down line l_{D}.
- the down-stroke (D) angle ϕ_{D}: the angle opposite to the up line l_{U}.

These three angles were calculated from the URD triangle, which was built by the intersection of the three lines l_{U}, l_{D} and l_{R} shown in Fig. 1. The specific methodology use to compute the angles ϕ_{U}, ϕ_{R} and ϕ_{D} inside the URD triangle was as follows:

1. The lines l_{U} and l_{D} were obtained by least square fitting the ECG signal, $x(n)$, in 8-ms windows centered at points of maximal inflection n_{U} and n_{D}, respectively:

$$l_{\mathrm{U}}(n) = \alpha_1 \cdot n + \alpha_0,\ n = n_{\mathrm{U}} - 4, ..., n_{\mathrm{U}} + 4 \tag{4.1}$$

$$l_{\mathrm{D}}(n) = \beta_1 \cdot n + \beta_0,\ n = n_{\mathrm{D}} - 4, ..., n_{\mathrm{D}} + 4 \tag{4.2}$$

   where n represents time measured in samples, and α_0, α_1, β_0 and β_1 are the coefficients obtained from the fitting. The slopes of the fitted lines l_{U} and l_{D} were given by the coefficients α_1 and β_1, respectively.

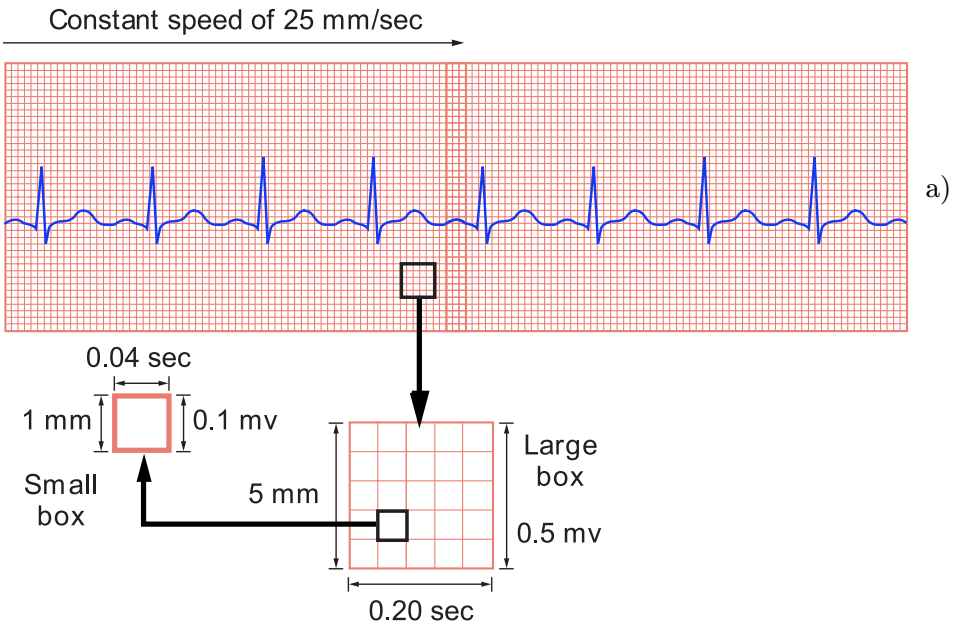

a)

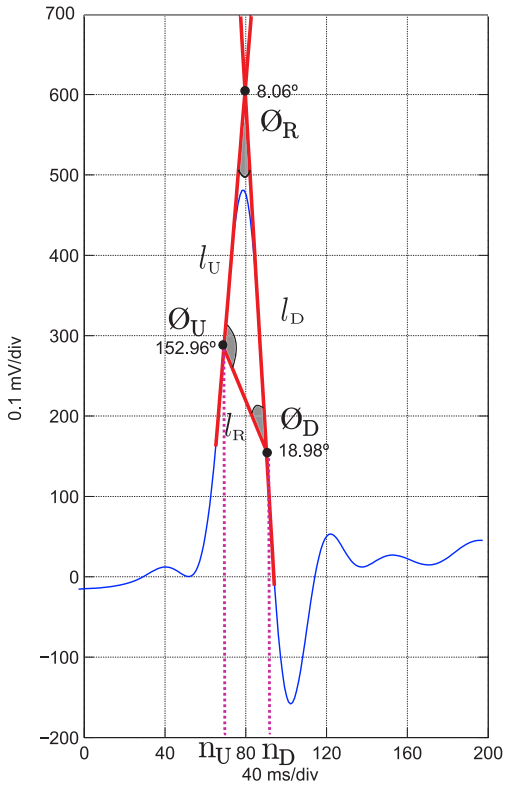

b)

Figure 4.1: a) Conventional ECG printouts calibrated for a speed of 25 mm/sec and gain of 10 mm/mV. b) Example of QRS angles computation for a particular beat of a recording analyzed in this chapter.

2. l_{R} was the line obtained by joining the points $[n_{\mathrm{U}}, x(n_{\mathrm{U}})]$ and $[n_{\mathrm{D}}, x(n_{\mathrm{D}})]$. The slope θ of l_{R} is given by:

$$\theta = \frac{x(n_{\mathrm{D}}) - x(n_{\mathrm{U}})}{n_{\mathrm{D}} - n_{\mathrm{U}}} \tag{4.3}$$

3. The angles ϕ_{U}, ϕ_{R} and ϕ_{D} were subsequently calculated in the following order. First, ϕ_{R} was assumed to be an acute angle (i.e., $\phi_{\mathrm{R}} < 90°$) and was calculated using the angular expression:

$$\phi = \arctan\left(\left|\frac{\alpha_1 - \beta_1}{1 + \alpha_1 \cdot \beta_1}\right|\right). \tag{4.4}$$

The above expression is the general equation assuming a two-dimensional (2D) euclidean space coordinate system. In this study, the units of the horizontal axis (time) and vertical axis (voltage) were re-scaled to match the particular case of conventional ECG tracings in clinical printouts, where a speed of 25 mm/s and a gain of 10 mm/mV are used. Equivalently, in clinical printouts 1 mm represents 40 ms in the horizontal direction and 0.1 mV (i.e. 100 μV) in the vertical one. Thus, in the equation for ϕ_{R}, both slopes α_1 and β_1 were multiplied by the factor 0.4 to convert from μV/ms to mm/mm (1 μV/ms = 0.01 mm/0.025 mm = 0.4 mm/mm), resulting in the following:

$$\begin{aligned}\phi_{\mathrm{R}} &= \arctan\left(\left|\frac{0.4(\alpha_1 - \beta_1)}{1 + 0.16\alpha_1\beta_1)}\right|\right), \\ &= \arctan\left(\left|\frac{\alpha_1 - \beta_1}{0.4(6.25 + \alpha_1\beta_1)}\right|\right).\end{aligned}$$

Second, depending on the sign of the slope θ, we first calculated ϕ_{U} or ϕ_{D}.

If $\theta > 0$,

$$\phi_{\mathrm{U}} = \arctan\left(\left|\frac{\alpha_1 - \theta}{0.4(6.25 + \alpha_1\theta)}\right|\right),$$

$$\phi_{\mathrm{D}} = 180° - (\phi_{\mathrm{U}} + \phi_{\mathrm{R}}). \tag{4.5}$$

else,

$$\phi_{\mathrm{D}} = \arctan\left(\left|\frac{\beta_1 - \theta}{0.4(6.25 + \beta_1\theta)}\right|\right),$$

$$\phi_{\mathrm{U}} = 180° - (\phi_{\mathrm{D}} + \phi_{\mathrm{R}}). \tag{4.6}$$

The above distinction was made to guarantee that the angles ϕ_U and ϕ_D were well-evaluated, as equation (4.4) that uses "arctan" was only valid for the smallest of the two angles generated by the interception of two lines (l_U and l_R or l_D and l_R, respectively). This was particularly relevant considering the different QRS complex morphologies found in the study, some of which are illustrated in Fig 4.2.

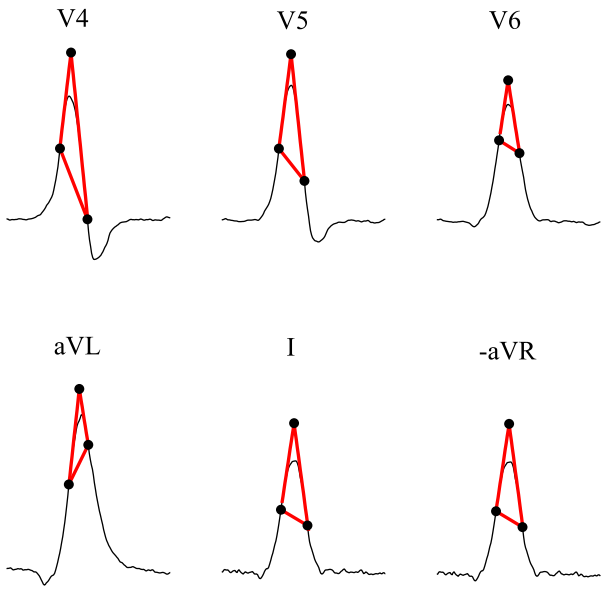

Figure 4.2: Different QRS morphologies corresponding to the same beat in different leads taken from one particular patient of the analyzed dataset.

4.2.2.1

Similarly to chapter 2, the QRS angles were also evaluated in those leads derived from the spatial QRS loops described in section 2.2.4. Other new leads derived from the PCA technique, using three contiguous leads rather than 8 leads (V1-V6, I-II), were also generated in this chapter, and described in detail in section 4.2.6.1. Those leads were considered to be used in an ischemia detector developed in this thesis and fully described in **??**.

4.2.3 ECG-derived indices for comparison

To assess the sensitivity of the QRS angles to the ischemia-induced changes in comparison to other depolarization indices, the upward slope ($\mathcal{I}_{US} = s_U$) and downward slope of the QRS complex ($\mathcal{I}_{DS} = s_D$) were evaluated as de-

scribed in chapter 2. The R-wave amplitude (R) and ST-segment deviation at J point (ST_J) were also determined in all patients as in chapter 3.

4.2.4 Spatio-temporal and statistical analysis

Absolute $\Delta\mathcal{I}$ and relative $\mathcal{R}_\mathcal{I}$ changes during the PCI procedure were tracked for each angle $\mathcal{I} = \{\phi_\mathrm{R}, \phi_\mathrm{U}, \phi_\mathrm{D}\}$. $\Delta\mathcal{I}(t)$ was calculated every 10 s from the start of occlusion ($t = 0$) until the end, by subtracting from the current value $\mathcal{I}(t)$ the initial reference $\mathcal{I}_{ref}$, which is given by the averaged value of the index $\mathcal{I}$ during the first 5 s of the occlusion. As can be noted, the way to compute absolute delta changes $\Delta\mathcal{I}$ in this chapter was different to that used in previous chapters, since, as it will be presented later, the evolution of the angle series during occlusion was less linearly gradual than that observed for the QRS slopes. $\mathcal{R}_\mathcal{I}(t)$ was calculated as the ratio between the absolute change observed during PCI, $\Delta\mathcal{I}(t)$, and the normal fluctuations of $\mathcal{I}$ observed during the control recording prior to the PCI (see equation 2.7).

Results for absolute and relative changes are presented as mean $\pm$ SD. For correlation analysis between the ECG indices and measures of ischemia, the Spearman rank correlation coefficient (r) was used because of the small number of patients. All statistical tests were 2-sided, and significance was defined as $p < 0.05$. Multiple linear regression (MLR) analysis was used to evaluate the additional value of QRS-angle changes to ST-segment changes when predicting the extent/severity of ischemia. Statistical analysis was performed using SPSS, version 19.0 (SPSS, Chicago, IL, USA).

4.2.5 Ischemia detection using a GLRT-based method

The behavior observed in the QRS angle series during coronary occlusion in patients of the STAFF III dataset was considered as a potential candidate to be used for detecting acute ischemic episodes. Particularly, the angles ϕ_U and ϕ_D were observed to have a sudden change in response to the induced ischemia, especially in those leads close to the ischemic region. Leveraging this particular phenomenon in the QRS angles, we extrapolated an approach used in a body postural change (BPC) detector[82] to our case due essentially to the similarity between the signature of the changes occurring in the QRS angles and other ECG-derived indices during BPC and during the induced ischemia. Indices used for BPC detection included Karhunen-Loève transform (KLT) coefficients for QRS and ST-T intervals, indices related to loop rotation angles evaluated over the VCG[83] and QRS-vector difference (QRS-VD) and ST change-vector magnitude (STC-VM) also obtained from the VCG[84].

The QRS angles presented a clear pattern of change in response to the induced ischemia during the PCI procedure and after balloon release. Those observations were translated into a detection problem where a step-like pat-

tern, but with a linear gradual transition rather than an abrupt switch, was searched for in a running observation window through the whole recording.

The angle series represented here as $\varphi_l[n]$, and computed for each lead l, were considered for determining whether an acute ischemic episode occurred (hypothesis $\mathcal{H}_1$) or only noise was present (hypothesis $\mathcal{H}_0$). The beginning of the observation interval was set at a running time instant $n = n_0$. Here, an acute ischemic episode was assumed to be represented by a unitary linearly gradual signature $h[n]$, which was scaled by a lead-dependent amplitude a_l and distorted by an additive, lead-dependent noisy signal $w_l[n]$ with mean value m_l (Laplacian noise model). The m_l value can be interpreted as the DC level of $\varphi_l[n]$ within the observation window. The signal model was represented as follows:

$$\begin{aligned} &\mathcal{H}_0 : \varphi_l[n] = w_l[n] && n = n_0, ..., n_0 + D - 1 \\ &\mathcal{H}_1 : \varphi_l[n] = a_l[n_0] \cdot h[n - n_0] + w_l[n] && n = n_0, ..., n_0 + D - 1 \end{aligned} \quad (4.7)$$

where $l = 1, ..., L$ represents the lead number and D represents the length of the observation window, being D an even-valued integer.

The acute ischemic episodes were here modeled as a step-like change with a gradual transition of a duration T (even-valued integer):

$$h[n] = \begin{cases} 1 & n = 0, ..., \frac{D-T}{2} - 1, \\ 1 - \frac{2}{T}(n - \frac{D-T}{2} + 1) & n = \frac{D-T}{2}, ..., \frac{D+T}{2} - 1 \\ -1 & n = \frac{D+T}{2}, ..., D - 1 \end{cases} \quad (4.8)$$

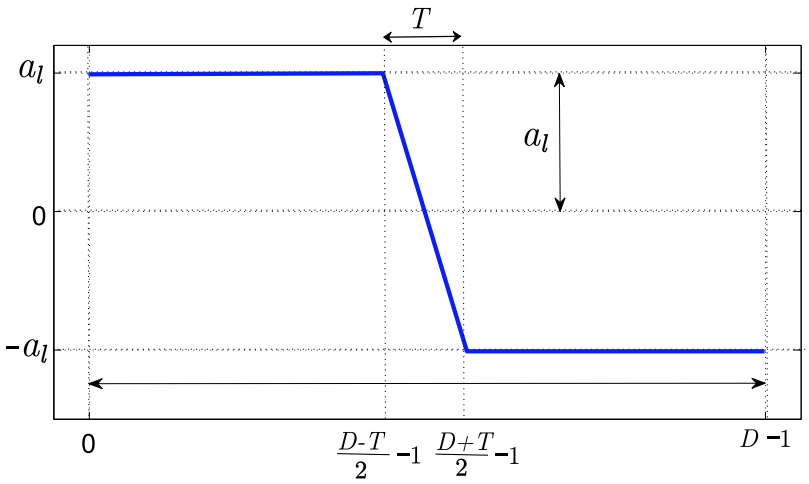

Figure 4.3: Step-like change with a transition of duration T.

The noise $w_l[n]$ was assumed to have a Laplacian probability density function (PDF):

$$p(w_l[n]) = \frac{1}{\sqrt{2}\sigma_l}\exp\left[-\frac{\sqrt{2}}{\sigma_l}\,|w_l[n] - m_l[n_0]|\right] \tag{4.9}$$

with mean $m_l[n_0]$ and variance σ_l^2. All variables were assumed to be mutually independent and uncorrelated to the observation signal $\varphi_l[n]$.

The generalized likelihood ratio test (GLRT), based on the Neyman-Pearson theorem, was used as the basis to design the ischemia detector. Basically, the GLRT allows to replace the unknown parameters of the signal model, under both hypothesis $\mathcal{H}_0$ and $\mathcal{H}_1$, with their maximum likelihood estimators (MLE). Thus, using the Laplacian distribution, the GLRT votes in favor of $\mathcal{H}_1$ if:

$$\Lambda_G(\boldsymbol{\varphi}) = \frac{p(\boldsymbol{\varphi}; \hat{a}_{l,\mathcal{H}_1}, \hat{m}_{l,\mathcal{H}_1}, \mathcal{H}_1)}{p(\boldsymbol{\varphi}; \hat{a}_{l,\mathcal{H}_0}, \mathcal{H}_0)}$$

$$= \frac{\exp\left[-\sqrt{\frac{2}{\sigma_l^2}}\sum_{n=n_0}^{n_0+D-1}|\varphi_l[n] - \hat{m}_{l,\mathcal{H}_1} - \hat{a}_{l,\mathcal{H}_1}\cdot h[n-n_0]|\right]}{\exp\left[-\sqrt{\frac{2}{\sigma_l^2}}\sum_{n=n_0}^{n_0+D-1}|\varphi_l[n] - \hat{m}_{l,\mathcal{H}_0}|\right]} > \gamma \tag{4.10}$$

where $\hat{a}_{l,\mathcal{H}_i}$ and $\hat{m}_{l,\mathcal{H}_i}$ denote the MLEs under the hypothesis $\mathcal{H}_i$. The unknown $\hat{m}_{l,\mathcal{H}_i}$ is regarded as a nuisance parameter.

4.2.5.1 Calculation of the MLEs of $\hat{m}_{l,\mathcal{H}_0}$, $\hat{m}_{l,\mathcal{H}_1}$ and $\hat{a}_{l,\mathcal{H}_1}$

The maximum likelihood estimator of $m_{l,\mathcal{H}_0}$ under the hypothesis $\mathcal{H}_0$ was obtained by maximizing the related log-likelihood function of the Laplacian noise model (see equation 4.9) with respect to $m_{l,\mathcal{H}_0}$:

$$\hat{m}_{l,\mathcal{H}_0} = \arg\max_{m_{l,\mathcal{H}_0}} \ln p(\boldsymbol{\varphi}_l; m_{l,\mathcal{H}_0}) \tag{4.11}$$

The above maximization was equivalent to minimizing the following cost function:

$$J(m_{l,\mathcal{H}_0}) = \sum_{n=n_0}^{n_0+D-1}|\varphi_l[n] - m_{l,\mathcal{H}_0}| \tag{4.12}$$

$$\frac{\partial J(m_{l,\mathcal{H}_0})}{\partial m_{l,\mathcal{H}_0}} = -\sum_{n=n_0}^{n_0+D-1}\mathrm{sgn}(\varphi_l[n] - m_{l,\mathcal{H}_0}) \tag{4.13}$$

whose minimum is reached when $m_{l,\mathcal{H}_0}$ takes the same value as the median of the observed data. This is because the sign function alternates between 1 and -1 depending on whether the expression inside is positive or negative, respectively. Thus, the MLE of $m_{l,\mathcal{H}_0}$ is:

$$\hat{m}_{l,\mathcal{H}_0} = \mathrm{med}(\varphi_l[n_0], ..., \varphi_l[n_0 + D - 1]) \tag{4.14}$$

Under the hypothesis $\mathcal{H}_1$, the MLEs of $m_{l,\mathcal{H}_1}$ and $\hat{a}_{l,\mathcal{H}_1}$ were obtained by maximizing:

$$[\hat{m}_{l,\mathcal{H}_1}, \hat{a}_{l,\mathcal{H}_1}] = \arg \max_{m_{l,\mathcal{H}_1}, a_{l,\mathcal{H}_1}} \ln p(\boldsymbol{\varphi}_l; m_{l,\mathcal{H}_1}, a_{l,\mathcal{H}_1}) \tag{4.15}$$

or, equivalently, by minimizing the cost function:

$$J(m_{l,\mathcal{H}_1}, a_{l,\mathcal{H}_1}) = \sum_{n=n_0}^{n_0+D-1} |\varphi_l[n] - m_{l,\mathcal{H}_1} - a_{l,\mathcal{H}_1} \cdot h[n-n_0]| \tag{4.16}$$

To obtained the MLEs both partial derivatives $\frac{\partial J(m_{l,\mathcal{H}_1}, a_{l,\mathcal{H}_1})}{\partial m_{l,\mathcal{H}_1}}$ and $\frac{\partial J(m_{l,\mathcal{H}_1}, a_{l,\mathcal{H}_1})}{\partial a_{l,\mathcal{H}_1}}$ were set to zero. In the case of $m_{l,\mathcal{H}_1}$,

$$\frac{\partial J(m_{l,\mathcal{H}_1}, a_{l,\mathcal{H}_1})}{\partial m_{l,\mathcal{H}_1}} = - \sum_{n=n_0}^{n_0+D-1} \text{sgn}(\varphi_l[n] - m_{l,\mathcal{H}_1} - a_{l,\mathcal{H}_1} \cdot h[n-n_0]) \tag{4.17}$$

which, when set to zero, yielded the following MLE:

$$\hat{m}_{l,\mathcal{H}_1} = \text{med}(\varphi_l[n] - a_{l,\mathcal{H}_1} \cdot h[n-n_0]) \tag{4.18}$$

with $n = n_0, ..., n_0 + D - 1$. The signal $\varphi_l[n] - a_{l,\mathcal{H}_1} \cdot h[n-n_0]$ inside the median operator represents, under the hypothesis $\mathcal{H}_1$, the Laplacian random noise signal $w_l[n]$, which is centered at m_l (see PDF in Fig. 4.4 (b)). One way to correctly interpreted this signal, is considering $\varphi_l[n]$ as the noise signal $w_l[n]$ shifted $+a_l$ in the first part, shifted $-a_l$ in the final part and modified in the intermediate part by a transition that includes a gradual displacement from $+a_l$ to -a_l. This will be manifested in the PDF of the signal $\varphi_l[n]$ as two sub-PDFs connected by a symmetric transition. Then, we can see the PDF of $\varphi_l[n] - a_{l,\mathcal{H}_1} \cdot h[n-n_0]$ as the PDF of $\varphi_l[n]$ shifted $+a_l$ and $-a_l$, and something proportional in the transition, as illustrated in Fig. 4.4 a and b. Thus, the median of $\varphi_l[n] - a_{l,\mathcal{H}_1} \cdot h[n-n_0]$ may be replaced by the median of $\varphi_l[n]$, since no knowledge of a_l is needed.

Regarding the partial derivative of the cost function with respect to $a_{l,\mathcal{H}_1}$ was:

$$\frac{\partial J(m_{l,\mathcal{H}_1}, a_{l,\mathcal{H}_1})}{\partial a_{l,\mathcal{H}_1}} = - \sum_{n=n_0}^{n_0+D-1} h[n-n_0] \cdot (\varphi_l[n] - m_{l,\mathcal{H}_1} - a_{l,\mathcal{H}_1} \cdot h[n-n_0]) \tag{4.19}$$

Inserting the definition of $h[n]$ (see equation 4.8) in the above equation:

$$\frac{\partial J(m_{l,\mathcal{H}_1}, a_{l,\mathcal{H}_1})}{\partial a_{l,\mathcal{H}_1}} = - \sum_{n=n_0}^{n_0+D/2-1} h[n-n_0] \cdot \text{sgn}(\varphi_l[n] - m_{l,\mathcal{H}_1} - a_{l,\mathcal{H}_1} \cdot h[n-n_0])$$

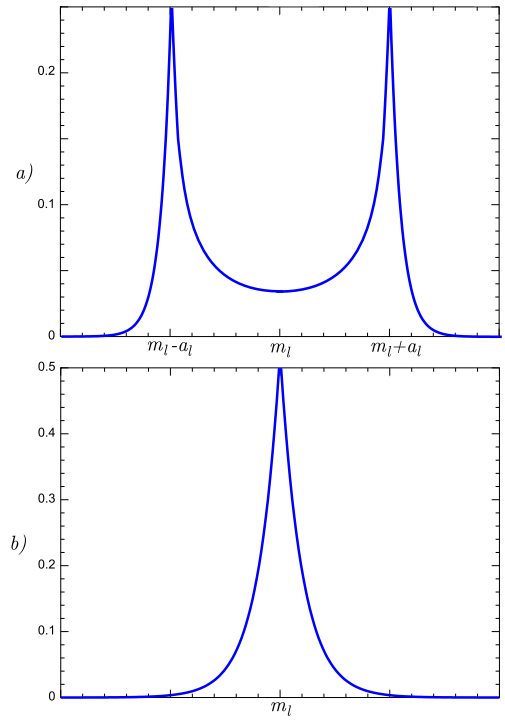

Figure 4.4: Schematic representation of: a) PDF of $\varphi_l[n]$, b) PDF of $\varphi_l[n] - a_{l,\mathcal{H}_1} h[n-n_0]$.

$$-\sum_{n=n_0+D/2}^{n_0+D-1} -h[n-n_0] \cdot \text{sgn}(-\varphi_l[n] + m_{l,\mathcal{H}_1} - a_{l,\mathcal{H}_1} \cdot (-h[n-n_0])) \tag{4.20}$$

$$= -\sum_{n=n_0}^{n_0+D-1} |h[n-n_0]| \cdot \text{sgn}\left(\frac{\varphi_l[n] - m_{l,\mathcal{H}_1}}{h[n-n_0]} - a_{l,\mathcal{H}_1}\right) \tag{4.21}$$

As the internal part of the sign function in equation 4.21 under hypothesis $\mathcal{H}_1$ is equal to $(w_l[n] - m_{l,\mathcal{H}_1})/h[n-n_0]$, whose sign is uncorrelated to $|h[n-n_0]|$, the MLE of $a_{l,\mathcal{H}_1}$ is:

$$\hat{a}_{l,\mathcal{H}_1} = \text{med}\left(\frac{\varphi_l[n] - m_{l,\mathcal{H}_1}}{h[n-n_0]}\right) \tag{4.22}$$

being $n = n_0, ..., n_0 + D - 1$.

As both MLEs $\hat{m}_{l,\mathcal{H}_1}$ and $\hat{a}_{l,\mathcal{H}_1}$ needed to be estimated together, an alternating optimization was applied. A suitable initial estimate for $m_{l,\mathcal{H}_1}$ was previously shown in Fig. 4.4, resulting as the median of $\varphi_l[n]$. This was included in 4.22 to estimate $\hat{a}_{l,\mathcal{H}_1}$. The obtained value was then included in equation 4.18 and so forth until convergence. Typically, stable values for $\hat{m}_{l,\mathcal{H}_1}$ and $\hat{a}_{l,\mathcal{H}_1}$ were achieved in less than 10 iterations.

4.2.5.2 Design of the GLRT detector $\mathbf{T}(\varphi_l)$

Considering the MLEs for the unknown parameters $\hat{m}_{l,\mathcal{H}_0}$, $\hat{m}_{l,\mathcal{H}_1}$ and $\hat{a}_{l,\mathcal{H}_1}$ and applying the logarithm to both sides of equation 4.10:

$$\begin{aligned}\ln \Lambda_G[n_0] &= -\frac{\sqrt{2}}{\sigma_l}\sum_{n=n_0}^{n_0+D-1}\left(|\varphi_l[n]-\hat{m}_{l,\mathcal{H}_1}-\hat{a}_{l,\mathcal{H}_1}\cdot h[n-n_0]|-|\varphi_l[n]-\hat{m}_{l,\mathcal{H}_0}|\right)\\ &= \frac{\sqrt{2}}{\sigma_l}\sum_{n=n_0}^{n_0+D-1}\left(|\varphi_l[n]-\hat{m}_{l,\mathcal{H}_0}|-|\varphi_l[n]-\hat{m}_{l,\mathcal{H}_1}-\hat{a}_{l,\mathcal{H}_1}\cdot h[n-n_0]|\right)\end{aligned} \tag{4.23}$$

which led to the following expression for the developed detector:

$$T[n_0]=\frac{\sqrt{2}}{\sigma_l}\sum_{n=n_0}^{n_0+D-1}\left(|\varphi_l[n]-\hat{m}_{l,\mathcal{H}_0}|-|\varphi_l[n]-\hat{m}_{l,\mathcal{H}_1}-\hat{a}_{l,\mathcal{H}_1}\cdot h[n-n_0]|\right)\gtrless_{\mathcal{H}_0}^{\mathcal{H}_1}\gamma' \tag{4.24}$$

being $\gamma'=\ln\gamma$. The standard deviation σ_l of the Laplacian noise was determined from an interval containing N_σ samples located at the beginning of $\varphi_l[n]$ ($n_0=0$) using the MLE:

$$\hat{\sigma}_l=\frac{\sqrt{2}}{N}\sum_{n=0}^{N_\sigma-1}\left|\varphi_l[n]-\hat{m}_{l,\mathcal{H}_0}[n_0]\right|. \tag{4.25}$$

The detector output given by $T[n_0]$ in equation 4.25 can be interpreted as a difference between the area $A_l{=}a_l\cdot h[n]$ and D times the standard deviation σ_l of the noise, $D\cdot\sigma_l$. If the constants in equation (4.25) are omitted, under hypothesis $\mathcal{H}_1$, the first term of the summation, i.e., $|\varphi_l[n]-\hat{m}_{l,\mathcal{H}_0}[n_0]|$, can be viewed as an estimate of the signal area, whereas the second term $|\varphi_l[n]-\hat{m}_{l,\mathcal{H}_1}-\hat{a}_{l,\mathcal{H}_1}\cdot h[n-n_0]|$ can be viewed as an estimate of the residual noise accounted for D times, thus, when both terms are subtracted we have an estimated values of $A_l-D\cdot\sigma_l$.

A simulated example is illustrated in Fig. 4.5 in order to visualize how the GLRT detector works. The involved parameters were selected to have values close to the real ones obtained from the analysis of the QRS angles. The step-like change with gradual transition was set with an amplitude of $a_l=50$ occurring at the time instant $n{=}300$. It was then contaminated with an additive Laplacian noise with mean $m_l{=}0$ and standard deviation $\sigma_l{=}5$. Three different time instants were selected to obtain the corresponding detection outputs before, just centered at the timing of the step-like change and after it. The sliding window duration for the GLRT filter was set at $D=100$ s with a transition duration of $T{=}20$ s.

To generate a random variable with Laplacian PDF and parameters μ and b, $\mathbf{w}\sim\mathcal{L}(\mu,b)$, the following equation was used:

$$\mathbf{w} = \mu - b \cdot \mathrm{sgn}(\zeta) \cdot \ln(1 - 2\,|\zeta|) \tag{4.26}$$

where ζ is a random variable with uniform distribution in the interval $[-\frac{1}{2}, \frac{1}{2}]$. The value of μ was determined from the median m_l estimated from the data as $\hat{\mu} = \mathrm{med}(w(n))$, and b was calculated in relation to the variance: $\sigma^2 = 2b^2$, leading to $b = \sigma_l/\sqrt{2}$, which can be estimated from the data as:

$$\hat{b} = \frac{1}{N} \sum_{n=1}^{N} |w[n] - \hat{\mu}|\,. \tag{4.27}$$

4.2.6 Blocks of the ischemia detector

To design the ischemia detector, we measured the ischemia-induced changes during the occlusion reflected on the QRS angles (ϕ_{U} and ϕ_{D}) not only in the standard 12-lead ECG, but also in composite leads obtained after applying the PCA technique over several contiguous standard leads. As ischemic changes are mainly reflected in those leads close to the ischemic region, applying the above GLRT-based detector to all standard leads may not provide valuable results. Even if we analyze all the leads, it is quite plausible that the step-like signature appears at different timings from one lead to another in the same patient. Therefore, the summation of the different GLRT detector outputs obtained for each particular lead (as considered in[82] for BPC detection) may not result in a unique event but in a mix of events occurring within a time interval rather than at a specific time instant. As an alternative the QRS angle series can be evaluated in those leads derived from the spatial QRS loop (as described in chapter 2) in order to have a unique, global input, to be supplied to the GLRT detector. The final design of the ischemia detector applied to any lead is represented in Fig. 4.6.

4.2.6.1 QRS angles block

Composite leads derived from the PCA technique were obtained by learning from three contiguous leads of the standard system (V1-V3, V2-V4, V3-V5,...). Then, the first transformed lead associated with the first principal component was selected. Ten new leads, denoted by $l_{C_1}(n), ..., l_{C_{10}}(n)$, were thus involved in this block of the GLRT detector.

$$l_{C_k}(n) = \mathbf{u}_k^T \cdot \mathbf{l}_k(n), \qquad k = 1, ..., 10. \tag{4.28}$$

where $\mathbf{u}_k$ is the first columns of the matrix $\mathbf{U}_k$ (see equations 2.4 and 2.5), representing the first principal component from matrix $\mathbf{L}_k$ decomposition and $\mathbf{l}_k(n)$ the three original leads.

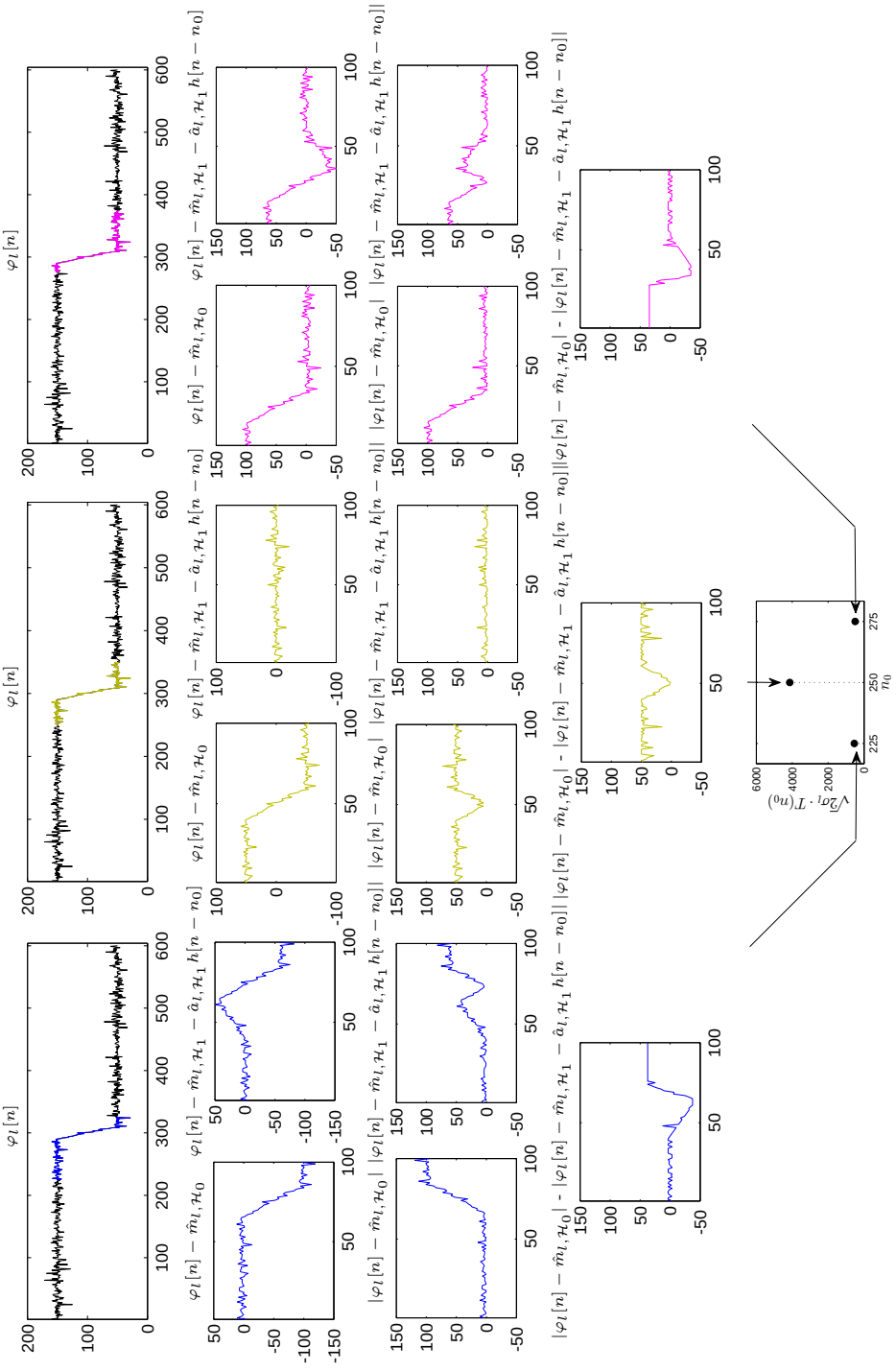

Figure 4.5: Example for three different positions (n_0=225, 250, 275) of the observation window (D=100, T=20) selected from the original input signal $\varphi_l[n]$. $\varphi_l[n]$ represents a step-like change with gradual transition occurring at n=300. The additive Laplacian noise has a median of m_l=0 and standard deviation of σ_l=5.

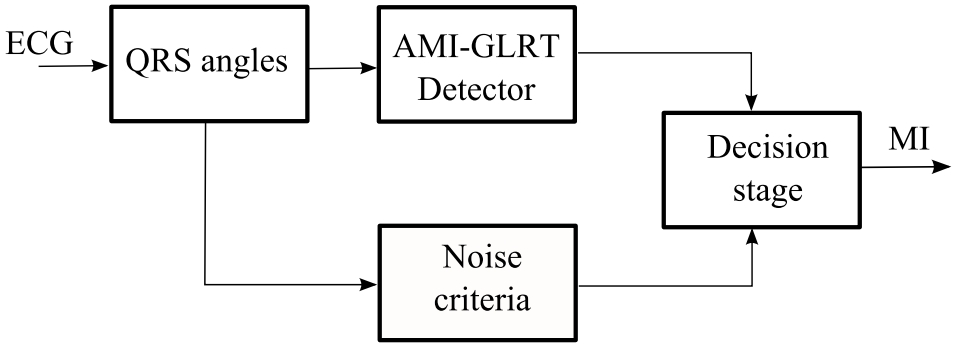

Figure 4.6: Block diagram of the designed AMI-GLRT detector.

In addition to this new PCA-derived leads, the standard and the loop-derived leads described in section 2.2.4 were also used to assess their performance for ischemia detection.

4.2.6.2 AMI-GLRT block

All QRS angles series evaluated on different standard and composite leads were filtered for outliers rejection, using a median absolute deviation (MAD) method[85]. Then, they were resampled to 1 Hz to have equidistant sample times.

For the GLRT detector the total length of the step-like change was set to 70 seconds, with a transition duration of 20 seconds in the middle part. This length was selected considering that the smallest occlusion duration is slightly above one and half minutes. Finally, as both QRS angles ϕ_{U} and ϕ_{D} are considered to be involved in the detection procedure, the same weight was assigned to each of them due to their complementary behavior. Then,

$$T_C[n_0] = \lambda_{\phi_{\mathrm{U}}} \cdot T_{\phi_{\mathrm{U}}}[n_0] + \lambda_{\phi_{\mathrm{D}}} \cdot T_{\phi_{\mathrm{D}}}[n_0] \tag{4.29}$$

with $\lambda_{\phi_{\mathrm{U}}}$ and $\lambda_{\phi_{\mathrm{D}}}$ values being equal to 0.5, and $T_{\phi_{\mathrm{U}}}$ and $T_{\phi_{\mathrm{D}}}$ being calculated following the equation (4.24).

4.2.6.3 Noise estimation

The estimates $\hat{\sigma}_l$ in equation 4.25, were obtained for each lead l at the beginning of the recording, taking the first 30 seconds. This implies that, even when the signal amplitude is very similar between leads, the estimates of the noise in each lead will determine the final amplitude of the corresponding detector outputs. With this in mind, the three individual detector outputs with the largest amplitude in $T_C[n]$ were selected to apply the final decision.

4.2.6.4 Decision stage

After lead selection (in the cases of the standard leads and PCA-composite leads), a threshold δ was selected so that the estimated amplitude of the change a_l was δ times greater than the standard deviation σ_l. This criteria ensured the presence of a significant change due to the induced ischemia. The above condition was imposed to be satisfied in at least two of the three selected leads. As the time positions determined for each lead differed the median of the three time instants was taken as the timing for the detected ischemic change.

4.2.6.5 Performance evaluation

To evaluate the performance of the proposed ischemia detector, the sensitivity (Se) and positive predictivity value (P_+) were assessed. Sensitivity measures the percentage of the actual positives (ischemic events) which are correctly identified or detected, and positive predictivity measures the percentage of detected episodes which correspond to actual positive ones:

$$Se = \frac{TP}{TP + FN} \times 100 \tag{4.30}$$

$$P_+ = \frac{TP}{TP + FP} \times 100 \tag{4.31}$$

where TP represents true positive, FN the false negative and FP false positive. For evaluation, all the PCI recordings were considered to have ischemia while all the control recordings were considered not to have ischemia. The performance evaluation was individually computed for each subgroup of patients according to the occlusion site. The Se and P_+ values were evaluated for different values of the threshold γ' in the ischemia detector, and the optimum one was selected.

4.3 Results and Discussion

4.3.1 QRS angles characterization

Figure 4.7 (a) shows an example of the QRS angles ϕ_{U}, ϕ_{R} and ϕ_{D} evaluated for a particular patient in lead V4. Figure 4.7 (b) and (c) display the QRS slopes $\mathcal{I}_{\mathrm{US}}$ and $\mathcal{I}_{\mathrm{DS}}$ and the R wave amplitude R_a, used here for comparison. As can be observed from Fig. 4.7, the QRS angles are stable at baseline (before of the start of coronary occlusion). In the beginning of the occlusion, ϕ_{U} and ϕ_{D} in particular show an abrupt change with an almost complementary behavior. The angle ϕ_{R}, on the other hand, presents a more gradual change compared to ϕ_{U} and ϕ_{D} during the occlusion period. From Fig. 4.7 it is possible to appreciate that the absolute variation of ϕ_{R} is approximately around 2.5°, whereas it is 155° for ϕ_{U} and ϕ_{D}. The QRS slopes and R wave

amplitude, evaluated for the same patient and lead, show notable changes during occlusion as well, with their evolution being similar to that of ϕ_R, however slower as compared to the angles ϕ_U and ϕ_D.

At baseline, the mean values of ϕ_R computed in each lead and averaged over patients, $\bar{\phi}_R(l)$, were 3.6 ± 1.7° for lead V4 and 20.3 ± 13.3° for lead III, which represent the lowest and highest values among all leads. Normal variations given by the SD of ϕ_R at baseline, averaged for all patients, $\bar{\sigma}_{\phi_R}(l)$, ranged between 0.17° and 2.74°, depending on the lead.

Regarding ϕ_U and ϕ_D, mean values $\bar{\phi}_U(l)$ and $\bar{\phi}_D(l)$ and normal variations $\bar{\sigma}_{\phi_U}(l)$ and $\bar{\sigma}_{\phi_D}(l)$ in control were considerably higher than for ϕ_R. $\bar{\phi}_U(l)$ varied between 66° (lead V6) and 163° (lead V3), while $\bar{\sigma}_{\phi_U}(l)$ ranged between 3.29° and 10.01°. $\bar{\phi}_D(l)$ varied between 7° (lead V3) and 105° (lead V6), while $\bar{\sigma}_{\phi_D}(l)$ ranged between 3.51° and 8.70°.

4.3.2 Evolution of ischemia-induced QRS angle changes

The evolution of changes observed for the QRS angles ϕ_U and ϕ_D is shown in Fig. 4.8. Absolute $\Delta\mathcal{I}(t)$ and relative $\mathcal{R}_\mathcal{I}(t)$ changes, averaged in the total population as well as the LAD subgroup, are displayed along 4 min of occlusion in leads V2 and V3. Maximum, relative changes of the three angles are shown in Table 4.1. In the LAD subgroup, maximum relative change of ϕ_U and ϕ_D were substantially larger than for the total population and for the other two subgroups RCA and LCX.

Regarding absolute changes $\Delta\mathcal{I}(t)$ for these two indices along the coronary occlusion, it can be observed from Figure 4.8 that the angles varied, in mean, around 75-90º in the LAD subgroup, whereas for the whole study population, the variation caused by the induced ischemia was around 15-23º. The variations observed for ϕ_R were considerably smaller as compared to ϕ_U and ϕ_D, which can be explained by the lower changes observed in the slopes of the lines l_U and l_D as compared to the l_R line.

The results obtained for the QRS angles, especially for ϕ_U and ϕ_D, far exceeded those obtained for other QRS-derived indices like QRS slopes, $\mathcal{I}_{US}$ and $\mathcal{I}_{DS}$, and the R-wave amplitude R_a. Maximum relative changes reached up to 9.3 (lead V3) for $\mathcal{I}_{DS}$ and 6.01 (lead V2) for $\mathcal{I}_{US}$ as previously reported (see chapter 2). In the case of R_a, the maximum relative change was achieved in lead II, achieving up to 7.7 times their normal variations at baseline.

4.3.3 Spatial distribution of ischemia-induced QRS-angle changes

Figure 4.9 shows mean ± standard error of the mean (SEM) for ϕ_U and ϕ_D in each lead computed for each of the three subgroups, both considering the whole study population (a) and the smaller subset (n=38) of patients with SPECT imaging data (b). The spatial distributions of $\Delta\phi_U$ and $\Delta\phi_D$ were very closely related, as the behaviour of the two angles during occlusion was almost complementary. Lead V1 is not represented in Fig. 4.9, as in several

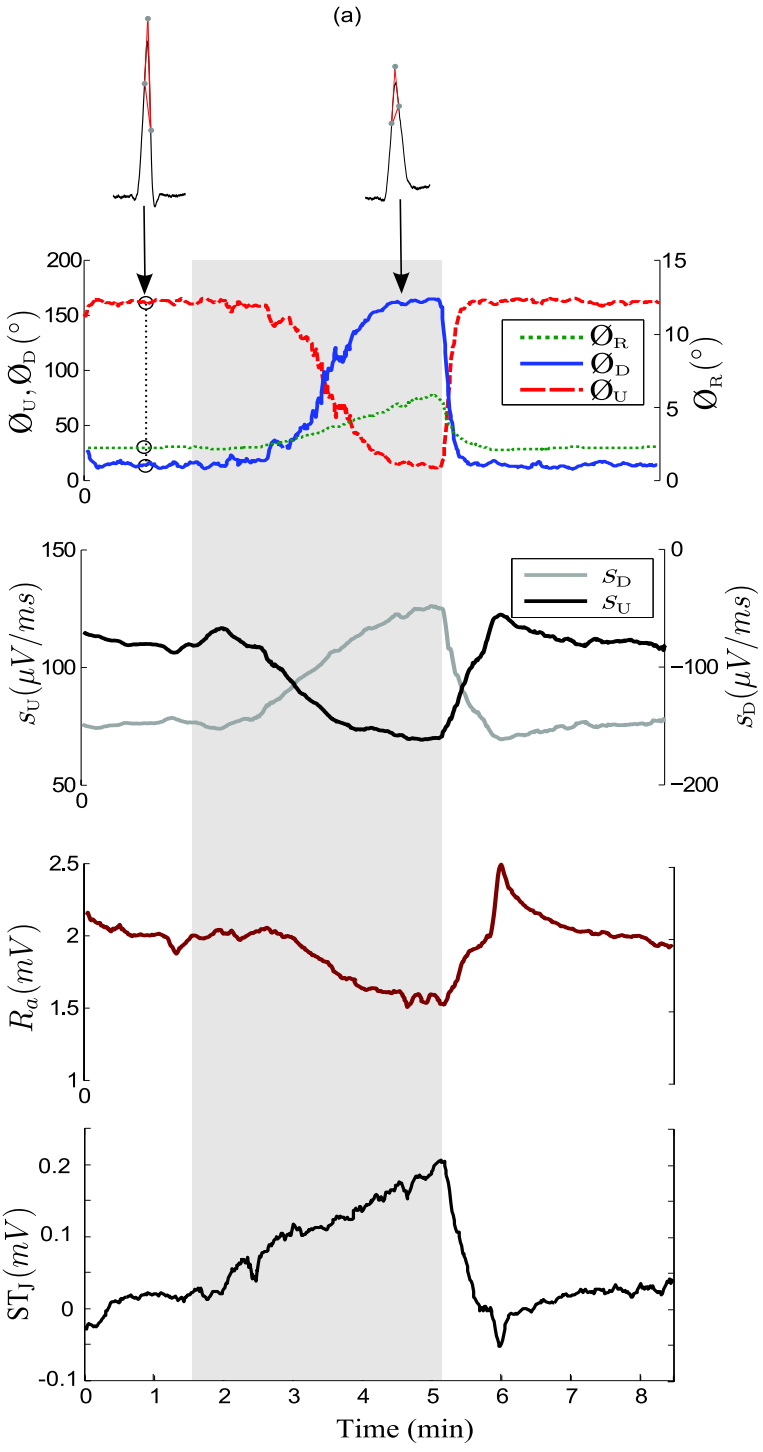

Figure 4.7: (a) Time course of QRS angles and illustrative beats taken at specific time instants representative of pre-occlusion and occlusion periods. (b) QRS slopes evolution. (c) R wave amplitude evolution. (d) Time course of ST level deviation. All represented indices were evaluated for a particular patient in lead V4. Gray zone indicates the occlusion period during the recording.

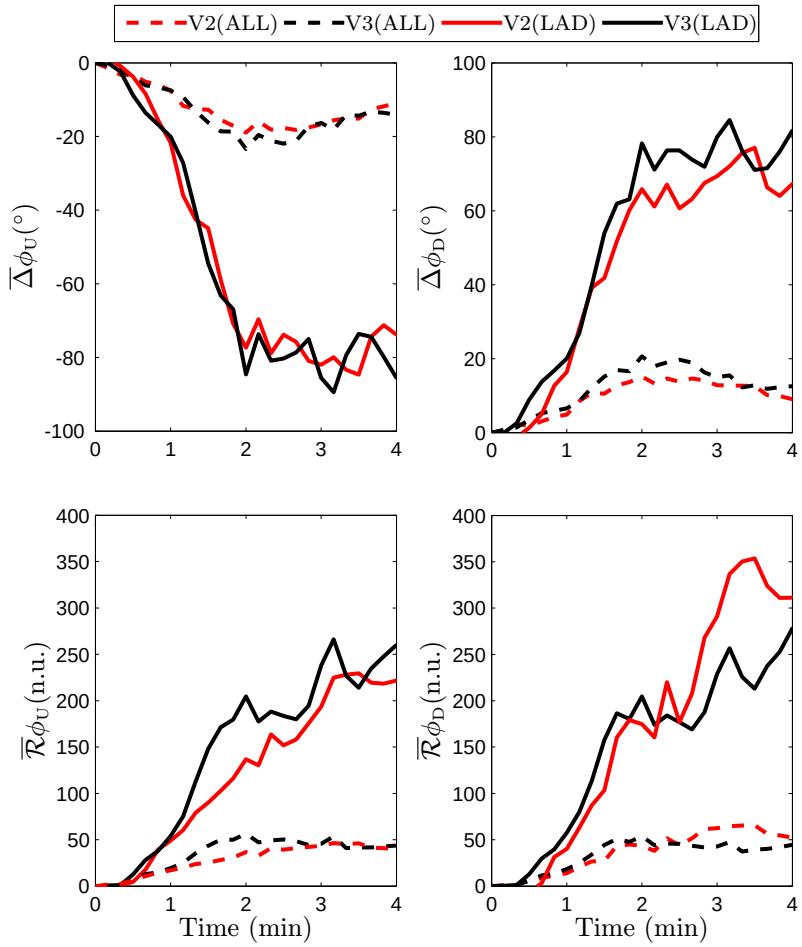

Figure 4.8: Averaged absolute $\Delta_{\mathcal{I}}(t)$ (top panels) and relative $\mathcal{R}_{\mathcal{I}}(t)$ (bottom panels) changes averaged during occlusion for patients in the LAD subgroup (solid lines) and the whole study population (dashed lines) in leads V2-V3.

Table 4.1: Maximum relative change $\mathcal{R}_{\mathcal{I}}$ and corresponding lead, evaluated for the three QRS angles ($\mathcal{I} = \phi_{\mathrm{R}}$, ϕ_{U}, ϕ_{D}) during the occlusion in the total study population and in the three artery subgroups.

$\mathcal{R}_{\mathcal{I}}$	**Total**	**LAD**	**LCX**	**RCA**
ϕ_{U}	V2: 56	V3: 266	V5: 11	III: 17
ϕ_{D}	V3: 65	V2: 354	V5: 10	III: 38
ϕ_{R}	V3: 18	V3: 63	V6: 18	II: 19

patients the QRS angles could not be measured in that lead due to the QRS morphology (usually QS complex). Those leads showing remarkable negative delta values (as leads V2-V4 in the LAD subgroup, Figure 4.9-a) indicate that the angle ϕ_{U} goes from higher values at baseline to lower values during occlusion. The opposite behaviour was found for ϕ_{D} in those cases.

According to the QRS-angle results shown in Figure 4.9 the LAD subgroup could be separated from the LCX and RCA subgroups by evaluating ϕ_{U} and ϕ_{D} changes in most of the leads except for V5, aVL and -aVR. The three subgroups could be separated using the same two angles in leads aVF and III. These results suggest that identification of the occluded artery is easier when distinguishing between the LAD subgroup and the other two subgroups (LCX and RCA) than when separating LCX from RCA.

Regarding changes of the angle ϕ_{R}, a less remarkable spatial lead profile was observed when absolute changes at the end of the occlusion were averaged. This could be due to the smaller range of variation presented by ϕ_{R}. However, when relative changes were analyzed for ϕ_{R}, the spatial lead profile showed more specific patterns, as illustrated in Figure 4.10. Also in this case the LAD subgroup could be easily distinguished from the other two subgroups, while separation of LCX and RCA subgroups was less clear.

4.3.4 Association between QRS changes and ischemia properties measured by SPECT

Properties of the PCI-induced were quantified by SPECT as extent and severity. Evaluation was made for the subset of patients (n=38) with available SPECT data as well as for subsets according to the occluded coronary artery. Absolute and relative changes of the QRS angles measured at the end of the occlusion were correlated with the extent and severity of ischemia.

4.3.4.1 Correlation using single-lead angle changes

Absolute changes of the QRS angles measured at the end of the occlusion were correlated with the extent/severity of ischemia, in each of the three subgroups (LAD, LCX and RCA) separately. Table 4.2 shows correlation

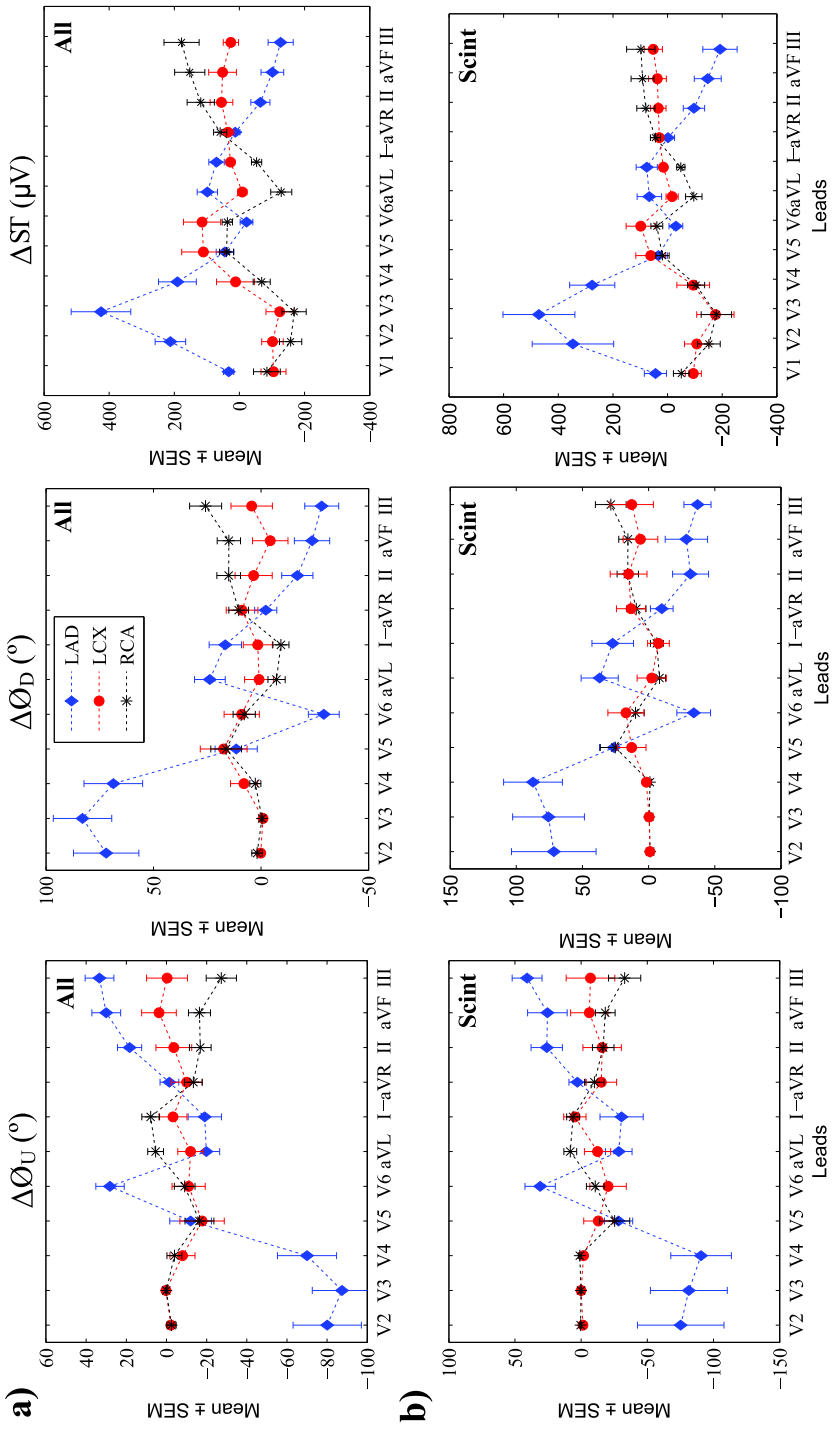

Figure 4.9: Lead-by-lead spatial profile of the averaged absolute changes for the angles ϕ_U and ϕ_D and for ST a) in the total population; b) In the subset of patients with available scintigraphic data (n=38).

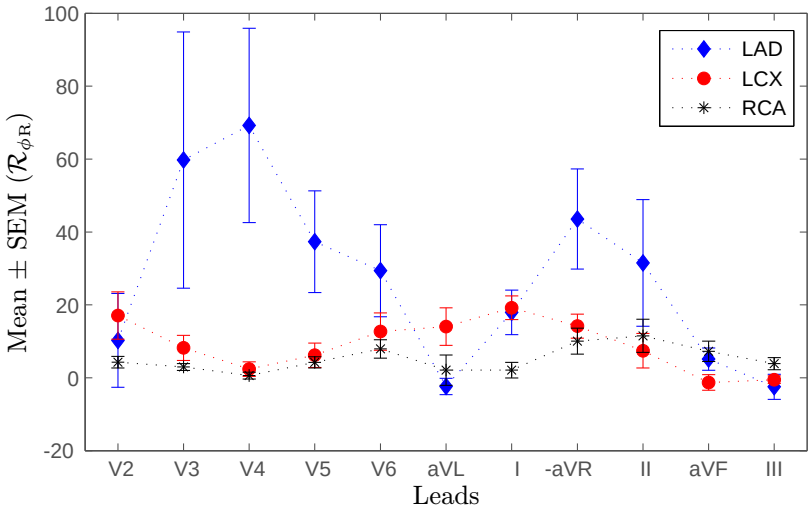

Figure 4.10: Lead-by-lead spatial profile of the averaged relative change for the angle ϕ_R.

coefficients between absolute changes in ϕ_R and ischemia in leads with a significant correlation within each artery group.

Table 4.2: Spearman rank correlation coefficients between absolute changes in ϕ_R and ischemia measures in the different subgroups according to the occluded coronary artery.

Coronary artery occluded	**Extent (% of LV)** $r(p)$	**Severity(%)** $r(p)$
LAD	V3: 0.91 (=0.002)	V4: 0.91 (=0.002)
	V4: 0.74 (=0.037)	V5: 0.86 (=0.007)
	I: 0.83 (=0.010)	V6: 0.86 (=0.007)
LCX	V5: 0.86 (=0.004)	V5: 0.73 (=0.026)
	V6: 0.83 (=0.005)	V6: 0.75 (=0.021)
RCA	V5: 0.67 (=0.001)	V4: 0.43 (=0.044)
	V6: 0.71 (=0.001)	V5: 0.71 (<0.001)
	II: 0.61 (=0.003)	V6: 0.67 (=0.001)
	III: 0.85 (=0.001)	aVF: 0.85 (<0.001)

4.3.4.2 Correlation using composite-lead angle changes

Additional correlation analysis was performed by combining changes measured in different leads. In particular, the sum of absolute changes in ϕ_R among leads and the maximal absolute change in ϕ_R in any lead were considered. The same correlation analysis was also performed considering relative

changes in ϕ_R. For relative ϕ_R measures (max and sum) significant correlations with the extent of ischemia were seen in all 3 subgroups, with the highest correlation coefficients found in the LAD group. When considering the sum of absolute ϕ_R changes, however, the correlation coefficients were considerably lower. For the total population, the correlation coefficients were r=0.45, p=0.005 for extent and r=0.39, p=0.015 for severity. Only the LAD subgroup showed a significant correlation with the extent of ischemia, however not with the severity. None of the other subgroups showed any significant correlation regarding the absolute ϕ_R changes (Table 4.3). The other two QRS angles, ϕ_U and ϕ_D, whose absolute and relative changes far exceeded those obtained for ϕ_R during coronary occlusion did not show any significant correlation with ischemia, either when measuring absolute or relative changes. Nevertheless, the obtained correlation coefficients were substantially higher when using relative changes rather than absolute changes.

Table 4.3: Spearman rank correlation coefficients between the ischemia measures and both maximal, positive single-lead change in ϕ_R, as well as the sum of positive changes in ϕ_R among all leads. Results are shown for both relative and absolute changes in ϕ_R.

	Relative changes		**Absolute changes**	
Coronary occluded artery	**Extent** (% of LV) $r(p)$	**Severity** (%) $r(p)$	**Extent** (% of LV) $r(p)$	**Severity** (%) $r(p)$
Total (n=38)				
Max_pos	0.68 (<0.001)	0.62 (<0.001)	0.25 (=0.128)	0.20 (=0.231)
Sum_pos	0.79 (<0.001)	0.86 (<0.001)	0.45 (=0.005)	0.39 (=0.015)
LAD (n=8)				
Max_pos	0.81 (=0.015)	0.81 (=0.015)	0.88 (=0.004)	0.38 (=0.352)
Sum_pos	0.95 (<0.001)	0.71 (=0.047)	0.81 (=0.015)	0.50 (=0.207)
LCX(n=9)				
Max_pos	0.73 (=0.025)	0.48 (=0.194)	0.13 (=0.732)	0.09 (=0.814)
Sum_pos	0.87 (=0.002)	0.66 (=0.053)	0.42 (=0.265)	0.20 (=0.604)
RCA(n=21)				
Max_pos	0.51 (=0.019)	0.36 (<0.108)	0.11 (=0.642)	0.24 (=0.298)
Sum_pos	0.64 (=0.002)	0.56 (=0.009)	0.22 (=0.348)	0.31 (=0.166)

The other two QRS angles, ϕ_U and ϕ_D, whose absolute and relative changes far exceeded those obtained for ϕ_R, did not show significant correlation with the extent and severity of myocardial ischemia either using absolute or relative changes during ischemia.

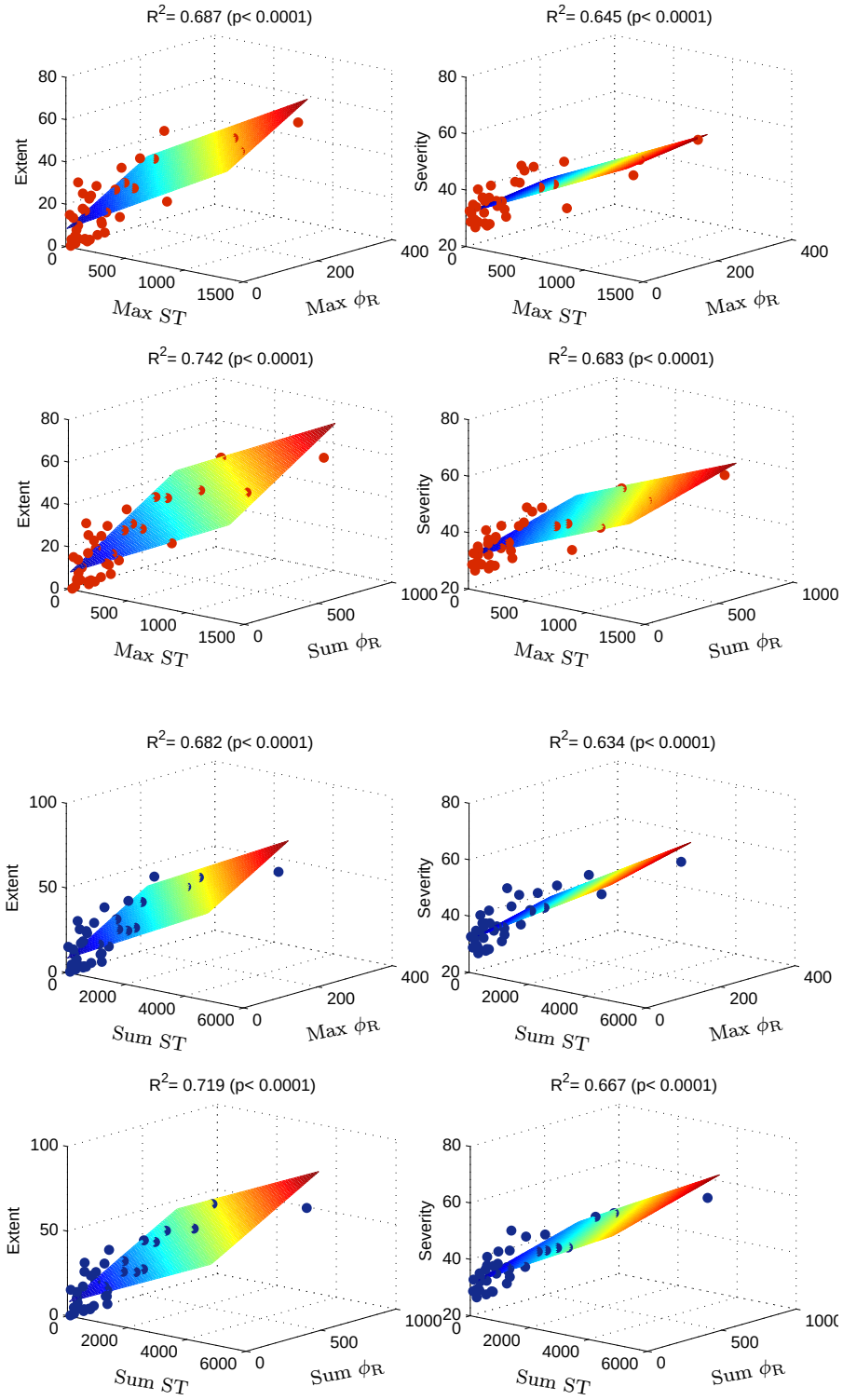

Figure 4.11: MLR analysis adding relative changes in angle ϕ_R to Max ST or Sum ST as predictor variables for explaining the extent and severity of ischemia (dependent variables).

4.3.4.3 Regression analysis involving both QRS-angle changes and ST-segment elevation

The sum of ST elevation among all leads and maximal single lead ST elevation were also considered for correlation with extent and severity of ischemia. Moreover, those two ST measures were used together with the same combinations in ϕ_R to evaluate their complementariness by multiple linear regression analysis. Table 4.4 summarizes the results of the regression analysis and shows the improvement in the prediction of ischemia when ϕ_R changes are added to the ST changes in each artery subgroup. In the LAD subgroup, no significant additive effect was seen as regards severity of ischemia either by absolute or relative ϕ_R changes. However a slightly higher additive effect by 11-12% was noted for extent when adding sum of relative ϕ_R changes to the respective ST measures. Furthermore, no extra value in the RCA subgroup was seen when adding absolute ϕ_R changes. However, an additive effect of between 22.6% and 24.6% was observed when adding sum of relative ϕ_R changes (Table 4.4). The most striking add-on effect of ϕ_R to the ST measures was noted for the LCX subgroup, in which the increase was up to 42.2% (absolute change) and 50.0% (relative change) for extent, whereas it was 15.8% for severity (relative change). When considering all occlusions together, regardless of location, the added value of ϕ_R was less noticeable, with corresponding percentages of improvement of 4.3% for the extent and 2.3% for the severity when considering absolute changes. When considering relative changes the percentages of improvement were of 16.7% for the extent and 7.9% for the severity. Figure 4.11 illustrates the MLR analysis performed for all different combinations involving both relative changes in ϕ_R and changes in ST as predictor variables.

4.3.5 Ischemia detection

The ischemia detector described in section 4.2.6 was applied in a subset of patients (n=48) of the STAFF III database whose associated PCI recording presented at least 20 seconds before the start of balloon inflation to avoid early ischemic episodes. Both control and PCI recordings were used for each analyzed patient and labeled as non-ischemic and ischemic recordings, respectively. Figure 4.12 illustrates an example of the angle ϕ_U measured in leads V2 (panel a) and V3 (panel b), as well as of the detector outputs for the 12 standard leads (panel c), in a patient belonging to the LAD subgroup. As evidenced from the figure, the three outputs with the highest peaks corresponded to leads V2-V4, while the rest of leads showed lower values, close to zero, which could be a hint of which artery is occluded (in this case LAD). Likewise, it is clear that the abrupt change associated with the onset of ischemia occurs at different timings in different leads.

The performance of the ischemia detector was separately tested for each

Table 4.4: Results of the MLR for prediction of the extent and severity of ischemia by combining maximal positive, or sum of changes across leads in the angle ϕ_R and the ST level. The increases, expressed as %, are referred to the value obtained using just the ST change (Sum ST or Max ST). Max ST= maximal ST elevation in any lead; Sum ST= summed ST elevation among all 12 leads; Max pos = maximal in any lead; Sum = summed among all 12 leads.

	Extent		**Severity**	
Predictor variables	**Absolute** ϕ_R change R^2, (p-value),	**Relative** ϕ_R change increase %	**Absolute** ϕ_R change R^2(p-value),	**Relative** ϕ_R change increase %
LAD (n=8)				
Max ST + Max ϕ_R	0.767 (.026)	0.768 (.026)	0.738 (.035)	0.759 (.028)
	3.2%	**3.3%**	**0.0%**	**2.1%**
Max ST + Sum ϕ_R	0.777 (.023)	0.848 (.009)	0.759 (.028)	0.759 (.029)
	4.2%	**11.3%**	**2.1%**	**2.1%**
Max ST	0.735 (.006)		0.738 (.006)	
Sum ST + Max ϕ_R	0.727 (.039)	0.807 (.016)	0.769 (.023)	0.735 (.036)
	0.3%	**8.3%**	**2.5%**	**0.0%**
Sum ST + Sum ϕ_R	0.728 (.039)	0.845 (.009)	0.735 (.036)	0.759 (.029)
	0.4%	**12.1%**	**0.0%**	**2.4%**
Sum ST	0.724 (.007)		0.735 (.036)	
LCX (n=9)				
Max ST + Max ϕ_R	0.617 (.056)	0.691 (.029)	0.389 (.229)	0.435 (.180)
	24.0%	**31.4%**	**6.7%**	**11.3%**
Max ST + Sum ϕ_R	0.799 (.032)	0.877 (.002)	0.504 (.122)	0.596 (.066)
	42.2%	**50.0%**	**18.2%**	**27.4%**
Max ST	0.377 (.078)		0.322 (.111)	
Sum ST + Max ϕ_R	0.729 (.020)	0.771 (.012)	0.541 (.097)	0.555 (.088)
	22.4%	**26.6%**	**6.5%**	**7.9%**
Sum ST + Sum ϕ_R	0.768 (.013)	0.873 (.002)	0.555 (.088)	0.634 (.049)
	26.3%	**36.8%**	**7.9%**	**15.8%**
Sum ST	0.505 (.032)		0.476 (.040)	
RCA (n=21)				
Max ST + Max ϕ_R	0.324 (.029)	0.449 (.005)	0.300 (.041)	0.465 (.001)
	0.6%	**13.1%**	**0.1%**	**16.6%**
Max ST + Sum ϕ_R	0.318 (.032)	0.550 (.001)	0.311 (.035)	0.525 (.001)
	0.0%	**23.2%**	**1.2%**	**22.6%**
Max ST	0.318 (.004)		0.299 (.010)	
Sum ST + Max ϕ_R	0.371 (.015)	0.531 (.001)	0.335 (.025)	0.539 (.001)
	0.5%	**16.7%**	**0.1%**	**20.5%**
Sum ST + Sum ϕ_R	0.365 (.017)	0.610 (<.001)	0.342 (.023)	0.576 (<.001)
	0.0%	**24.6%**	**0.8%**	**24.2%**
Sum ST	0.364 (.004)		0.334 (.006)	

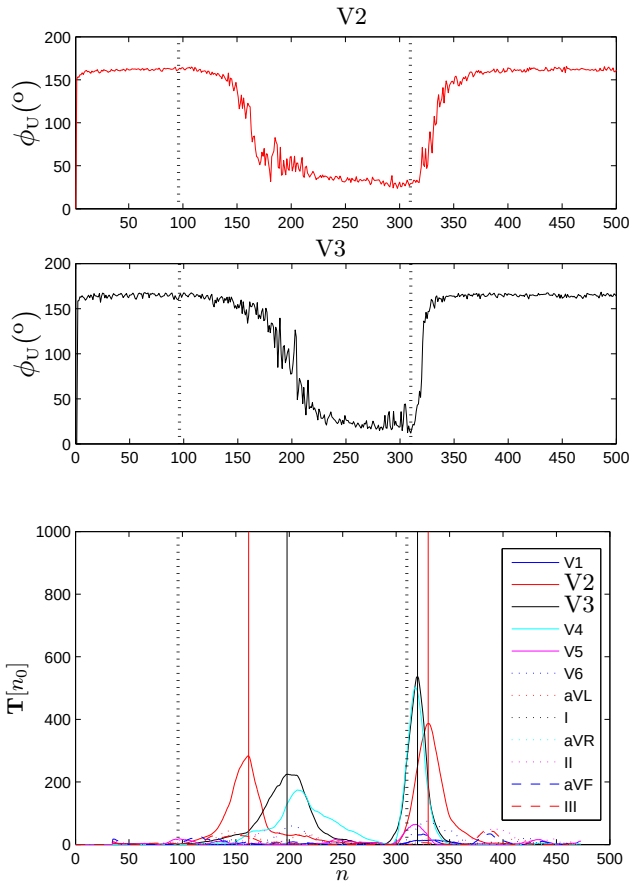

Figure 4.12: Evolution of the angle ϕ_U in leads V2 and V3 during the PCI recording for a particular patient. The bottom panel displays the different outputs given by the GLRT detector for each 12 standard lead. Vertical dashed lines indicate the start and end of occlusion.

artery subgroup, varying the threshold δ in each case. Results obtained for the loop-derived leads were poorer than those obtained for the standard leads. Basically, the reason for that was due to the fact that, in some patients, no change was observed in the angles series evaluated in the loop-derived leads, despite notable changes being present in some individual standard leads (see Fig. 4.13). This masking of changes makes the detector unable to determine if there is a change and thereby producing a FN, and thus, a lower sensitivity. In table 4.5 the values of S_e and P_+ in the different subgroups, using a threshold that makes the estimated index change ($2a_l$), at least, $\delta = 6$ times greater than the standard deviation σ_l, are summarized. The results for the LAD subgroup are better than those of the other two subgroups in terms of S_e and P_+ which is expected since it is

the group with the largest changes in the QRS angles.

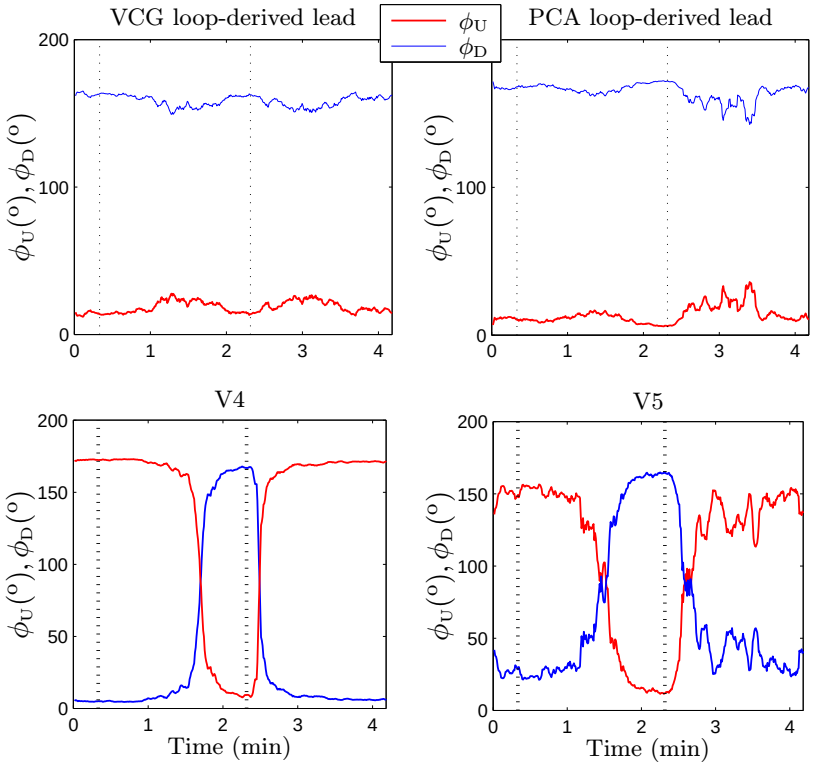

Figure 4.13: Time course of the angles ϕ_U and ϕ_D evaluated in the loop-derived leads (top panels) and standard leads V4 and V5 (bottom panels). Vertical dashed lines in black indicate the start and end of occlusion.

In the case of the ischemia detector applied over the PCA-derived leads l_{C_i} described in 4.2.6.1, the lead combinations involving V1-V3, V2-V4 and V3-V5 achieved values of S_e above 60% (maximum 70.9%) and P_+ ranging between 91.7 and 100% in the LAD subgroup. On the other hand, the RCA and LCX subgroups presented poor values of S_e and P_+ in most of the combinations.

4.4 Discussion

In this chapter three new indices, ϕ_R, ϕ_U and ϕ_D, quantifying angles within the QRS complex, have been proposed and evaluated in 12-lead ECG recordings during myocardial ischemia produced by prolonged, elective PCI. The computation of these angles is straightforward and robust as to measure alterations within the QRS complex during ischemia. The three angles showed high stability at baseline, as assessed by their standard deviations measured

Table 4.5: Performance of the ischemia detector for the three artery subgroups in terms of sensibility (S_e) and positive predictive value (P_+).

Coronary artery occluded	S_e(%)	P_+(%)
LAD	82.3	93.3
LCX	12.5	100.0
RCA	21.7	100.0

in the recording prior to the PCI. If absolute changes during the coronary occlusion are made relative to fluctuations at baseline, the QRS angles turn out to be very sensitive indices to the ischemia-induced changes as compared with other QRS-derived indices like QRS slopes and R wave amplitude, already analyzed in chapter 2. Regarding the temporal evolution of the QRS angles during ischemia, an important difference was noted between the angle ϕ_{R} and the other two angles, ϕ_{U} and ϕ_{D}. While ϕ_{R} presented a gradual change, ϕ_{U} and ϕ_{D} developed a larger and very abrupt change some time after the start of the occlusion, reaching a maximal value at a given time and remaining stable from that time on. The differences observed between the three angles can be attributed to the fact that ischemia-induced changes in QRS amplitudes and/or QRS width have larger effects on the l_{R} line (which determines ϕ_{U} and ϕ_{D}) than on the l_{U} or l_{D} lines (defining ϕ_{R}). Results obtained in most of the analyzed leads suggest a widening of the QRS complex due to the induced ischemia.

The spatial distribution of changes in the QRS angles suggest that their lead profiles could distinguish between the LAD subgroup and the other two subgroups (LCX and RCA), particulary considering the notable differences found in leads V2-V4. Discrimination between the LCX and RCA subgroups was more challenging, with the largest differences found in lead III. Similar results regarding the distinction between artery groups were reported by García *et al.* using ECG indices derived from the Karhunen-Loève transform in the same study population [61]. These results suggest that ischemia-induced depolarization changes may be tracked by leads overlying the ischemic region, however, they do not seem to be more sensitive than ST-segment changes in terms of localization of ischemia.

The relationship between absolute changes in the QRS angles and scintigraphic ischemia measures was evaluated by correlation analysis. A positive correlation was found between lead specific changes in the angle ϕ_{R} and the quantified ischemia for the different occluded arteries, indicating that a local increase in the ϕ_{R} value could indicate larger extent and severity of the ischemia. For RCA occlusions, however, the non-significant correlation between changes in the inferior leads aVF and III and the ischemia measures was somewhat surprising, however significant correlation to extent was seen

for lead II and anterolateral precordial leads in these patients. When patients were separated into groups according to their occluded artery, only changes in a few leads from the twelve standard leads were significantly correlated to the ischemia measures.

Despite larger changes in the angles ϕ_{U} and ϕ_{D} along PCI, no significant correlations with ischemia were observed. A possible explanation for that may be that changes in ϕ_{U} (and ϕ_{D}, respectively) were clustered into two groups of either very low or very high values, depending on the patient and lead, showing a clear non-linear relation with the ischemia measures, which are more evenly distributed along their respective ranges.

By presenting the QRS angle ϕ_{R} as maximal positive, single lead change, or sum of positive changes among all leads at the end of occlusion, relative changes proved to be better predictors of ischemia as compared to absolute values. The significant association between ϕ_{R} and the amount of ischemia by SPECT in the present study is interesting in comparison to our earlier findings regarding correlation between ischemia and QRS slopes as well as R wave amplitude changes, using the same dataset (see chapter 3). In chapter 3 the maximal correlation with the extent and severity of the ischemia was found when considering changes in the downward slope of the R wave, with the highest correlation coefficients (Spearman) being of r=0.71 (p<0.001) and r=0.73 (p<0.001) for extent and severity, respectively. In the study of this chapter, relative changes in the angle ϕ_{R} led to maximal correlation coefficients of r=0.78 (p<0.001) and r=0.73 (p<0.001), respectively. This suggests that the R wave angle seems to be at least as good predictor of ischemia as the down-slope of the R wave. The improvement with respect to other depolarization indices is especially true for LAD occlusions, both regarding extent and severity of the ischemia. In LCX and RCA subgroups there was either no correlation or low correlation to severity if considering either the maximum or the sum of ϕ_{R} values among all leads, although significant relation to extent was seen. More severe ischemia in the LAD occlusions and thus more evident slowing of the regional depolarization wavefront through the ischemic region could possibly explain this difference between artery subgroups.

By regression analysis relative changes in the angle ϕ_{R} used in conjunction with ST changes led to highly variable performance in the additional prediction of extent and severity of the ischemia as compared to the ST changes alone. The additive effect was modest in the LAD group, but more evident in patients with RCA occlusion. However, the largest and most striking improvement was seen in the LCX subgroup. In this group the additional value of absolute ϕ_{R} changes was high. In general, considering the 12-lead standard ECG, the evaluation of ischemia produced by LCX occlusions is difficult in terms of ST segment deviation. The present finding of the additive value of ϕ_{R} changes to that of ST changes, concerning

particularly the LCX occlusions, raises interesting questions of whether this may have important clinical implications for ischemia prediction within this region. The results of our study corroborate the importance of using several indices corresponding to different phases of the ECG to better describe the amount of ischemia. Comparing the results of the present study with those reported in chapter 3 for the QRS slopes and the R wave amplitude, the added value of using ϕ_{R} changes was found to be slightly lower than that of the downward QRS slope when combined with ST changes.

The results of the ischemia detector proposed in this chapter, based on a Laplacian noise model, showed that changes in the angles ϕ_{U} and ϕ_{D} could be potentially useful in the detection of acute ischemia episodes, as both ϕ_{U} and ϕ_{D} present very abrupt transitions after the start of ischemia. Despite the fact that the LAD subgroup was the most sensitive to the acute ischemia, with higher values of sensitivity and positive predictive value (specially in the standard leads), the detector was to some extent able to track acute ischemic episodes in the other artery subgroups. Our results suggest that it could be suitable that the values of the design parameters in the ischemia detector (threshold, transition and length of the step-like function) were set according to the level of change occurring in each ischemic site. Also, the ischemia detector could be used to identify the occluded artery, as the leads with the highest amplitude in the detector output tend to correspond with the leads close to the ischemic area. The performance of the ischemia detector was lower when using the loop-derived leads, where sometimes ischemic changes were not reflected even if there was a substantial change in the standard leads. Nevertheless, the use of PCA-derived leads obtained from contiguous standard leads improved the performance of the ischemia detector compared with that of the loop-derived leads, with the added value of using a lower number of leads.

As a conclusion, the QRS angles ϕ_{U} and ϕ_{D} can be used for ischemia detection and for identification of the occluded artery, particularly in distinguish the LAD subgroup from the LCX and RCA subgroups. On the other hand, the angle ϕ_{R}, which may be seen as a robust surrogate measure of particularly QRS duration, could be used for prediction of the extent and severity of the ischemia.

4.4.1 Limitations

This particular database represents a unique human model of about 5 minutes of controlled ischemia by PCI, and also provides myocardial scintigraphy as the gold standard for the amount of ischemia in a subset of patients (n=38). The latter subset is small, in particular when considering artery-specific results. Therefore, the statistical findings regarding multiple correlation analyses between ECG changes and ischemia must be interpreted with this in mind. Besides, generalization of the present results to

other clinical scenarios is not straightforward, as there is not usually a baseline ECG recorded immediately before ischemia followed by another ECG recorded throughout the ischemic process, and thus relative ECG changes are not often possible to assess, and only absolute changes can be measured. Therefore gradual QRS changes may be most likely evaluated in monitoring situations, such as during pre-hospital transport of STEMI patients to primary PCI (pPCI) in-hospital evaluation of patients with acute coronary syndrome including post-revascularization evaluation of recurrent ischemia as well as in stress test situations. However, further analysis is required to assess the effect of additional factors such as movement artifacts, among others.

The developed ischemia detector has been designed using a fixed window duration for the step-like change function, with a specific transition. However, the observed transitions vary from one patient to another, as well as between leads of the same patient, so an optimal detector would be one able to estimate the transition duration, so that the final window size can be updated as appropriate.

Chapter 5

Analysis of ischemia by depolarization-based ECG methods in a porcine model of myocardial infarction

5.1 Introduction

The ST-elevation myocardial infarction (STEMI) criteria are based solely upon changes in the repolarization phase of the ECG. However, severe myocardial ischemia due to lack of ischemia protection in the myocardium (such as collaterals and/or metabolic preconditioning) causes slowing of the conduction through the ischemic myocardium, thus producing changes also in the depolarization phase (QRS complex). Since longer time is needed for the activation wavefront to propagate through the ischemic area, the normal, balanced ventricular depolarization is altered, thus producing changes in the QRS complex. The more severe ischemia makes the progression of irreversible necrosis due to evolving myocardial infarction faster over time compared to a situation when the myocardium is more protected. By also considering changes in the depolarization phase (QRS complex) in the early triage of patients, important risk stratification can be made, adding prognostic information as well as enabling tailoring of the acute management.

More studies are needed to understand the pathophysiological bases of these QRS changes, but also to develop robust and validated methods to correctly characterize and quantify them. In chapter 2 a method was proposed for evaluation of depolarization changes by analyzing the slopes of the QRS complex: upward slope between Q and R waves ($\mathcal{I}_{\mathrm{US}}$) and downward slope between R and S waves ($\mathcal{I}_{\mathrm{DS}}$), in both standard leads and leads derived from the spatial QRS loop. During coronary artery occlusion by PCI in hu-

mans, the QRS slopes became considerably less steep than in the control situation, in particular for $\mathcal{I}_{\mathrm{DS}}$, as a combined result of both changes in the QRS amplitude and duration. The method showed very low intra-individual variation in a control situation, and both changes in $\mathcal{I}_{\mathrm{US}}$ and $\mathcal{I}_{\mathrm{DS}}$ during the ischemia significantly correlated with the amount of ischemia determined by myocardial scintigraphy, as reported in chapter 3.

A number of animal experiments have been carried out to investigate whether changes in the ECG, mostly in the ST-T interval, are related to the amount of ischemia assessed either by different image techniques or by histochemical analysis. In pigs, during regional ischemia produced by clamping one of the coronary arteries (mainly the LAD artery), changes were reflected as T-Q depression, decreased action potential amplitude and upstroke velocity [86–88]. Also, changes in QRS vector (magnitude and direction) [89] and ST vector [90] have been reported, and have been shown to correlated with the myocardium at risk during the initial minutes of ischemia.

In this chapter the slope indices of the ventricular depolarization phase have been further evaluated by expanding the model from short-term ischemia in humans to an experimental porcine model of myocardial infarction. The specific aims of this chapter were to:

- Characterize the dynamic and temporal behavior of depolarization and repolarization indices during balloon-induced ischemia in pigs in the 12 standard ECG leads, normalized leads and QRS loop-derived leads.
- Correlate changes in the indices to the amount of ischemia given by myocardium at risk (MaR) and to the final infarct size (IS) determined by MPS.

5.2 Materials and Methods

5.2.1 Study population

The study population investigated in this chapter comprised 13 domestic male and female pigs with a weight range between 40-50 kg. During anesthesia, ischemia was induced by a long occlusion of the LAD artery achieved by inflation of a percutaneous transluminal balloon placed in the middle part of the vessel. MPS was used to evaluate the amount of myocardium at risk as well as the size of the infarct achieved during the experiment. A detailed description of the experimental setup is described below [91].

5.2.1.1 Description of experimental protocol

The total duration of the occlusion period was 40 minutes. To verify the complete occlusion of the vessel and the correct balloon positioning, a coro-

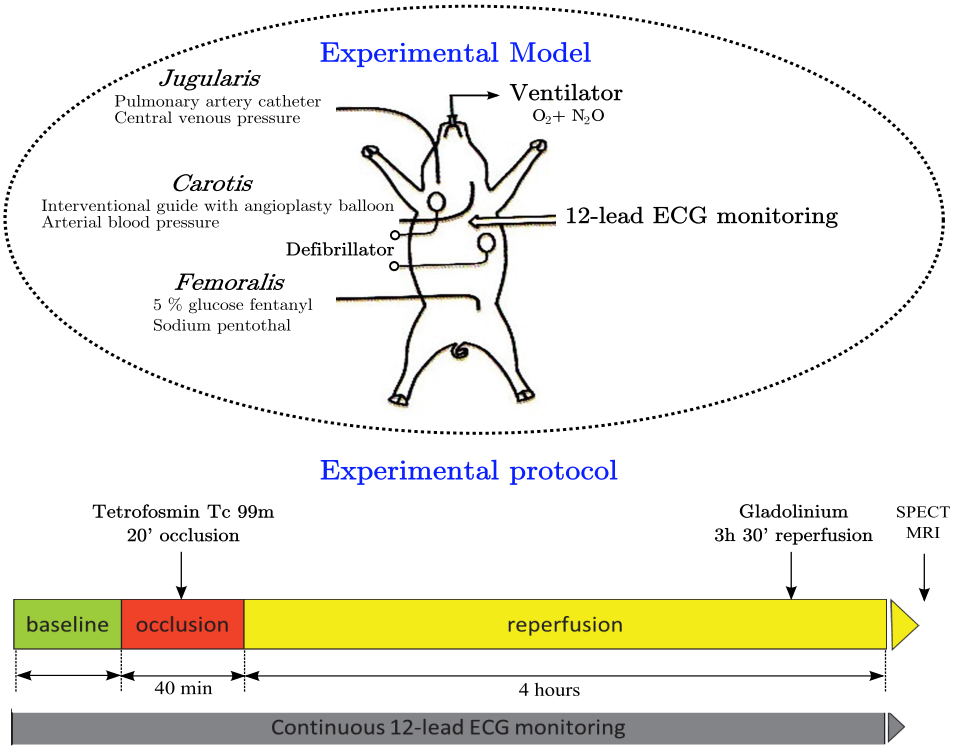

Figure 5.1: Top panel shows the global design of the experimental model with specifications of the different connections. Bottom panel shows the duration of the different stages of the experiment.

nary angiography after inflation of the balloon and before deflation was performed. A subsequent angiogram after balloon deflation was performed to verify the complete restoration of coronary flow in the previously occluded artery. Before starting of occlusion, a continuous 12-lead ECG monitoring was initiated, which lasted during all the experiment (around 5 hours). At the 20^{th} minute of occlusion, Tc tetrofosmin was injected for subsequent SPECT acquisition. The reperfusion period lasted 4 hours. Just at 30 minutes before the end of the experiment, gadolinium was injected for subsequent MRI acquisition. After termination of the experiment, the heart was explanted and SPECT and MRI were performed to assess the MaR and IS, respectively. Further details of the experiment preparation are documented in [91]. A global schema of the experimental model and protocol is shown in Fig. 5.1 while a real view in the laboratory is displayed in Fig. 5.2.

5.2.1.2 ECG recording

A standard 12-lead ECG recording was continuously acquired during occlusion by using a digital ECG monitor ("Kardiotechnica-04-8m", Incart, St.

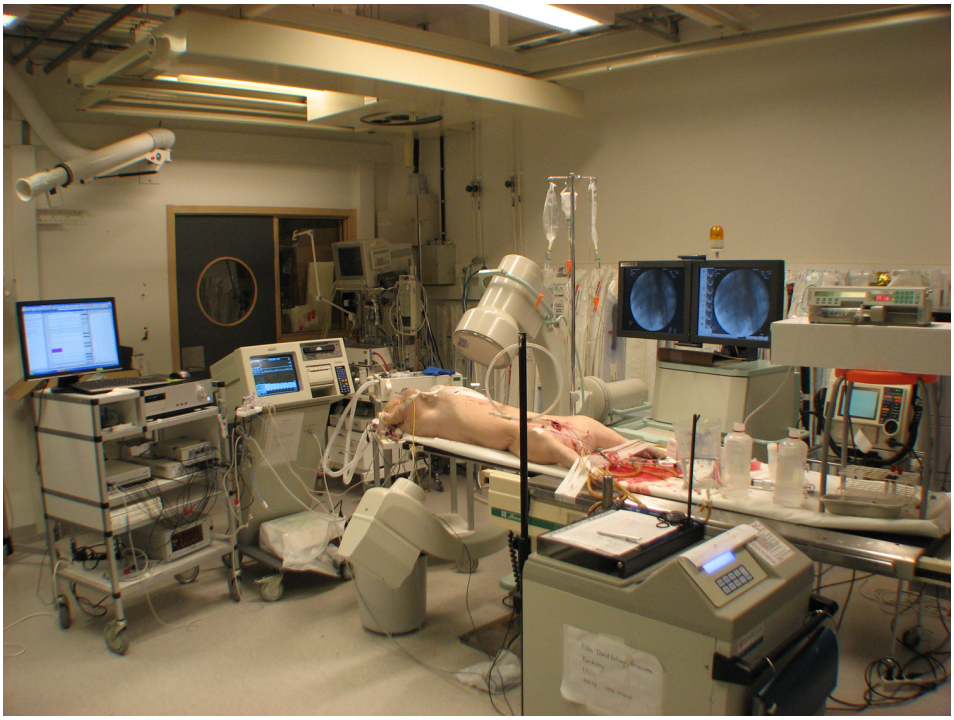

Figure 5.2: General view of the experimental laboratory.

Petersburg, Russia) with a sampling rate of 1024 Hz and amplitude resolution of 1.4 μV. In addition, both a baseline ECG recording before occlusion as well as a 4-hour reperfusion recording after the 40-minute occlusion were acquired, thus achieving a total experiment protocol duration of 5 hours. In this chapter only the 40 minutes corresponding to the occlusion period were considered for analysis.

5.2.1.3 Assessment of MaR by SPECT

Approximately 1000 MBq of Tetrofosmin Tc-99m was injected intravenously in each pig at 20 minutes of occlusion. The MPS ex-vivo imaging was carried out by a dual-head camera (Skylight, Philips, Best, The Netherlands) at 32 projections (40 seconds per projection) with 64 x 64 matrix yielding a digital resolution of 5 x 5 x 5 mm. A low resolution Butterworth filter with a cutoff frequency of 0.6 of Nyquist and order 5 was applied for iterative reconstruction using maximum likelihood-expectation maximization. Short- and long-axis images were reconstructed [91].

The MaR was defined as the perfusion defect size, determined by the area within the left ventricular myocardium with counts lower than 55% of the maximum (normal) counts, and expressed as a percentage of the total LV myocardium.

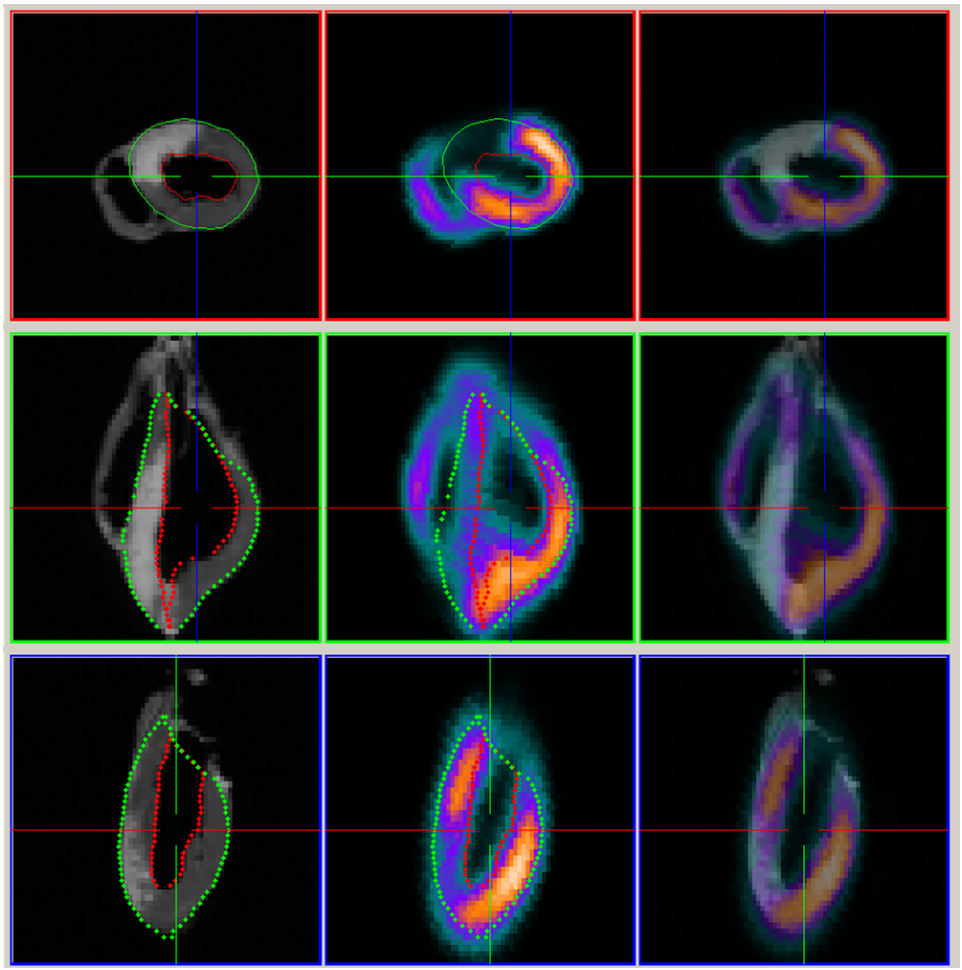

Figure 5.3: Reproduced from Demidova et al.[92] Images representing MaR and final IS after experimentally induced ischemia. Left column: MRI performed for visualization of the ant infarction. Dark gray indicates viable myocardium and white indicates infarction. Middle column: SPECT used to assess MaR by visualization of the anteroseptal perfusion defect. Warm colors indicate adequate perfusion and cold/absent colors indicate decreased/lack of perfusion. Right column: Fusion of MRI and SPECT images. Endocardial and epicardial borders of the left ventricle were manually delineated in the MRI images and fused with the co-registered SPECT images.

5.2.1.4 Assessment of IS by ex vivo MRI

To assess the IS, cardiac MRI was used, as described in detail in previous works.[93–95] In brief, a gadolinium-based contrast agent (Dotarem, gadoteric acid, Gothia Medical AB, Billdal, Sweden) was administered intravenously (0.4 mmol/kg) 30 minutes before removal of the heart. MRI was performed using a 1.5-T MR scanner (Intera, Philips) after removal of the heart. T1-weighted images (repetition time = 20 milliseconds, echo time = 3.2 milliseconds, flip angle = 70°, and 2 averages) with an isotropic resolution of 0.5 mm covering the entire heart were then acquired using a quadrature head coil. The endocardial and epicardial borders of the LV myocardium were manually delineated in short-axis ex-vivo images. The myocardium with a signal intensity greater than 8 SD above the average intensity of the non-affected remote myocardium was defined as the infarcted myocardium. The size of the infarcted myocardium, IS, was then quantified as the product of the slice thickness and the area of hyperenhanced myocardium. The IS was expressed as a percentage of the LV myocardium.

To analyzed the MPS data and assess the MaR and the IS (see Fig. 5.3) the freely available software Segment v1.700 (http://segment.heiberg.se, Medviso, Lund, Sweden) was used[96].

5.2.2 Preprocessing of the ECG signals

All the ECG recordings analyzed in this chapter were preprocessed before computing depolarization and repolarization indices. QRS complexes were automatically detected by using a wavelet-based technique[54], and were then visually checked using the BiosigBrowser tool[97]. This software was also used to manually classify the abnormal beats (ectopic, supraventricular, etc) from the automatic QRS complex detection, and discard them from further processing. This step was crucial in the analysis of this dataset due to the large presence of ectopic and other abnormal beats in the signals. Additionally, ECG segments presenting VT/VF episodes as a consequence of the sustained ischemia were also discarded (see Fig 5.4, bottom panel). Subsequent steps of the preprocessing included baseline drift attenuation via cubic spline interpolation and delineation using a wavelet-based technique as in previous chapters. Only leads V1 to V6 were considered for further analysis.

5.2.3 Depolarization indices and lead configurations applied

5.2.3.1 QRS slopes and R-wave amplitude

For each pig the following depolarization indices were evaluated in the standard leads V1-V6:

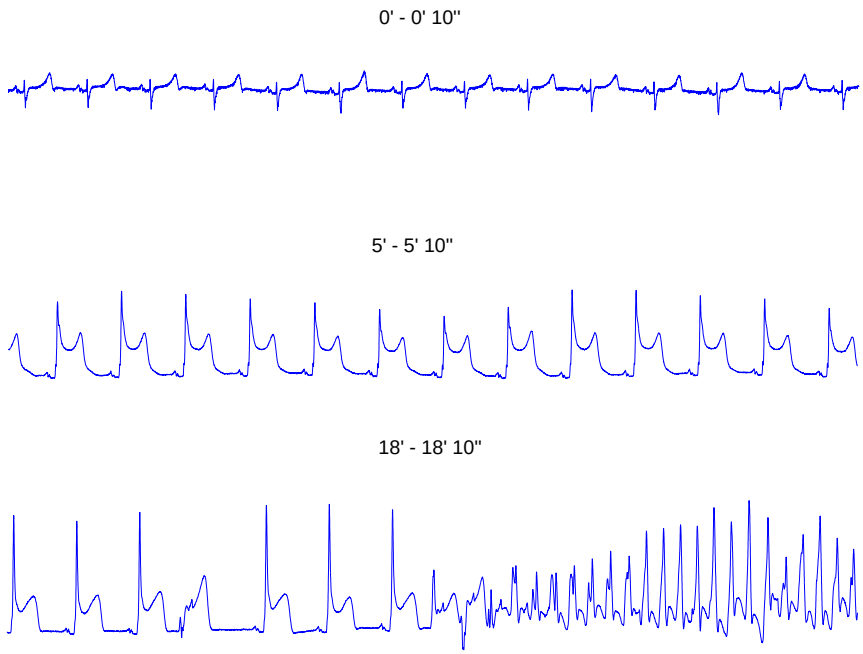

Figure 5.4: ECG tracing for a particular pig, lead V3, taken at different time instants during occlusion.

- $\mathcal{I}_{\text{US}}$: the upward slope of the R wave.
- $\mathcal{I}_{\text{DS}}$: the downward slope of the R wave.
- R_a: R-wave amplitude.

The full methodology used to compute the QRS slope indices $\mathcal{I}_{\text{US}}$ and $\mathcal{I}_{\text{DS}}$ was described in chapter 2. The R-wave amplitude R_a was measured as described in chapter 3. $\mathcal{I}_{\text{US}}$ and $\mathcal{I}_{\text{DS}}$ were also evaluated in the lead derived from the spatial QRS loop built using the vectorcardiogram (VCG), as in section 2.2.4.1.

In addition to the standard and loop-derived leads, other normalized ECG leads were generated. In brief, the maximum vector magnitude within the spatial QRS loop was used as a normalization factor for each corresponding beat. This maximum vector magnitude was denoted by QRS_{max_i}, where i represents the beat index used to normalize each i-th beat in each lead l (V1-V6), $b_{i,l}(n)$, and the normalized beat $\bar{b}_{i,l}(n)$ was computed as:

$$\bar{b}_{i,l}(n) = \frac{b_{i,l}(n)}{QRS_{max_i}}. \tag{5.1}$$

Details on how to estimate QRS_{max_i} are given in the next subsection.

The six normalized leads, obtained from precordial leads V1-V6 and denoted by nV1-nV6, were used to evaluate the $\mathcal{I}_{\text{US}}$ and $\mathcal{I}_{\text{DS}}$ indices as a way to investigate the relevance of slope changes generated just by QRS width changes, avoiding R wave amplitude influence. In this way it is possible to ascertain whether the slope-relevant information comes mostly from variations in QRS width or amplitude.

5.2.3.2 VCG-derived QRS_{max} and QRS_{mean}

Other indices reported in the literature derived from the VCG were also evaluated in this study [89]:

- QRS_{max}: maximum spatial QRS vector magnitude.
- QRS_{mean}: mean spatial QRS vector magnitude.

QRS_{max} was obtained for each beat i by identifying the sample index $n_{0,i}$ associated with the main direction within the loop, as formulated in equation (2.2). Then QRS_{max_i} was calculated as:

$$QRS_{max_i} = \sqrt{x_i^2(n_{0,i}) + y_i^2(n_{0,i}) + z_i^2(n_{0,i})}. \tag{5.2}$$

QRS_{mean} was obtained for each beat i by calculating:

$$QRS_{mean_i} = \frac{1}{n_{\text{OFF}_i} - n_{\text{ON}_i}} \sum_{n=n_{\text{ON}_i}}^{n_{\text{OFF}_i}-1} \sqrt{(x_i^2(n) + y_i^2(n) + z_i^2(n)}. \tag{5.3}$$

where n_{ON_i} and n_{OFF_i} are the QRS onset and offset of beat i.

5.2.4 Repolarization indices

5.2.4.1 ST level

Conventional ST level deviation was also determined in the precordial standard leads V1-V6. For this particular study, and following the same line as in previous studies performed on this database, the ST level was measured 40 ms after the J point, with the PR segment used as the isolectrical level, and denoted by ST_{40}.

5.2.4.2 VCG-derived $STVM$ and $STCVM$

Two additional indices related to the ST segment were also calculated using the orthogonal leads X, Y and Z as described in [90]. The first one represents

the spatial ST vector magnitude ($STVM$), calculated from J point at a position n_{20} ($J + 20\ ms$) in the X, Y and Z leads according to the equation:

$$STVM_i = \sqrt{x_i^2(n_{20,i}) + y_i^2(n_{20,i}) + z_i^2(n_{20,i})}. \tag{5.4}$$

The second additional index represents the spatial ST change vector magnitude ($STCVM$), determined by the magnitude of the vector difference between the reference (mean of $x_i(n_{20,i})$, $y_i(n_{20,i})$ and $z_i(n_{20,i})$ in the first 5 seconds of the occlusion, denoted by x_0, y_0 and z_0, respectively) and the current ST vector at $J + 20\ ms$ of the i-th beat:

$$\begin{aligned} \delta x_i &= x_i(n_{20,i}) - x_0, \\ \delta y_i &= y_i(n_{20,i}) - y_0, \\ \delta z_i &= z_i(n_{20,i}) - z_0, \\ STCVM_i &= \sqrt{\delta x_i^2 + \delta y_i^2 + \delta z_i^2}. \end{aligned} \tag{5.5}$$

where the subindex i represents the current beat and the subindex 0 denotes the ST reference vector. $STVM$ and $STCVM$ indices, as well as the other indices described in 5.2.3, were evaluated on a beat-to-beat basis during the whole occlusion period.

5.2.5 Quantification of ECG changes

The absolute change during the coronary occlusion was calculated for each analyzed index $\mathcal{Y}$ ($\mathcal{Y} \in \{\mathcal{I}_{\text{US}}, \mathcal{I}_{\text{DS}}, R_a, ST_{40}, QRS_{max}, QRS_{mean}, STVM, STCVM\}$) in each lead l ($l = 1, ..., 6$ for leads V1, ..., V6) by the parameter $\Delta\mathcal{Y}(t)$. This parameter was computed every 10 seconds from the beginning of the occlusion ($t = 0$) until the end ($t = 40$ min) in each lead l, and was defined as the difference between the index value at time instant t, $\mathcal{Y}(t)$, and the reference value $\mathcal{Y}_{ref}$ given by the mean of $\mathcal{Y}$ in the first 5 seconds of occlusion, $\Delta\mathcal{Y}(t) = \mathcal{Y}(t) - \mathcal{Y}_{ref}$.

Delta changes $\Delta\mathcal{Y}(t)$ during the occlusion were averaged over pigs for each index $\mathcal{Y}$ to assess global behavior. Values for maximum delta change $\Delta\mathcal{Y}^l_{max}$ for each index were determined in each lead l for the relevant peaks along the occlusion period. Their corresponding timings t^l_{max} were identified, in both individual subjects and as mean for the whole population.

Different combinations of changes were defined and were correlated with MaR. Maximum change regardless lead, $\Delta\mathcal{Y}_{max}$, was defined as:

$$\Delta\mathcal{Y}_{max} = \max_l\{\max_t\{\Delta\mathcal{Y}_l(t)\}\} \text{ for positive peaks,}$$

$$\Delta\mathcal{Y}_{max} = \min_l\{\min_t\{\Delta\mathcal{Y}_l(t)\}\} \text{ for negative deflections,}$$

$$l = 1, ..., 6; \quad t = 0, 10, 20, ..., 2400 \ \ s. \tag{5.6}$$

The timing associated with $\Delta\mathcal{Y}_{max}$ was denoted by t_{max}. Other types of changes were computed as:

$$\Delta\mathcal{Y}_{pos/neg} = \sum_{l \in P} \Delta\mathcal{Y}_l(t_{max}),$$

$$P = \{l_j, j = 1, ..., 6 | \Delta\mathcal{Y}_{l_j}(t_{max}) > 0\} \text{ for positive peaks or}$$

$$P = \{l_j, j = 1, ..., 6 | \Delta\mathcal{Y}_{l_j}(t_{max}) < 0\} \text{ for negative deflections.} \tag{5.7}$$

$$\Delta\mathcal{Y}_{abs} = \sum_{l=1}^{6} |\Delta\mathcal{Y}_l(t_{max})| \,. \tag{5.8}$$

$$\Delta\mathcal{Y}_{real} = \sum_{l=1}^{6} \Delta\mathcal{Y}_l(t_{max}). \tag{5.9}$$

The latter three defined combinations of changes represent: $\Delta\mathcal{Y}_{pos}$, sum of positive or negative changes among leads; $\Delta\mathcal{Y}_{abs}$, sum of absolute changes for all leads; $\Delta\mathcal{Y}_{real}$, sum of all changes over leads keeping their original sign. Particularly for equations (5.6) and (5.7) there are two possibilities depending on whether the peak observed in the index is positive or negative.

In addition to the above combinations of change defined in equations (5.6) - (5.9), $\Delta\mathcal{Y}^l_{max}$ and t^l_{max} values were also correlated with MaR, both individually and in combination ($\Delta\mathcal{Y}^l_{max}/t^l_{max}$ and $\Delta\mathcal{Y}^l_{max} \cdot t^l_{max}$), each of them taken separately for each lead l. The definition of $\Delta\mathcal{Y}^l_{max}$ and its corresponding timing t^l_{max} is analogous to that of equation (5.6), but just for an individual lead l. For those indices that presented more than one remarkable peak along the occlusion, the time lasted between both peaks was also used for correlating with MaR.

All depolarization and repolarization indices, evaluated either in original, normalized and loop derived leads or derived from VCG, as well as the different combinations of change defined above are summarized in table 5.1.

Because the relationship between acute ischemia, quantified by MaR, and the final size of the infarct, determined by IS, is not exactly proportional, since there are many factors involved in the rate progression of the necrotic process.

Table 5.1: A) Summary of the ECG indices of the depolarization and repolarization phases and in which leads they were calculated. B) Different ways the dynamic changes of the parameters were expressed (either as a single-lead maximum value or as a summation among leads), and later used for correlation analyses.

A) Index ($\mathcal{Y}$)	Description	Lead configurations applied
$\mathcal{I}_{\mathrm{US}}$	Upward slope of the R wave	V1-V6, nV1-nV6 and LDL
$\mathcal{I}_{\mathrm{DS}}$	Downward slope of the R wave	V1-V6, nV1-nV6 and LDL
R_a	R-wave amplitude	V1-V6
ST_{40}	ST level at $J + 40\ ms$	V1-V6
QRS_{max}	maximum QRS vector magnitude	VCG (vectorcardiogram)
QRS_{mean}	mean QRS vector magnitude	VCG
$STVM$	ST vector magnitude	VCG
$STCVM$	ST change vector magnitude	VCG

B) Different combinations of changes

$\Delta\mathcal{Y}_{max}$ (*): maximum change regardless lead
$\Delta\mathcal{Y}_{pos/neg}$ (*): sum of the positive/negative changes among leads evaluated at t_{max}
$\Delta\mathcal{Y}_{abs}$ (*): sum of absolute changes for all leads evaluated at t_{max}
$\Delta\mathcal{Y}_{real}$ (*): sum of all changes over leads keeping their original sign
$\Delta\mathcal{Y}^{l}_{max}$, $l = 1, ..., 6$ (leads V1-V6) or another transformed lead (LDL or from VCG)
t^{l}_{max}, $l = 1, ..., 6$ (leads V1-V6) or another transformed leads (LDL or from VCG)

(*) Only evaluated for $\mathcal{I}_{\mathrm{US}}$, $\mathcal{I}_{\mathrm{DS}}$, R_a and ST_{40} measured in standard leads V1-V6.

5.2.6 Correlation analysis along occlusion

5.2.6.1 Individual ECG variables vs MaR/IS

In addition to the correlation analysis described in previous section where MaR/IS were related to ECG changes computed at time instants associated with relevant peaks and valleys during occlusion, additional correlation analysis was performed where ECG changes were calculated every 10 sec from the beginning of the occlusion. In brief, the absolute value for each index, $\Delta\mathcal{Y}(t)$, was measured every 10 sec in each lead (V1-V6) and in each pig (n=13) and was correlated with MaR and IS. Determining the correlation in this way allows to estimate approximately when each marker (MaR and IS) achieves its maximal relationship with ECG changes.

5.2.6.2 Combined ECG variables vs MaR/IS

A more powerful way to figure out the existing relationship between acute myocardial ischemia/infarction, as quantified by MaR and IS, and the ischemic-induced ECG changes can be provided by considering MLR in which changes observed in different ECG indices are analyzed together. The rationale for this is given by the fact that the analyzed indices, some of them related to depolarization and others to repolarization, are affected by different mecha-

nisms so that ischemia-induced changes can begin to manifest in some cases before than in others.

To find the combination of indices (independent variables) that can better explain the quantified ischemia as well as the size of the final infarct (dependent variables), the following model is used:

$$\mathrm{V}_D = b_0 + b_1\Delta\mathcal{Y}_1(t) + b_2\Delta\mathcal{Y}_2(t) + ... + b_n\Delta\mathcal{Y}_n(t) \quad (5.10)$$

where $\mathbf{b} = [b_0, b_1, ..., b_n]^T$ are the coefficients obtained for the model indicating the weights corresponding to each predictor variable, and n represents the number of predictor variables $\mathcal{Y}$ ($\mathcal{Y} \in \{\mathcal{I}_{\mathrm{US}}, \mathcal{I}_{\mathrm{DS}}, R_a, ST_{40}\}$) used for each particular set. MLR analysis was performed in this study considering each of the independent variables measured every 10 sec in each lead V1-V6.

5.2.7 Statistical methods

Results are presented as mean ± SD. Because of the small number of subjects (n=13) in the study, nonparametric tests were used. Spearman rank correlation coefficient (r) was used for correlation analysis. All statistical tests were 2-sided, and significance was defined as $p < 0.05$. Statistical analyses were performed using SPSS, version 19, for Windows (SPSS, Chicago, IL).

5.3 Results

5.3.1 Time-course evolution of ECG changes

Slope indices: An illustrative example of the evolution of QRS slopes during coronary occlusion is shown in Fig. 5.5 (a). The displayed $\mathcal{I}_{\mathrm{US}}$ and $\mathcal{I}_{\mathrm{DS}}$ series correspond to precordial leads V1-V6 of a particular recording without any VT/VF episodes. That behavior is representative of most of the PCI recordings analyzed in the study.

For the case of the $\mathcal{I}_{\mathrm{US}}$ index, the highest absolute changes were individually achieved between the 11^{th} and 24^{th} minute (related to the second remarkable peak shown in Fig. 5.5 (a)) after the start of occlusion. Mean ± SD and range for the timing of $\mathcal{I}_{\mathrm{US}}$ peaks in the leads with the greatest changes (V2-V4) are summarized in Table **??**. In relation to this, two different incremental phases (two marked positive peaks) were found in $\mathcal{I}_{\mathrm{US}}$ during the occlusion. The first peak was less prominent than the second one (see Fig. 5.5 (a)). During the second half of the occlusion (approximately from minute 20), $\mathcal{I}_{\mathrm{US}}$ normally started to decrease until the end of the recording, where it reached approximately the value observed before the occlusion started.

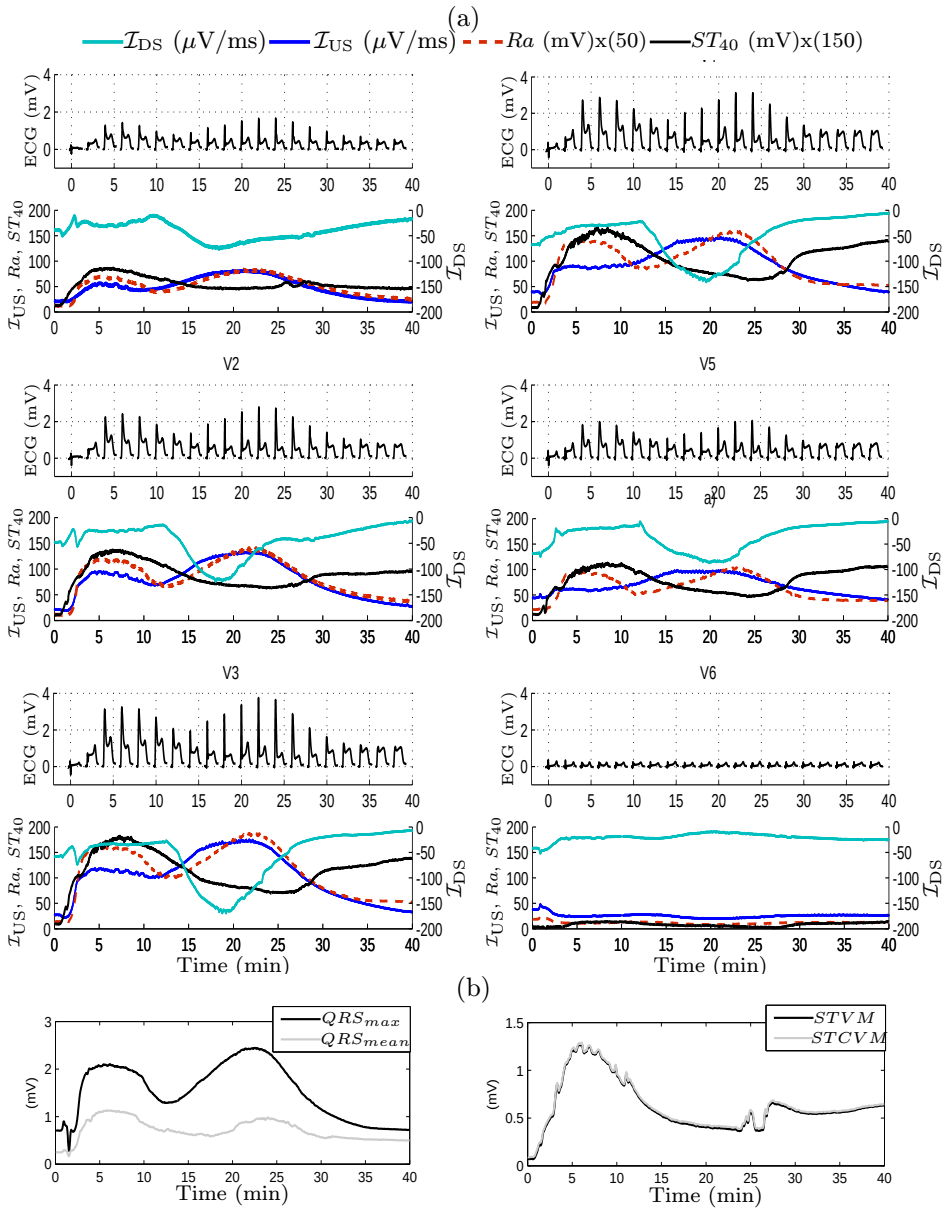

Figure 5.5: (a) Time course evolution of $\mathcal{I}_{\text{US}}$, Ra and ST_{40} (left axis), as well as $\mathcal{I}_{\text{DS}}$ (right axis), during 40-minute occlusion for one particular recording, evaluated in precordial standard leads V1-V6. Odd rows display heartbeats recorded every 2 minutes in each precordial lead, and even rows present the series of the analyzed indices along the occlusion. (b) Time course evolution of indices derived from the VCG: QRS_{mean}, QRS_{max}, $STVM$ and $STCVM$.

Table 5.2: Average values and range for the timing of predominant peaks observed in $\mathcal{I}_{\mathrm{US}}$ and $\mathcal{I}_{\mathrm{DS}}$ in standard leads showing the largest changes (V2-V4) as well as in the lead derived from the QRS loop.

Lead	Timing of 1^{st} peak Mean ± SD (range) (min) ($\mathcal{I}_{\mathrm{US}}$)	Timing of 2^{nd} peak Mean ± SD (range) (min) ($\mathcal{I}_{\mathrm{US}}$)	Timing of 1^{st} peak Mean ± SD (range) (min) ($\mathcal{I}_{\mathrm{DS}}$)	Timing of 2^{nd} peak Mean ± SD (range) (min) ($\mathcal{I}_{\mathrm{DS}}$)
V2	4.6±1.3 (2.3:6.7)	18.3±2.4 (14.5:24.2)	4.9±1.6 (3.5:7.7)	14.9±4.0 (10.5:19.9)
V3	4.5±1.5 (2.3:6.7)	18.2±3.2 (14.7:23.5)	5.7±2.7 (3.7:12.6)	14.5±3.1 (10.4:19.8)
V4	—	16.3±2.9 (11.3:19.9)	5.6±3.1 (3.1:13.3)	14.7±4.0 (7.1:19.7)
LDL	—	16.5±2.5 (13.9:21.5)	4.7±1.2 (3.0:7.5)	13.8±4.0 (8.4:19.8)

The time course of $\mathcal{I}_{\mathrm{DS}}$ was substantially different to that of $\mathcal{I}_{\mathrm{US}}$. The main difference was observed in the first half of the recording, where $\mathcal{I}_{\mathrm{DS}}$ became lower in absolute value tending to zero (flatter slope) during the first 2 to 13 minutes of the occlusion. Then, $\mathcal{I}_{\mathrm{DS}}$ started to decrease, achieving either a large negative peak or sometimes just a small negative deflection. The timing for the largest negative peak of $\mathcal{I}_{\mathrm{DS}}$ ranged between the 7^{th} and 20^{th} minute after the start of occlusion. Mean ± SD and range for the timing of $\mathcal{I}_{\mathrm{DS}}$ peaks are summarized in Table 5.2.

Regarding results obtained for the slopes evaluated in leads derived from the spatial QRS loop, mean ± SD of the timing corresponding to maximum (second positive peak) for $\mathcal{I}_{\mathrm{US}}$ and both maximum (first positive peak) and minimum (second negative peak) for $\mathcal{I}_{\mathrm{DS}}$ are also shown in Table 5.2. In addition, Fig. 5.6 presents the time course of QRS slopes evaluated in the loop-derived lead for the same recording illustrated in Fig. 5.5. As can be observed from Fig. 5.6, the first positive peak in $\mathcal{I}_{\mathrm{US}}$ was found to be less pronounced than in precordial leads (illustrated in Fig. 5.5), while the second one was the most pronounced. In some cases, the first positive peak in $\mathcal{I}_{\mathrm{US}}$ became negative, which is due to changes in the direction of the maximum magnitude vector within the QRS loop. In the case of $\mathcal{I}_{\mathrm{DS}}$, the initial increase leading to the first positive peak was more relevant in the loop-derived lead, and then $\mathcal{I}_{\mathrm{DS}}$ remained quite flat until the start of the negative deflection, keeping from that point on a similar behavior to that observed in precordial leads.

The time course of QRS slopes evaluated in normalized leads nV2-nV4 during coronary occlusion is displayed in Fig. 5.6. It can be observed that $\mathcal{I}_{\mathrm{DS}}$ evaluated in these three precordial leads shows a similar behavior to that observed in the loop-derived lead. Nevertheless, while in the original leads V2-V4 the evolution of $\mathcal{I}_{\mathrm{DS}}$ is quite flat at the beginning of the occlusion, the normalized leads show a remarkable increase in $\mathcal{I}_{\mathrm{DS}}$ during the first five minutes of occlusion. Subsequently, the $\mathcal{I}_{\mathrm{DS}}$ index remains approximately constant during several minutes, which are followed by a large

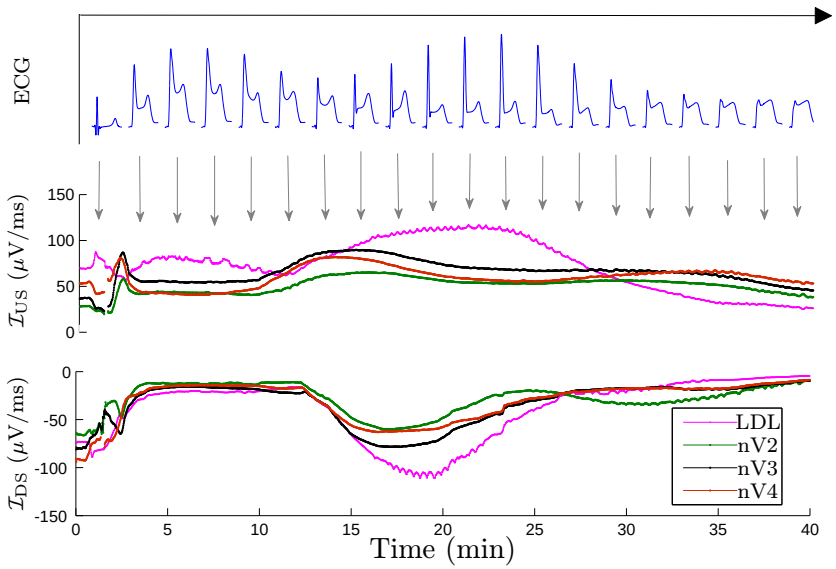

Figure 5.6: QRS slopes evaluated in the loop-derived lead (LDL) and in the normalized leads nV2–nV4 for the same pig of Fig. 5.5. Top panel displays representative beats in the loop-derived lead every 2 minutes during the coronary occlusion.

negative deflection. This behavior suggests that two important increases of QRS duration occur during the coronary occlusion in accordance with the two $\mathcal{I}_{DS}$ increases observed in normalized leads. In contrast, the behavior of $\mathcal{I}_{US}$ in normalized leads was quite different from that observed in the original leads (Fig. 5.5 (a)) and in the loop-derived lead. In fact, only one clear positive peak was observed during the occlusion, which normally occurred in the time interval between the two positive peaks observed in the original leads. The observed differences in the evolution patterns of $\mathcal{I}_{US}$ and $\mathcal{I}_{DS}$ when analyzed in normalized and original ECG leads can be explained by the normalization process applied to the original leads, which separates the changes that occur in the slopes due to changes in the QRS duration and due to changes in the QRS amplitude.

Conventional ECG indices: R-wave amplitude, R_a, and ST level deviation, ST_{40}, used here as conventional depolarization and repolarization indices, respectively, are shown in Fig. 5.5 (a) for leads V1-V6. As can be observed from the figure, the R_a evolution during ischemia presents a similar behavior to that observed for $\mathcal{I}_{US}$. In this case, a remarkable increase in R_a quickly developed at the start of occlusion, due to the fact that the rS complex configuration observed during the initial minutes turned into a monophasic, giant R wave. The initial R_a increase was transiently reduced until a second and more pronounced increase developed between the $11^{th}$and

24^{th} minute. In the case of ST_{40}, a clear and unique positive peak was observed in most of the analyzed leads. This main peak in ST_{40}, indicating abrupt ST elevation, occurred between the 5^{th} and 12^{th} minute after the start of occlusion.

Vectorcardiogram-derived indices: In Fig. 5.5 (b) four indices evaluated by using the VCG loop generated from orthogonal leads X, Y and Z are displayed. The left panel presents the QRS_{max} and QRS_{mean} series and the right panel, the $STVM$ and $STCVM$ series. A strong relationship was observed between the evolution of QRS_{max} calculated from the VCG and R_a evaluated in leads V1-V6, with two distinct phases clearly distinguished (see Fig. 5.5). A strong similarity was also found between $STVM/STCVM$ and ST_{40}, with a predominant positive peak occurring during the first 10 minutes of occlusion.

5.3.2 Quantitative and dynamic ECG changes

The amount of changes induced by balloon inflation, as expressed by the parameter $\Delta\mathcal{Y}(t)$, was determined. Averaged values of delta change for all pigs, $\overline{\Delta\mathcal{Y}}(t)$, ($\mathcal{Y} \in \{\mathcal{I}_{\text{US}}, \mathcal{I}_{\text{DS}}, R\text{a}, ST_{40}\}$), were computed in the precordial leads V1-V6. Similarly, $\overline{\Delta\mathcal{Y}}(t)$ values corresponding to those indices evaluated in leads derived from the QRS loop, $\mathcal{Y} \in \{\mathcal{I}_{\text{US}}, \mathcal{I}_{\text{DS}}\}$, and the VCG, $\mathcal{Y} \in \{QRS_{max}, QRS_{mean}, STVM, STCVM\}$, were also calculated.

The leads with the most substantial changes during occlusion were V2-V4 for the indices $\mathcal{I}_{\text{US}}$, $\mathcal{I}_{\text{DS}}$, R_a and ST_{40}. In Fig. 5.7 (top panels) averaged values, expressed as mean ± SD, for these four indices in lead V3 are shown. The first two panels at the top also display the averaged delta values for $\mathcal{I}_{\text{US}}$ and $\mathcal{I}_{\text{DS}}$ evaluated in normalized lead V3. Bottom panels of the same figure display the averaged delta values for $\mathcal{I}_{\text{US}}$ and $\mathcal{I}_{\text{DS}}$ evaluated in the

Table 5.3: Distribution of the largest changes across leads averaged over pigs for the different indices, expressed as mean ± SD. $\mathcal{I}_{\text{US}}$ and $\mathcal{I}_{\text{DS}}$ delta values are shown in both precordial and QRS loop-derived leads.

Lead	V2	V3	V4	LDL	VCG
	Mean ± SD	Mean ± SD	Mean ± SD	Mean ± SD	Mean ± SD
$\Delta\mathcal{I}_{\text{US}}$ (μV/ms)	47.3 ± 32.2	63.4 ± 36.2	43.9 ± 39.6	1.79 ± 34.6	—
$\Delta\mathcal{I}_{\text{DS}}$ (μV/ms)	31.2 ± 25.5	51.6 ± 31.4	53.7 ± 36.4	38.4 ± 27.3	—
ΔR_a (mV)	1.04 ± 0.49	1.36 ± 0.72	0.96 ± 0.78	—	—
ΔST_{40} (mV)	0.59 ± 0.33	0.74 ± 0.36	0.57 ± 0.34	—	—
ΔQRS_{max} (mV)	—	—	—	—	0.36 ± 0.41
$\Delta STCVM$ (mV)	—	—	—	—	0.66 ± 0.29

loop-derived lead as well as QRS_{max} and $STCVM$ indices evaluated from the VCG. It is important to mention that, due to the presence of VT/VF episodes during occlusion, abnormal beats were discarded and it is thus possible that, at some time instants, not all pigs analyzed in this study

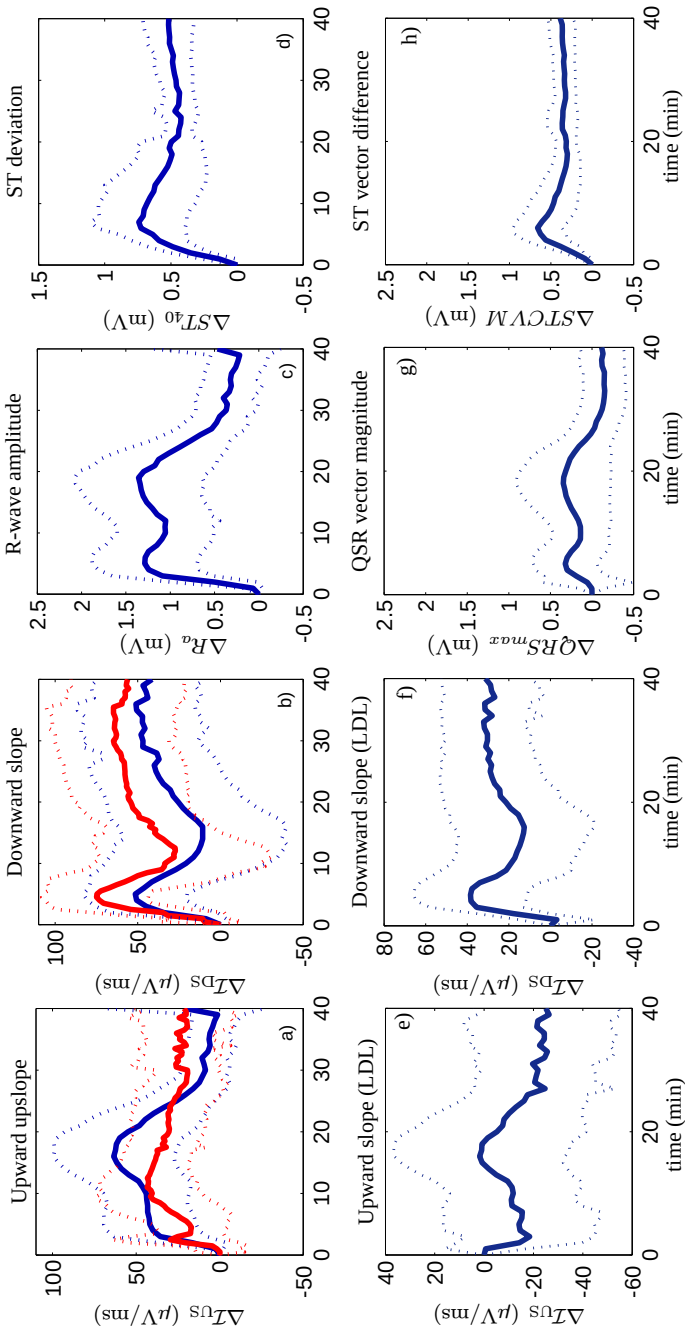

Figure 5.7: Top panels display mean ± SD of delta changes $\Delta\mathcal{Y}$, $\mathcal{Y} \in \{\mathcal{I}_{\text{US}}, \mathcal{I}_{\text{DS}}, R_a, ST_{40}\}$ for all pigs in lead V3, calculated every minute from the start of occlusion: (a) $\mathcal{I}_{\text{US}}$ in the original (dark blue) and normalized lead V3 (red); (b) $\mathcal{I}_{\text{DS}}$ in the original (dark blue) and normalized lead V3 (red); (c) R_a; (d) ST_{40}. Bottom panels display mean ± SD of $\mathcal{Y}$, with $\mathcal{Y}$ being: (e) $\mathcal{I}_{\text{US}}$ evaluated in QRS loop-derived lead; (f) $\mathcal{I}_{\text{DS}}$ evaluated in QRS loop-derived lead; (g) QRS_{max}; (h) $STCVM$.

are involved in the averages shown in Fig. 5.7. A summary of the most prominent changes found for all the indices shown in Fig. 5.7 is presented in Table 5.3.

5.3.3 Correlation analysis between ECG changes and MaR

5.3.3.1 Correlation with MaR using absolute ECG changes during occlusion

Changes in the ECG indices during the occlusion were correlated with the MaR marker defined in section 5.2.1.3. The averaged value and range of MaR in the study population was 39.0 ± 9.9 $(28:57)$% of the LV.

Upward slope change: Correlation analysis was performed considering $\Delta\mathcal{I}_{\text{US}}$ evaluated at the two prominent peaks identified during the occlusion in all the recordings. Results of the correlation analysis in the standard leads V1-V6 were non-significant for the second prominent peak, while for the first one a significant correlation was found between $\Delta\mathcal{Y}_{abs}$ ($\mathcal{Y} = \mathcal{I}_{\text{US}}$) and MaR, $r = 0.69$ ($p = 0.0167$). Table 5.4 presents the correlation coefficients obtained for all combinations of change defined in section 5.2.5. Additionally, correlation analysis was performed for $\mathcal{I}_{\text{US}}$ evaluated in the loop-derived lead, and poor correlation values were obtained between MaR and the maximum positive change $\Delta\mathcal{Y}_{max}$ for the two peaks.

R wave amplitude change: The R-wave amplitude changes, ΔR_a, in the two relevant peaks, were separately correlated with MaR. Correlation was, however, non-significant for any combination of change, as shown in Table 5.4.

Table 5.4: Correlation values between MaR and $\Delta\mathcal{Y}$, $\mathcal{Y} \in \{\mathcal{I}_{\text{US}}, \mathcal{I}_{\text{DS}}, R_a, ST_{40}\}$, evaluated at the timings corresponding to the relevant peaks observed for each of those indices during the occlusion.

MaR vs $\Delta\mathcal{Y}$	$\Delta\mathcal{Y}_{max}$ $r(p)$	$\Delta\mathcal{Y}_{pos}$ $r(p)$	$\Delta\mathcal{Y}_{abs}$ $r(p)$	$\Delta\mathcal{Y}_{real}$ $r(p)$
$\mathcal{I}_{\text{US}}$ 1^{st} peak	0.54 (0.0850)	0.52 (0.0971)	0.69 (0.0167)*	0.26 (0.4312)
$\mathcal{I}_{\text{US}}$ 2^{nd} peak	0.42 (0.1929)	0.44 (0.1774)	0.41 (0.2092)	0.36 (0.2692)
R_a 1^{st} peak	0.21 (0.5353)	0.43 (0.1825)	0.51 (0.1115)	0.44 (0.1724)
R_a 2^{nd} peak	0.28 (0.4230)	0.34 (0.3025)	0.32 (0.3307)	0.20 (0.5628)
$\mathcal{I}_{\text{DS}}$ 1^{st} peak	-0.75 (0.0045)*	-0.65 (0.0220)*	-0.63 (0.0265)*	-0.66 (0.0184)*
$\mathcal{I}_{\text{DS}}$ 2^{nd} peak	-0.67 (0.0237)*	-0.71 (0.0345)*	-0.08 (0.8101)	-0.77 (0.0054)*
ST_{40} peak	-0.25 (0.4351)	-0.34 (0.2814)	-0.34 (0.2805)	-0.34 (0.2828)

Downward slope change: As can be observed in Table 5.4, there was a significant, negative correlation between this index and MaR. In the case of the first positive peak, these negative correlation values mean that more pos-

itive $\Delta\mathcal{I}_{\mathrm{DS}}$ values ($\mathcal{I}_{\mathrm{DS}}$ becoming less steep) correspond to smaller MaR. For the second negative deflection, these negative correlation values mean that lower $\Delta\mathcal{I}_{\mathrm{DS}}$ values ($\mathcal{I}_{\mathrm{DS}}$ becoming steeper) correspond to larger MaR. Regarding the first positive peak in the evolution of $\Delta\mathcal{I}_{\mathrm{DS}}$ during occlusion, the most significant correlation was found between MaR and $\Delta\mathcal{Y}_{max}$, $r = 0.75$ ($p = 0.0040$), whereas for the second negative deflection in $\Delta\mathcal{I}_{\mathrm{DS}}$, the most significant correlation was found between MaR and $\Delta\mathcal{Y}_{real}$, $r = -0.77$ ($p = 0.0054$). The delta value corresponding to the second negative deflection following the initial first positive peak takes either negative or positive value depending on the evaluated subject, and in average is close to zero, as can be appreciated in Fig. 5.8, which shows $\Delta\mathcal{I}_{\mathrm{DS}}$ averaged over pigs every 10 sec during occlusion in lead V3. The correlation results obtained for all combinations of change in $\Delta\mathcal{I}_{\mathrm{DS}}$ are shown in Table 5.4.

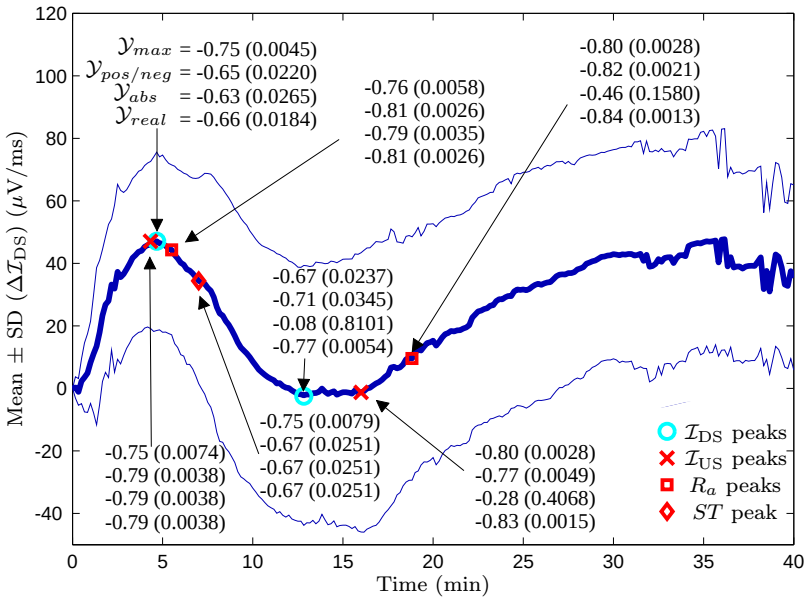

Figure 5.8: Average delta values of $\Delta\mathcal{I}_{\mathrm{DS}}$ (mean ± SD) evaluated every 10 s from the start of occlusion. Red marks indicate the timings of the relevant peaks found for each of the other indices, i.e. R_a, $\mathcal{I}_{\mathrm{US}}$ and ST_{40}. The blue circles indicate the timing of $\Delta\mathcal{I}_{\mathrm{DS}}$ positive peak and negative deflection. The numbers inside the graph express the correlation values obtained for $\mathcal{I}_{\mathrm{DS}}$ combinations of change (ordered like in equations (5.6)–(5.9)) at specific time instants, which are pointed to their corresponding marks by black arrows.

ST level change: The positive peak observed in ST_{40} during the first 10 minutes of occlusion is the most prominent one for this index. Similarly to the results obtained for $\Delta\mathcal{I}_{\mathrm{DS}}$, correlation between ST_{40} and MaR was negative, although non-significant, as summarized in Table 5.4.

Fig. 5.8 shows the time course evolution of $\Delta\mathcal{I}_{\mathrm{DS}}$ averaged for all pigs and expressed as mean ± SD. Correlation values between MaR and the different combinations of change evaluated for $\Delta\mathcal{I}_{\mathrm{DS}}$, but at the timings corresponding to the peaks found for each of the other indices, are displayed in the figure in association with their positions in time. Increased correlation between $\Delta\mathcal{I}_{\mathrm{DS}}$ and MaR was observed at some of those other temporal positions. Similarly to the results presented in Figure 5.8 for $\Delta\mathcal{I}_{\mathrm{DS}}$, correlation analysis was additionally performed for all the other indices, i.e. R_a, ST_{40} and $\Delta\mathcal{I}_{\mathrm{US}}$, considering their delta changes evaluated at time instants associated with relevant peaks observed in the rest of the analyzed indices. Correlation values with MaR did not increase with respect to the results shown in table 5.4, except for $\Delta\mathcal{Y}_{max}$ for $\mathcal{Y} = \Delta\mathcal{I}_{\mathrm{US}}$, evaluated at the timing of the positive peak corresponding to $\mathcal{I}_{\mathrm{DS}}$, for which correlation with MaR was $r = 0.76$ ($p = 0.01$).

Evaluation of the correlation between MaR and $\Delta\mathcal{I}_{\mathrm{US}}$ and $\Delta\mathcal{I}_{\mathrm{DS}}$ in normalized leads did not lead to higher correlation coefficients. For both indices, this correlation was non-significant in all cases. Evaluation of $\Delta\mathcal{I}_{\mathrm{US}}$ and $\Delta\mathcal{I}_{\mathrm{DS}}$ in normalized leads but considering the time instants corresponding to relevant peaks observed in the original leads did not increase the correlation values directly obtained for the original precordial leads.

Table 5.5: Correlation values between MaR and changes observed in $STCVM$, QRS_{max} and QRS_{mean}, at their most relevant peaks during occlusion.

Index	$r(p)$
$STCVM$(max)	0.19 (0.5219)
QRS_{max} 1^{st} peak	0.47 (0.1661)
QRS_{max} 2^{nd} peak	0.42 (0.2202)
QRS_{mean} 1^{st} peak	0.45 (0.1920)
QRS_{mean} 2^{nd} peak	0.45 (0.1920)

Finally, correlation analysis carried out for QRS_{max}, QRS_{mean} and $STCVM$ indices are summarized in Table 5.5. None of these indices showed any significant correlation with MaR.

5.3.3.2 Correlation with MaR adding the temporal aspects of the peaks

The timings of relevant peaks in any lead and for any of the indices analyzed in this study did not correlate strongly with MaR. However, differences between the timings of the two more prominent peaks of R_a significantly correlated with MaR in lead V3, $r = -0.62$ ($p = 0.04$), indicating that shorter time between the two marked peaks was associated with larger MaR.

Indices combining absolute ECG changes occurring at prominent peaks

with their corresponding timings, quantified by $\Delta\mathcal{Y}^l_{max}{\cdot}t^l_{max}$ and $\Delta\mathcal{Y}^l_{max}/t^l_{max}$, were also correlated with MaR. In lead V3, both indices showed a negative correlation with MaR when $\Delta\mathcal{I}_{\text{DS}}$ was taken at the second negative peak ($r = -0.72$; $p = 0.01$ for $\Delta\mathcal{Y}^l_{max} \cdot t^l_{max}$ and $r = -0.68$; $p = 0.02$ for $\Delta\mathcal{Y}^l_{max}/t^l_{max}$. Likewise, the correlation was significant in lead V2, but just for $\Delta\mathcal{Y}^l_{max}/t^l_{max}$, with $r = -0.62$ ($p = 0.04$). In all other cases the correlation was NS.

5.3.4 Correlation between ECG changes and IS

Table 5.6 summarizes the correlation coefficients obtained for the same combinations of ECG changes presented in table 5.4, but correlated to IS rather than to MaR. Results show that the indices that best correlate with IS are the ST level deviation ST_{40} and the downward slope $\mathcal{I}_{\text{DS}}$ (first positive peak), suggesting that changes developed in the latter part of the QRS complex and in the ST segment are more associated with the final size of the infarct than changes observed in the early part of the QRS complex. Similar to the results obtained for MaR, there is an inverse but strong correlation between $\mathcal{I}_{\text{DS}}$ or ST_{40} and IS. Changes in ST_{40} were significantly correlated with IS in all possible combinations of changes whereas for $\mathcal{I}_{\text{DS}}$ only $\Delta\mathcal{Y}_{max}$ (r= -0.65, p=0.0217) and $\Delta\mathcal{Y}_{real}$ (r= -0.53, p=0.0265) were significantly correlated.

Indices derived from the VCG ($STCVM$, QRS_{max} and QRS_{mean}) were also correlated with IS but low, non-significant correlation was found in all cases.

Table 5.6: Correlation values between IS and $\Delta\mathcal{Y}$, $\mathcal{Y} \in \{\mathcal{I}_{\text{US}}, \mathcal{I}_{\text{DS}}, R_a, ST_{40}\}$, evaluated at the timings corresponding to the relevant peaks observed for each of those indices during the occlusion. The (*) mark indicates significant correlation ($p < 0.05$).

IS vs $\Delta\mathcal{Y}$	$\Delta\mathcal{Y}_{max}$ $r(p)$	$\Delta\mathcal{Y}_{pos/neg}$ $r(p)$	$\Delta\mathcal{Y}_{abs}$ $r(p)$	$\Delta\mathcal{Y}_{real}$ $r(p)$
$\mathcal{I}_{\text{US}}$ 1^{st} peak	0.51 (0.1099)	0.46 (0.1543)	0.61 (0.1518)	0.25 (0.4512)
$\mathcal{I}_{\text{US}}$ 2^{nd} peak	0.20 (0.5573)	0.18 (0.5952)	0.24 (0.4854)	0.07 (0.8388)
R_a 1^{st} peak	0.30 (0.3710)	0.17 (0.6144)	0.25 (0.4512)	0.18 (0.5952)
R_a 2^{nd} peak	0.26 (0.4345)	0.26 (0.4345)	0.20 (0.5575)	0.12 (0.7342)
$\mathcal{I}_{\text{DS}}$ 1^{st} peak	-0.65 (0.0217)*	-0.51 (0.0923)	-0.49 (0.1085)	-0.53 (0.0265)*
$\mathcal{I}_{\text{DS}}$ 2^{nd} peak	-0.42 (0.2695)	-0.13 (0.7435)	-0.13 (0.7435)	-0.13 (0.7435)
ST_{40} peak	-0.59 (0.0431)*	-0.67 (0.0162)*	-0.68 (0.0157)*	-0.67 (0.0168)*

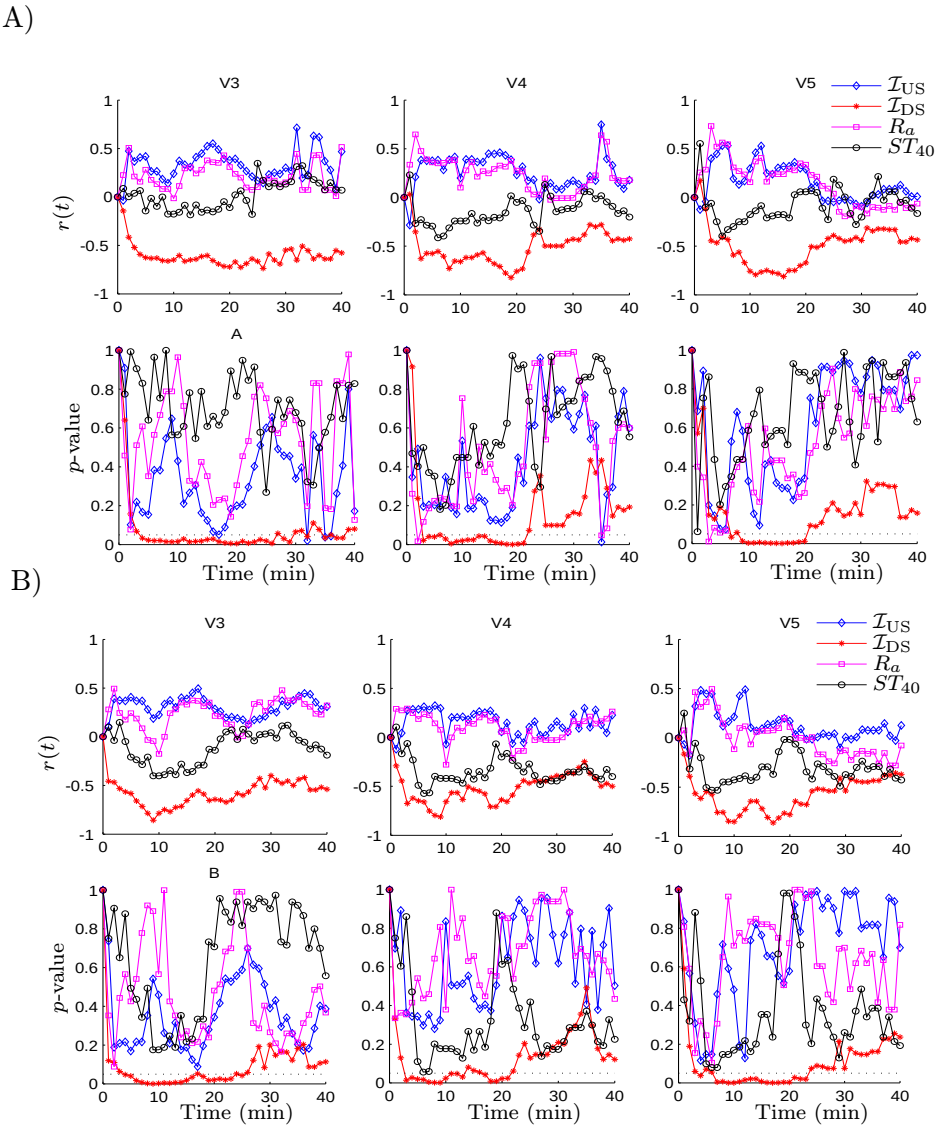

Figure 5.9: Dynamic correlation along the occlusion period between the changes in the ECG indices and A) MaR, B) IS.

5.3.5 Dynamic relationship between ECG changes and MI

The evolution of the dynamic correlation between each of the indices $\mathcal{I}_{\text{US}}$, $\mathcal{I}_{\text{DS}}$, R_a and ST_{40} and MaR/IS throughout the occlusion was analyzed in precordial leads V1-V6. Fig. 5.9 shows the time-course of the obtained correlation coefficients in leads V3-V5. As can be observed, all correlation values obtained for $\mathcal{I}_{\text{DS}}$ during the occlusion were negative, corroborating its inverse relationship with MaR and IS. A similar observation can be noted for the ST level, but in this case correlation is non-significant at any time. The timing where changes in $\mathcal{I}_{\text{DS}}$ start to be significantly correlated with MaR and IS lies within the interval between the first 3-4 minutes after the start of occlusion and minute 22. The maximum correlation values were achieved around minute 9 for IS (see Fig. 5.9 B), while for MaR the maximum value was dependent on the lead (see Fig. 5.9 A). For the rest of indices, correlation was non-significant along the occlusion.

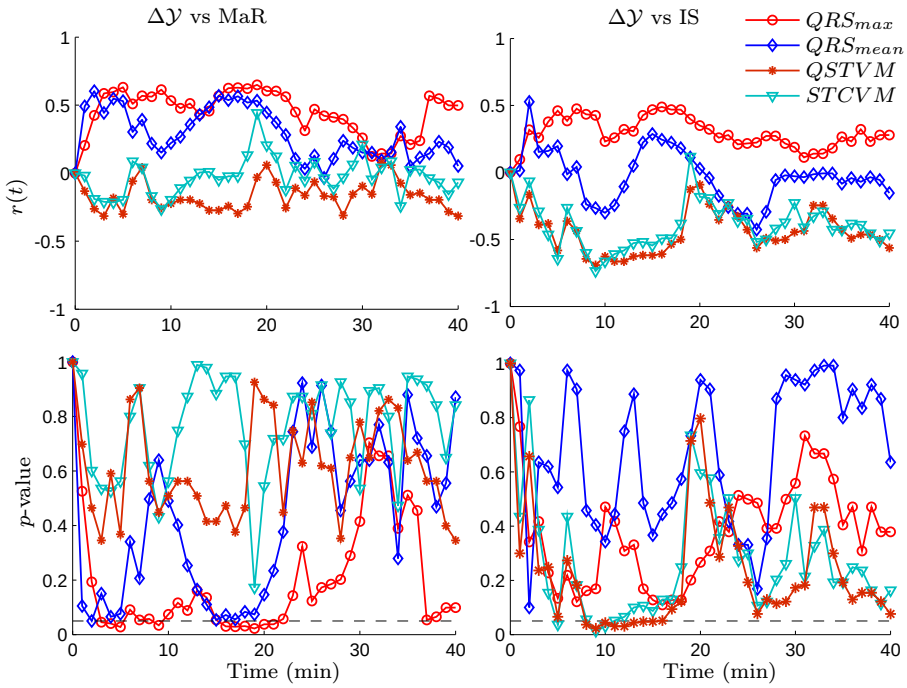

Figure 5.10: Time-course correlation between changes in the VCG-derived indices and MaR (left column) and IS (right column).

The same analysis was performed for the indices derived from the VCG ($STVM$, $STCVM$, QRS_{max} and QRS_{mean}) and results are shown in Fig. 5.10. From the figure it is clear that QRS$_{max}$ and QRS_{mean} better correlated better with MaR while $STVM$ and $STCVM$ better correlated with IS. The timing of maximum correlation between $STVM/STCVM$ and IS was

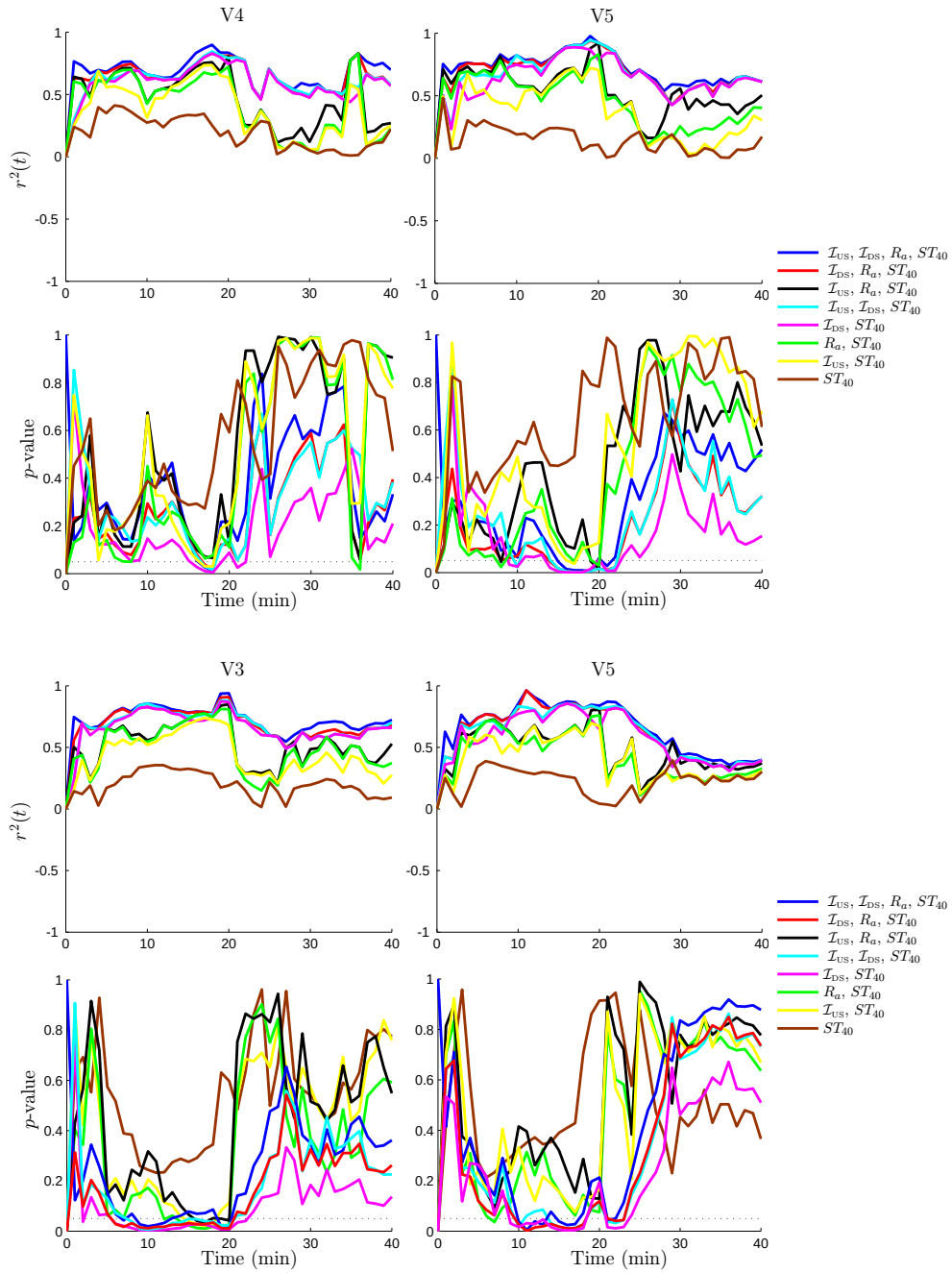

Figure 5.11: Results from the MLR analysis compared with the single linear regression analysis between ST changes and A) MaR, B) IS.

around minute 9-10. After that moment, correlation begins to decrease and only some fluctuations can be observed at the end of occlusion. Regarding QRS_{max} and QRS_{mean} and their correlation to MaR, two important peaks, with significant correlation values, can be observed in the first 20 minutes of occlusion, which may be associated with the two peaks observed in the time-course evolution of those indices.

As can be observed, all correlation values obtained for $\mathcal{I}_{\text{DS}}$ during occlusion time were negative corroborating its inverse relationship with the MaR and IS. The same is also noted with the ST level but being not significant at any time. The timing where changes in $\mathcal{I}_{\text{DS}}$ start to be significantly correlated with MaR and IS are found in the first 3-4th minutes after start of occlusion, and lasted until minute 22th. The maximum correlation values were achieved around minute 9th for IS marker (see Fig. 5.9 B) since for MaR is more changing depending on the lead (see Fig. 5.9 A). For the rest of indices, not significant correlation was observed during occlusion.

The results described above are restricted to the analysis of the correlation between a particular ECG index and MaR/IS. However, if more than one ECG index is analyzed to explain the ischemia or the size of the infarct, better results are obtained. Fig. 5.11 shows the evolution of the outcome from the MLR analysis during occlusion considering different combinations of ECG indices. The ST level (ST_{40}) was firstly correlated with MaR and IS independently (Pearson correlation coefficient, r^2). Subsequently, QRS-derived indices were added one-by-one, individually and also in combination. Increases in the percent of explanation of the MaR and IS markers is clearly evident when adding QRS changes on top of ST changes. Also in this case, after approximately minute 22 the strong correlation achieved between ECG changes and MaR/IS markers gradually begins to fall and only some fluctuations can be observed at the end of the occlusion. The combination involving changes in all indices ($\mathcal{I}_{\text{US}}$, $\mathcal{I}_{\text{DS}}$, R_a and ST_{40}) explains the developed MaR and IS.

5.4 Discussion

Ischemia-induced ECG changes in depolarization and repolarization

In this study several indices derived from the ECG signal during both depolarization and repolarization phases were evaluated in an experimental, closed chest porcine myocardial infarction model produced by 40-minute coronary balloon inflation.

Depolarization changes observed in R_a, $\mathcal{I}_{\text{US}}$ and QRS_{max} presented temporal patterns during the coronary occlusion that showed two well-defined phases, with two marked positive peaks. These two phases have been de-

scribed for other electrophysiological indices and have been related to the incidence of arrhythmias[98,99]. In the present study population, the largest changes of these QRS-derived indices, especially for $\mathcal{I}_{\text{US}}$ and QRS_{max}, were seen during the second phase rather than the first one, and were located in time between the 11^{th} and 22^{nd} minutes of occlusion.

QRS_{max} and $\mathcal{I}_{\text{US}}$ are directly influenced by the R wave amplitude. As illustrated in Figure 5.5, a giant R wave quickly developed during the first 4 minutes of coronary occlusion, and also later in time around 11–22 minutes. This particular finding has been reported in previous studies carried out in experiments with pigs[86] and also in humans[100]. However, those other studies did not focus their attention on the two different peaks in R_a evolution. Chang *et al.*[86] studied the presumable genesis for this giant R wave during transient transmural ischemia and hyperacute phase of transmural myocardial infarction by the analysis of different factors. They concluded that the origin of the giant R wave is the slowed conduction velocity into the ischemic tissue, which led to the formation of a homogeneous and discrete wavefront advancing toward the center of the ischemia from its lateral and subendocardial areas. These two local wavefronts do not cancel but instead complement each other. Thus, the activation of the ischemic tissue remains temporally isolated from the non-ischemic one giving rise to the development of a giant R wave. This appreciation was confirmed by Birnbaum and Drew[101], who additionally mentioned that many other factors influence the R wave amplitude, so that this parameter is not helpful in determining the amount of the developed myocardial ischemia, as corroborated in our study.

A somewhat different behavior was observed for the $\mathcal{I}_{\text{DS}}$ index, which presented a biphasic pattern, starting with a substantial decrease during the first 5 minutes (positive peak in $\Delta\mathcal{I}_{\text{DS}}$) followed by an increase until around the 12^{th} minute, reflected in $\Delta\mathcal{I}_{\text{DS}}$ by a negative deflection. Subsequently, a second gradual decrease in $\mathcal{I}_{\text{DS}}$ was observed until the end of the occlusion (Figure 5.7 (b) and (f)). That biphasic pattern was even more marked when $\mathcal{I}_{\text{DS}}$ was evaluated in normalized leads, suggesting an evident increase in the QRS width during the first minutes of occlusion, despite the fact that the QRS amplitude also increases during those first minutes. Figure 5.7 (b) shows how the normalization procedure applied to the QRS amplitude emphasizes the first positive peak in $\Delta\mathcal{I}_{\text{DS}}$ of the normalized leads with respect to $\Delta\mathcal{I}_{\text{DS}}$ evaluated in the original precordial leads. Some minutes later during the occlusion and after the second negative deflection in $\Delta\mathcal{I}_{\text{DS}}$, $\mathcal{I}_{\text{DS}}$ became less steep again, even though QRS amplitude (see R_a and QRS_{max} indices in Figure 5.7 (c) and (g)) increased until around minute 20 and ST elevation became less marked. Finally, the further diminution of the R wave amplitude combined with the remaining ST elevation from minute 20 until the end of occlusion led to the continuous decline of the $\mathcal{I}_{\text{DS}}$ index.

ST-segment elevation, a classical index traditionally used for detecting

transmural ischemia, developed a clear peak during the first 5–12 minutes of the occlusion in almost all the analyzed leads. After this time, the ST level started to decrease until the end of the occlusion, reaching around 50% of its maximal developed change (see Figure 5.7 (d) and (h)). The maximum peak of ST elevation at approximately 5–12 minutes as well as the latter decrease until the end of the coronary occlusion was similarly reported by Kjekshus *et al.*[102]. Likewise, ST elevation was postulated as a valid marker of myocardial ischemia only in the first few minutes following the coronary occlusion, confirming that it became maximal around the initial 10–15 minutes with a subsequent decline after this time[103]. As described earlier[104], a plausible mechanism underlying the subsequent decline (after minutes 15–20) may be related to an increase of resistance between adjacent cells, affecting the gap junctions and leading to cell-to-cell uncoupling. This cell-to-cell uncoupling has been suggested to be triggered by a change in intracellular $[Ca^{2+}]$[105–107].

Regarding the amount of change quantified by the parameter $\Delta\mathcal{Y}$ for all the analyzed indices, $\mathcal{Y} \in \{\mathcal{I}_{\text{US}}, \mathcal{I}_{\text{DS}}, R_a, ST_{40}\}$, it was found that lead V3 was the most sensitive one, even more than leads derived from the spatial QRS loop, in contrast with our previous results in patients undergoing PCI[81]. This finding can be associated with the marked rotation observed in the maximum vector magnitude direction within the QRS loop, also reported in[89], which is used to project the VCG onto its dominant direction to obtain the QRS loop-derived lead. Care should be taken when interpreting changes just looking to electrophysiology and not realizing of the geometrical implications.

Correlation between ECG changes and the amount of ischemia

In the correlation analysis the only parameters showing a significant correlation to MaR were the QRS slope changes. Of the classical ECG indices, neither ST elevation nor R_a showed any significant correlation to the amount of ischemia. However, in contrast to our previous findings in a human model of shorter transmural ischemia produced by PCI[108], this longer, porcine experimental infarction model showed negative correlation between changes in the R-wave downslope, $\mathcal{I}_{\text{DS}}$, and MaR. This finding cannot be fully explained and further studies are needed to elucidate its underlaying basis.

Changes in the R-wave upslope, $\mathcal{I}_{\text{US}}$, showed a significant, however positive correlation to MaR, as quantified using the sum of absolute change $\Delta\mathcal{Y}_{abs}$ in V1-V6 in the first peak, as well as the maximum change $\Delta\mathcal{Y}_{max}$ at the timing of the first, positive peak of $\mathcal{I}_{\text{DS}}$.

The correlation between MaR and QRS_{max}, which is a spatial projection of the maximum amplitude of the QRS complex, was also positive, a finding consistent with the results reported in[89], although in the present study it was non-significant.

As shown before, the QRS slope changes are dependent on both changes in the QRS amplitude and duration[24]. This is furthermore supported in this study by the results of the R wave normalization, with loss of significance when correlating $\Delta\mathcal{I}_{\mathrm{DS}}$ with MaR in the normalized leads, indicating that the combination of both QRS amplitude and duration variations reflected by $\Delta\mathcal{I}_{\mathrm{DS}}$ better correlate with MaR than changes in $\mathcal{I}_{\mathrm{DS}}$ due to the QRS width only. Additionally, it was shown that correlation was non-significant between ΔR_a and MaR.

Another important finding of the present study was that all significant correlation values were found in standard precordial leads V1-V6. No extra value was added by using loop-derived leads, or vector-based QRS or ST indices.

Negative, non-significant correlation coefficients were obtained when ST_{40} changes were correlated with MaR, in agreement with the results reported by Demidova *et al.*[91] when investigating ST level changes in a subset of the present population. Many other studies, however, have shown opposite results when correlating ST level and MaR, both in humans and in animal experiments[102,109,110]. Our finding of negative correlation between MaR and ST_{40} cannot be clearly explained and needs to be further explored in future studies. One possible explanation could perhaps be that all subjects in the present study developed large anterior MaR (mean 39 ± 9.9, range 28 to 57 % of the LV), and within this range and location the correlation between ECG indices and MPS might be different from the one evaluated for a wider range of ischemic areas including also much smaller areas as well as different locations of ischemia. However, this hypothesis needs to be confirmed in future studies.

Although the ST segment elevation during acute myocardial ischemia has been widely studied by many authors in both humans and animals, the relationship between alterations in depolarization and later signs of ischemic damage have been less studied. This study has shed light on that relationship.

Correlation between ECG changes and the infarct size

As in the correlation with MaR, the $\mathcal{I}_{\mathrm{DS}}$ and ST_{40} changes negatively correlated with IS, being in this case significant for the ST_{40} index as well. All defined combinations of change for ST_{40} strongly correlated with IS whereas only $\Delta\mathcal{Y}_{max}$ and $\Delta\mathcal{Y}_{real}$ referred to the first peak did so for $\mathcal{I}_{\mathrm{DS}}$. On the other hand, neither R_a nor $\mathcal{I}_{\mathrm{US}}$ presented any significant relationship with IS for any of the combinations of change. These results suggest that the IS marker could be better related to changes in the ST segment and the second half of the QRS complex than with the changes occurring at the beginning of it. To confirm this statement, changes in all indices, taken every minute, were correlated with MaR and with IS throughout the occlusion. As expected,

indices associated with the QRS complex like QRS_{max} and QRS_{mean} were better related to MaR than indices related to the ST level ($STVM$ and $STCVM$), while the latter were better related to IS (see Fig. 5.10). In precordial leads V1-V6, the changes in the ST level showed strong correlation with IS, however, changes in the R-wave amplitude and the upward slope did not strongly correlated with MaR. Meanwhile, the downward slope showed a negative, but very good correlation with both markers, mostly with IS (see Fig. 5.9).

Timing of ECG changes

One of the main observations of this study is that ST elevation peaked earlier in time than QRS_{max} and $\mathcal{I}_{\text{US}}$ (referring to the second peak of those two indices, of larger amplitudes than the first one), indicating that more changes are still occurring during depolarization when changes at repolarization have already reached their maximum levels. Thus, changes in depolarization occurring some minutes later during occlusion could be in better correspondence with MaR or IS as determined by MPS.

In relation to that, the correlation between $\mathcal{I}_{\text{DS}}$ and MaR was strong when the changes were evaluated at the most relevant peaks (positive and negative) observed in $\mathcal{I}_{\text{DS}}$, but even stronger for the second peak occurring later in time. Furthermore, the correlation between $\mathcal{I}_{\text{DS}}$ changes and MaR was not only significant when evaluated at its own peak values during the occlusion, but also when evaluated at the timing of the peaks of other indices, as displayed in Figure 5.8. All the above arguments postulate the downward slope $\mathcal{I}_{\text{DS}}$, which combines both QRS amplitude and duration, as a potential predictor of the ischemic process.

Chapter 6
Conclusions and future extensions

6.1 Conclusions

In the following the most important contributions of this thesis are summarized.

6.1.1 QRS slopes for ischemia monitoring

In this thesis a robust methodology was developed to quantify the three main slopes within the QRS complex, namely the R-wave upward slope ($\mathcal{I}_{\mathrm{US}}$), the R-wave downward slope ($\mathcal{I}_{\mathrm{DS}}$) and the S-wave slope ($\mathcal{I}_{\mathrm{TS}}$). The methodology includes a normalization step that improves sensitivity of the QRS slopes to ischemia-induced changes, caused by elective PCI in patients with stable angina pectoris.

The first study of the thesis, presented in chapter 2, showed that QRS slopes and their variations at resting state after normalization present a high intra-individual stability, thus being suitable for characterizing dynamic changes due to ischemia. The downward slope of the R-wave, $\mathcal{I}_{\mathrm{DS}}$, was the one with the most marked changes due to ischemia, however with a similar behavior to that of the S-wave slope, $\mathcal{I}_{\mathrm{TS}}$, confirming that the effects of ischemia are most likely to be found in the latter part of the depolarization phase. Evolution of QRS slopes in leads obtained by projection of spatial QRS loops led to improved sensitivity to the induced ischemia as compared to evaluation of QRS slopes in the standard ECG leads.

Temporal analysis during PCI showed that significant changes in QRS slopes $\mathcal{I}_{\mathrm{US}}$ and $\mathcal{I}_{\mathrm{DS}}$ occurred between 30 s and 2 min after initiation of the coronary occlusion, depending on the analyzed lead. Changes in the downward slope, $\mathcal{I}_{\mathrm{DS}}$, usually occurred earlier than in the upward slope $\mathcal{I}_{\mathrm{US}}$. Our findings point out that QRS slope analysis could be used as a robust

method of depolarization evaluation, providing additional information to that from the repolarization phase for risk stratification during monitoring of patients with acute ischemia.

6.1.2 Spatial profiles of QRS slope changes

The QRS slopes evaluated during ischemia additionally showed remarkable spatial lead-by-lead profiles for each of the analyzed sites (LAD, RCA and LCX), suggesting that they could be used for identification of the occluded artery. In particular, the downward slope $\mathcal{I}_{\mathrm{DS}}$ presented a spatial profile similar to those obtained for the S-wave amplitude (S_a) and the ST level (ST), indicating a strong dependence of $\mathcal{I}_{\mathrm{DS}}$ on those two indices. Dynamic changes of $\mathcal{I}_{\mathrm{DS}}$ during coronary artery occlusion strongly correlated to the extent and severity of ischemia assessed by myocardial scintigraphy, providing information beyond that obtained by conventional ST-segment analysis, as corroborated by a multiple regression analysis involving changes in both indices.

6.1.3 Ischemia detection by a QRS angle-based method

A new QRS angle-based approach was proposed for evaluation of ischemia-induced changes during PCI. The approach involved the evaluation of three angles within the QRS complex: the R-wave angle (ϕ_{R}), the up-stroke angle (ϕ_{U}) and the down-stroke angle (ϕ_{D}). Changes in the R-wave angle (ϕ_{R}), seen as a surrogate marker of QRS duration, were suggested to be used as predictors of the extent and severity of the ischemia, both by themselves and in conjunction to ST changes. The suggestion was based on the fact that changes in ϕ_{R}, particularly when evaluated in relative terms with respect to baseline, strongly correlated with ischemia characteristics.

On the other hand, the angles ϕ_{U} and ϕ_{D} showed a sudden and very abrupt change in response to the induced ischemia, as compared to the more gradual change seen in ϕ_{R}. The behavior of ϕ_{U} and ϕ_{D} suggested that they could be used in the development of an ischemia detector. The detector was implemented by modeling ischemia-induced changes as step-like changes with a linearly gradual transition plus additive Laplacian noise. Results showed a high sensitivity and positive predictive value in the detection of ischemic events, particularly in patients with LAD occlusion, as they presented the highest ECG changes following coronary occlusion.

6.1.4 Depolarization analysis applied to a porcine model of myocardial infarction

The ECG indices analyzed in chapters 2 and 3 were subsequently evaluated in a porcine model of myocardial ischemia and infarction. Analysis of ECG

recordings acquired during 40-min LAD occlusion in pigs revealed that indices associated with the earlier part of the depolarization phase (upward slope $\mathcal{I}_{\mathrm{US}}$ and maximum QRS vector magnitude QSR_{max}) presented temporal patterns of variation during coronary occlusion similar to that of the R-wave amplitude (R_a), and did not correlate with the myocardium at risk. On the other hand, indices associated with the latter part of the depolarization phase (downward slope $\mathcal{I}_{\mathrm{DS}}$), reflecting changes both in the amplitude and width of the QRS complex as well as distortion in the final part of the complex, are better predictors of the myocardium at risk in acute myocardial ischemia. The first 4–21 minutes of coronary occlusion represented the most significant ones in terms of correlation between changes in ECG-derived indices and the myocardium at risk. Despite species differences, the findings in the animal experiments analyzed in this thesis served to understand the electrophysiological changes occurring following long periods of ischemia.

6.2 Future extensions

6.2.1 Evaluation of QRS slopes in other clinical settings

A robust method for quantification of QRS slopes was developed and evaluated in two different ischemia models, based on a human and pig population, respectively. The sensitivity of the QRS slopes to the ischemia-induced changes and its relationship with ischemia properties was reported. However, the method could have a potential application in monitoring stress tests, where ischemia develops as stress progresses. The main challenge in this application is the high level of noise present in that type of recordings. Specific filters to avoid or attenuate such noise could be considered alongside with the QRS slopes calculation.

Another aspect of QRS slopes that deserves further attention is its potential use for identification of the occluded artery. Both the 2D and 3D spatial lead profiles presented in chapter 3 indicated that the QRS slopes could be used for that purpose. Different classifiers should be evaluated and their performance should be tested for separation of the different artery groups, particularly for distinguishing RCA and LCX, which is the most challenging one.

6.2.2 Ischemia detection

Robust ischemia detectors are required to identify ischemic events in clinical situations. The ischemia detector proposed in chapter 4 of this thesis used the QRS angles as trigger inputs and showed good performance in the specific model of PCI-induced myocardial ischemia, particularly in patients with LAD occlusion. Additional validation should be provided by evaluation in other databases, such as the European Society of Cardiology ST-T database

(ESCDB) and the Long Term ST Database (LTSTDB), which contain ECG recordings of 2-hour and 24-hour duration, respectively, and a considerable number of annotated ischemic and non-ischemic ST-segment changes in real situations.

The ischemia detector could be further improved by including a step in its design in which the duration of the ischemic changes transition was estimated, and thus the size of the analysis window could be set accordingly.

On top of providing information on the timing of ischemic events, the detector could additionally inform about the site of the damaged/occluded artery. Since the leads where the ECG changes are the largest, are those close to the ischemic region, the detector could quantify the outputs for the different analyzed leads and assess the most probable site of occlusion. Alternatively, three independent detectors could be designed each working on the set of leads usually affected by one of the three main coronary arteries (LAD, RCA, LCX).

Appendix A
Scientific publications

Most contributions derived from the present thesis have been published in the following works:

Journal articles:

- D. Romero, M. Ringborn, P. Laguna, O. Palhm, E. Pueyo. Depolarization changes during acute myocardial ischemia by evaluation of QRS slopes. Standard lead and vectorial approach. *IEEE Transactions on Biomedical Engineering*, 2011, 58(1), 110-120.
- M. Ringborn, D. Romero, E. Pueyo, O. Pahlm, G.S. Wagner, P. Laguna and P.G. Platonov. Evaluation of depolarization changes during acute myocardial ischemia by analysis of QRS slopes. *Journal of Electrocardiology,* 2011, 44(4), 416-424.
- D. Romero, M. Ringborn, M. Demidova, S. Koul, P. Laguna, P. Platonov, E. Pueyo. Characterization of ventricular depolarization and repolarization changes in a porcine model of myocardial infarction. *Physiological Measurement*, 2012, 33(12), 1975.
- D. Romero, M. Ringborn, P. Laguna and E. Pueyo. Detection and quantification of acute myocardial ischemia by morphologic evaluation of QRS changes by an angle-based method. *Journal of Electrocardiology,* 2013, 46(3), 204-214.

International conferences contributions:

- D. Romero, E. Pueyo, M. Ringborn, P. Laguna. QRS slopes for ischemia monitoring in PCI recording. In *World Congress on Medical Physics and Biomedical Engineering, September 7-12, 2009, Munich, Germany* (pp. 1695-1698). Springer Berlin Heidelberg.
- D. Romero, E. Pueyo, M. Ringborn, P. Laguna. Spatial characterization of ischemia in 12-lead ECG recordings during PCI using both depolarization and repolarization indices. *In Computers in Cardiology, 2009.* IEEE, 2009. p. 113-116.

- D. Romero, E. Pueyo, M. Ringborn, P. Laguna. Pendientes del QRS para la monitorización de isquemia en registros de intervención coronaria percutánea. *Proceedings XXVII Congreso Anual de la Sociedad Española de Ingeniería Biomédica*, pp.

- M. Ringborn, D. Romero, O. Pahlm, G. Wagner, P. Laguna, E. Pueyo, P. Platonov. Analysis of QRS slopes as a measure of depolaritazion change during acute myocardial ischemia. *37th International Congress on Electrocardiology*, 2010. Lund, Sweden.

- D. Romero, M. Ringborn, P. Laguna, O. Pahlm, E. Pueyo. A Vectorial Approach for Evaluation of Depolarization Changes during Acute Myocardial Ischemia. *In Computing in Cardiology, 2010.* IEEE 2010, pp.

- D. Romero, M. Ringborn, P. Laguna, O. Pahlm, E. Pueyo. Análisis Espacial en la Evaluación de Cambios de la Despolarización Cardíaca durante Isquemia Aguda de Miocardio. *In V Congreso Latinoamericano de Ingeniería Biomédica*, CLAIB 2011, pp:1-4.

- D. Romero, M. Ringborn, E. Pueyo, O. Palhm, G.S. Wagner, P. Laguna, P. Platanov. Análisis de la despolarización en isquemia de miocardio mediante la evaluación de las pendientes del QRS. *Proceedings XXIX Congreso Anual de la Sociedad Española de Ingeniería Biomédica.* pp. 41-44.

- D. Romero, P. Laguna, E. Pueyo. Detecting acute myocardial ischemia by evaluation of QRS angles. *VII Workshop on Biosignal Interpretation (BSI 2012).* 2012. Published in the International Journal of Bioelectromagnetism, vol. 15, No. 1 pp. 77-82, 2013.

Collateral contributions not included in the thesis:

- M. Demidova, A. Martin-Yebra, J.P. Martínez, V. Monasterio, S. Koul, Jesper van der Pals, D. Romero et al. T-wave alternans in experimental myocardial infarction: time course and predictive value for the assessment of myocardial damage. *J Electrocardiol.* 2013, 46(3), 263-9

- A. Alcaine, R. Bailón, D. Romero, E. Pueyo, P. Laguna. ECG amplitude Modulation in the Very-Low-Frequency Band in Patients with Angina Pectoris. *In Computing in Cardiology*, Hangzhou, China, 2011.

- L. PB Meijs, L. Galeotti, E. Pueyo, D. Romero *et al.* Increased T-amplitude with decreased ST-elevation characterizes ischemic preconditioning: A Simulation, Experimental and Clinical Study. *ISCE 2012 Annual Meeting*, Harrisburg (USA).

Appendix B

Acronyms

3D	Three-dimensional
AF	Atrial fibrillation
AFL	Atrial flutter
AP	Action potential
APD	Action potential duration
AV	Atrioventricular node
BPC	Body postural changes
CAD	Coronary artery disease
CT	Computed tomography
CVD	Cardiovascular disease
ECG	Electrocardiogram
EGE	Early Gd enhancement, equivalent to early ce-MRI
EMG	Electromyogram
EPS	Electrophysiology study
FDA	Food and Drug Administration
FP	False positive
Gd	Gadolinium contrast
GLRT	Generalized likelihood ratio test
HR	Heart rate
HRV	Heart rate variability
IS	Infarct size
KLT	Karhunen-Loève transform
LA	Left arm
LAD	Left anterior descendent artery
LBBB	Left bundle branch block
LCX	Left circumflex artery
LGE	late Gd enhancement, equivalent to late ce-MRI
LL	Left leg
LV	Left ventricle
MAD	Median absolute deviation
MaR	Myocardium at risk

MBq	Megabecquerel, 10^6 becquerel (Bq). Unit of radioactivity
MI	Myocardial infarction
MLE	Maximum likelihood estimator
MLR	Multiple linear regression
MPS	Myocardial perfusion imaging
MRI	Magnetic resonance images
PCI	Percutaneous coronary intervention
pPCI	primary percutaneous coronary intervention
PCA	Principal components analysis
PDF	Probability density function
PSVT	Paroxysmal supraventricular tachycardia
PTCA	Primary transluminal coronary angioplasty
QRS_{VCG}	QRS loop obtained from the VCG
QRS_{PCA}	QRS loop obtained from the PCA technique
RA	Right arm
RBBB	Right bundle branch block
RCA	Right coronary artery
SA	Sinoatrial node
SCD	Sudden cardiac death
SEM	Standard error of the mean
SD	Standard deviation
SPECT	Single photon emission computed tomography
SPCs	Supraventricular premature contractions
SPSS	Statistical Product and Service Solutions
STEMI	ST segment elevation myocardial infarction
SVD	Singular value decomposition
SVT	Supraventricular tachycardia
TN	True negative
TP	True positive
TWA	T wave alternans
VCG	Vectorcardiogram
VF	Ventricular fibrilation
VT	Ventricular tachycardia
WCT	Wilson's central terminal
WPW	Wolff-Parkinson-White syndrome

Bibliography

[1] V.L. Roger, A.S. Go, D.M. Lloyd-Jones, E.J. Benjamin, J.D. Berry, W.B. Borden, D.M. Bravata, S. Dai, E.S. Ford, C.S. Fox, et al. Heart Disease and Stroke Statistics – 2012 Update a Report from the American Heart Association. *Circulation*, 125(1):e2–e220, 2012.

[2] M.L. Daviglus, G.A. Talavera, M.L. Avilés-Santa, M. Allison, J. Cai, M.H. Criqui, M. Gellman, A.L. Giachello, N. Gouskova, R.C. Kaplan, et al. Prevalence of major cardiovascular risk factors and cardiovascular diseases among hispanic/latino individuals of diverse backgrounds in the United States cardiovascular diseases and US hispanics/latinos. *JAMA: the Journal of the American Medical Association*, 308 (17):1775–1784, 2012.

[3] M. Gheorghiade and R.O. Bonow. Chronic heart failure in the united states: a manifestation of coronary artery disease. *Circulation*, 97(3): 282–289, 1998.

[4] M. Gheorghiade, G. Sopko, L. De Luca, E.J. Velazquez, J.D. Parker, P.F. Binkley, Z. Sadowski, K.S. Golba, D.L. Prior, J.L. Rouleau, et al. Navigating the crossroads of coronary artery disease and heart failure. *Circulation*, 114(11):1202–1213, 2006.

[5] E. Carmeliet. Cardiac ionic currents and acute ischemia: from channels to arrhythmias. *Physiological Reviews*, 79(3):917–1017, 1999.

[6] M.J. Janse and A.L. Wit. Electrophysiological mechanisms of ventricular arrhythmias resulting from myocardial ischemia and infarction. *Physiological Reviews*, 69(4):1049–1169, 1989.

[7] N. Luqman, R.J. Sung, C.L. Wang, and C.T. Kuo. Myocardial ischemia and ventricular fibrillation: pathophysiology and clinical implications. *International Journal of Cardiology*, 119(3):283–290, 2007.

[8] M.T. Keating and M.C. Sanguinetti. Molecular and cellular mechanisms review of cardiac arrhythmias. *Cell*, 104:569–580, 2001.

[9] L. Sörnmo and P. Laguna. *Bioelectrical signal processing in cardiac and neurological applications*, volume 1. Elsevier Academic Press, 2005.

[10] E. Pueyo, J.P. Martínez, and P. Laguna. Cardiac repolarization analysis using the surface electrocardiogram. *Philosophical Transactions of the Royal Society A: Mathematical, Physical and Engineering Sciences*, 367(1887):213–233, 2009.

[11] R. Myerburg and A. Castellanos. *Heart disease: a textbook of cardiovascular medicine, ch. Cardiac arrest and sudden cardiac death.* Philadelphia: WB Saunders, 2001.

[12] A. Bayï¿½s de Luna. *Clinical electrocardiography: A textbook*. Armonk, N.Y.: Futura Publishing Company, 1998.

[13] K.H.W.J. Ten Tusscher and A.V. Panfilov. Cell model for efficient simulation of wave propagation in human ventricular tissue under normal and pathological conditions. *Physics in Medicine and Biology*, 51(23): 6141, 2006.

[14] William F Ganong et al. *Review of medical physiology*, volume 21. McGraw-Hill Medical New York:, 2005.

[15] S.A. Jones. *ECG notes: Interpretation and management guide*. FA Davis Company, 2005.

[16] E. Frank. An accurate, clinically practical system for spatial vectorcardiography. *Circulation*, 13(5):737–749, 1956.

[17] L. Edenbrandt and O. Pahlm. Vectorcardiogram synthesized from a 12-lead ECG: superiority of the inverse Dower matrix. *Journal of Electrocardiology*, 21(4):361–367, 1988.

[18] J.A. Kors, J.L. Talmon, and J.H. Van BemmeL. Multilead ECG analysis. *Computers and Biomedical Research*, 19(1):28–46, 1986.

[19] H.C. Bazzet. An analysis of the time-relations of electrocardiograms. *Heart*, 7:353–370, 1920.

[20] L.S. Fridericia. The duration of systole in an electrocardiogram in normal humans and in patients with heart disease. *Annals of Noninvasive Electrocardiology*, 8(4):343–351, 2003.

[21] A. Sagie, M.G. Larson, R.J. Goldberg, J.R. Bengtson, and D. Levy. An improved method for adjusting the qt interval for heart rate (the framingham heart study). *The American Journal of Cardiology*, 70 (7):797–801, 1992.

[22] P. Gomis, D.L. Jones, P. Caminal, E.J. Berbari, and P. Lander. Analysis of abnormal signals within the QRS complex of the high-resolution electrocardiogram. *IEEE Transactions on Biomedical Engineering*, 44 (8):681–693, 1997.

[23] A. Beker, A. Pinchas, J. Erel, and S. Abboud. Analysis of high frequency QRS potential during exercise testing in patients with coronary artery disease and in healthy subjects. *Circulation*, 19(12):2040–2050, 1996.

[24] E. Pueyo, L. Sörnmo, and P. Laguna. QRS slopes for detection and characterization of myocardial ischemia. *IEEE Transactions on Biomedical Engineering*, 55(2):468–477, 2008.

[25] T. Watanabe, M. Yamaki, H. Tachibana, I. Kubota, H. Tomoike, et al. Decrease in the high frequency QRS components depending on the local conduction delay. *Japanese Circulation Journal*, 62(11):844, 1998.

[26] J. Pettersson, O. Pahlm, E. Carro, L. Edenbrandt, M. Ringborn, L. Sï¿½rnmo, S.G. Warren, and G.S. Wagner. Changes in high-frequency QRS components are more sensitive than ST-segment deviation for detecting acute coronary artery occlusion. *Journal of the American College of Cardiology*, 36(6):1827, 2000.

[27] M. Fernández. *Obtención de micropotenciales cardíacos latido a latido por vía superficial*. PhD thesis, 1996.

[28] Anthony S Fauci et al. *Harrison's principles of internal medicine*, volume 2. McGraw-Hill Medical New York, 2008.

[29] A. Florian, R. Jurcut, C. Ginghina, and J. Bogaert. Cardiac magnetic resonance imaging in ischemic heart disease: A clinical review. *Journal of Medicine and Life*, 4(4):330, 2011.

[30] A.E. Arai. Magnetic resonance imaging for area at risk, myocardial infarction, and myocardial salvage. *Journal of Cardiovascular Pharmacology and Therapeutics*, 16(3-4):313–320, 2011.

[31] M. Ishida, S. Kato, and H. Sakuma. Cardiac MRI in ischemic heart disease. *Circulation Journal: official journal of the Japanese Circulation Society*, 73(9):1577, 2009.

[32] C.B. Higgins, R. Herfkens, M. J Lipton, R. Sievers, P. Sheldon, L. Kaufman, and L.E. Crooks. Nuclear magnetic resonance imaging of acute myocardial infarction in dogs: alterations in magnetic relaxation times. *The American Journal of Cardiology*, 52(1):184–188, 1983.

[33] R.C. Hendel, M.R. Patel, C.M. Kramer, M. Poon, J.C. Carr, N.A. Gerstad, L.D. Gillam, J.M.B. Hodgson, R.J. Kim, J.R. Lesser, et al. ACCF/ACR/SCCT/SCMR/ASNC/NASCI/SCAI/SIR 2006 appropriateness criteria for cardiac computed tomography and cardiac magnetic resonance imaging: A report of the American College of Cardiology Foundation quality strategic directions committee appropriateness criteria working group, American College of Radiology, Society of Cardiovascular Computed Tomography, Society for Cardiovascular Magnetic Resonance, American Society of Nuclear Cardiology, North American Society for Cardiac Imaging, Society for Cardiovascular Angiography and Interventions, and Society of Interventional Radiology. *Journal of the American College of Cardiology*, 48(7):1475, 2006.

[34] B.J. Maron, W.J. McKenna, G.K. Danielson, L.J. Kappenberger, H.J. Kuhn, C.E. Seidman, P.M. Shah, W.H. Spencer III, P. Spirito, F.J. Ten Cate, et al. American College of Cardiology/European Society of Cardiology clinical expert consensus document on hypertrophic cardiomyopathy: a report of the American College of Cardiology Foundation Task Force on Clinical Expert Consensus Documents and the European Society of Cardiology Committee for Practice Guidelines. *Journal of the American College of Cardiology*, 42(9):1687, 2003.

[35] A. Wagner, H. Mahrholdt, T.A. Holly, M.D. Elliott, M. Regenfus, M. Parker, F.J. Klocke, R.O. Bonow, R.J. Kim, and R.M. Judd. Contrast-enhanced MRI and routine single photon emission computed tomography (SPECT) perfusion imaging for detection of subendocardial myocardial infarcts: an imaging study. *The Lancet*, 361(9355): 374–379, 2003.

[36] T. Ibrahim, H.P. Bülow, T. Hackl, M. Hörnke, S.G. Nekolla, M. Breuer, A. Schömig, and M. Schwaiger. Diagnostic value of contrast-enhanced magnetic resonance imaging and single-photon emission computed tomography for detection of myocardial necrosis early after acute myocardial infarction. *Journal of the American College of Cardiology*, 49(2):208–216, 2007.

[37] C. Manhenke, I.S. Anand, I. Squire, E. Nagel, T. Edvardsen, K. Dickstein, et al. Effect of left ventricular scar size, location, and transmurality on left ventricular remodeling with healed myocardial infarction. *The American Journal of Cardiology*, 99(8):1109–1114, 2007.

[38] G. Mariani, L. Bruselli, T. Kuwert, E.E. Kim, A. Flotats, O. Israel, M. Dondi, and N. Watanabe. A review on the clinical uses of SPECT/CT. *European Journal of Nuclear Medicine and Molecular Imaging*, 37(10):1959–1985, 2010.

[39] V. Fuster, R.W. Alexander, R.A. O'Rourke, R. Roberts, S.B. King, and H. JJ Wellens. *Hurst's the Heart, 2-Vol Set*. McGraw-Hill Professional Publishing, 2000.

[40] A. Elhendy, J.J. Bax, and D. Poldermans. Dobutamine stress myocardial perfusion imaging in coronary artery disease. *Journal of Nuclear Medicine*, 43(12):1634–1646, 2002.

[41] N. B. Wagner, D. C. Sevilla, M. W. Krucoff, K. L. Lee, K. S. Pieper, K. K. Kent, R. K. Bottner, R. H. Selvester, and G. S. Wagner. Transient alterations of the QRS complex and ST segment during percutaneous transluminal balloon angioplasty of the left anterior descending coronary artery. *American Journal of Cardiology*, 62(16):1038–1042, 1988.

[42] S. Charlap, J. Shani, N. Schulho, B. Herman, and E. Lichstein. R- and S-wave amplitude changes with acute anterior transmural myocardial ischaemia. *Chest*, 97(3):566–571, 1990.

[43] E. Pueyo, J. García, G. Wagner, R. Bailón, L. Sörnmo, and P. Laguna. Time course of ECG depolarization and repolarization changes during ischemia in PTCA recordings. *Methods of Information in Medicine*, 43(1):43–46, 2004.

[44] P. Weston, P. Johanson, L. M. Schwartz, C. Maynard, R. B. Jennings, and G. S. Wagner. The value of both ST-segment and QRS complex changes during acute coronary occlusion for prediction of reperfusion-induced myocardial salvage in a canine model. *Journal of Electrocardiology*, 40(1):18–25, 2007.

[45] J. García, G. Wagner, L. Sörnmo, S. Olmos, P. Lander, and P. Laguna. Temporal evolution of traditional versus transformed ECG-based indexes in patients with induced myocardial ischemia. *Journal of Electrocardiology*, 33(1):37–47, 2000.

[46] Y. Birnbaum, I. Herz, S. Sclarovsky, B. Zlotikamien, A. Chetrit, L. Olmer, and G. I. Barbash. Prognostic significance of the admission electrocardiogram in acute myocardial infarction. *Journal of the American College of Cardiology*, 27(5):1128–1132, 1996.

[47] J. Pettersson, O. Pahlm, E. Carro, L. Edenbrandt, M. Ringborn, L. Sörnmo, S. G. Warren, and G. S. Wagner. Changes in high-frequency QRS components are more sensitive than ST-segment deviation for detecting acute coronary artery occlusion. *Journal of the American College of Cardiology*, 36(6):1827–1834, 2000.

[48] S. Abboud, R. J. Cohen, A. Selwyn, P. Ganz, D. Sadeh, and P. L. Friedman. Detection of transient myocardial ischemia by computer analysis of standard and signal-averaged high-frequency electrocardiograms in patients undergoing percutaneous transluminal coronary angioplasty. *Circulation*, 76(3):585–596, 1987.

[49] G. Dori, A. Rosenthal, S. Fishman, Y. Denekamp, B.S. Lewis, and H. Bitterman. Changes in the slope of the first major deflection of the ECG complex during acute coronary occlusion. *Computers in Biology and Medicine*, 35(4):299–309, 2005.

[50] R. Correa, E. Laciar, P. Arini, and R. Jané. Analysis of QRS loop changes in the beat-to-beat Vectocardiogram of ischemic patients undergoing PTCA. In *Proceedings of the Annual International Conference of the IEEE, EMBC 2009. IEEE Engineering in Medicine and Biology Society*, pages 1750–1753, 2009.

[51] R. Correa, P.D. Arini, E. Laciar, P. Laguna, and R. Jané. Study of morphological parameters of QRS loop using singular value decomposition during ischemia induced by coronary angioplasty. In *Proceedings of Computers in Cardiology, IEEE Computer Society Press*, pages 693–696, 2009.

[52] R.E. Mason and I. Likar. A new system of multiple-lead exercise electrocardiography. *American Heart Journal*, 71(2):196–205, 1966.

[53] G.B. Moody and R.G. Mark. Development and evaluation of a 2-lead ECG analysis program. In *Proceedings of Computers in Cardiology, IEEE Computer Society Press*, pages 39–44, 1982.

[54] J.P. Martínez, R. Almeida, S. Olmos, A.P. Rocha, and P. Laguna. A wavelet-based ECG delineator: evaluation on standard databases. *IEEE Transactions on Biomedical Engineering*, 51(4):570–581, 2004.

[55] F. Castells, P. Laguna, L. Sörnmo, A. Bollmann, and J.M. Roig. Principal component analysis in ECG signal processing. *EURASIP Journal on Advances in Signal Processing*, 2007. ID:74580, doi:10.1155/2007/74.

[56] D. Romero, E. Pueyo, M. Ringborn, and P. Laguna. QRS slopes for ischemia monitoring in PCI recordings. In *Proceedings of World Congress on Medical Physics and Biomedical Engineering*, pages 1695–1698, 2009.

[57] N.B. Wagner, D.C. Sevilla, M.W. Krucoff, K.S. Pieper, K.L. Lee, R.D. White, K.M. Kent, R. Renzi, R.H. Selvester, and G.S. Wagner. Transient alterations of the QRS complex and ST segment during percutaneous transluminal balloon angioplasty of the right and left circumflex

coronary arteries. *American Journal of Cardiology*, 63(17):1208–1213, 1989.

[58] P. Laguna, G.B. Moody, J. García, A.L. Goldberger, and R.G. Mark. Analysis of the ST-T complex of the electrocardiogram using the Karhunen-Loève transform adaptive monitoring and alternans detection. *Medical and Biological Engineering and Computing*, 37(2):175–189, 1999.

[59] P. Johanson, Y. Fu, S.G. Goodman, M. Dellborg, P.W. Armstrong, M.W. Krucoff, L. Wallentin, and G.S. Wagner. A dynamic model forecasting myocardial infarct size before, during, and after reperfusion therapy: an ASSENT-2 ECG/VCG substudy. *European Heart Journal*, pages 1726–1733, 2005.

[60] P. Johanson, G.S. Wagner, M. Dellborg, and M.W. Krucoff. ST-segment monitoring in patients with acute coronary syndromes. *Current Cardiology Reports*, 5:278–283, 2003.

[61] J. García, G. Wagner, L. Sörmno, P. Lander, and P. Laguna. Identification of the occluded artery in patients with myocardial ischemia induced by prolonged percutaneous transluminal coronary angioplasty using traditional vs transformed ECG-based indexes. *Computers and Biomedical Research*, 32(5):470–482, 1999.

[62] B. Surawicz. Reversible QRS changes during acute myocardial ischemia. *Journal of Electrocardiology*, 31(3):209–220, 1998.

[63] J.S. Floyd, C. Maynard, P. Weston, P. Johanson, R.B. Jennings, and G.S. Wagner. Effects of ischemic preconditioning and arterial collateral flow on ST-segment elevation and QRS complex prolongation in a canine model of acute coronary occlusion. *Journal of Electrocardiology*, 42(1):19–26, 2009.

[64] B. Surawicz, C.M. Orr, J.B. Hermiller, K.D. Bell, and R.P. Pinto. QRS changes during percutaneous transluminal coronary angioplasty and their possible mechanisms. *Journal of the American College of Cardiology*, 30(2):452–458, 1997.

[65] C.K. Wong, W. Gao, R.A.H. Stewart, N. van Pelt, J.K. French, P.E.G. Aylward, H.D. White, et al. Risk stratification of patients with acute anterior myocardial infarction and right bundle-branch block. importance of QRS duration and early ST-segment resolution after fibrinolytic therapy. *Circulation*, 114(8):783–789, 2006.

[66] C.K. Wong, W. Gao, R.A.H. Stewart, J.K. French, P.E.G. Aylward, and H.D. White. Relationship of QRS duration at baseline and changes

over 60 min after fibrinolysis to 30-day mortality with different locations of ST elevation myocardial infarction: results from the Hirulog and Early Reperfusion or Occlusion-2 trial. *Heart*, 95(4):276–282, 2009.

[67] Y. Birnbaum, D.A. Criger, G.S. Wagner, B. Strasberg, A. Mager, K. Gates, C.B. Granger, A.M. Ross, and G.I. Barbash. Prediction of the extent and severity of left ventricular dysfunction in anterior acute myocardial infarction by the admission electrocardiogram. *American Heart Journal*, 141(6):915–924, 2001.

[68] A. Wolak, S. Yaroslavtsev, G. Amit, Y. Birnbaum, C. Cafri, S. Atar, H. Gilutz, R. Ilia, and D. Zahger. Grade 3 ischemia on the admission electrocardiogram predicts failure of st resolution and of adequate flow restoration after primary percutaneous coronary intervention for acute myocardial infarction. *American Heart Journal*, 153(3):410–417, 2007.

[69] T. Billgren, C. Maynard, T.F. Christian, M.A. Rahman, M. Saeed, S.C. Hammill, G.S. Wagner, and Y. Birnbaum. Grade 3 ischemia on the admission electrocardiogram predicts rapid progression of necrosis over time and less myocardial salvage by primary angioplasty. *Journal of Electrocardiology*, 38(3):187–194, 2005.

[70] R.J. Gibbons, M.S. Verani, T. Behrenbeck, P.A. Pellikka, M.K. O'Connor, J.J. Mahmarian, J.H. Chesebro, and F.J. Wackers. Feasibility of tomographic 99mTc-hexakis-2-methoxy-2-methylpropyl-isonitrile imaging for the assessment of myocardial area at risk and the effect of treatment in acute myocardial infarction. *Circulation*, 80 (5):1277–1286, 1989.

[71] H.L. Haronian, M.S. Remetz, A.J. Sinusas, J.M. Baron, H.I. Miller, M.W. Cleman, B.L. Zaret, and F.J.T. Wackers. Myocardial risk area defined by technetium-99m sestamibi imaging during percutaneous transluminal coronary angioplasty: comparison with coronary angiography. *Journal of the American College of Cardiology*, 22(4):1033–1043, 1993.

[72] E. Persson, J. Palmer, J. Pettersson, S.G. Warren, S. Borges-Neto, G.S. Wagner, and O. Pahlm. Quantification of myocardial hypoperfusion with 99mTc-sestamibi in patients undergoing prolonged coronary artery balloon occlusion. *Nuclear Medicine Communications*, 23(3): 219–228, 2002.

[73] E.V. Garcï¿½a, C.D. Cooke, K.F. Van Train, R. Folks, J. Peifer, E.G. DePuey, J. Maddahi, N. Alazraki, J. Galt, N. Ezquerra, et al. Technical aspects of myocardial SPECT imaging with technetium-99m sestamibi. *The American Journal of Cardiology*, 66(13):E23–E31, 1990.

[74] E. Persson, J. Pettersson, M. Ringborn, L. Sörnmo, S.G. Warren, G.S. Wagner, C. Maynard, and O. Pahlm. Comparison of ST-segment deviation to scintigraphically quantified myocardial ischemia during acute coronary occlusion induced by percutaneous transluminal coronary angioplasty. *The American Journal of Cardiology*, 97(3):295–300, 2006.

[75] M. Ringborn, J. Pettersson, E. Persson, S.G. Warren, P. Platonov, O. Pahlm, and G.S. Wagner. Comparison of high-frequency QRS components and ST-segment elevation to detect and quantify acute myocardial ischemia. *Journal of Electrocardiology*, 43(2):113–120, 2010.

[76] P. Laguna, R. Jané, P. Caminal, et al. Automatic detection of wave boundaries in multilead ECG signals: Validation with the CSE database. *Computers and Biomedical Research*, 27(1):45–60, 1994.

[77] T.L. Shook, V. Valvo, M. Hubelbank, C.L. Feldman, P.H. Stone, and K.L. Ripley. Validation of a new algorithm for detection and quantification of ischemic ST segment changes during ambulatory electrocardiography. In *Proceedings of Computer in Cardiology, IEEE Computer Society Press*, pages 57–62, 1987.

[78] R.W. Stadler, S.N. Lu, S.D. Nelson, and L. Stylos. A real-time ST-segment monitoring algorithm for implantable devices. *Journal of Electrocardiology*, 34(4):119–126, 2001.

[79] A. Smrdel and F. Jager. Automated detection of transient ST-segment episodes in 24h electrocardiograms. *Medical and Biological Engineering and Computing*, 42(3):303–311, 2004.

[80] A. Taddei, G. Costantino, R. Silipo, M. Emdin, and C. Marchesi. A system for the detection of ischemic episodes in ambulatory ECG. In *Proceedings of Computers in Cardiology, IEEE Computer Society Press*, pages 705–708, 1995.

[81] D. Romero, M. Ringborn, P. Laguna, O. Pahlm, and E. Pueyo. Depolarization changes during acute myocardial ischemia by evaluation of QRS slopes: standard lead and vectorial approach. *IEEE Transactions on Biomedical Engineering*, 58(1):110–120, 2011.

[82] A. Mincholé, L. Sï¿½rnmo, and P. Laguna. ECG-based detection of body position changes using a Laplacian noise model. In *Proceedings of the Annual International Conference of the IEEE: Engineering in Medicine and Biology Society, EMBC*, pages 6931–6934. IEEE, 2011.

[83] J. García, M. Astrom, J. Mendive, P. Laguna, and L. Sï¿½rnmo. ECG-based detection of body position changes in ischemia monitoring. *IEEE Transactions on Biomedical Engineering*, 50(6):677–685, 2003.

[84] B.L. Nørgaard, B.M. Rasmussen, M. Dellborg, and K. Thygesen. Positional changes of spatial QRS-and ST-segment variables in normal subjects: Implications for continuous vectorcardiography monitoring during myocardial ischemia. *Journal of Electrocardiology*, 33(1):23–30, 2000.

[85] F. Hampel, E. Ronchetti, P. Rousseeuw, and W. Stahel. Robust Statistics, ser. Probability and Mathematical Statistics. 1986.

[86] W.S. Chang, T. Akiyama, J.F. Richeson, R.T. Faillace, and P. Serrino. Origin of the giant R wave in acute transmural myocardial infarction in the pig. *Japanese Heart Journal*, 30(6):863–883, 1989.

[87] M.J. Janse, J. Cinca, H. Morena, J.W. Fiolet, A.G. Kleber, G.P. De Vries, A.E. Becker, and D. Durrer. The border zone in myocardial ischemia. an electrophysiological, metabolic, and histochemical correlation in the pig heart. *Circulation Research*, 44(4):576–588, 1979.

[88] H. Morena, M.J. Janse, J.W. Fiolet, W.J. Krieger, H. Crijns, and D. Durrer. Comparison of the effects of regional ischemia, hypoxia, hyperkalemia, and acidosis on intracellular and extracellular potentials and metabolism in the isolated porcine heart. *Circulation Research*, 46(5):634–646, 1980.

[89] U. Näslund, S. Häggmark, G. Johansson, and S. Reiz. Ischaemia and reperfusion induced transient QRS vector changes: relationship to size of the ischaemic territory. *Cardiovascular Research*, 27(2):327–333, 1993.

[90] U. Näslund, S. Häggmark, G. Johansson, and S. Reiz. Quantification of myocardium at risk and detection of reperfusion by dynamic vectorcardiographic ST segment monitoring in a pig occlusion-reperfusion model. *Cardiovascular Research*, 27(12):2170–2178, 1993.

[91] M.M. Demidova, J. van der Pals, J.F.A. Ubachs, M. Kanski, H. Engblom, D. Erlinge, V.M. Tichonenko, and P.G. Platonov. ST-segment dynamics during reperfusion period and the size of myocardial injury in experimental myocardial infarction. *Journal of Electrocardiology*, 44(1):74–81, 2011.

[92] M.M. Demidova, J. van der Pals, J.F.A. Ubachs, M. Kanski, H. Engblom, D. Erlinge, V.M. Tichonenko, and P.G. Platonov. St-segment dynamics during reperfusion period and the size of myocardial injury in experimental myocardial infarction. *J. Electrocardiol.*, 44(1):74–81, 2011.

[93] M. Götberg, G. Olivecrona, H. Engblom, M. Ugander, J. Van Der Pals, E. Heiberg, H. Arheden, and D. Erlinge. Rapid short-duration hypothermia with cold saline and endovascular cooling before reperfusion reduces microvascular obstruction and myocardial infarct size. *BMC Cardiovascular Disorders*, 8(1):7, 2008.

[94] R.J. Kim, D.S. Fieno, T.B. Parrish, K. Harris, E.L. Chen, O. Simonetti, J. Bundy, J.P. Finn, F.J. Klocke, and R.M. Judd. Relationship of MRI delayed contrast enhancement to irreversible injury, infarct age, and contractile function. *Circulation*, 100(19):1992–2002, 1999.

[95] E. Heiberg, M. Ugander, H. Engblom, M. Götberg, G.K. Olivecrona, D. Erlinge, and H. Arheden. Automated quantification of myocardial infarction from MR images by accounting for partial volume effects: Animal, phantom, and human study1. *Radiology*, 246(2):581, 2008.

[96] E. Heiberg, J. Sjögren, M. Ugander, M. Carlsson, H. Engblom, and H. Arheden. Design and validation of segment-freely available software for cardiovascular image analysis. *BMC Medical Imaging*, 10(1):1, 2010.

[97] J. Bolea, R. Almeida, P. Laguna, L. Sï¿½rnmo, and J.P. Martï¿½nez. BioSigBrowser, biosignal processing interface. In *9th International Conference on Information Technology and Applications in Biomedicine, ITAB 2009.*, pages 1–4. IEEE, 2009.

[98] J.R. De Groot and R. Coronel. Acute ischemia-induced gap junctional uncoupling and arrhythmogenesis. *Cardiovascular Research*, 62(2): 323–334, 2004.

[99] J.R. De Groot, F.J.G. Wilms-Schopman, T. Opthof, C.A. Remme, and R. Coronel. Late ventricular arrhythmias during acute regional ischemia in the isolated blood perfused pig heart role of electrical cellular coupling. *Cardiovascular Research*, 50(2):362–372, 2001.

[100] R.T. Faillace, T. Akiyama, and W. Chang. The giant R wave of acute myocardial infarction. *Japanese Heart Journal*, 26(2):165, 1985.

[101] Y. Birnbaum and B.J. Drew. The electrocardiogram in ST elevation acute myocardial infarction: correlation with coronary anatomy and prognosis. *Postgraduate Medical Journal*, 79(935):490–504, 2003.

[102] J.K. Kjekshus, P.R. Maroko, and B.E. Sobel. Distribution of myocardial injury and its relation to epicardial ST-segment changes after coronary artery occlusion in the dog. *Cardiovascular Research*, 6(5): 490–499, 1972.

[103] A.G. Kleber, M.J. Janse, FJ Van Capelle, D. Durrer, et al. Mechanism and time course of ST and TQ segment changes during acute regional myocardial ischemia in the pig heart determined by extracellular and intracellular recordings. *Circulation Research*, 42(5):603–613, 1978.

[104] A. van Oosterom. *Cardiac potential distributions*. PhD thesis, Amsterdam: University of Amsterdam, 1978.

[105] A. Noma and N. Tsuboi. Dependence of junctional conductance on proton, calcium and magnesium ions in cardiac paired cells of guinea-pig. *The Journal of Physiology*, 382(1):193, 1987.

[106] L. Firek and R. Weingart. Modification of gap junction conductance by divalent cations and protons in neonatal rat heart cells. *Journal of Molecular and Cellular Cardiology*, 27(8):1633–1643, 1995.

[107] L.R.C. Dekker, J.W.T. Fiolet, E. VanBavel, R. Coronel, T. Opthof, J.A.E. Spaan, and M.J. Janse. Intracellular Ca^{2+}, intercellular electrical coupling, and mechanical activity in ischemic rabbit papillary muscle: effects of preconditioning and metabolic blockade. *Circulation Research*, 79(2):237–246, 1996.

[108] M. Ringborn, D. Romero, E. Pueyo, O. Pahlm, G.S. Wagner, P. Laguna, and P.G. Platonov. Evaluation of depolarization changes during acute myocardial ischemia by analysis of QRS slopes. *Journal of Electrocardiology*, 44(4):416–424, 2011.

[109] J.E. Lowe, K.A. Reimer, and R.B. Jennings. Experimental infarct size as a function of the amount of myocardium at risk. *The American Journal of Pathology*, 90(2):363, 1978.

[110] T.F. Christian, R.J. Gibbons, I.P. Clements, P.B. Berger, R.H. Selvester, and G.S. Wagner. Estimates of myocardium at risk and collateral flow in acute myocardial infarction using electrocardiographic indexes with comparison to radionuclide and angiographic measures. *Journal of the American College of Cardiology*, 26(2):388–393, 1995.

Que te parece desto, Sancho – Dijo Don Quijote –
Hay encantos que valgan contra la verdadera valentía.
Bien podrán los encantadores quitarme la ventura,
pero el esfuerzo y el nimo, será imposible.

Miguel de Cervantes
II parte del Ingenioso Caballero
Don Quijote de la Mancha